AD A110032

STRUCTURAL ANALYSIS OF NATURAL TEXTURES

by

Felicia Mary D'Auria Vilnrotter

September 1981

Intelligent Systems Group
Departments of Electrical Engineering
and Computer Science

University of Southern California

STRUCTURAL ANALYSIS OF

NATURAL TEXTURES

by

Felicia Mary D'Auria Vilnrotter

September 1981

Intelligent Systems Group
Departments of Electrical Engineering
and Computer Science

SECURITY CLASSIFICATION OF THIS PAGE *(When Data Entered)*

REPORT DOCUMENTATION PAGE		READ INSTRUCTIONS BEFORE COMPLETING FORM
1. REPORT NUMBER USCISG 100 USCIPI 1040	2. GOVT ACCESSION NO. AD-A110 032	3. RECIPIENT'S CATALOG NUMBER
4. TITLE *(and Subtitle)* STRUCTURAL ANALYSIS OF NATURAL TEXTURES		5. TYPE OF REPORT & PERIOD COVERED Technical Report, Sept. 1981
		6. PERFORMING ORG. REPORT NUMBER USCISG 100, USCIPI 1040
7. AUTHOR(s) FELICIA MARY D'AURIA VILNROTTER		8. CONTRACT OR GRANT NUMBER(s) F-33615-80-C-1080
9. PERFORMING ORGANIZATION NAME AND ADDRESS Departments of Electrical Engineering and Computer Science, University of Southern California Los Angeles, California 90007		10. PROGRAM ELEMENT, PROJECT, TASK AREA & WORK UNIT NUMBERS DARPA Order No. 3119
11. CONTROLLING OFFICE NAME AND ADDRESS Defense Advanced Research Projects Agency 1400 Wilson Boulevard Arlington, VA 22209		12. REPORT DATE September 1981
		13. NUMBER OF PAGES 328 pages
14. MONITORING AGENCY NAME & ADDRESS*(if different from Controlling Office)* Air Force Wright Aeronautical Laboratories Wright-Patterson Air Force Base Dayton, OHIO 45433		15. SECURITY CLASS. *(of this report)* UNCLASSIFIED
		15a. DECLASSIFICATION/DOWNGRADING SCHEDULE

16. DISTRIBUTION STATEMENT *(of this Report)*

Approved for release: distribution unlimited

17. DISTRIBUTION STATEMENT *(of the abstract entered in Block 20, if different from Report)*

18. SUPPLEMENTARY NOTES

19. KEY WORDS *(Continue on reverse side if necessary and identify by block number)*

Texture Analysis, Texture Description, Texture Identification, Structural Analysis, Image Understanding, Image Processing, Texture Gradients.

20. ABSTRACT *(Continue on reverse side if necessary and identify by block number)*

In this dissertation a general method is presented for the structural analysis of natural texture images. Edge Repetition Arrays(ERAs) are calculated for the edge and direction images corresponding to the natural texture image being analyzed. Each ERA entry is the normalized frequency of occurrence of specific types of edge matches occurring with a particular angle and distance separation. The two types of edge matches sought are for element size and spacing. Hence, a one-dimensional structural texture profile can be inferred from the information inherent in these arrays. An algorithm designed to automatically interpret

DD FORM 1 JAN 73 1473 EDITION OF 1 NOV 65 IS OBSOLETE

SECURITY CLASSIFICATION OF THIS PAGE *(When Data Entered)*

39 1141

ERA results is presented. This algorithm produces a one-dimensional structural description of the texture, and provides a starting point for the two-dimensional texture primitive search.

A texture primitive extraction algorithms is also developed. It uses the information inherent in the above-mentioned texture description to identify the locations of various type of elements within the texture image. The results produced are in the form of individual and composite texture primitive masks as well as descriptions for the individual texture primitive types.

A structural texture description should include information about the manner in which the primitives are arranged within the texture. Since the texture primitive masks pinpoint the texture element locations they can be used to calculate a set of rules which characterize this arrangement. An algorithm is developed which extracts the most frequently occurring interprimitive placement rules, and in case the texture being analyzed is homogeneous and regular a minimum set of rules necessary to characterize the underlying texture pattern is also chosen. Finally, a texture reconstruction algorithm is developed to produce a reconstruction of the original texture using the minimum placement rule set and a set of average primitive templates. In this way, a visual comparison can be made to determine how closely the grid relations chosen capture the spatial relations of the original texture image.

A scheme is presented for texture classification (of 11 texture types) using the structural texture descriptions discussed above. An overall success rate of 91.23% was achieved. The techniques developed in this thesis are also applied to the surface orientation determination problem. A general algorithm is outlined for determining the orientation of textures surfaces. Preliminary results are presented and discussed.

Accession For

NTIS GRA&I
DTIC TAB
Unannounced
Justification

By
Distribution/
Availability Codes
Avail and/or
Dist   Special

DTIC
COPY
INSPECTED
1

ACKNOWLEDGEMENTS

ii

Finally, I would like to thank the Hughes Aircraft Company for its generous financial support.

iii

TABLE OF CONTENTS

v

LIST OF TABLES

ABSTRACT

In this dissertation a general method is presented for the structural analysis of natural texture images. Edge Repetition Arrays (ERAs) are calculated for the edge and direction images corresponding to the natural texture image being analyzed. Each ERA entry is the normalized frequency of occurrence of specific types of edge matches occurring with a particular angle and distance separation. The two types of edge matches sought are for element size and spacing. Hence, a one-dimensional structural texture profile can be inferred from the information inherent in these arrays. An algorithm designed to automatically interpret ERA results is presented. This algorithm produces a one-dimensional structural description of the texture, and provides a starting point for the two-dimensional texture primitive search.

A texture primitive extraction algorithms is also developed. It uses the information inherent in the above-mentioned texture description to identify the locations of various type of elements within the texture image. The results produced are in the form of individual and composite texture primitive masks as well as

descriptions for the individual texture primitive types.

A structural texture description should include information about the manner in which the primitives are arranged within the texture. Since the texture primitive masks pinpoint the texture element locations they can be used to calculate a set of rules which characterize this arrangement. An algorithm is developed which extracts the most frequently occurring interprimitive placement rules, and in case the texture being analyzed is homogeneous and regular a minimum set of rules necessary to characterize the underlying texture pattern is also chosen. Finally, a texture reconstruction algorithm is developed to produce a reconstruction of the original texture using the minimum placement rule set and a set of average primitive templates. In this way, a visual comparison can be made to determine how closely the grid relations chosen capture the spatial relations of the original texture image.

A scheme is presented for texture classification (of 11 texture types) using the structural texture descriptions discussed above. An overall success rate of 91.23% was achieved. The techniques developed in this thesis are also applied to the surface orientation determination problem. A general algorithm is outlined for determining the orientation of textured surfaces. **Preliminary results are presented and discussed.**

CHAPTER 1

INTRODUCTION

When interpreting natural scenes the human visual system uses the textural characteristics of the objects it perceives as well as their shapes and intensities. When we differentiate a brick wall from a field of grass or an aerial ocean view from one of a city we are interpreting textural cues within the image. A texture can be thought of as a spatial pattern of light intensities. This pattern, or arrangement, can be regular (periodic) or random. Likewise, the elements composing the texture can be uniform or varying in shape, intensity, and orientation. Since texture is a pervasive characteristic of natural scenes, texture analysis should be included in image understanding systems.

Computer vision systems need to have the capacity to draw on this wealth of textural information within the image. This information could be helpful in:

1) segmenting the image into homogeneously textured regions,

1

2) providing more complete region descriptions,

3) giving cues to help predict surface orientation; and,

4) aiding in region identification or recognition.

Automatic analysis of naturally occurring textures is the subject of this thesis. An attempt is made to identify the structural characteristics of the textures being analyzed. Descriptions are generated for homogeneous texture regions, textural elements are extracted and described, and a set of placement rules necessary for texture reconstruction is automatically determined whenever possible.

1.1 Statistical Versus Structural Analysis Methods

A variety of methods have been used for texture analysis and classification. These approaches can, for the most part, be divided into two major categories, namely, statistical and structural. In the former, statistical measures are sought which can be used to characterize or classify image textures. The experimental findings of perceptual psychologist, Bela Julesz [1] lend support to this method of analysis. Julesz found that textures whose first- or second-order statistics were different could be distinguished immediately by human observers. However, textures differing only in their

2

third- or higher-order statistics could not be easily distinguished. It was therefore conjectured that the second-order statistics of a texture were sufficient for texture characterization. Later work by others, including Pratt, Faugeras, and Gagalowicz [2], has served to sharpen this result. It has been determined that while second-order statistical measures should be sufficient, the mean, variance, and autocorrelation functions, by themselves, were not.

Structural analysis methods, on the other hand, attempt to characterize textures in terms of primitives and their relative placement within the texture image. Texture primitives can be regions of uniform intensity or more complex structures such as tiles or mosaic cells.

Consider the brick wall mosaic in Fig. 1-1. The statistical description of these 4 brick subwindows might be in the form of feature vectors containing statistical measures designed to capture textural characteristics such as contrast or coarseness. (It is assumed that the types of measures chosen are nearly uniform over homogeneously textured regions.) On the other hand, structural descriptions for these 4 brick patterns include size, shape and intensity information for the brick and mortar texture primitives. They would also provide descriptions

(a) Brick Mosaic
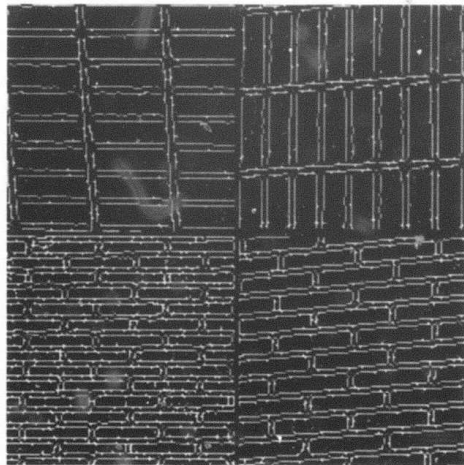
(b) Non-Maximal Suppressed
Edges from (a)

Figure 1-1. Brick Mosaic and Edges

4

of how these primitives are arranged in each of the 4 subpatterns. Therefore, it should be clear from these descriptions that:

1) The brick primitives in the top row images are arranged in rectangular grid patterns, while the images in the bottom row show shifted arrangements.

2) The horizontal dimension of the brick primitives in the left top row image is larger than the vertical dimension. The opposite is true of the brick primitives in the right top subimage.

3) The brick primitives in the left bottom subimage are smaller than the ones on the right. (This information could be useful in determining the relative distance from the observer.)

The two basic approaches need not be used in isolation. Statistical methods have been used to extract structural information while some structural textural properties may need to be described statistically [3].

1.2 Related Work

A large variety of techniques have been developed for analyzing natural textures. A few are mentioned briefly below. Some of these techniques are discussed in greater

5

detail in later chapters. An excellent survey of texture analysis techniques can be found in [4].

Bajcsy [5], [6] produced symbolic descriptions for natural texture images by analyzing the 2-dimensional Fourier transform of the image. By examining certain regions within the transform image, information pertaining to periodicity, directionality, and other texture characteristics was inferred.

Haralick, Shanmugam, and Dinstein [7] developed a technique for calculating certain textural features based on the gray-tone spatial dependencies inherent in texture images. A set of N x N matrices are calculated for given angle and distance pixel separations where N is the number of gray levels in the image. The entries of these "co-occurrence" matrices are counts of how often one gray tone appears in a specific spatial relationship to another gray tone. In [7] fourteen measures are suggested for calculating textural features from these matrices. (See Chapter 2, Section 2.2 for some examples.)

In [8] Price and Nevatia used the co-occurrence technique on edge images corresponding to natural texture images. In this way the number of gray levels to consider is only 2 while the image used retains the basic structure of the texture under consideration.

Davis, Johns, and Aggarwal [9] generalized the co-occurrence technique. Their generalized co-occurrence matrices reflect the spatial interdependence of sets of local features (not necessarily gray levels).

Clearly, the number of possible spatial relationships, and thus co-occurrence matrices, is very large for a given texture image. In [10] Zucker and Terzopoulos present a statistical approach to finding the spatial relationships best suited to capture the structural features within a texture image.

Conners [11] and Conners and Harlow [12] make use of one of the co-occurrence measures to determine the size, shape and orientation of the unit cell or tile which can be repeated to produce a given regular texture. This is an example of using a statistical texture analysis method to extract structural information.

Another approach to texture analysis is the syntactic approach. It is suggested here that the placement rules for primitives (basic elements comprising the texture) can be compared to the production rules of a grammar. Texture classification is then the determination of whether or not a particular texture image exhibits a pattern which belongs to a given language. This model was used by Carlucci [13], Lu and Fu [14], [15], and Zucker [16]. In

7

[16] Zucker defines natural (observable) textures as ideal patterns which have undergone certain transformations.

Primitive extraction is an important part of the structural texture analysis process. However, the definition of "texture primitive" is not unique. Primitives can be, for example, line segments [13], pixels [14], or tiles [12]. In [17], Ehrich and Foith define primitives as gray level peaks. Then the method of relational trees is used to recursively form more complex regions. In [18], Wang, Velasco, Wu, and Rosenfeld compare three threshold based primitive extraction techniques. The primitives found by these methods are then essentially connected regions with gray level values restricted to a certain range (as defined by the threshold). In [19], Maleson, Brown, and Feldman describe a texture analysis scheme whereby the texture image is divided into uniform intensity regions which are then approximated by ellipses. These ellipses are their texture primitives.

Once the primitives are defined and extracted their spatial arrangements must be ascertained. In [19], Maleson, et al. discuss the types of spatial relationships sought between elements of a given class. Elements are thought to be parallel or collinear depending

8

on how their major axes align. In [20], Matsuyama, Saburi, and Nagao use regularity vectors and their respective sets of element pairs to characterize commonly occurring inter-primitive spatial relations within the texture. In [21], Davis presents a scheme for computing the underlying grid relations for rectangular cellular textures.

In this thesis methods will be presented for:

1) generating structural descriptions for natural textures;

2) extracting and describing textural primitives; and,

3) describing inter-primitive spatial relations within the texture pattern.

1.3 Overview

The main algorithms presented in this thesis are outlined in Fig. 1-2. The texture description process begins by creating edge and direction images for the texture image. Fig. 1-1 provides examples of texture images and their corresponding edge images. The bricks and mortar strips are clearly outlined, thus providing primitive size, shape, and arrangement information. Edge repetition arrays (ERAs) are calculated for edge and

TEXTURE IMAGE → EDGE DETECTION → EDGE & DIRECTION IMAGES → ERA CALCULATION → SIZE & SPACING ERAs → INTERPRETATION ROUTINE → TEXTURE DESCRIPTION

(a) Describing Natural Textures

TEXTURE IMAGE →
EDGE IMAGE →
DIRECTION IMAGE →
TEXTURE DESCRIPTION → PRIMITIVE EXTRACTION ROUTINE → PRIMITIVE DESCRIPTIONS / PRIMITIVE MASKS
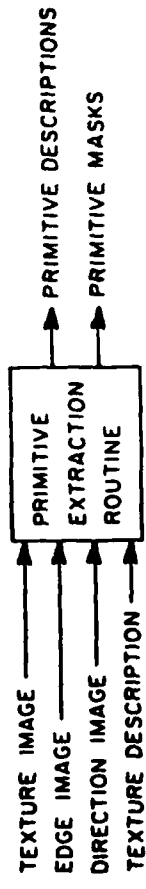
(b) Extracting Texture Primitives

PRIMITIVE MASKS → AVERAGE PRIMITIVE TEMPLATE CALCULATION → PLACEMENT RULE & PRIMITIVE TEMPLATES → PLACEMENT RULES / PRIMITIVE TEMPLATES → GRID RELATION EXTRACTION → GRID RELATIONS → TEXTURE RECONSTRUCTION ALGORITHM → TEXTURE RECONSTRUCTION
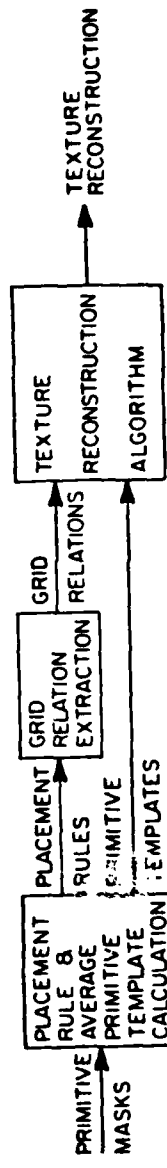
(c) Analyzing Interprimitive Spatial Relations

Figure 1.2. Structural Texture Analysis Processes

direction image pairs. An ERA entry is the normalized frequency of occurrence of specific types of edge matches occurring with a specified angle and distance separation within the texture image. Every picture element (pixel) within the image is examined in turn. Starting at a given pixel the image is scanned in 6 directions for a user specified range of distances. When a pair of edges with directions perpendicular to the line of scan are encountered the matrix entry noting the particular type of match and spatial relationship is updated.

There are 2 types of matches sought. The first type of match involves edges which define the opposite sides of textural elements, e.g., opposite sides of the same brick in Fig. 1-1(b). In this case the distance at which the match occurred would be the dimension of the element in that scan direction. The second type of match involves the corresponding edges of 2 neighboring elements, e.g., the left edge of 2 neighboring bricks which occur in the same row in Fig. 1-1(b). In this case the distance at which the match occurred would be the period of repetition of the texture elements in the given scan direction. After the ERAs are calculated an interpretation routine generates a texture description. This routine analyzes peaks and their repetitions in the element size and spacing ERAs. The description generation process is

11

outlined in Fig. 1-2(a).

The texture primitive extraction process uses the
internal form of the texture description as its starting
point. The information contained in the texture
description is element size and spacing information for
relatively dark and light texture elements found in 5 scan
directions. Using the relative intensity, size, and scan
direction for each of the given elements their exact
locations can be found within the original texture image.
This is done by rescanning in the particular direction in
which the element was found. However, the scan is now
only for elements exhibiting a particular relative
intensity and size.

When all of the locations for the element are found
they are marked and expanded in a blank primitive mask
image. A region extractor is then used to examine the
primitives one by one to determine some average
characteristics of the element type under consideration.
Further analysis is done to determine if there is more
than one primitive mask referring to the same primitive
type, or if one mask refers to more than one primitive
type. In these cases the element masks are merged or
separated, respectively. The end product of the primitive
extraction process is a set of primitive masks and

descriptions.   (See Fig. 1-2(b).)

Determination of inter-primitive placement rules is an important part of the structural texture analysis process. The primitive masks created by the primitive extraction process are the inputs to this algorithm.

The centroid of each individual primitive is computed.   Then 12 directional scans are initiated from each centroid location in each primitive mask.   That is, if (i,j) is the location of the centroid of a primitive of type A, and there are primitives of type A, B, and C then 12 directional scans are started from location (i,j) in primitive masks A, B, and C.   The scans are continued until a second primitive is found or the boundary of the mask image is reached.   When another primitive is encountered the angle and distance between the 2 primitive centroids is noted and the frequency of that particular placement rule is increased by 1. The placement rule frequencies are then normalized and the rules with the highest rate of occurrence are kept.

If the texture being considered is homogeneous and regular then a minimum set of rules necessary to characterize the underlying grid pattern is extracted. This reduced set of rules along with a set of average texture primitives is used to create a reconstructed

13

texture image. A visual comparison can then be made to determine how closely the grid relations chosen capture the spatial relations of the original texture image. The spatial relation analysis scheme is shown in Fig. 1-2(c).

1.4 Organization

The organization of this thesis will be discussed below. It should be noted that most of the texture samples displayed and analyzed in this thesis are taken from a photographic album of texture images compiled by Brodatz [22].

In Chapter 2 a method for automatically generating texture image descriptions is presented. First, the edge repetition array (ERA) and its precursor, the gray level co-occurrence matrix, are both discussed in detail. ERA results are then displayed and interpreted for a number of natural textures. (The information inherent in these arrays is period and element size information in pixels for a number of specific scan directions.) The technique used to automate the interpretation process is next described, and some automatically generated descriptive results are presented.

In Chapter 3 a method for automatically extracting and describing textural elements is presented. First, an

"intelligent" primitive search which uses the one-dimensional textural information extracted by the algorithm described in Chapter 2 is explained in detail. Results of this search are in the form of individual and composite primitive image masks. Masks automatically generated for a number of natural textures are presented and discussed. The primitive analysis technique is explained and the primitive descriptions for several texture images are examined.

In Chapter 4 a method for automatically determining inter-primitive placement rules is presented. The role of individual primitive masks in the rule extraction process is explained in detail. Sets of placement rules for several periodic textures are examined. A technique for extracting minimum sets of rules for completely characterizing homogeneous, regular textures is examined. Then a texture reconstruction process using this set of rules, primitive templates, and primitive descriptions is described. Reconstruction results for a number of periodic textures are displayed for comparison with the original texture image.

The texture analysis techniques presented in Chapters 2, 3, and 4 can be used for more than texture description generation. In Chapter 5 two texture analysis

applications are discussed. A scheme for texture
recognition (for 11 texture classes) is presented. Both
texture and primitive descriptions are used in the
decision process. Results for 11 natural textures are
examined. A second application is the determination of
surface orientation from texture. A surface orientation
analysis algorithm is outlined. It uses methods suggested
by Bajcsy [5] and Stevens [23], as well as the texture
analysis techniques developed in this thesis. Preliminary
results for a number of texture images exhibiting non-zero
texture gradients are discussed.

In the final chapter a summary of results is given
along with a discussion of the possible extensions of this
work. Areas for further research in natural texture
analysis are discussed.

CHAPTER 2

AUTOMATIC GENERATION OF DESCRIPTIONS FOR
NATURAL TEXTURE IMAGES

2.1 Introduction

In this chapter a technique is presented for automatically generating descriptions of natural textures. These descriptions will include information pertaining to the period of repetition within the texture, the size of textural elements, and the direc'ionality of the texture. Although this information will not completely characterize the texture under consideration it gives a strong indication of the nature of the texture and provides valuable cues for further analysis. In particular, the descriptions generated by the algorithm presented in this chapter will be used as the starting point of the primitive extraction algorithm to be described in Chapter 3.

2.2 Some Approaches to Texture Feature Extraction

A natural statistical approach to texture analysis is via spatial frequency analysis. A two dimensional Fourier transform of an image would be expected to reveal

17

periodicity within the texture field as well as directional information. Bajcsy [5] developed a technique for extracting such information from the power spectrum of the discrete Fourier transform, i.e., from the magnitude of its complex results. By studying annular sections of the power spectrum, directional information could be detected. A flat annular function would indicate a non-directional texture, while peaks in this section indicate directionality. In the case of a non-directional texture, peaks in power spectrum wedges would indicate the presence of blob-like structures within the texture field [6]. This technique has been successfully used on images containing various types of natural texture regions.

There are some difficulties in working with the Fourier transform of an image. In natural scenes, where even regular or periodic textures are not very exact, the power spectrum results are quite diffuse. Also, the results can be misleading since a single strong edge within the image may have the effect of indicating textural directionality. An example of a set of natural textures and their respective 2-D Fourier transform magnitude is given in Fig. 2-1.

An approach aimed at defining a set of meaningful texture features to be extracted from natural texture

18
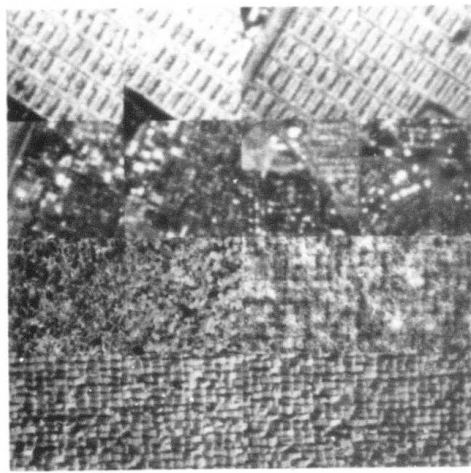
(a) Texture Subwindows (Aerial City, Grass, Sand, Wool, Raffia)
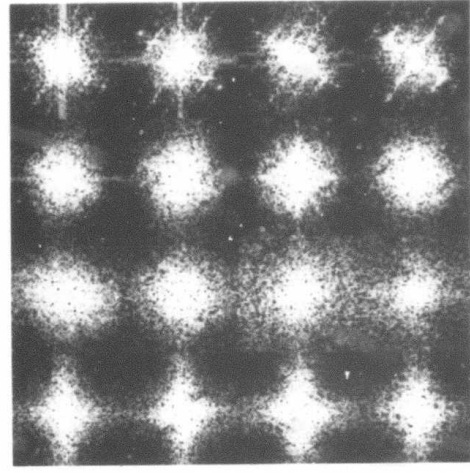
(b) Fourier Transforms of subwindows in (a)
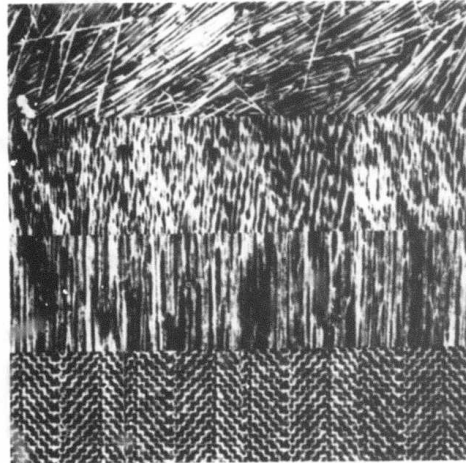
(c) Brodatz Texture Sub-windows (Straw, Water, Wood, Herringbone)
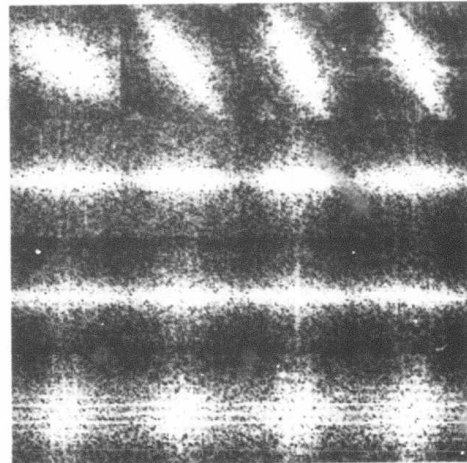
(d) Fourier Transfors of subwindows in (c)

Figure 2-1.   Texture Mosaics and their Corresponding Fourier Transforms (from [36]).

images was presented by Tamura, Mori, and Yamawaki in [25]. They approximated six textural features, namely, coarseness, contrast, directionality, line-likeness, regularity, and roughness, and compared them with psychological measurement taken for human subjects. They found that 3 of these features correlated well with human subject response. These were the coarseness, contrast and directionality measures. The other three features showed some correspondence, but it was explained that further work with these features would be required. A possible problem with this technique is the subjectivity of human textural interpretation. A different group of subjects might have produced completely different texture measurement results.

Due to the Julesz hypothesis [1] that human texture discrimination depends on second-order statistics, much attention has been given to the spatial gray level dependence matrix, or co-occurrence matrix technique proposed by Haralick, Shanmugam, and Dinstein [7].

The co-occurrence matrix, $P_{\theta,d}(i,j)$, is an approximation to the joint probability density function defining the probability of a pixel with intensity level i being separated by angle, θ, and distance, d, from a pixel whose intensity level is j, where θ is measured with

respect to the horizontal. It was not suggested that the matrix elements themselves would serve as textural features; but that certain measures defined on them would. For example,

$$f_{ENT}(\theta,d) = \sum_{i=0}^{N_g-1} \sum_{j=0}^{N_g-1} P_{\theta,d}(i,j) \log(P_{\theta,d}(i,j)),$$

where N_g is the number of distinct gray levels within the quantized image, is an entropy measure on the elements of $P_{\theta,d}(i,j)$. In [7] twenty-eight texture features are suggested for use in texture image classification schemes. (These are the mean and range for 14 co-occurrence measures.) Image classification results are discussed for 3 separate groups of natural terrain and sand-stone images. Different sets of features were used to classify images from the 3 groups to produce results ranging between 82.3 and 89 percent correct classification.

Further endorsement of the spatial gray level dependence method (SGLDM) came from two separate studies. An experimental study [26] by Weszka, Dyer, and Rosenfeld and a theoretical comparison [27] by Conners and Harlow. In both studies the SGLDM was compared to 3 other methods the gray level difference method, the gray level run length method, and the power spectrum method. In each

21

case, the SGLDM was determined to be the most powerful algorithm of the four.

In [11] Conners uses the inertia measure to determine unit cell size within the texture image. The inertia measures is defined as follows,

$$f_{INT}(\theta,d) = \sum_{i=0}^{N_g-1} \sum_{j=0}^{N_g-1} (i-j)^2 P_{\theta,d}(i,j) \quad ,$$

where N_g is the number of gray levels within the quantized image.

In [11] it is explained that this measure reaches a minimum when the two unit patterns match best in the mean square sense, that is, when the square of the intensity differences is minimized. Therefore, analysis of plots of inertia measures over varying distances for a variety of angles should produce information about the tile size in regular texture images.

One drawback in using this method is its computational complexity. For each angle and distance to be examined there is an N_g x N_g matrix to be calculated. It is not uncommon to have 8 bits per pixel, requiring each matrix to have 256 x 256 entries. (It should be noted that calculations are usually carried out for no

more than 16 quantized gray levels.) Also, in order for meaningful statistics to be calculated a reasonably large texture region should be used.

In [8] Price and Nevatia used the co-occurrence matrix technique not on the image itself but on an edge image corresponding to the original texture image. In such an edge image, non-maximal points along rows or columns are set to zero. Hence, an edge is represented by a single line. Since the image being analyzed is made up of essentially binary points, noting the presence or absence of an edge, co-occurrence analysis would be quite simple computationally. It remained to determine whether meaningful texture features could be extracted from a texture edge image. This is the subject of the following section (2.3).

2.3 Using Edge Repetition Arrays for Structural Feature Extraction

An ERA is like a co-occurrence matrix on the edge and direction images corresponding to a gray level image. Basically, a match occurs when there are two edges with the proper directions and relative locations.

Figure 1-1(b) is the edge image mosaic corresponding to the brick image mosaic in Fig. 1-1(a). These edge

images retain the basic structural definition of their corresponding gray level images. Bricks and mortar strips are clearly outlined, thus providing not only primitive size and shape information, but primitive arrangement information as well. Another example of a gray level image with its corresponding edge image is the raffia (woven palm) texture sample given in Fig. 2-2. The primitives comprising this natural texture are not as uniform as the brick primitives of the image in Fig. 1-1(a). This is reflected in its corresponding edge image. These edge images (Figs. 1-1(b) and 2-2(b)) have been thinned by non-maximal suppression to produce edges composed of single lines.

All of the edge images used in this thesis have been produced by using the set of 5 x 5 convolution masks [28] shown in Fig. 2-3. Each of these masks or operators is applied on every 5 x 5 window within the gray level image to produce a magnitude and a direction (1 of 12). The magnitude chosen for a window is the highest magnitude in absolute value over the six convolution results. The direction is determined by the mask producing the maximum result, and the sign of this result as well. In Fig. 2-4(a) the 12 directions are shown. In each case, the higher intensity or lighter pixels are to the right of the vector when facing in the vector's direction, see

24
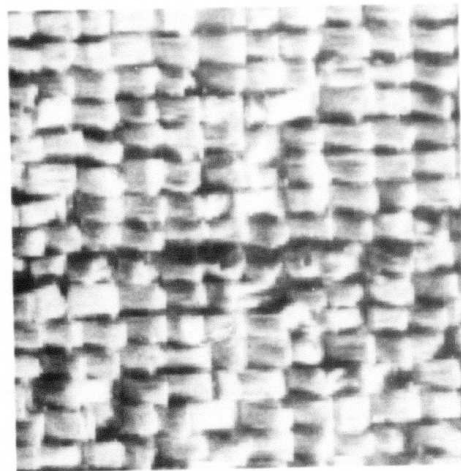
(a) Raffia (Woven Palm) Texture Image

(b) Non-Maximal Suppressed Edges from (a)

Figure 2-2. Raffia and Edges.

```
-100 -100    0   100  100              -100    32  100  100  100

-100 -100    0   100  100              -100   -78   92  100  100

-100 -100    0   100  100              -100  -100    0  100  100

-100 -100    0   100  100              -100  -100  -92   78  100

-100 -100    0   100  100              -100  -100 -100  -32  100

         (a)  0°                               (b)  30°


 100  100  100  100  100               100   100  100  100  100

 -32   78  100  100  100               100   100  100  100  100

-100  -92    0   92  100                 0     0    0    0    0

-100 -100 -100  -78   32              -100  -100 -100 -100 -100

-100 -100 -100 -100 -100              -100  -100 -100 -100 -100

         (c)  60°                               (d)  90°


 100  100  100  100  100               100   100  100   32 -100

 100  100  100   78  -32               100   100   92  -78 -100

 100   92    0  -92 -100               100   100    0 -100 -100

  32  -78 -100 -100 -100               100    78  -92 -100 -100

-100 -100 -100 -100 -100               100   -32 -100 -100 -100

         (e)  120°                              (f)  150°
```

Figure 2-3.   Covolution Masks.

26
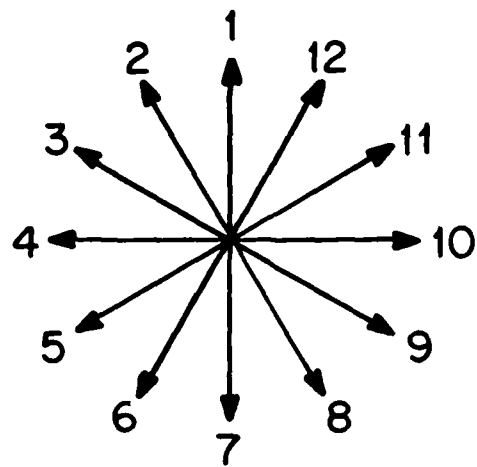
(a) 12 Edge Directions
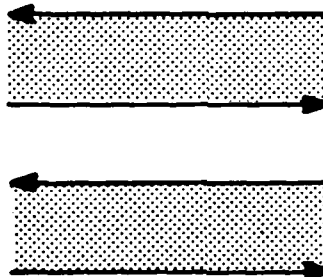
(b) Horizontal Edges
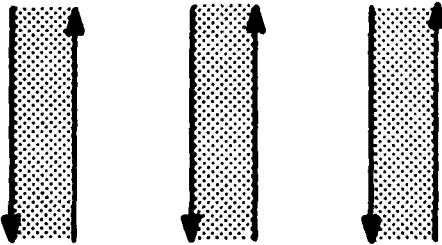
(c) Vertical Edges

Figure 2-4.   Edge Directions as Determined
              by Edge Operators of Fig. 2-3.

27

Figs. 2-4(b) and (c). In this way each pixel in the original gray level image is replaced by an edge magnitude and direction. After the edges have been thinned the edge and direction information is ready for analysis.

Consider the top left edge image in Fig. 1-1(b). If one examines a vertical strip of pixels from the center of the line of bricks a pattern could be established. Edges separate short (length 2) strips of zeros corresponding to the mortar interiors from long (length 12) strips of zeros representing the brick interiors. If this happens often enough in the image then it can be said that 2 types of texture primitives have been found. One has vertical dimension 2 and the other has vertical dimension 12. A period of repetition can also be established from this sequence of pixel values. It is the number of pixels from the beginning of one string of 12 zeros to the beginning of the next similar string. Hence, a one-dimensional scan through the edge image can uncover meaningful structural information. ERAs are computed by considering edge placements in pixel strips extending in 6 directions from every pixel in the edge image.

It might seem at first that suppressed edges alone would provide enough information to easily extract the interesting textural features. However, when scanning in

28

a certain direction, e.g. horizontal, and a like direction (horizontal) edge is encountered, there will be a match at every distance smaller than or equal to the length of the edge. While edge lengths may be a meaningful measure it is not necessarily helpful in determining period and element size within the image. It was therefore decided that the edge directions would be used to determine which kinds of edge matches to consider. In particular, only edges whose directions are perpendicular to the direction of scan are considered potential matching edges.

Both element size and spacing (or period) information for a given direction is produced by each directional scan. This information is in the form of peaks at element size and spacing values and their repetitions. A natural next objective is to separate the information for these features so that the correct interpretation of these matrices can be expedited.

Some simple observations can be made by studying Fig. 2-4(b) and (c). Element spacing or period is the distance between like oriented edges while oppositely oriented edges form element boundaries. Therefore, the distances at which like oriented edges match measures element spacing in that direction, while the distances at

29

which oppositely oriented edges match measures the size of texture primitives in the given direction. Further, it can be determined whether the sizes and spacings refer to dark or light intensity objects. For examples, in Fig. 2-4(c) a dark object which has vertical edges will be bounded on the left by a down-pointing edge and on the right by an up-pointing edge; and the opposite can be said of light objects with vertical edges. Therefore, the intensity of the element under consideration can also be discovered by using edge and direction information.

2.3.1 Algorithm Details

Some of the details of the ERA method as used in this thesis follow. The inputs to this algorithm are the edge and direction images corresponding to the original texture image, as well as a range of distances over which to scan.

Edge matches are considered only for pairs of edges whose directions are perpendicular to the direction of scan. Therefore, the set of scan directions is determined by the set of possible edge directions. The scan directions used are 0°, 30°, 60°, 90°, 120°, and 150° taken clockwise from the horizontal, see Fig. 2-5(a). The set of edge directions are given in Fig. 2-4(a). If more accuracy is needed the number of edge directions (and scan directions) could be increased. However, along with these

30
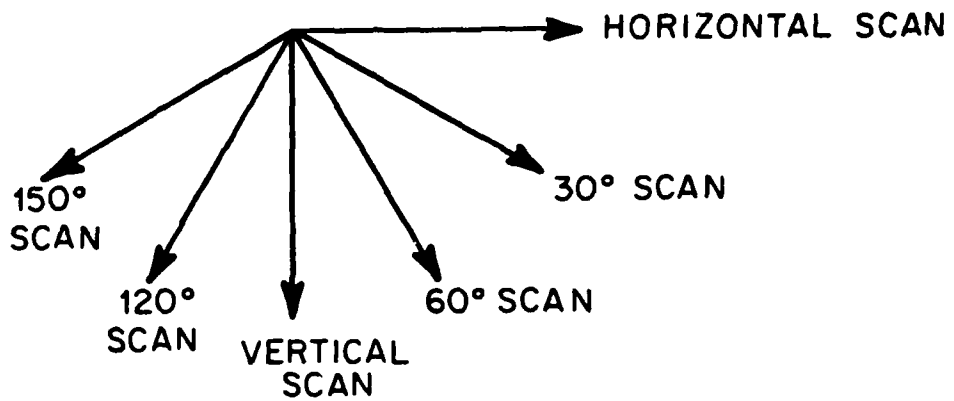
(a) Edge Repetition Array Scan Directions
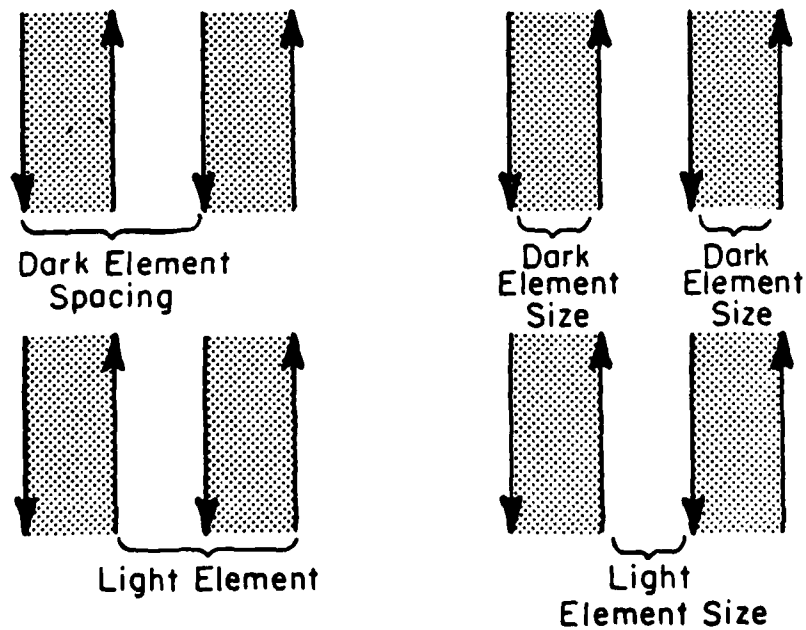
(b) Types of Matches for Horizontal Scan

Figure 2-5. ERA Scan Directions and Types of Horizontal Edge Matches

31

increases there would be a proportional increase in the amount of time and space needed for the execution of this algorithm.

Separate matrices are calculated for spacings and sizes of both dark and light intensity elements. For example, when scanning horizontally the following four types of matches are sought at each distance within the user specified range:

1. Matching pairs of vertical down-pointing edges, which indicate element spacing for dark objects;

2. A down-pointing vertical edge followed by an up-pointing vertical edge, which indicate element size for dark objects;

3. Matching pairs of vertical up-pointing edges, which indicate element spacing for light objects; and,

4. An up-pointing vertical edge followed by a down-pointing vertical edge, which indicate element size for light objects. (See Fig. 2-5(b)).

Information for twenty-four separate graphs is generated for each texture image. However, there are only 4 values for each (angle, distance) pair. Each ERA entry is the number of matches of a particular type, for example

two like up-pointing vertical edges, occurring at a given angle and distance. This number is then normalized by the number of matches added to the number of times only one of the two desired edges occurred in the proper location. It is then multiplied by 100.0 to form a percentage. It tells what percent of the time a match occurred given that at least one of the edges appeared in the proper place.

The entries are not normalized by the number of possible locations within the image in which the given angle and distance relationship is satisfied because this would cause the values of the entries to depend on the size of the objects or periods being measured. In Fig. 2-6, the effects of these two normalization schemes are illustrated. NORM1 is the total number of locations where a match can occur. NORM2 is the number of locations where at least one of the two matching edges occurs in the correct location. In each case all of the edge points were present for the given period size. However, NORM1 causes the entry value to decrease as the period size increases while NORM2 allows the entry value to remain constant. Each ERA entry is of the form:

$$100 \text{ x } \frac{\text{Number of matches at distance d}}{\text{Normalization count for d}}$$

where d is within the user specified range.

Distance = 2
$\theta = 0°$ $\dfrac{\#\text{Matches}}{\text{NORM 1}} = \dfrac{8}{15} = .53$ $\dfrac{\#\text{Matches}}{\text{NORM 2}} = \dfrac{8}{8} = 1.0$

Distance = 4
$\theta = 0°$ $\dfrac{\#\text{Matches}}{\text{NORM 1}} = \dfrac{4}{13} = .31$ $\dfrac{\#\text{Matches}}{\text{NORM 2}} = \dfrac{4}{4} = 1.0$

Distance = 8
$\theta = 0°$ $\dfrac{\#\text{Matches}}{\text{NORM 1}} = \dfrac{2}{9} = .22$ $\dfrac{\#\text{Matches}}{\text{NORM 2}} = \dfrac{2}{2} = 1.0$
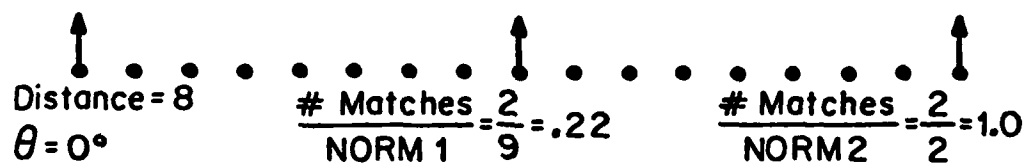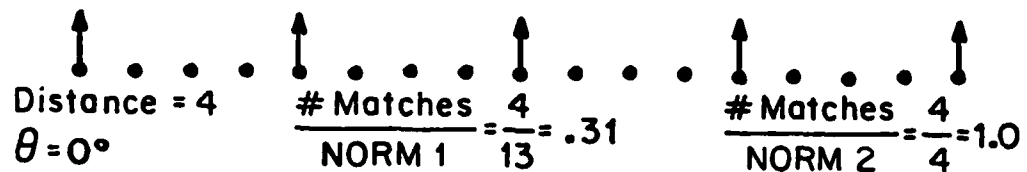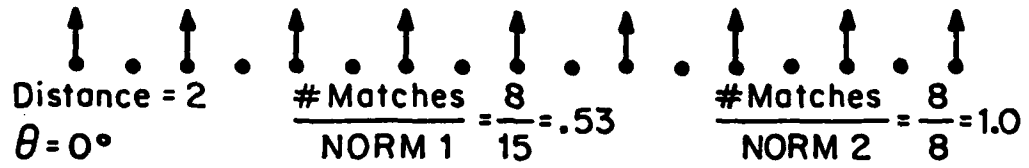
Figure 2-6.   Comparison of 2 Normalization Schemes.
(Actual ERA Entries are then Multiplied
by 100.0.)

34

The order of this algorithm is DP, where D is the number of distances to be examined at each angle and P, is the number of pixels in the image. The average CPU time needed to calculate a set of ERAs for a 128 x 128 pixel image at 31 distances is 1.5 minutes (on a DEC KL-10 processor). For purposes of comparison it is noted that six 5 x 5 masks can be convolved with a 128 x 128 pixel image to produce edge magnitudes and directions for each pixel in 15 CPU seconds.

2.3.2 Some ERA Results

The edge repetition arrays for the raffia texture image in Fig. 2-2(a) are given in Fig. 2-7. The element spacing graphs are on the left, the element size graphs are on the right. The broken line graphs are light element ERAs, while the solid line graphs are for dark elements. The two numbers appearing below each graph are the normalization numbers for the smallest distance entries for dark and light elements, respectively. These numbers give a rough idea of the number of edges found in that particular scan direction.

First, consider the actual texture image (Fig. 2-2(a)). Raffia is a natural texture which is periodic in the vertical direction due to the similarity of widths of the pieces of palm used in the weave. It is

35

Element Spacing   Element Size
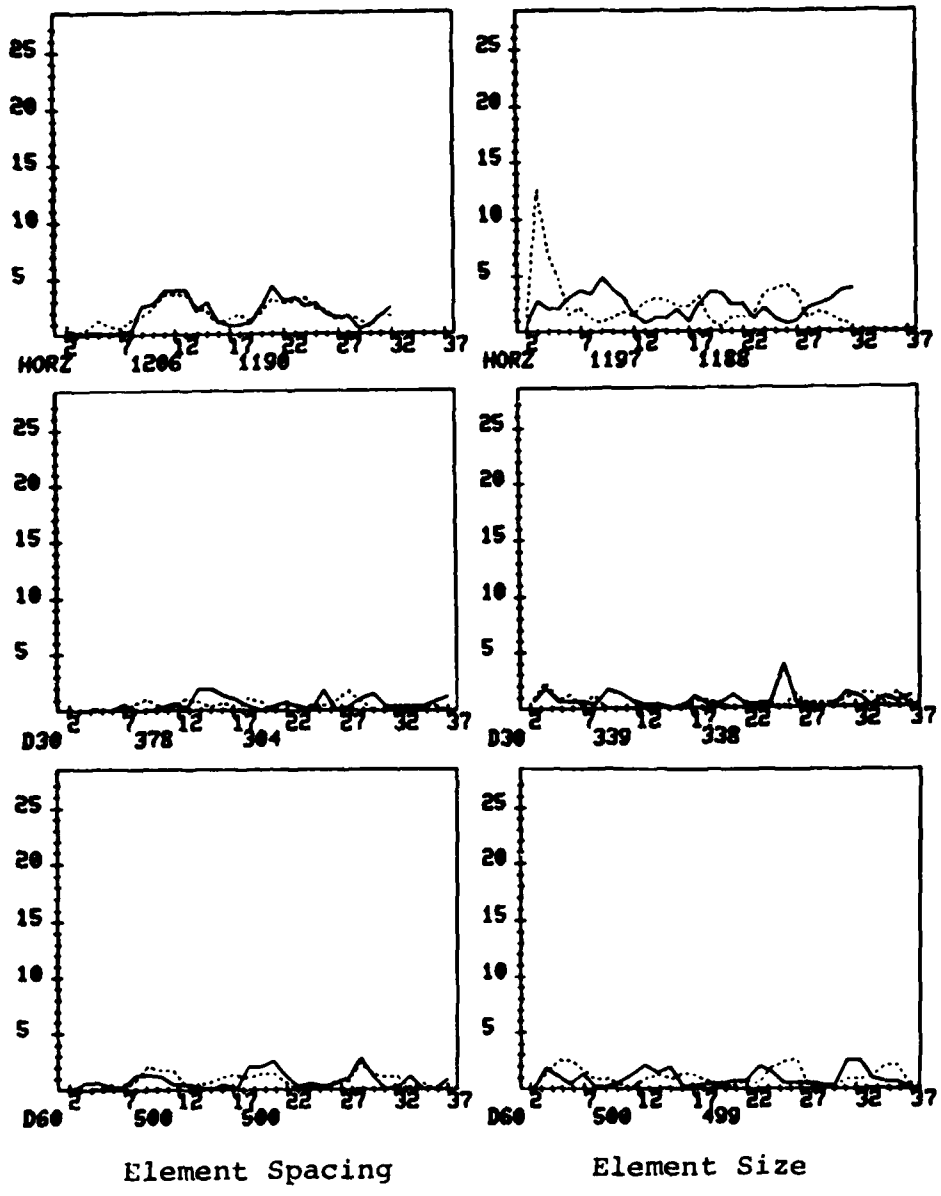
Figure 2-7. Raffia ERA Graphs

36

Element Spacing   Element Size
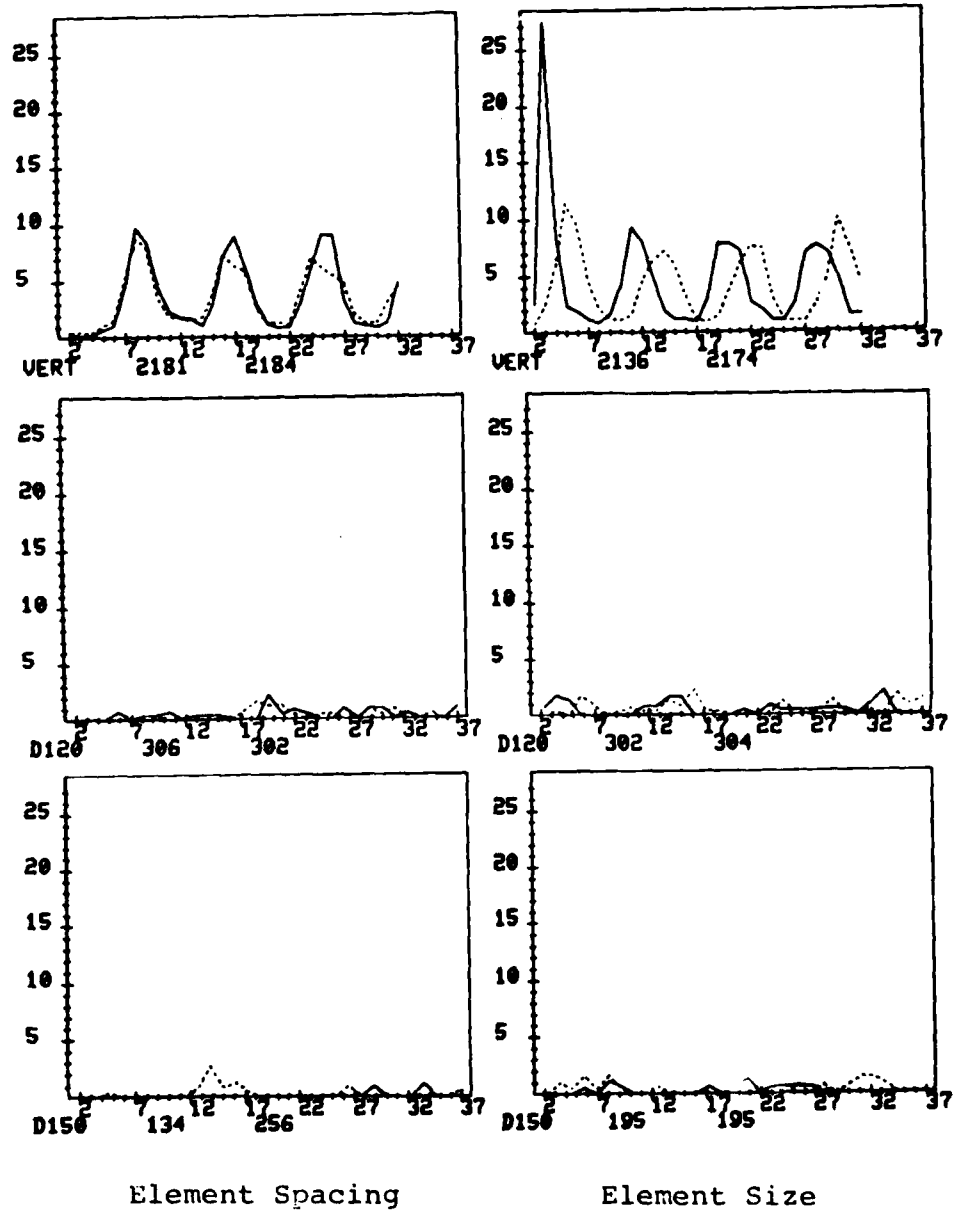
Figure 2-7. Continued

only loosely periodic in the horizontal direction due to the irregularities of the weave. The predominant texture primitives are bright rectangular regions and the dark elongated regions separating them. In some parts of the image a light vertical strip (highlight) separates the large rectangles. This can be considered a third primitive type.

Next, consider the ERA results shown in Fig. 2-7. The most significant results appear in the vertical and horizontal scan directions. The vertical element spacing graphs for both dark and light intensity objects have peaks at multiples of 8, which indicates a vertical period of 8 pixels. Dark objects with vertical dimension 3 are strongly indicated by the high amplitude peak at pixel distance 3 in the solid line element size graph for the vertical scan direction. Likewise, a vertical element size of 5 is strongly indicated for light objects. It should be noted that peaks also occur at intervals of approximately 8 starting from the initial element size peaks for both light and dark objects. This is further indication of the vertical period of 8 pixels.

The most significant peak in the set of horizontal graphs occurs in the light element size graph at pixel distance 3. No obvious peak repetitions occur.

The information one can extract from these graphs agrees well with the structural description of the image, when considering one dimension at a time.

Figure 2-8(a) is a texture image mosaic containing samples of 4 regular textures. Each subimage is 128 x 128 pixels. The corresponding edge image mosaic is given in Fig. 2-8(b). There are 2 aerial images of a section of San Francisco in the top row of the mosaic. In the second row there is a picture of a floor grating on the left, and a piece of herringbone material on the right. Figures 2-9 through 2-12 are the edge repetition arrays for these texture images.

In the leftmost city image the streets line up exactly with the vertical and horizontal scan directions. Therefore, one would expect the strongest ERA results appear in the vertical and horizontal graphs. This is shown in Fig. 2-9. In the horizontal element spacing graphs for both dark and light elements there is strong evidence of a period size of 7 pixels. This is supported in the horizontal element size graphs since peaks in these graphs repeat at intervals of 7. The first element size peaks are at 3 for dark objects and 4 for light objects. These sizes corresponds to the dark vertical strips and the light vertical strips separating them, respectively.
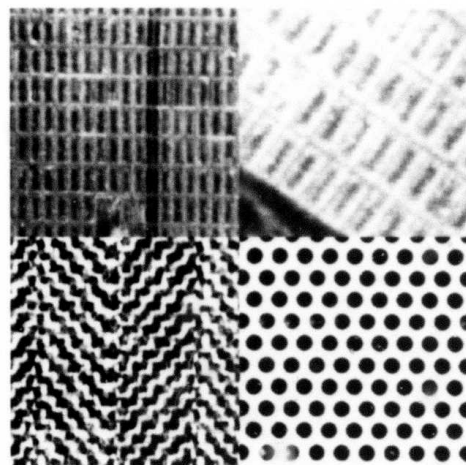
(a) Texture Mosaic Including City1, City2, Herringbone, and Grating Images
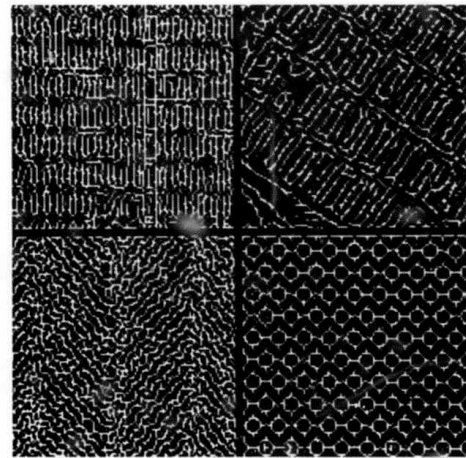
(b) Non-Maximal Suppressed Edges From (a)

Figure 2-8.   Periodic Texture Mosaic and Edges

40

Element Spacing   Element Size

Figure 2-9. City1 ERA Graphs

41

Element Spacing   Element Size
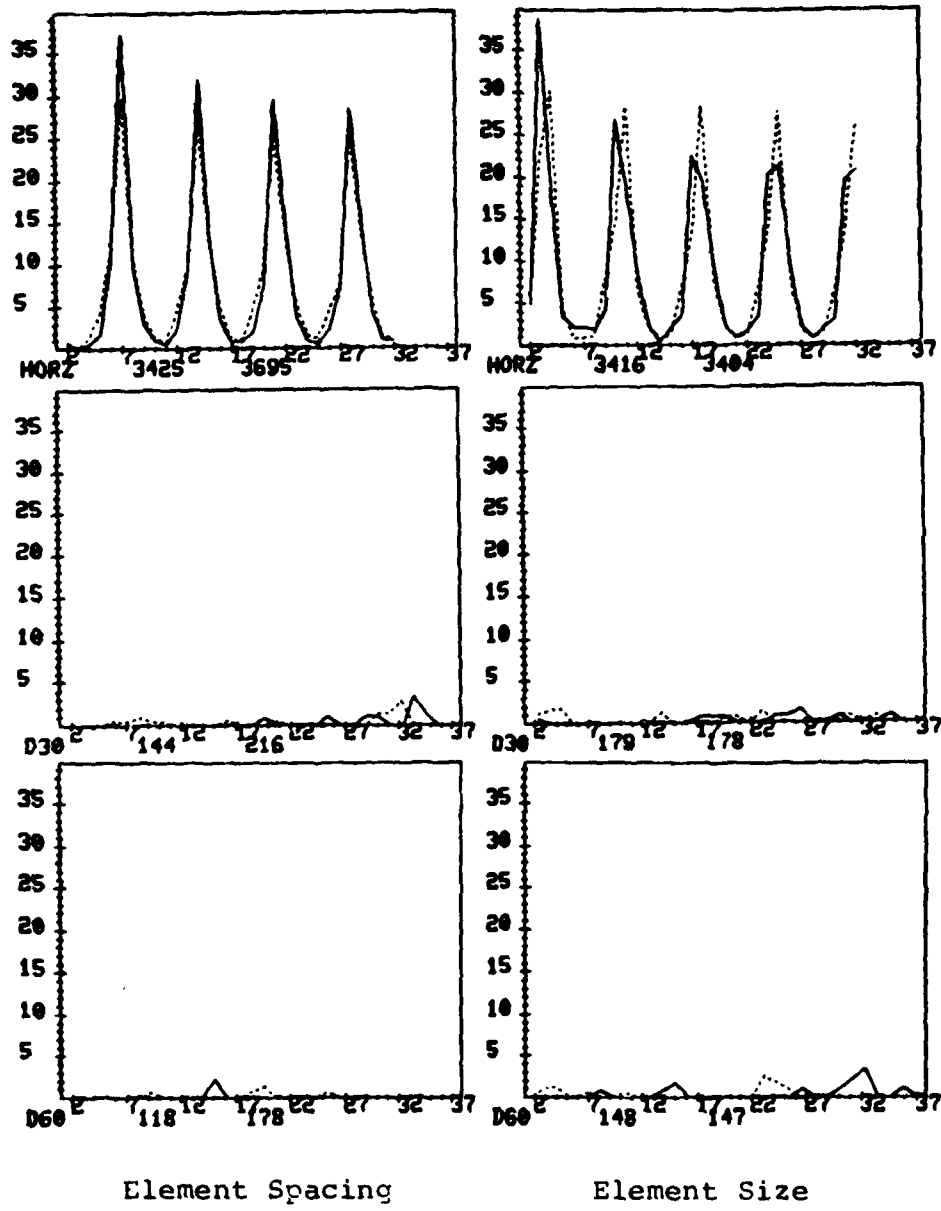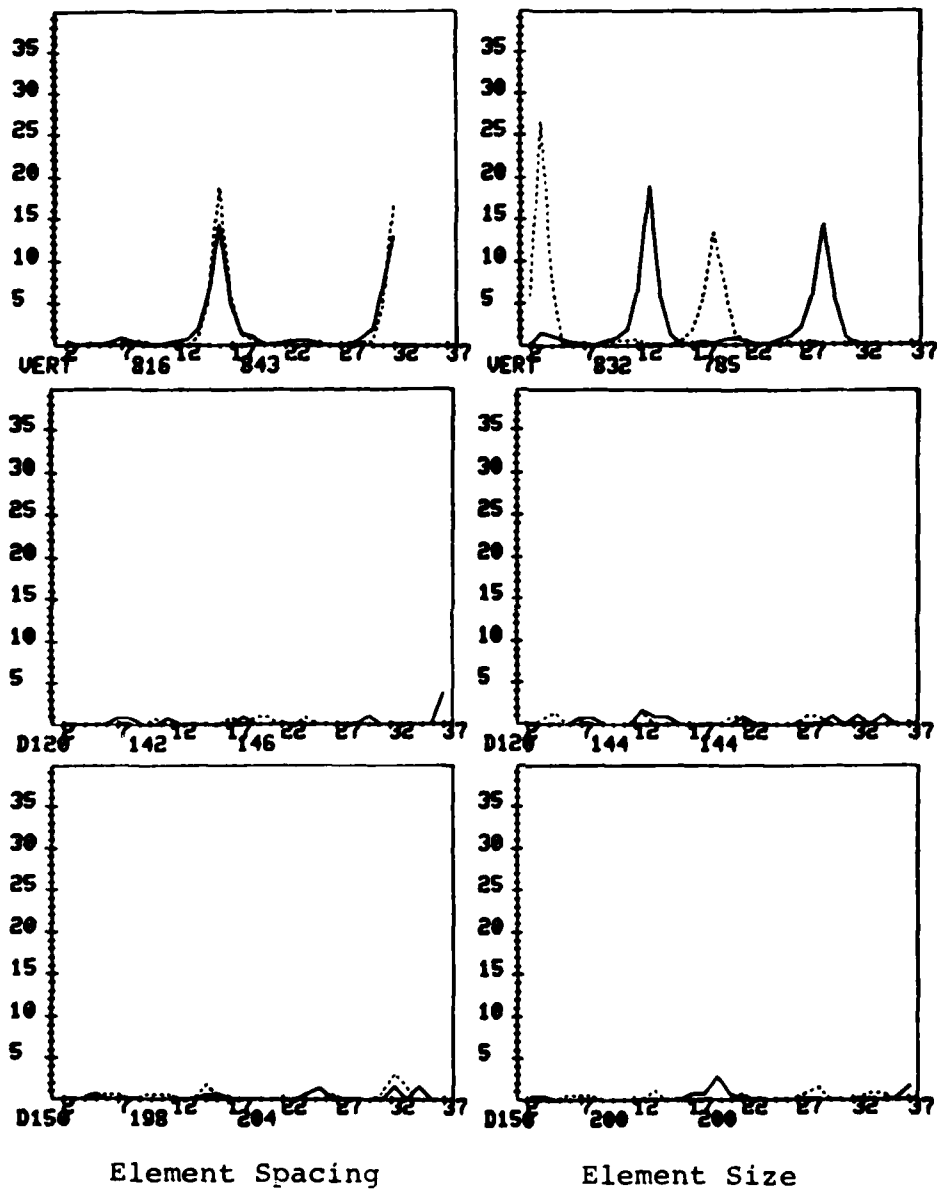
Figure 2-9.   Continued

42

The vertical scan direction ERAs also exhibit signs of periodicity. The period for both dark and light elements is 16 in the vertical direction. The element sizes in this direction are 3 for light objects and 13 for dark objects. It would seem that the same dark strips were found in a second scan direction and that the shorter light regions above and below these dark areas are the light primitives with vertical dimension 3.

The second aerial city picture is a picture of the same general area taken at a different angle and resolution. As expected the strongest results are in the 30 degree scan direction which is the closest scan angle perpendicular to the street direction, see Fig. 2-10(a). The 30 degree scan picks up 2 distinct element sizes per intensity repeating at the same periods. Looking at the image, this would seem to be caused by the fact that there are 3 types of colored strips in each line of city blocks, a black strip beside a dark gray strip, beside a light gray strip. In Fig. 2-10(b) the effect of this phenomenon is examined. As one would expect, one light element period (14), and 3 dark element periods (6, 9, and 15) are found. Also two light element sizes (5 and 10) and two dark element sizes (5 and 10) can be found in this same scan direction. Similar sizes and spacings can be found in the horizontal direction. Due to slight irregularities

43

Element Spacing   Element Size
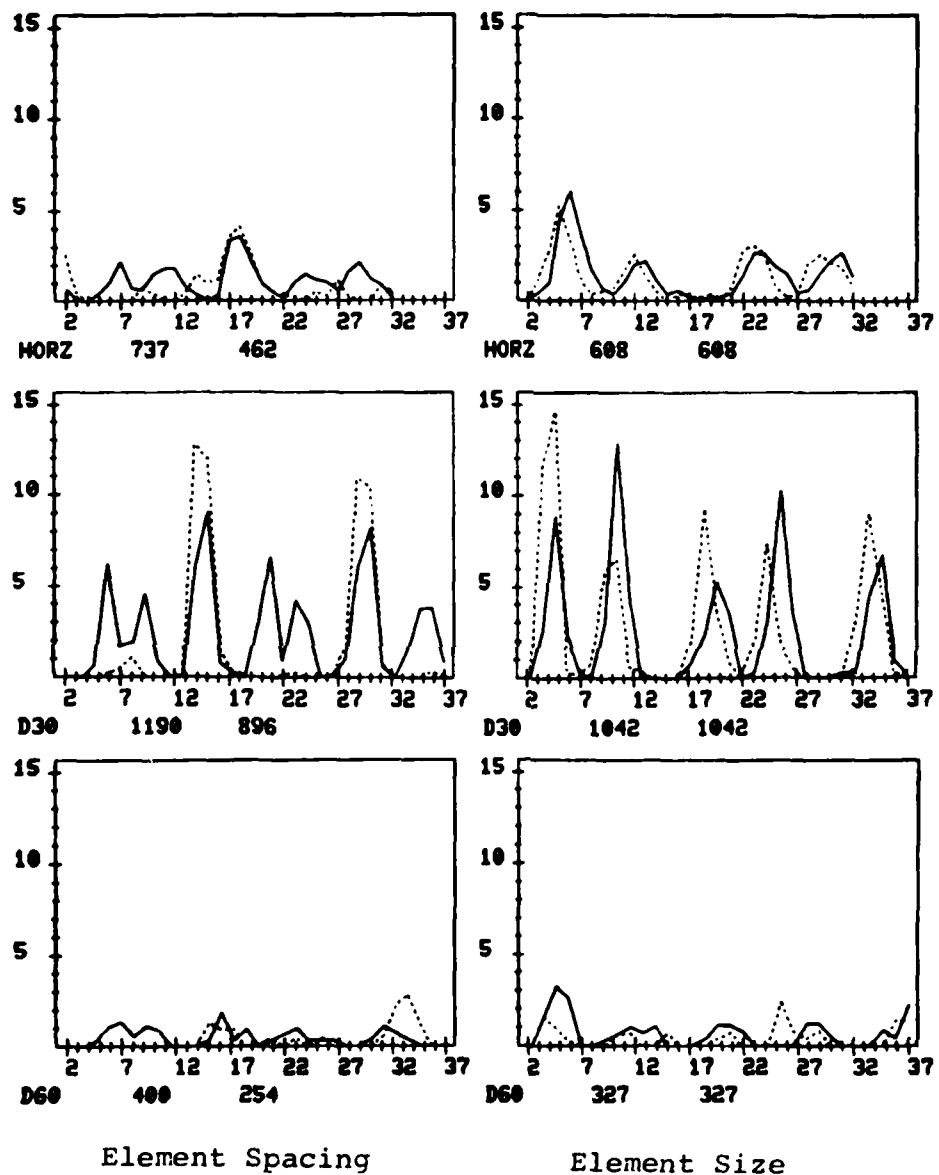
Figure 2-10(a). City2 ERA Graphs

44

Element Spacing   Element Size
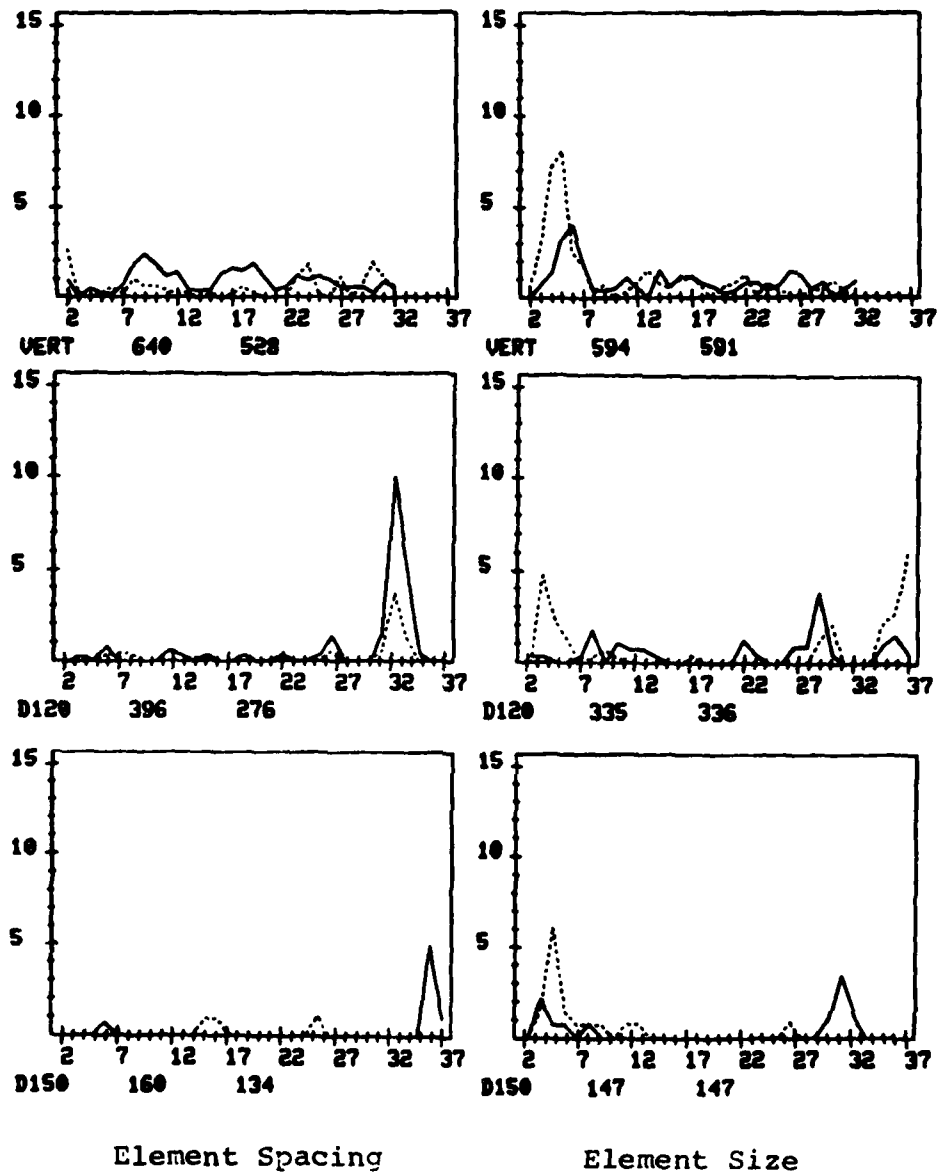
Figure 2-10(a).   Continued

45
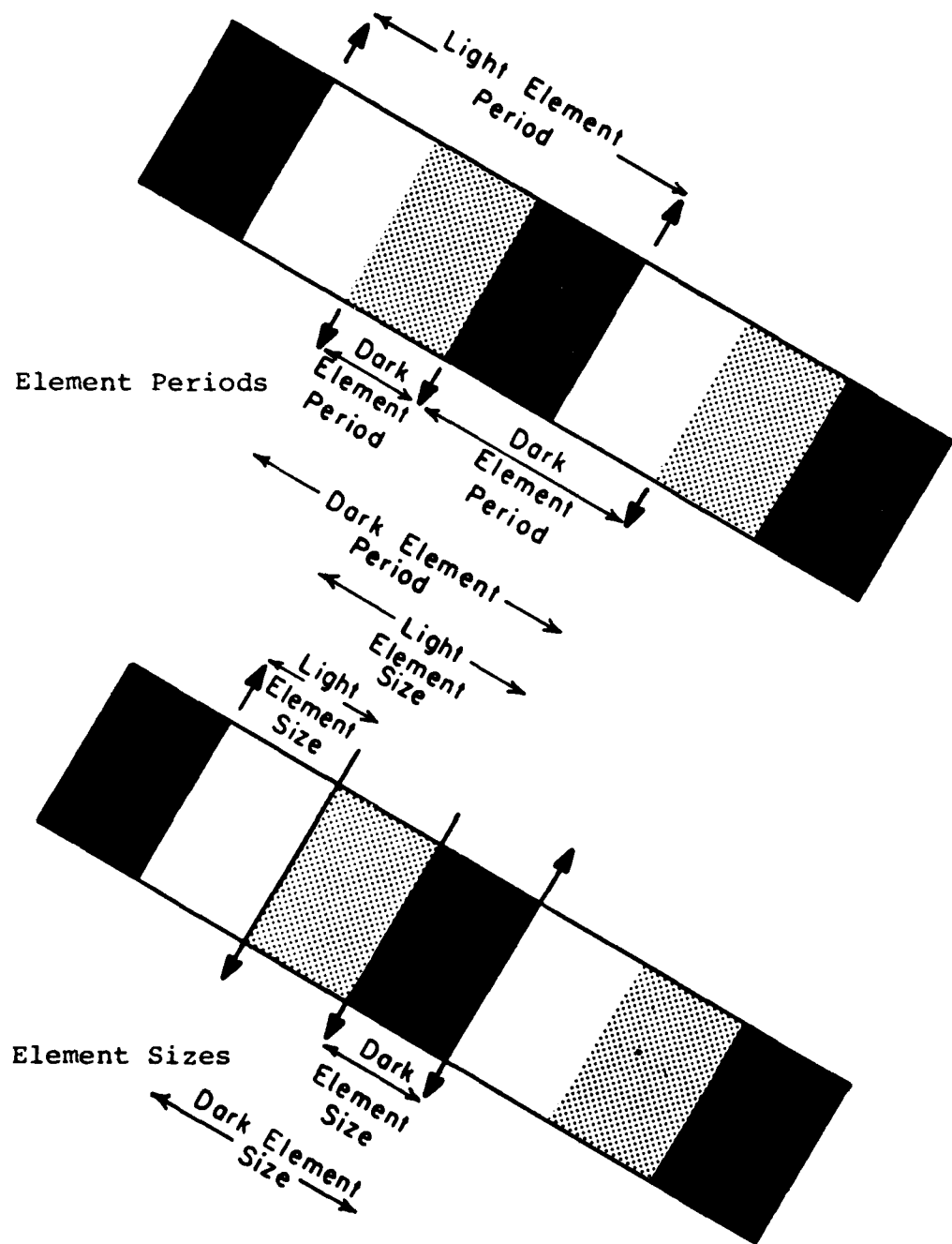
Figure 2-10(b).   Element Periods and Sizes due to 3
Alternating Gray Levels.

46

in the shapes of the primitives some edges were determined to be 90 degrees instead of 120 degrees. This would explain returns in the horizontal scan direction. Element size peaks also occur at other scan directions but no periodic repetitions seem to occur.

Herringbone material is the texture occurring in the lower left section of the texture mosaic of Fig. 2-8(a). At first glance one might be tempted to think that most of the elements had orientation 45 or 135 degrees and so element sizes and periods would be least likely to appear in the vertical and horizontal scan directions. However, a closer look at this texture reveals that the textural primitives are really little rectangular regions chained together. These rectangles, which are actually the threads of which the material is constructed, have most of their edges occurring with direction 0 or 90 degrees. The ERAs with the strongest returns should then be in the vertical and horizontal directions.

In Fig. 2-11(a), we see that both the vertical and horizontal element spacing graphs report strong evidence of periodicity. The periodicity is the same for both dark and light intensity objects. Multiple element sizes are apparent for both dark and light objects. This can be explained by the weave of the material. (See

Element Spacing   Element Size
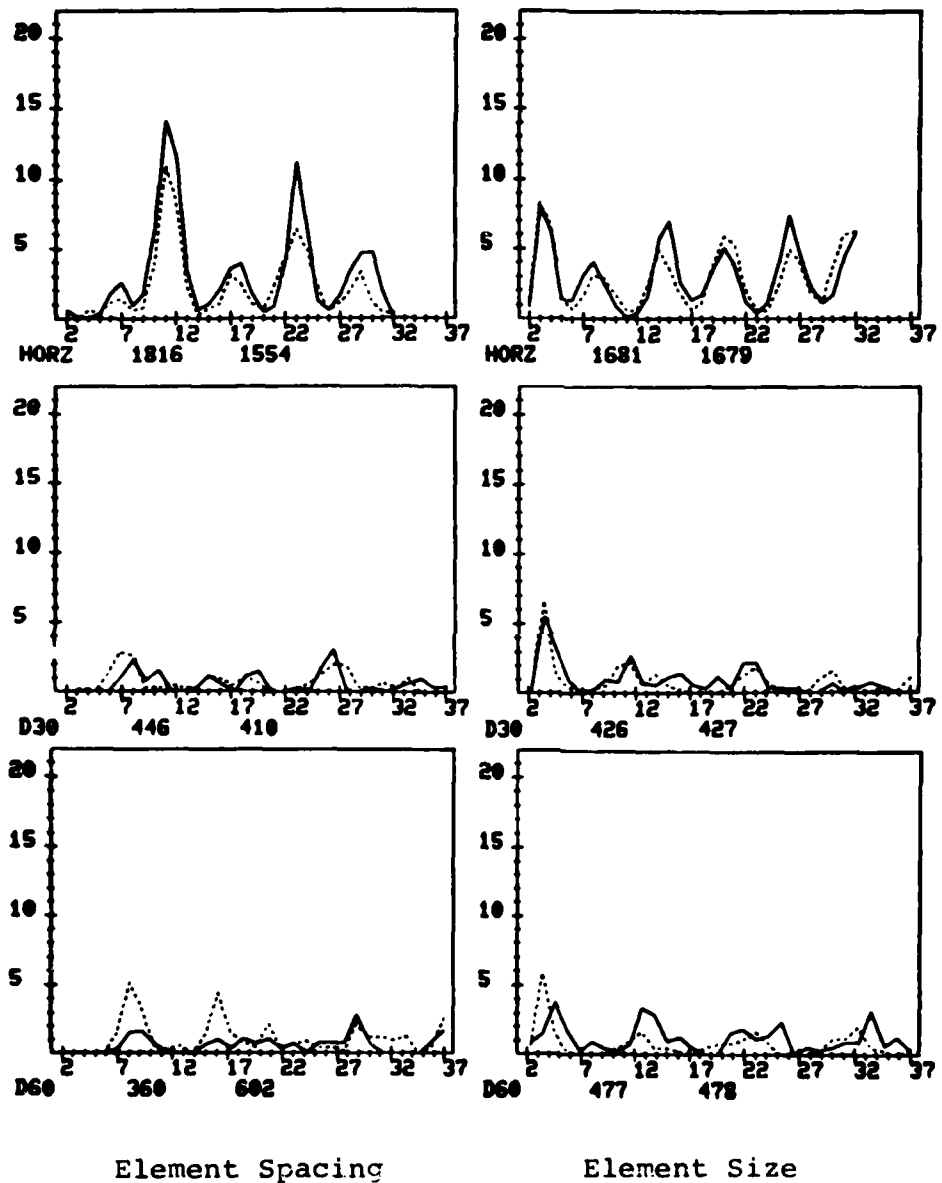
Figure 2-11(a).   Herringbone ERA
Graphs

48

Element Spacing   Element Size
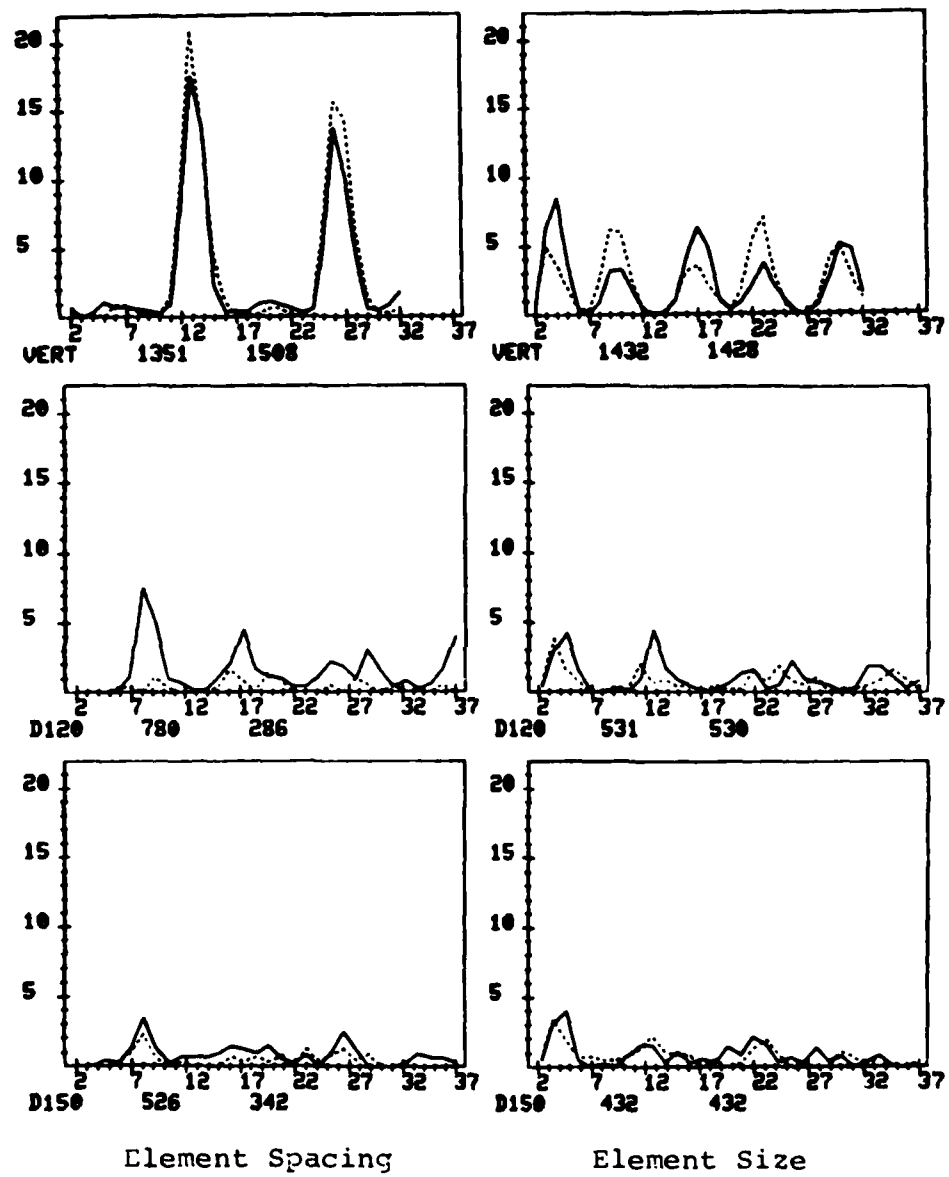
Figure 2-11(a). Continued

49
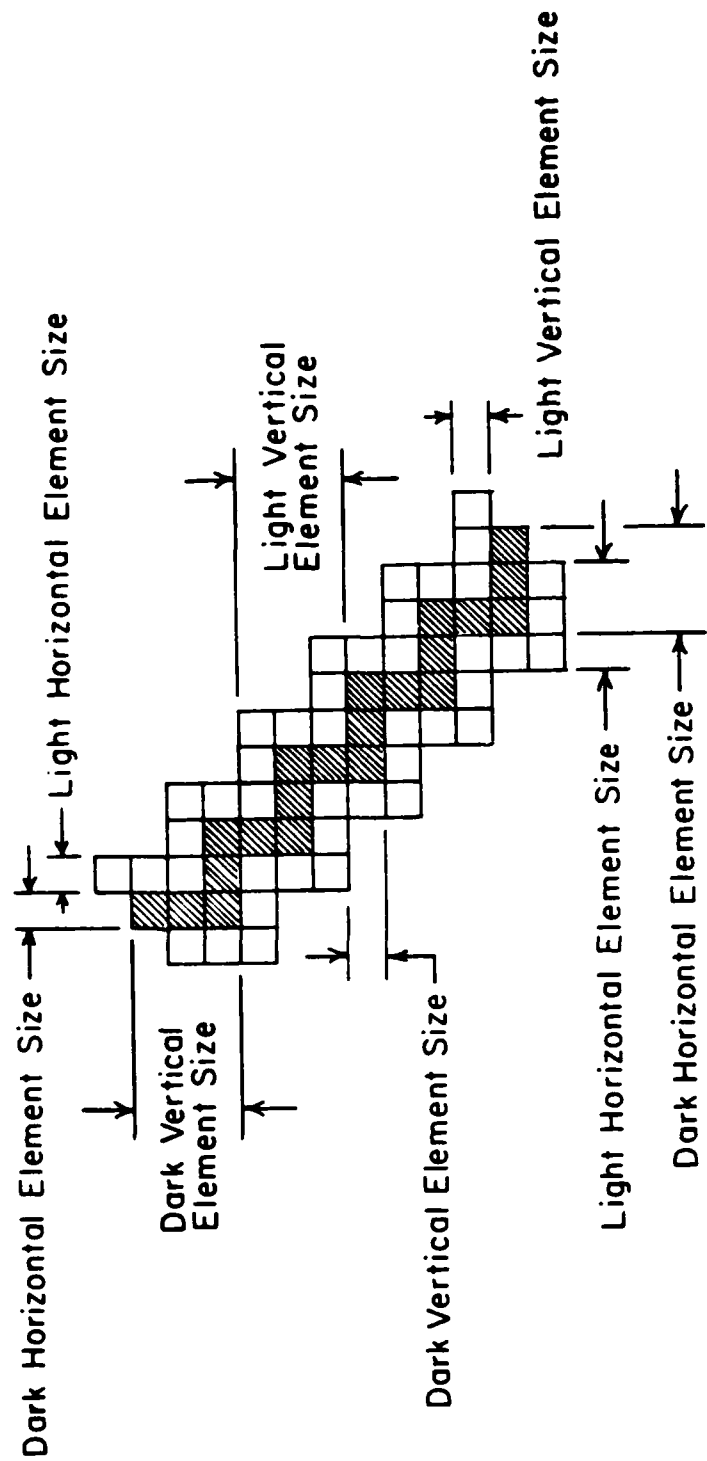
Figure 2-11(b). Herringbone Weave Element Sizes

50

Fig. 2-11(b)). In all of the remaining scan directions some element sizes can be found but there is no strong evidence of repetition.

The final image in this mosaic is the floor grating (black dot) pattern. The ERAs in Fig. 2-12 show that every scan direction produces element size and spacing peaks for both dark and light intensity objects. This is not surprising since the boundary of the black dots must approximate a circle and so each possible edge direction should be represented. The smallest dark element size peak is approximately 8 for all directions, while the smallest light element size peaks vary widely. This can be explained by the black dot diameters being roughly constant while the size of the light region between the dots varies with the scan direction.

In Fig. 2-13(a), there is another natural texture mosaic. The 4 texture subwindows are each 128 x 128 pixels. None of the textures in this image are regular, i.e., periodic. However, in some it seems that a pattern does emerge. The top left texture is a picture of ocean waves; to the right of it is a wood grain texture. In the second row there are 2 pictures of straw, one which is uni-directional, and one which has pieces of straw at several different orientations. Figure 2-13(b) is a

Element Spacing   Element Size
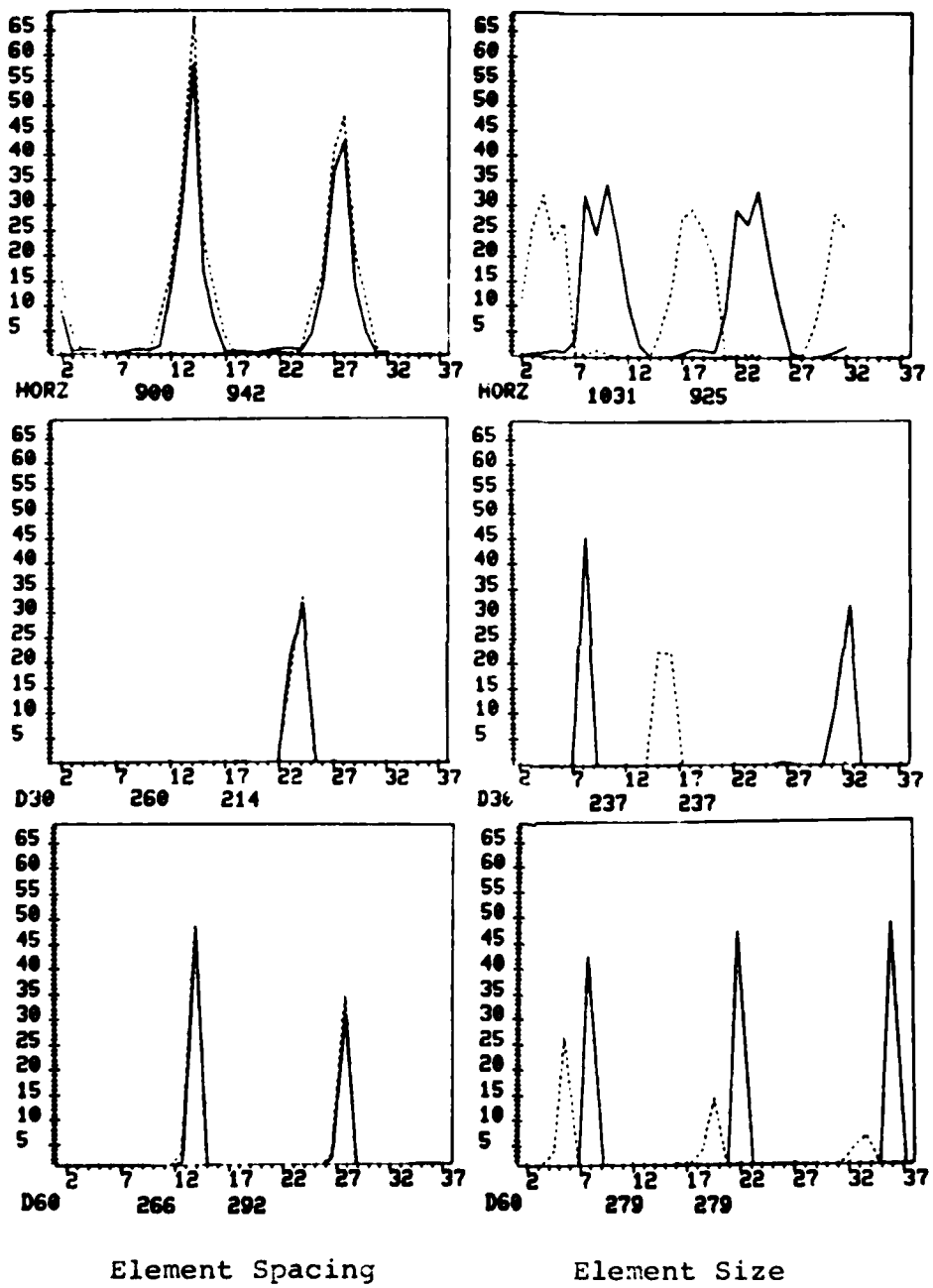
Figure 2-12.   Floor Grating ERA Graphs

52

Element Spacing   Element Size
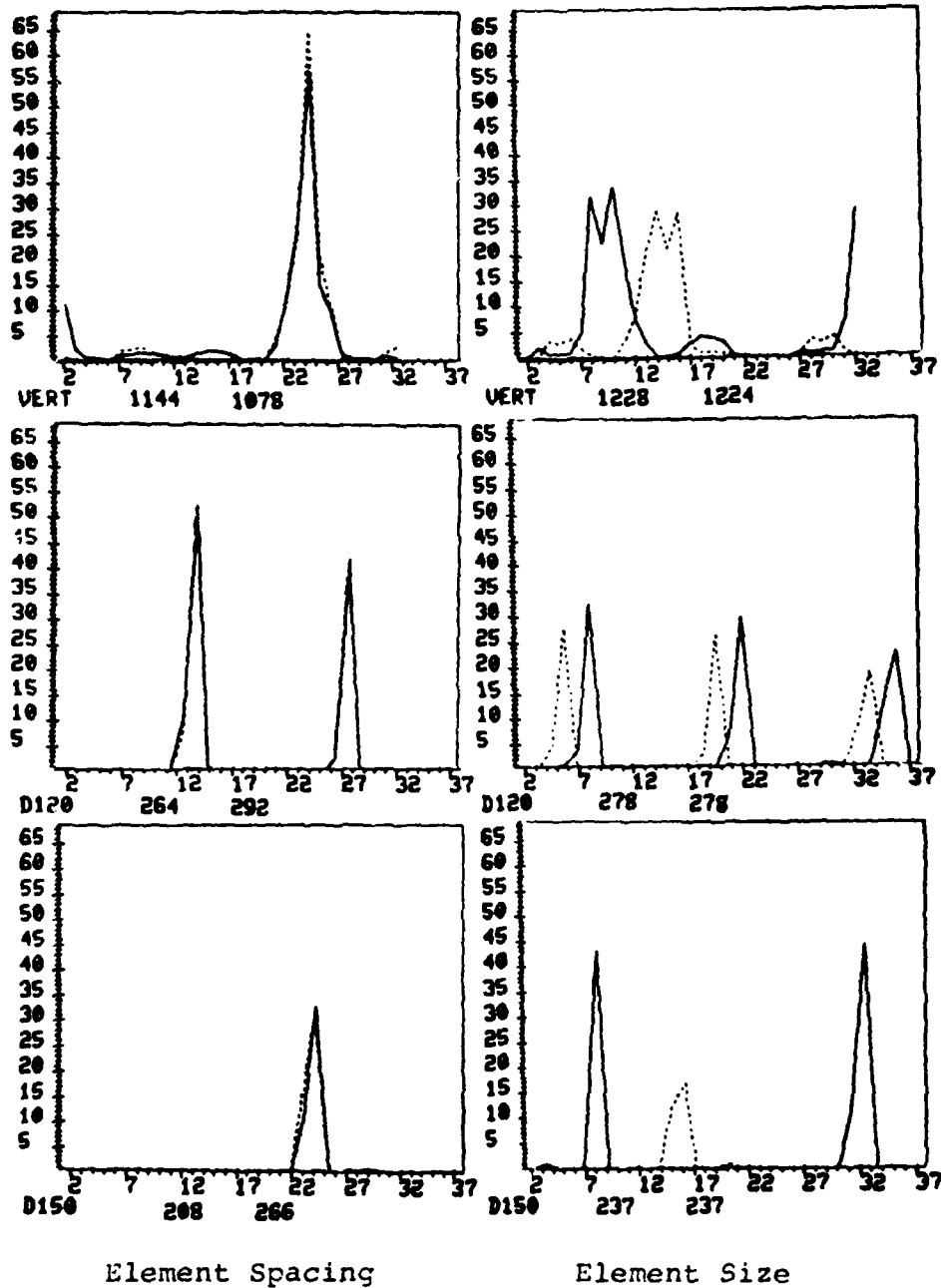
Figure 2-12.   Continued

53

(a) Texture Mosaic Including Water,
Wood, Straw1, and Straw2 Images
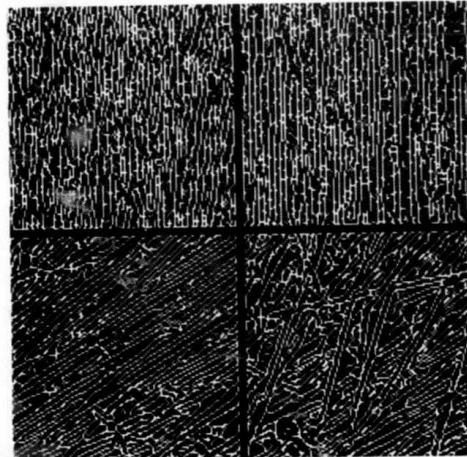
(b) Non-Maximal Suppressed Edges from (a)

Figure 2-13. Non-Periodic Texture Mosaic and Edges

54

mosaic of the edge images corresponding to the texture images in (a).

An observation one might make concerning the two top row images in Fig. 2-13(a) is that they are somewhat similar. The primitives of both are elongated or line-like dark regions, oriented in a vertical direction. One distinguishing feature is the length of these objects (shorter for the water image). Looking at the ERAs for the water (Fig. 2-14) and wood grain (Fig. 2-15) images one can observe their similarity as well. The only ERA graphs showing significant results are the ones in the horizontal scan direction. No period seems to be evident for either water or wood. However, there are strong indications for element size of 3 for dark and light elements in both texture images. Since there are many small elements with vertical edges randomly spaced throughout the image, many element spacing matches and element size repetitions will occur in the horizontal scan direction at all distances giving the graph a high floor value after the initial peak and/or valley. This type of graph should be characteristic of highly directional random patterns, i.e., patterns with a high density of elements oriented in the same direction.

In the bottom row of the texture mosaic

Element Spacing   Element Size
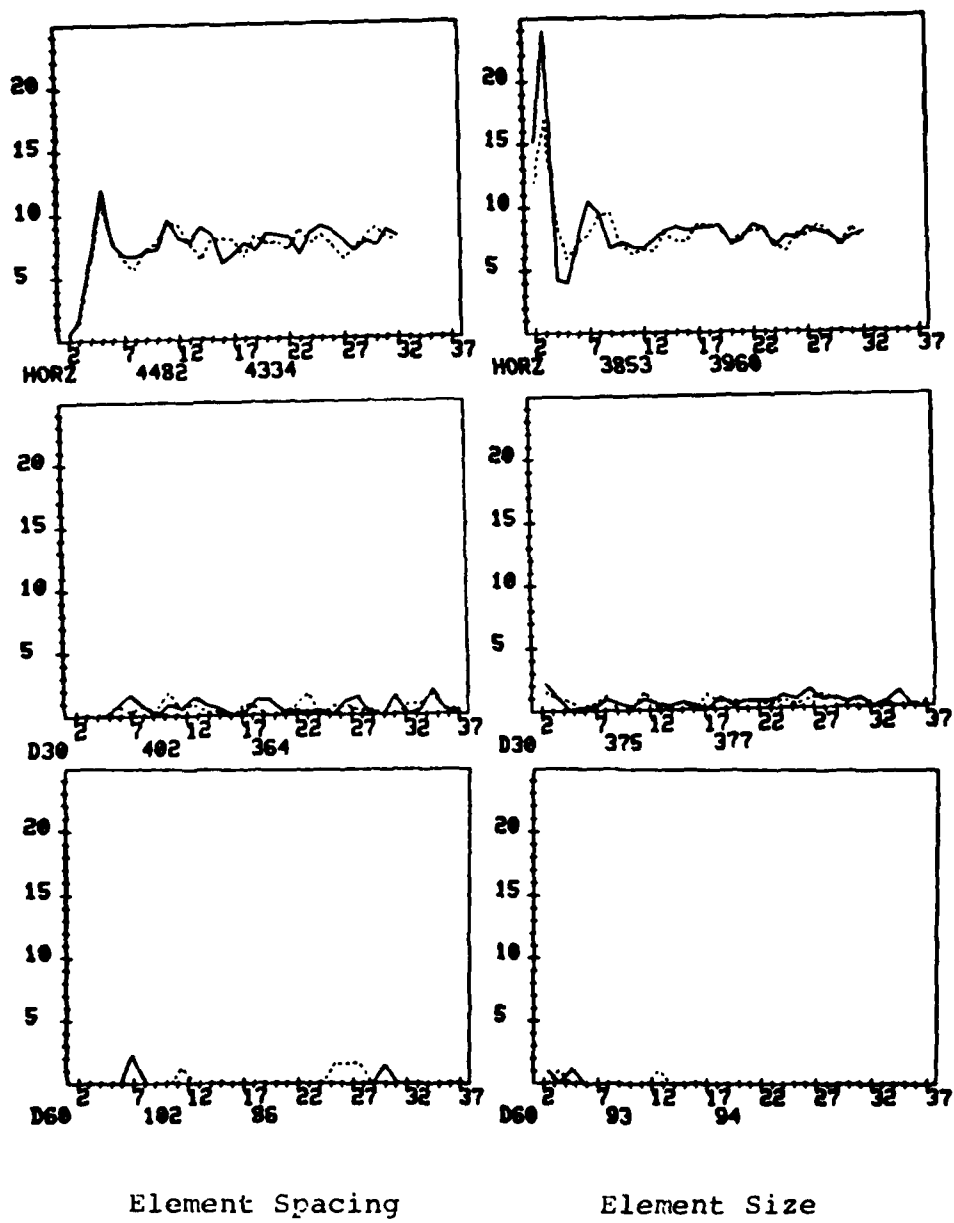
Figure 2-14. Water ERA Graphs

56

Element Spacing   Element Size

Figure 2-14.   Continued

57

Element Spacing   Element Size
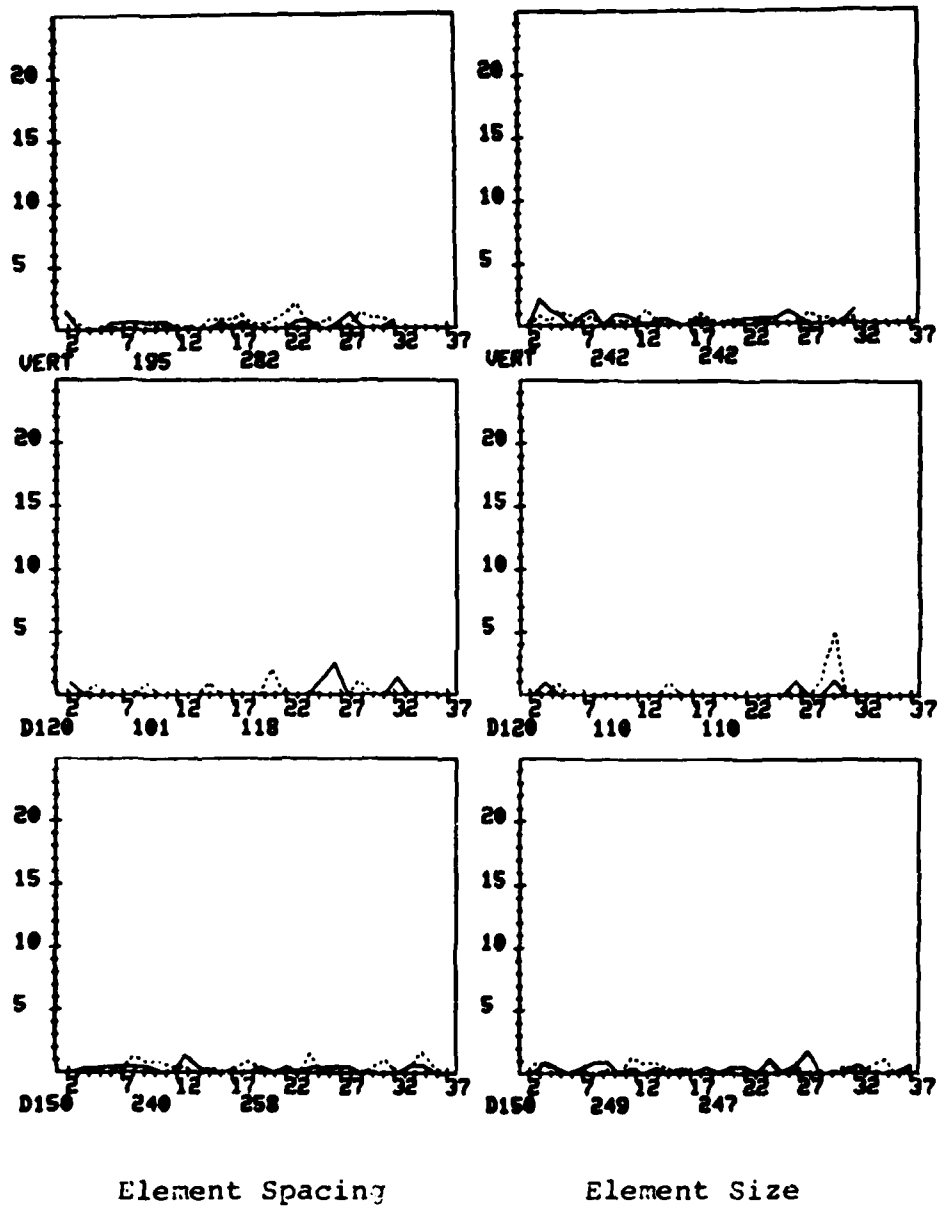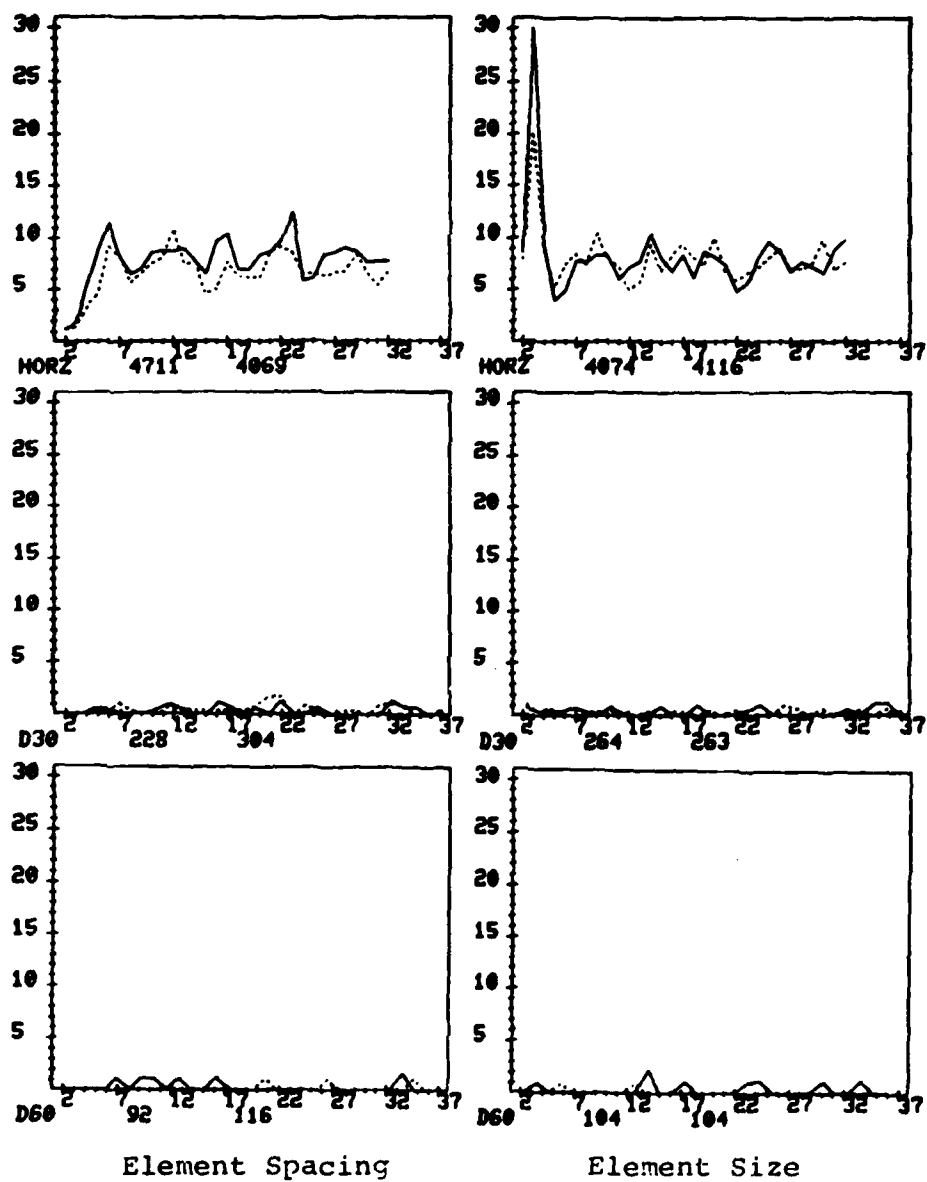
Figure 2-15.   Wood ERA Graphs

58

Element Spacing   Element Size
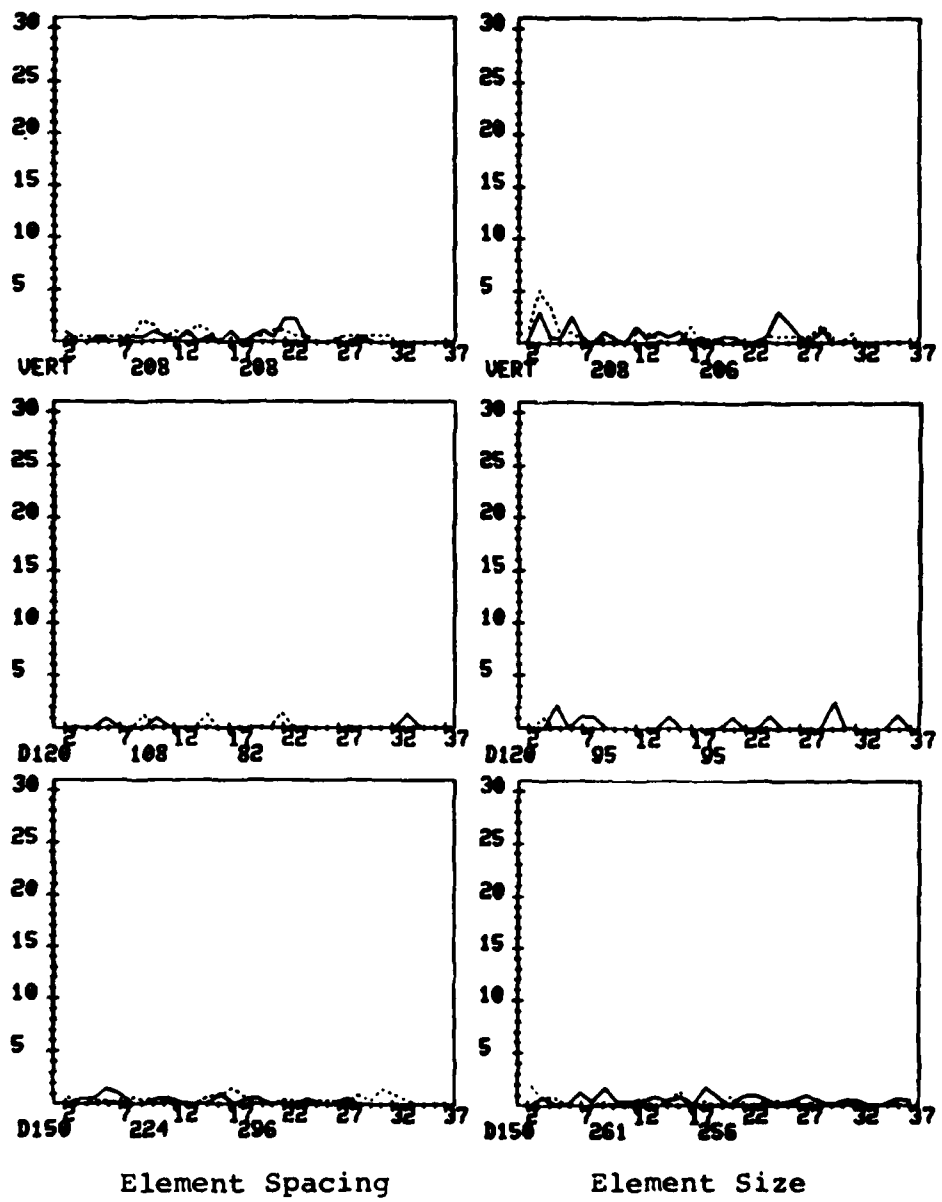
Figure 2-15.   Continued

59

(Fig. 2-13(a)) there are two pictures of straw. As would be expected the strongest results for the first image occur in the 60 degree scan direction (see Fig. 2-16). This is because the individual pieces of straw in the image are oriented at approximately 150 degrees. Some smaller element size peaks also occur in the vertical scan direction graphs. However, a comparison of the normalization numbers for both directions would indicate that many more edge matches occurred at 60 degrees. In the second straw image there are pieces of straw at various orientations within the image causing high element size peaks to occur in a number (4) of the scan direction graphs, (see Fig. 2-17). These straw images are not considered to be regular texture images, even though there is weak evidence of a period in the 60 degree scan direction graphs for the first straw image. This evidence is not nearly as convincing as the evidence found in the vertical scan direction graphs for the raffia image (Fig. 2-7).

The element size for dark and light elements in both straw images is from 2 to 3 pixels for all scan directions where element size peaks occur.

In Fig. 2-18(a), there is a third texture image mosaic. This mosaic contains four 128 x 128 pixel

Element Spacing   Element Size

Figure 2-16.   Strawl ERA Graphs

61

Element Spacing   Element Size

Figure 2-16. Continued

Element Spacing　　　　Element Size
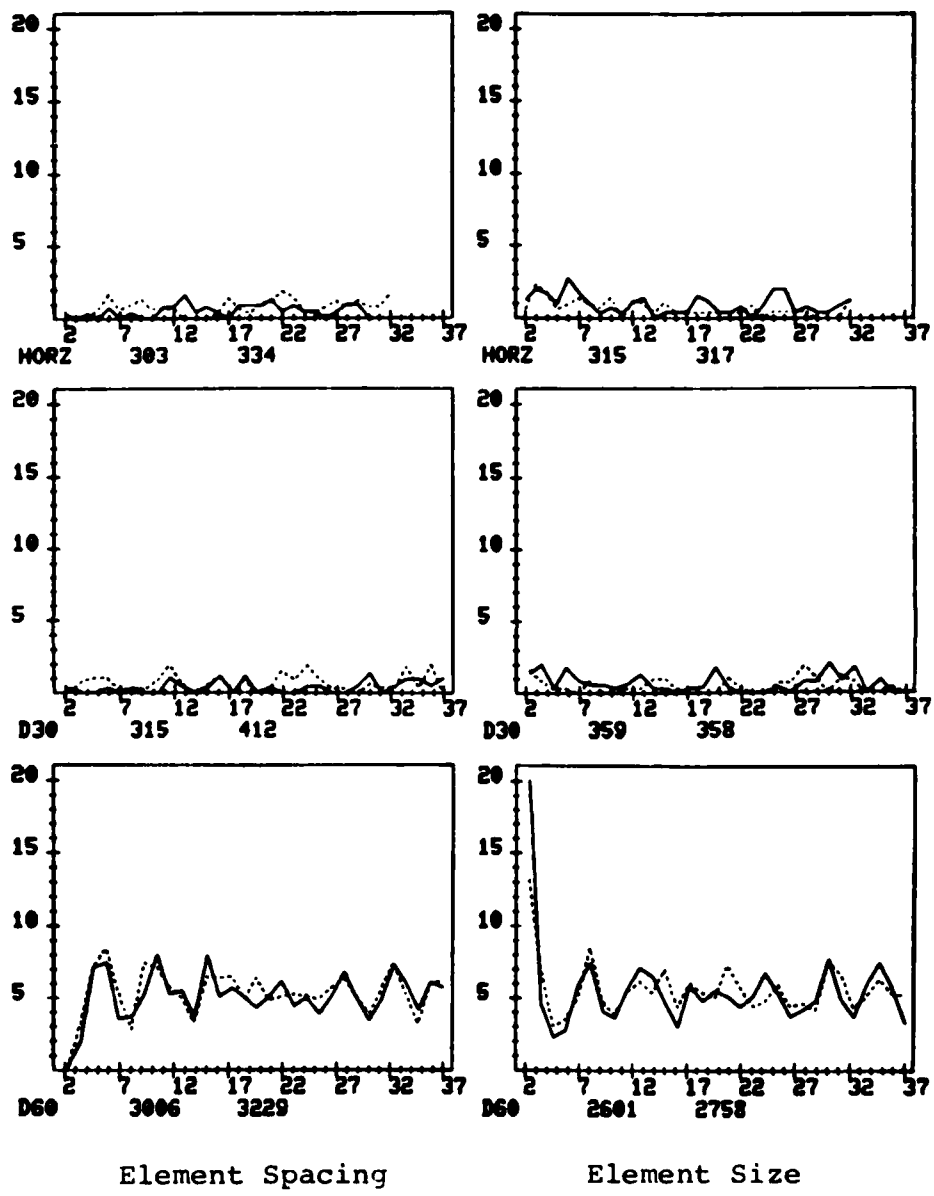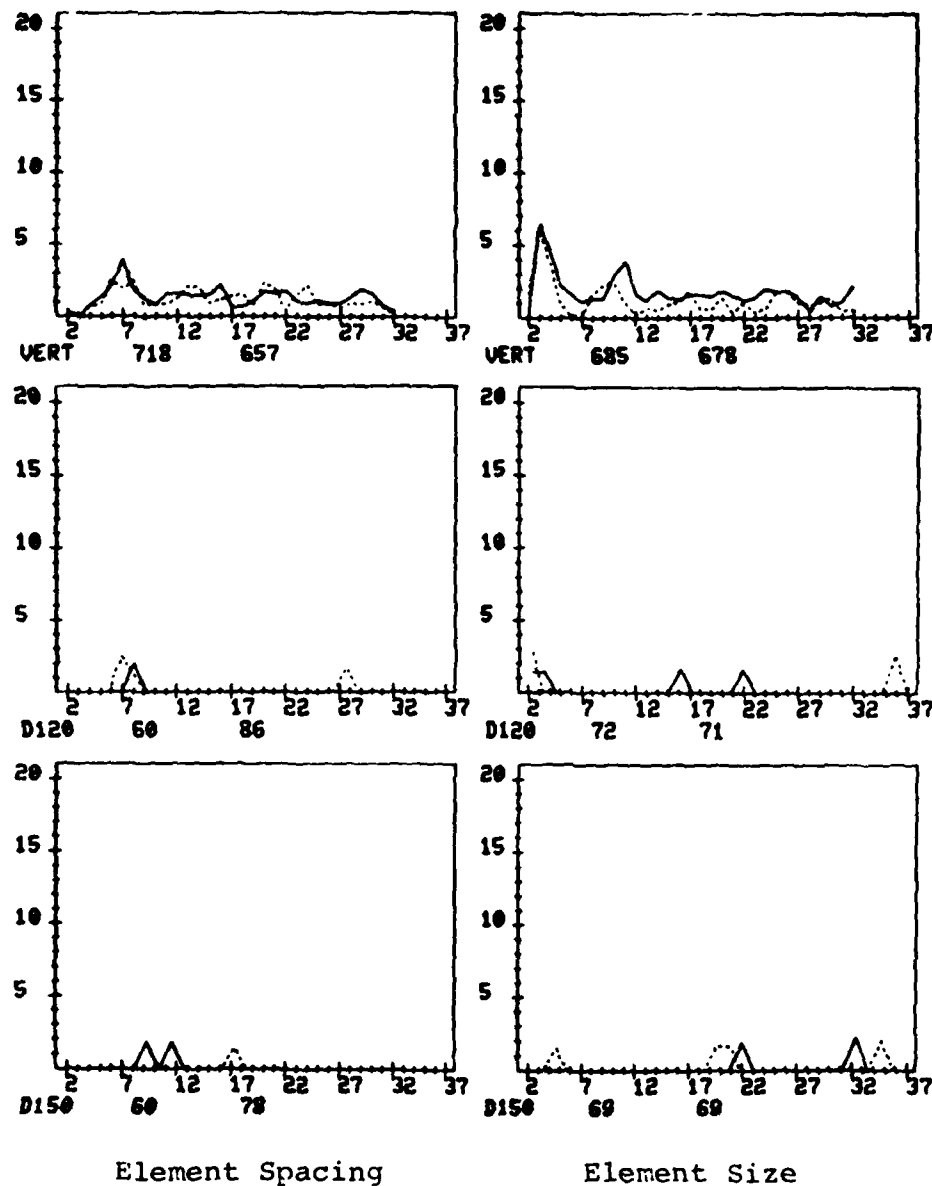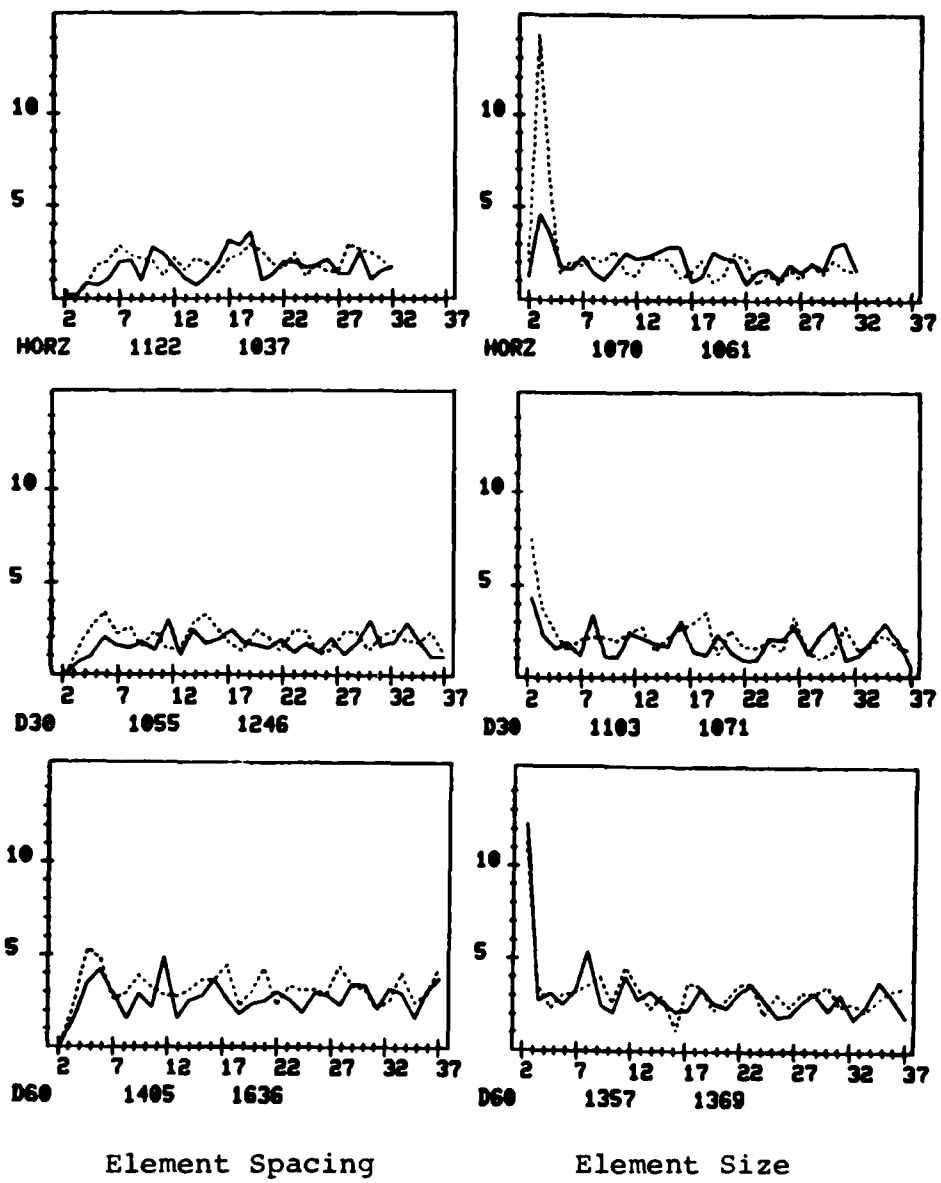
Figure 2-17.　Straw2 ERA Graphs

63

Element Spacing   Element Size
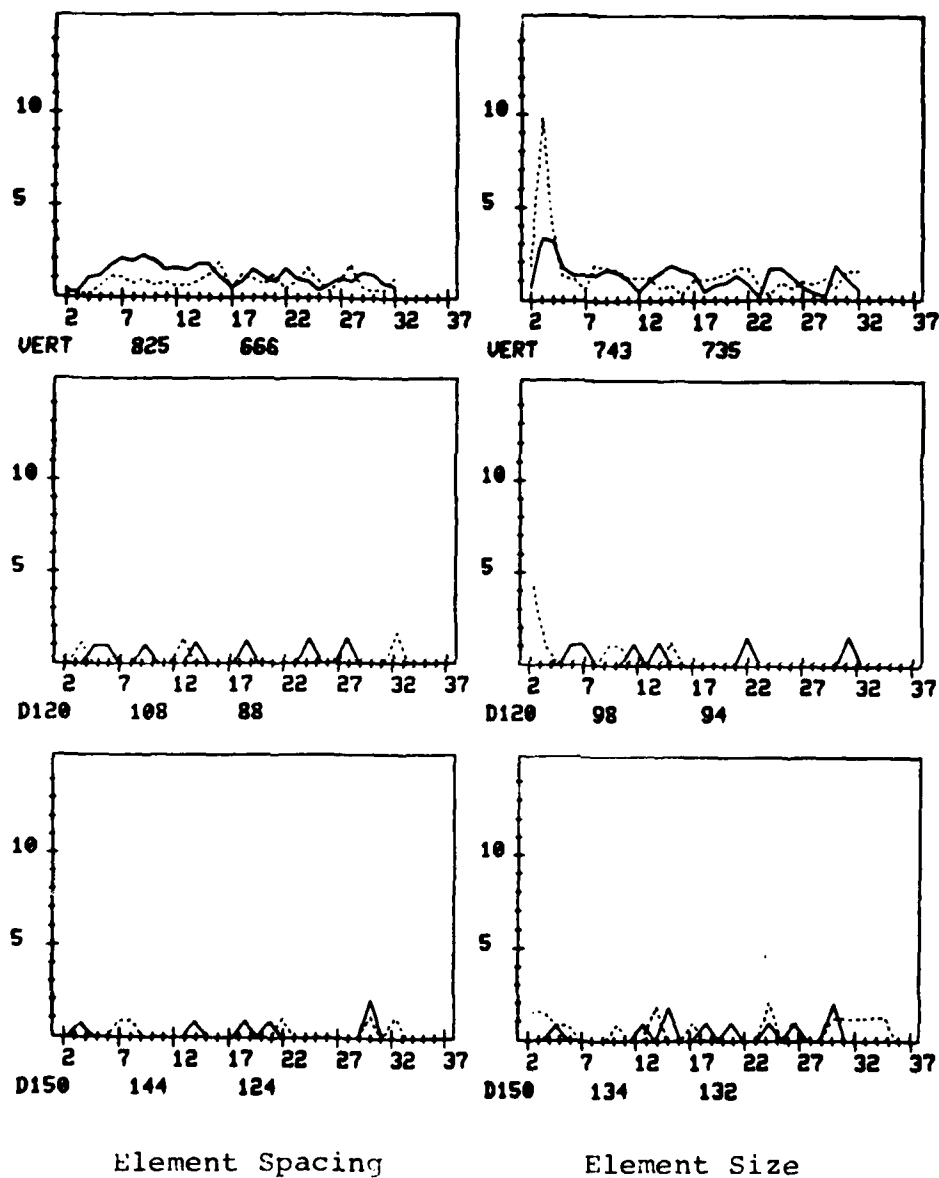
Figure 2-17.   Continued

64
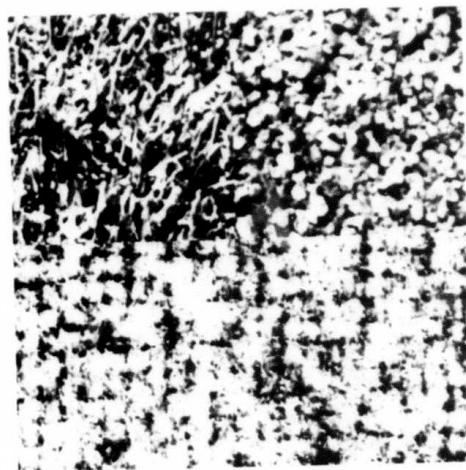
(a) Texture Mosaic Including Grass, Sand, Wool 1 and Wool 2 Images
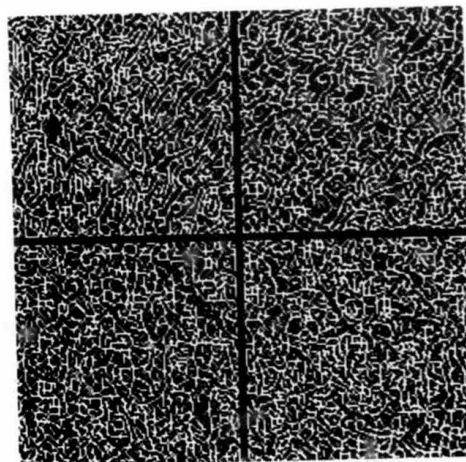
(b) Non-Maximal Suppressed Edges from (a)

Figure 2-18.   Random Texture Mosaic and Edges

subimages. The textures included in this mosaic are the most random ones to be examined. The edge image corresponding to the mosaic in Fig. 2-18(a) is given in Fig. 2-18(b). The textures represented in these mosaics are grass and sand in the first row from left to right, and two wool images in the second row.

The ERAs for grass and sand are given in Figs. 2-19 and 2-20, respectively. Neither pattern shows any evidence of periodicity but both show evidence of element size in their horizontal and vertical scan direction graphs. The predominant element size for grass is 3 for both dark and light objects. Element sizes for sand are 3 for dark objects and 4 for light objects.

The information extracted for these two textures is very similar, even though the textures look quite different to the human observer. After taking a cursory look at the sand texture image one would be tempted to say that the sand texture was made up of perfectly circular pieces of sand, all extremely close in size, but scattered randomly throughout the image. However, on closer inspection one will notice that only relatively few of the sand pebbles in the image are round and there is great variation with respect to pebble size. The shadows between the pebbles are probably more of a constant within

66
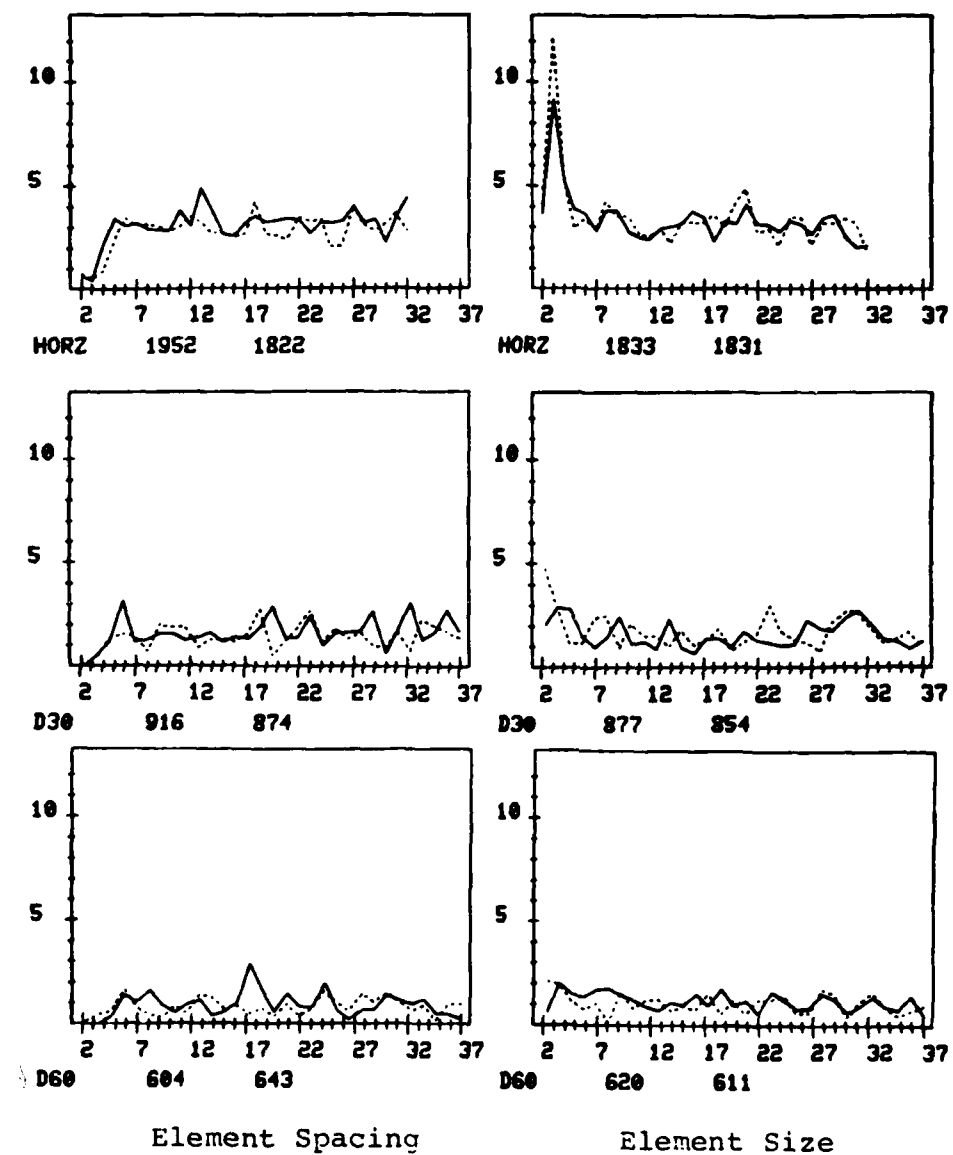
Figure 2-19. Grass ERA Graphs

67

VERT   1189   1101   VERT   1133   1121

D120   378   354   D120   362   359

D150   474   438   D150   453   440

Element Spacing   Element Size

Figure 2-19. Continued

HORZ   1413   1395

HORZ   1402   1405

D30   584   654

D30   611   617

D60   578   684

D60   622   620
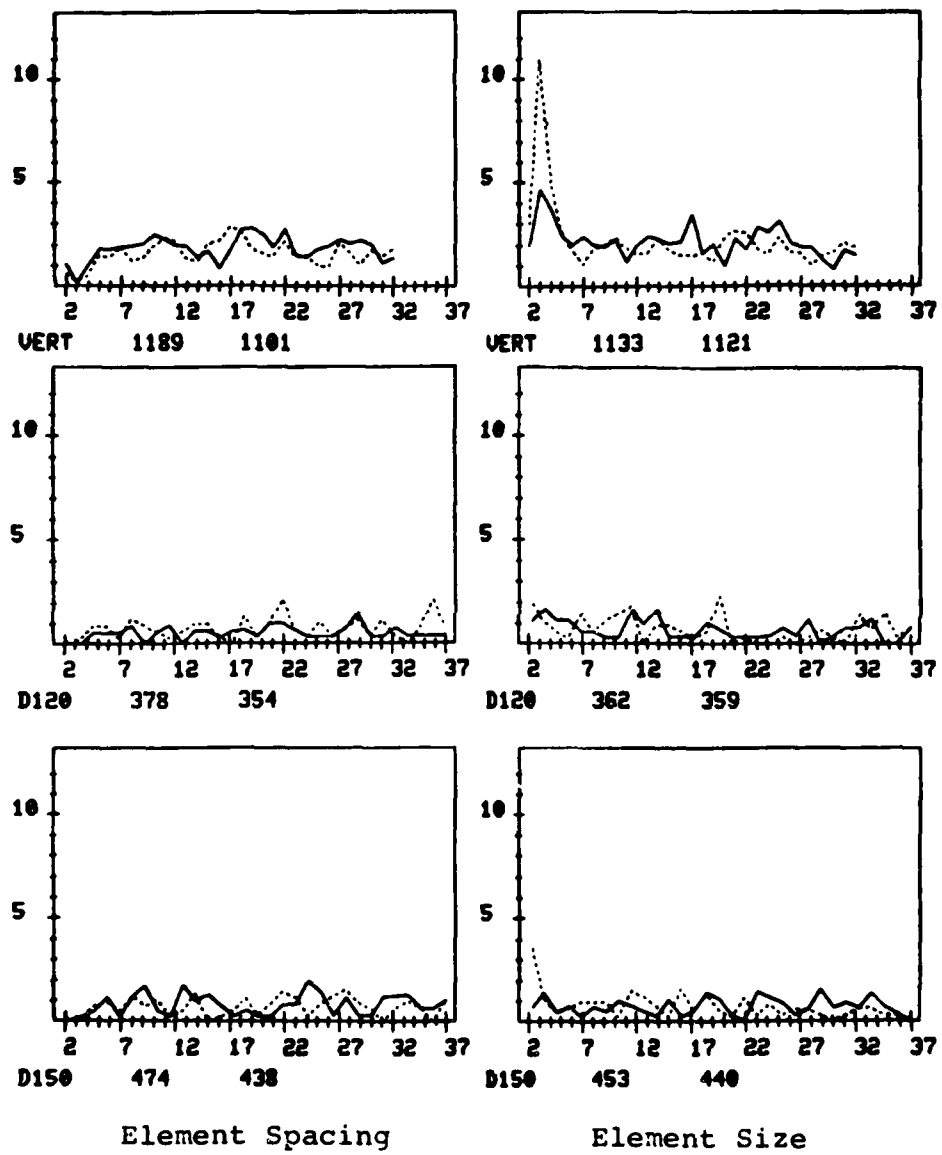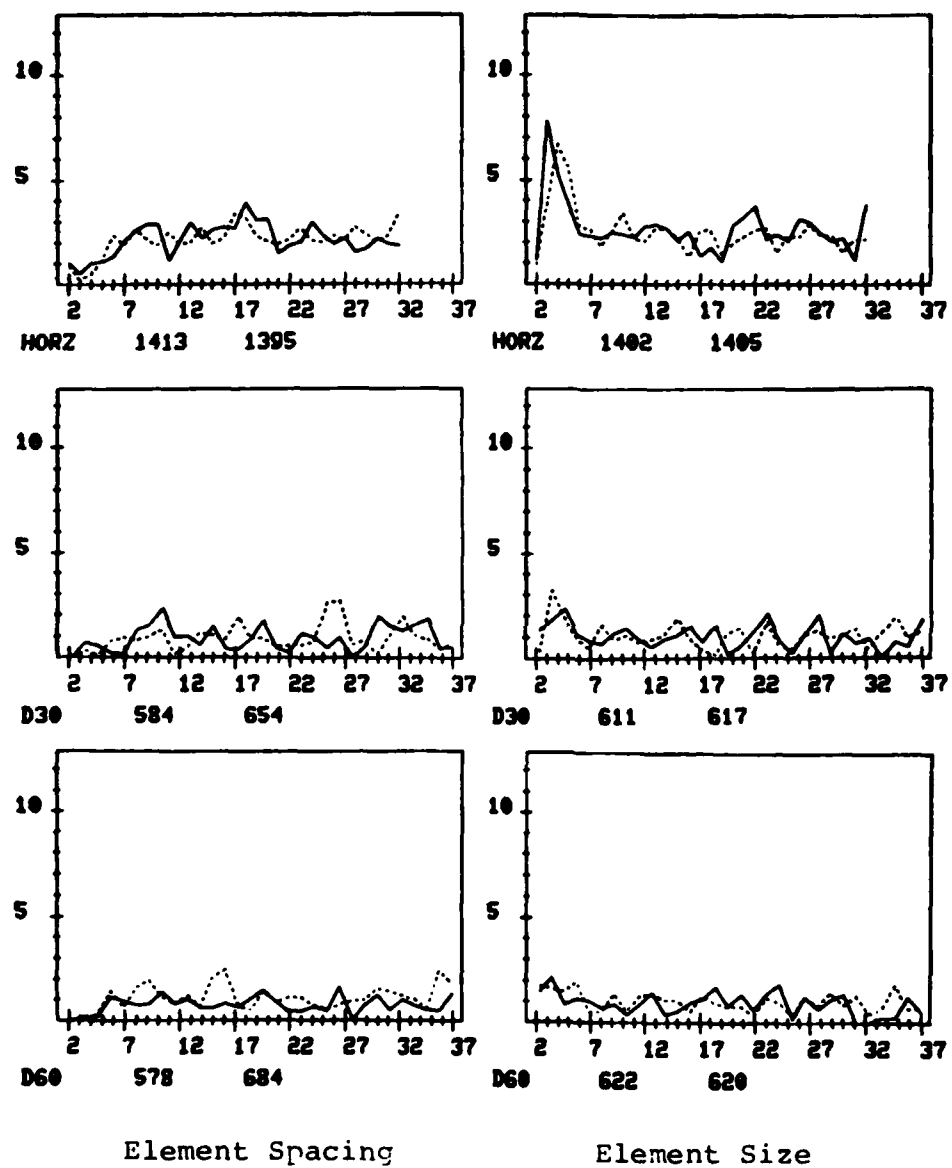
Element Spacing   Element Size

Figure 2-20.   Sand ERA Graphs

Element Spacing   Element Size
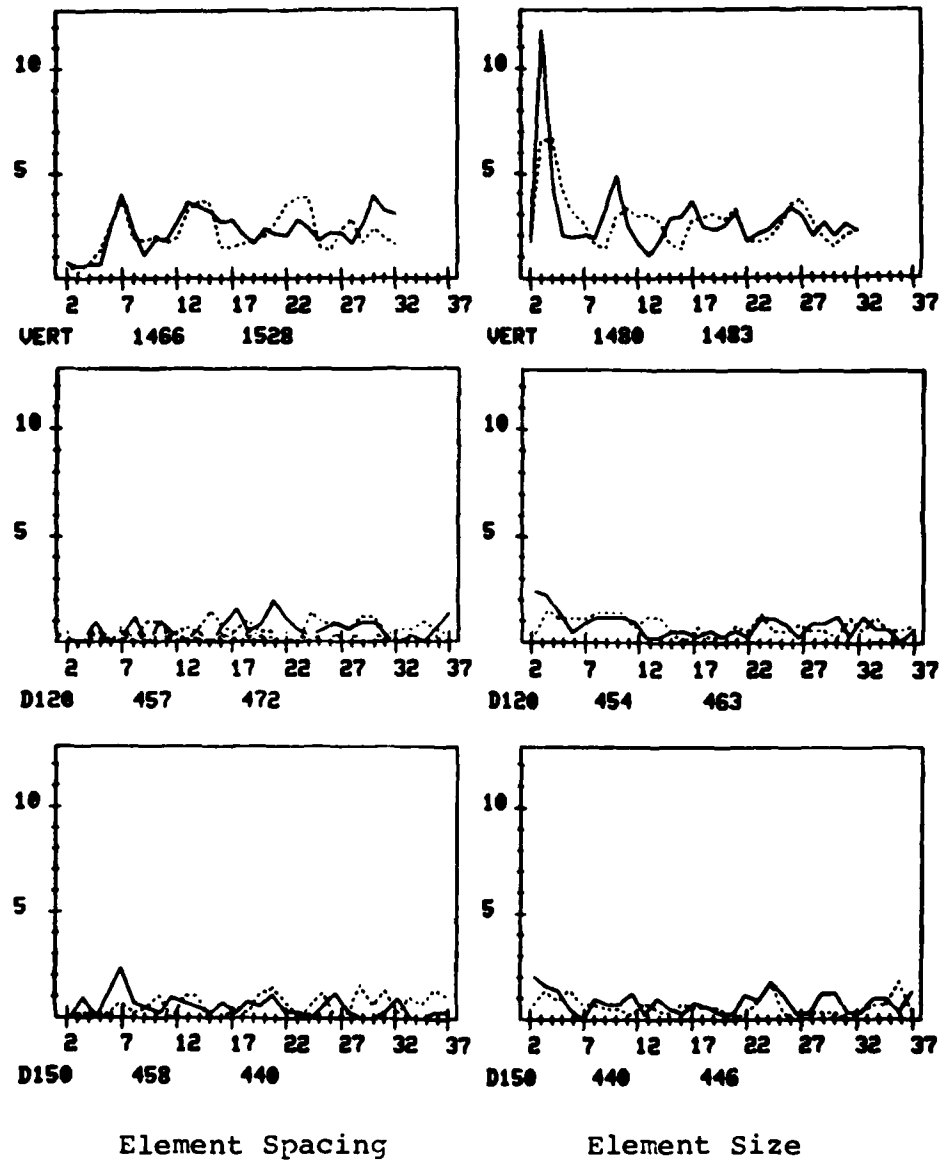
Figure 2-20.   Continued

70

the image. It would seem then that the sand element size peaks are measuring only the smallest of the sand pebbles and the spaces between grains and not the large circular pebbles which our eye tends to pick out.

The two texture images in the second row of the mosaic in Fig. 2-18(a) are wool texture subwindows. Their ERAs appear in Figs. 2-21 and 2-22. As in grass and sand the strongest amplitudes are in the horizontal and vertical scan direction element size graphs. The results for dark elements are stronger than those for light elements in both images. There is very weak evidence for periodicity of dark elements in the horizontal scan direction. When we look at the wool images in Fig. 2-18(a), we have no trouble finding squares which repeat at definite periods. A closer look will reveal that in fact there are very few if any square elements in the image. The one dimensional scans have a better chance of finding the dark strips (shadows) which separate some of the "square" sections.

2.4 Automatic Interpretation of ERA Results

The results given in Section 2.3.2 have shown that the edge repetition array is a useful device for identifying certain structural texture properties. The next step in the texture analysis process is to automate

71

Element Spacing   Element Size
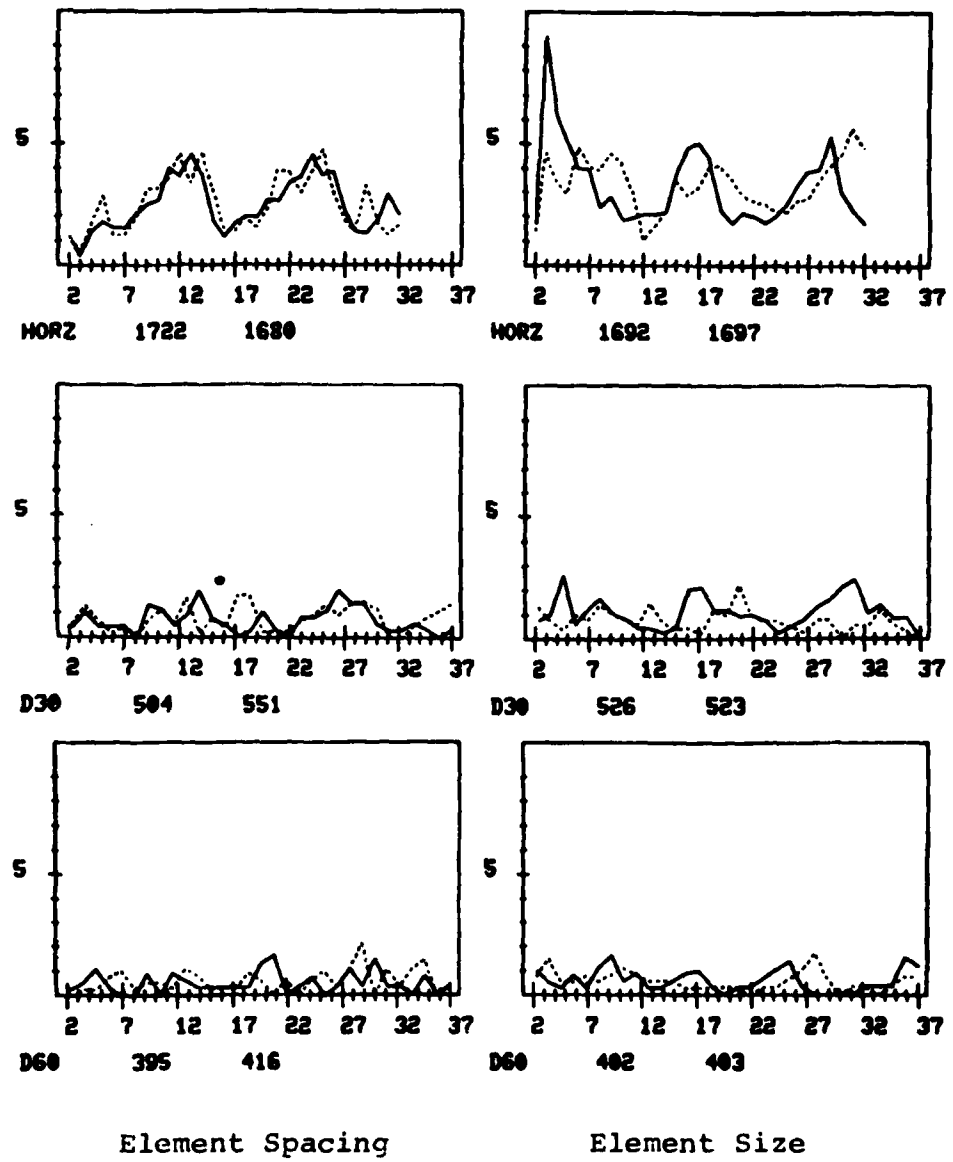
Figure 2-21. Wool 1 ERA Graphs

72

VERT   1323   1300

VERT   1298   1306

D120   554   555

D120   544   546

D150   602   644

D150   615   618

Element Spacing   Element Size

Figure 2-21. Continued

73

HORZ 1550 1672

HORZ 1594 1603

D30 560 493

D30 525 523

D60 460 461

D60 456 456

Element Spacing   Element Size
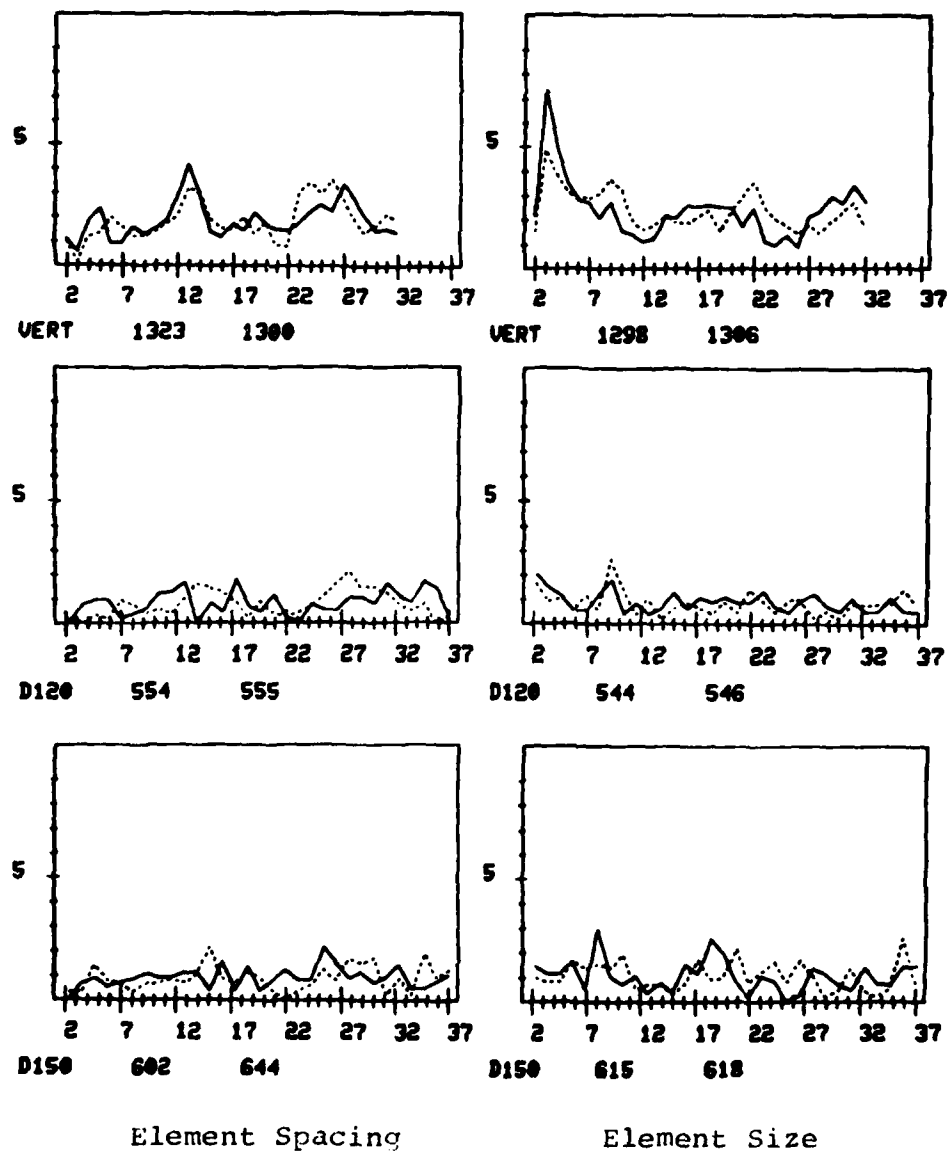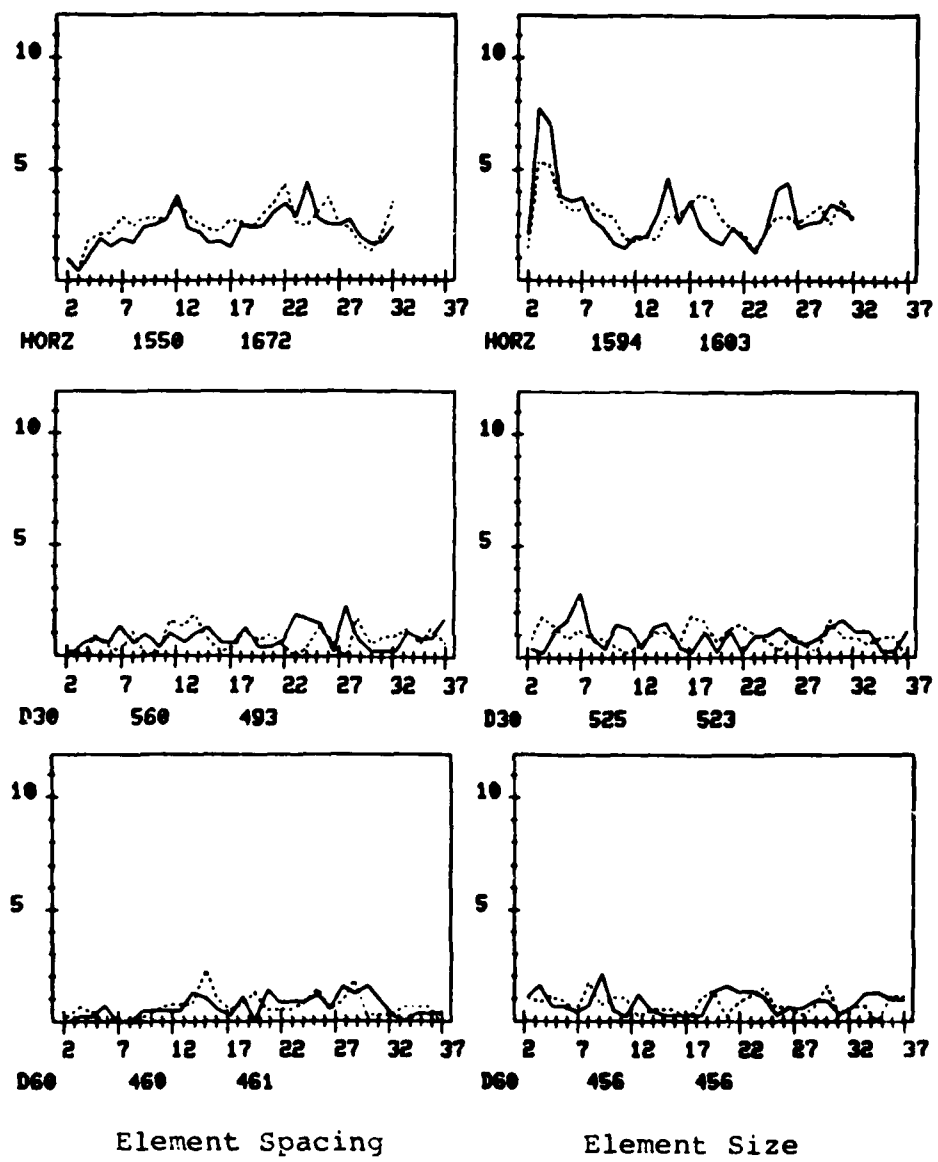
Figure 2-22. Wool 2 ERA Graphs

Element Spacing   Element Size
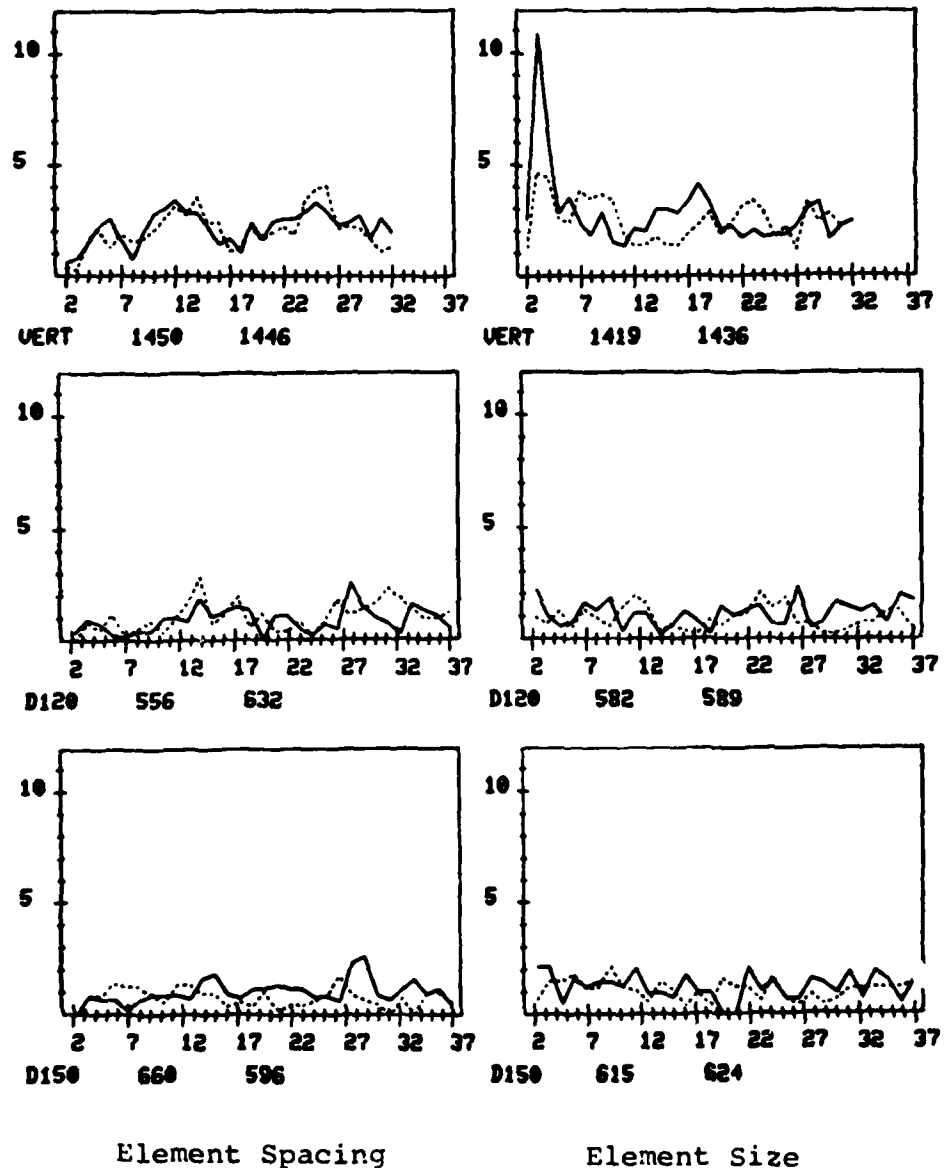
Figure 2-22.   Continued

75

the ERA interpretation process. That is, to automatically generate texture descriptions from ERA results.

Before one can design an algorithm to perform an intelligent process it is necessary to have a clear understanding of the process one wishes to imitate. The following is a brief descriptive outline of the approach taken by the author to extract the pertinent structural information from sets of ERA graphs.

2.4.1 The ERA Interpretation Process

For each (direction, intensity) pair there are two graphs, namely, an element spacing graph and an element size graph. The first step in the examination process is to locate and classify all of the peaks indicated in this pair of graphs. When the most significant or highest peaks are found it is necessary to determine whether they carry important structural information or are simply part of the noise. If both graphs are nearly constant all that can be said is that there are no obvious element sizes or periods. However, when peaks with significant peak to valley separation are found the next level of analysis can begin.

If the element spacing graph shows strong peaks at all multiples of a certain distance then periodicity in

the scan direction of the graph pair is suspected. When this is further supported by element size peaks repeating at intervals of the indicated spacing value then this hypothesis is confirmed. The texture is considered to be regular and the period and directionality are known. At this point it is necessary to determine the sizes of the textural elements or primitives in the given scan direction.

If there are no indications of periodicity, but there is at least one strong peak in the element size graph then it is assumed that the texture is composed of randomly placed, similar-sized textural elements. The dimension of the texture primitives in the indicated scan direction is taken to be the pixel distance at which the peaks in element size values occur. If there is a high floor value following the initial element size peak then it is likely that there is a high density of edges oriented perpendicular to the direction of scan. Since there are many matches at every element size, their placement is probably random. In this case the texture under consideration is determined to be a <u>highly directional random pattern</u>.

The analysis described above is repeated for each (direction, intensity) pair, producing a structural

description for the texture with respect to light and dark intensity objects in each of six scan directions.

2.4.2 Descriptive Outline of the ERA
Interpretation Program

The program designed to automatically interpret ERA results follows the procedure described in Section 2.4.1 very closely. The first program section deals with peak detection and classification. Initially each point in the graph is labelled as a peak, a valley, or a hillside. All peaks are catalogued with certain descriptive information, e.g., peak width, amplitude, valley to valley width, etc. An attempt is then made to classify the peaks as major, minor or subminor. This classification process takes into account both absolute and relative peak amplitudes. A detailed description of the classification process is given in Section 2.4.3. Even the largest peaks in a graph will be ignored if they are not above a reasonable value, as in the 150 degree scan direction graphs in Fig. 2-14. On the other hand, all of the peaks in a graph might be classified as major. See the horizontal scan direction graphs in Fig. 2-9. Classification of the peaks in these 2 examples is fairly straightforward. However, there are cases where the classification decision is not as clear cut.

An attempt has been made to design an algorithm flexible enough to correctly identify meaningful graphic information even when the amplitudes are fairly low. However, some absolute and dynamic cutoffs are used in an attempt to filter out misleading or noisy information. For example, no peak with amplitude less than 2 is considered as a major or minor peak. This is reasonable when we consider that the value 2 means that a match occurred only 2 percent of the time that at least one of the edge types necessary for the match was in the proper location. Clearly, a peak with amplitude 2 does not reflect any major structural feature of the texture pattern.

Choosing the value, 2, as a cutoff does not mean that peaks with amplitude 2.0 are considered to be far more important than peaks with amplitude 1.9. The threshold 2.0 is a conservative choice. It is low enough so that no significant textural feature is in danger of being missed. However, it is useful in that many small peaks which are part of the noise are excluded from further consideration.

Along with peak detection and classification some general graph descriptors are calculated in this program section. One description classifies each graph as to how closely it approximates a constant. Another descriptor

flags graphs which have a high floor value after their initial peak and valley. Therefore, graphs which have a high floor value after an initial high peak, an initial low valley, or a high peak followed by a low valley are flagged.

The next major program section determines whether the texture is periodic in the given scan direction, and if so it determines its period. Major peaks in the element spacing graph are examined to determine if peaks exist at all multiples of a given spacing value. If this occurs then all but the first peak are tagged as multiples and the next untagged major element spacing peak is examined. In this process the strength of the repetition is noted. If there are major peaks at all the multiples of a given value the repetition is considered to be stronger than if only minor peaks occur at the multiples of this value. The repetition descriptor assigned has one of 4 possible values (FAIL, IC, PK, or MPK). The exact criterion used to assign these values is explained in detail in a later section.

After all of the major element spacing peaks have been considered as possible periods of repetition the element size graph is analyzed. Support for potential element spacing values is sought. Each major and minor

element size peak is examined to determine if repetitions occur at intervals of a potential element spacing value. That is, if M is a possible texture period value and N is a value at which a major or minor element size peak occurs, then peaks are sought at the ele..ent size values of N+M, N+2M, N+3M, etc. If such peaks are found then the strength of repetition is noted and all repetitions of the element size peak are tagged with respect to the specific element spacing peak under consideration.

The final section of this program is the interpretation or description generation section. All of the descriptors previously generated are considered in a specific order. This program section is logically equivalent to a small production system with rules of the form:

    IF(COND1 AND COND2 AND...AND CONDN)
    THEN PRINT(Appropriate Descriptive Message)

Some specific examples of the production rules used are given at the end of the following section.

2.4.3 The ERA Interpretation Program in Detail

In this section the ERA interpretation program will be explained in detail. The major program sections to be discussed below perform the following tasks:

1)   Peak-Valley Signature Calculation

2)   Amplitude Descriptor Calculation

3)   Constant   Profile   and   Directionality   Descriptor
     Calculation

4)   Peak Information Collection

5)   Major Peak Extraction

6)   Repetition Descriptor Calculation

7)   Description Generation

Peak-Valley Signature Calculation

A peak-valley signature (P-VS) is calculated for every element size and spacing ERA. This is a vector of dimension $D = M2-M1+1$, where M1 and M2 are the smallest and largest distances to be scanned when calculating the ERAs. Each P-VS value is either a P, V, or H depending on whether the corresponding ERA value is a peak, a valley, or a hillside, respectively. Plateaus occur when 2 neighboring values differ by less than the minimum of one third of the amplitude of the ERA entry being considered and the value .6. As an example, consider the solid line, vertical scan direction, element spacing graph given in Fig. 2-12. The P-VS values for the distances 18 through

82

32 are as follows: V, V, H, H, H, H, P, H, H, H, H, H, V, P, V. Later in the program, when peaks are further classified as major, minor, or subminor the peaks in the signature are adjusted to reflect this classification. The P-VS is used to provide easy access to location, width and classification of peaks.

Amplitude Descriptor Calculation

The amplitude, A, of each point on the graph is classified as follows:

a) VERY STRONG if A is greater than 15;

b) STRONG if A is greater than 10 but not greater than 15;

c) MODERATE if A is greater than 5 but not greater than 10;

d) WEAK if A is greater than 2 but not greater than 5; and,

e) VERY WEAK if A is not greater than 2.

Constant Profile and Directionality Descriptor Calculation

Both of these calculations are performed in order to provide information about the overall shape of the graph.

83

The following 3 conditions are described:

1) near constant amplitude throughout the ERA;

2) relatively constant amplitude starting with the second ERA peak; and,

3) high ERA floor value over all but a small number of points.

A near constant graph has little structural information to offer. It indicates that no predominant element size or spacing is likely to be found in the given scan direction. An example is the 30 degree scan direction ERA in Fig. 2-15.

Some textures have like-sized elements, but they are randomly placed. In this case a predominant element size will be indicated by a high amplitude peak in the element size graph. However, since the texture is not periodic, element size repetitions at every distance may be equally likely. Therefore, after the first peak, the graph may tend to be relatively constant. An example is the horizontal ERA for light objects in Fig. 2-17.

A graph with most of its points above a relatively high value usually indicates that there is a high density of edges with direction perpendicular to the scan

direction. If the texture were periodic then deep valleys should be found between multiples of the element spacing distance, therefore it is also likely that the texture is random. A texture with a graph exhibiting a high minimum value over most of its entries will then be labelled as a directional random pattern. The horizontal ERAs in Fig. 2-14 exhibit this phenomenon.

Descriptors for these 3 general classes of graphs are calculated as follows:

1) If the difference between the highest and lowest graph values is not greater than two(three) the graph is considered to be strongly (moderately) constant.

2) If the different between the highest and lowest graph values beginning with the second peak is less than the maximum of one-fourth of the largest graph value and the value 2 then the ERA is considered to be strongly constant after the first peak. If this difference is less than the maximum of one-third of the maximum graph value and the value 3 then the ERA is considered to be moderately constant after the first peak.

3) Let $T = M2-M1-2$, i.e., all but 3 points of the graph, where M1 and M2 are the smallest and largest pixel distances to be considered when calculating the ERA.

If at least T graph values are greater than or equal to the maximum of one-fourth of the largest graph amplitude and the value 3 then it is assumed that the texture is a highly directional random pattern. If at least T graph values are greater than or equal to the maximum of one-fifth of the largest graph amplitude and the value 2 then it is assumed that the texture is a moderately directional random pattern. If neither occurs then the directionality descriptor is set to zero to indicate that the texture is non-directional.

If neither (1) nor (2) above occurs then the constant profile is set to zero. If, at a later point in the program, it is obvious that the texture is periodic in the given direction and the directionality descriptor is zero for both element spacing and size graphs then the constant profile for these 2 graphs set to zero. In short, evidence of periodicity is given preference over evidence of randomness in borderline cases.

The thresholds used in this section were chosen after examining ERA graphs for a wide range of textures. Both dynamic and absolute thresholds are used to lend flexibility to the basic classification scheme. These thresholds were conservatively chosen to insure that their use would not affect the robustness of the algorithm.

86

Peak Information Collection

The following information is catalogued for each peak for use later in the program:

a) peak amplitude;

b) peak width;

c) valley to valley width;

d) location of left valley;

e) location of right valley;

f) difference in amplitude between peak and left valley; and,

g) difference in amplitude between peak and right valley.

A list of peaks is also formed in this section to facilitate the sequential examination of peaks. Peaks with maximum peak-valley variation (the maximum of c and d above) greater than a minimum of 2 are labelled minor peaks. At a later point in the program, some of the minor peaks may be reclassified as major peaks. At this point, if a peak is not labelled as minor its classification will remain as subminor.

87

Major Peak Extraction

The list of major peaks is formed in this program section. There are two separate sets of criteria for major peak classification. The first set pertains to both element spacing and element size peaks. However, the second set is used only for element spacing peaks. This latter set of conditions enables an element spacing peak which would normally be classified as minor to be considered along with the other major element spacing peaks in the search for texture period. It is hoped that if the peak representing the period of the texture falls short of the basic set of major peak conditions then the second set of conditions will provide enough algorithm flexibility to make up for it. The first set of major peak conditions are as follows:

a) the peak amplitude must be greater than or equal to the maximum of two-thirds of the maximum graph value and 3; and,

b) both left and right peak to valley differences must be greater than 3.

In (a), an effort is made to select the highest element size and spacing peaks in each graph. However, none below amplitude 3 are considered. In (b), the degree

88

of peak definition is examined. Thus, major peaks should be among the highest peaks in the graph and have well-defined peak to valley separations. Since the texture period is such an important piece of structural information a second set of constraints has been added to allow weaker element spacing peaks to be considered along with major peaks in the search for texture period. This new class of peaks will not be considered as true major peaks but as major-minor peaks. The constraints are as follows:

a) The peak must be a minor peak;

b) It must have amplitude at least as great as one-fifth of the maximum graph value; and,

c) The pixel distance at which this peak occurs must be within 1.5 pixels of the difference between 2 major element size peak distances.

In (a) and (b), the peak amplitude and peak-valley separations are somewhat constrained. In (c), it is required that there be evidence that the element spacing value is indeed a candidate for the texture period.

In Appendix A, an effort is made to derive some indication of the robustness of the peak classification algorithm. When working with natural scenes it is likely

89

that the edge and direction images will exhibit some form of degradation. In low contrast images some edges may be missed, in noisy images edges may be found where there are no corresponding object edges, and at times edges are out of place by a small number of pixels. The effects of these three types of edge image degradations are examined. It was determined that for probability of deletion as great as .8 the true texture period can be expected to be classified as a major peak. In all of the test cases considered for insertions and shifts, the peak occurring at the true texture period in the element spacing ERA would have been successfully classified as a major peak. A more complete statement of results can be found in Section A.1 of the appendix. This study examined each type of degradation in isolation. Future studies should be made to determine the combined effects of these types of degradations.

Consider the set of element spacing graphs in Fig. 2-12. As would be expected only one major peak is found in the 30 degree, 150 degree and vertical scan directions for both dark and light objects. These are found by using the first set of conditions. In all of the other graphs one would expect to find that 2 major peaks were discovered. This was true of all but the dark element graph for the 60 degree scan direction. The

second peak is just below the amplitude threshold. Therefore, it is considered to be only minor. After the second set of conditions were used, this peak and one other were reclassified as major-minor peaks. The second peak was found at pixel distance 2 for light objects in the horizontal scan direction. Neither of these 2 peaks are at the texture period for their respective scan directions. However, the peak which was added for the 60 degree scan graph was clearly a strong multiple of the actual texture period peak, the first one in the graph. Although the peak near distance 2 of the horizontal light element graph was neither the texture period nor one of its multiples, considering this peak as a possible texture period cause no problems. It was weeded out in the next level of processing when no strong evidence could be found to support it as the horizontal texture period.

In light of the above example it might seem that peak classification is unnecessary. Perhaps all element spacing peaks should be considered in the search for texture period. This would probably work very well for artificially generated regular textures with perfect edge and direction images. Every peak in the element spacing graph would either be the period of the texture or one its multiples. Hence, peak detection and a simple repetition detection scheme would work well. However, when working

with natural textures extra steps must be taken to insure that the interpretation being made is backed up by strong enough evidence. Consider the 120° and 150° ERA graphs in Fig. 2-19. These graphs were produced for the grass subwindow of Fig. 2-18(a). Using the repetition descriptor algorithm to be defined in the next section without discriminating between the types of peaks encountered, we would find that grass is periodic in at least these 2 directions, a claim which is not observationally well-founded. It is therefore necessary to use some form of peak classification scheme to properly weight the evidence observed.

Repetition Descriptor Calculation

In this section the periodicity of the texture in the given scan directions is examined. At first, element spacing information is used. If a possible texture period value is found, then more support is sought from the element size data. It should be noted that whenever multiples or peak repetitions are sought a margin of 1.5 to the left and right is given. Both element spacing and element size repetition descriptors are calculated in this section. The process is described below.

The first major peak is considered as a possible element spacing value. Checks are made to determine if

peaks occur at multiples of this value. Then the appropriate element spacing repetition descriptor is assigned as explained below.

The descriptor is assigned MPK if each multiple of the value being considered is the location of a major peak. At least one repetition must be found.

The descriptor is assigned PK if at least one multiple of the value being considered is the location of a major peak and the rest are at least minor peaks, i.e., minor peaks or major-minor peaks. Again at least one multiple must be found.

The descriptor is assigned IC if all of the constraints of PK are met except that one of the peak repetitions is missing. At least 1 repetition must be found. The descriptor is assigned FAIL (i.e., zero) if none of the above cases apply.

If the assigned descriptor is not FAIL, all repetitions of the peak under consideration are tagged. The next untagged major peak is then considered. When all untagged major peaks have been considered, the untagged major-minor peaks are then examined.

If a non-zero element spacing repetition descriptor, say D1, has been assigned to any element spacing value, N,

then attention is shifted to the element size graph in search of further support. This support, if it exists, will be a non-zero element size repetition descriptor. The descriptor calculation process is described below.

Element spacing values are considered in order of decreasing positive element spacing repetition descriptor value D1. If peaks occur at locations M, M+N, M+2N,... for element size M and element spacing value N then the size repetition descriptor, say D2, for N is set to MPK, PK, IC, or FAIL as explained below.

The descriptor is set to MPK if each of M, M+N, M+2N,... is the location of a major peak. At least one repetition must be found.

The descriptor is set to PK if each of M, M+N, M+2N,... is the location of a peak which is at least minor. Again, at least one repetition must be found.

The descriptor is set to IC if all the constraints of PK are met except that one of the peak repetitions is missing. At least 1 repetition must be found. The descriptor is set to FAIL (i.e., zero) if none of the above cases apply.

If the descriptor produced while considering element size M is not equal to FAIL then repetitions of the peak,

94

namely, M+N, M+2N,... are both temporarily and permanently tagged. For a given N, D2 is maximized over element size peaks which are not temporarily tagged. After all element size peaks which are at least minor peaks and are not temporarily tagged are considered, the temporary tags are removed and the next element spacing value having non-zero D1 is considered.

If the descriptor, D2, produced for N while considering element size M is greater than zero then element size, M, is assigned an ordered pair, <S1,S2>, where S1 = N and S2 = D2. S1 and S2 are reset only if a descriptor greater than S2 is produced while using element size M. Therefore, the ordered pair <S1,S2> is changed only to maximize S2 over all element spacing values with positive D1.

The repetition descriptors D1 and D2 associated with element spacing values as well as the ordered pairs <S1,S2> associated with non-permanently tagged element size peaks are considered when descriptions are being generated in the interpretation section described below.

For the horizontal scan direction ERAs of Fig. 2-12 the element spacing value 14 has D1 = D2 = MPK for both dark and light objects. The element size values 10 (for dark objects) and 4 (for light objects) have

$\langle S1,S2\rangle = \langle 14, MPK\rangle$.

Description Generation Section

A simplified outline of this program section is given in Fig. 2-23. If all of the case statements and nested conditionals were expanded this section would essentially consist of a set of production rules of the form

IF(COND1 AND COND2 AND...AND CONDN)

THEN PRINT(Appropriate Descriptive Message).

A small subset of these expanded production rules follows:

Rule 1: IF(Element size graph closely approximates a constant)

THEN PRINT ("No evidence of periodicity or predominant element size").

Rule 2: IF(Element spacing graph closely approximates a constant)

AND (Element size graph has constant profile 0)

AND (There exists a major peak at element size value N with amplitude descriptor STRONG)

THEN PRINT("No evidence of periodicity. STRONG evidence of element size of N").

Rule 3: IF(Element size graph has constant profile 0)

96
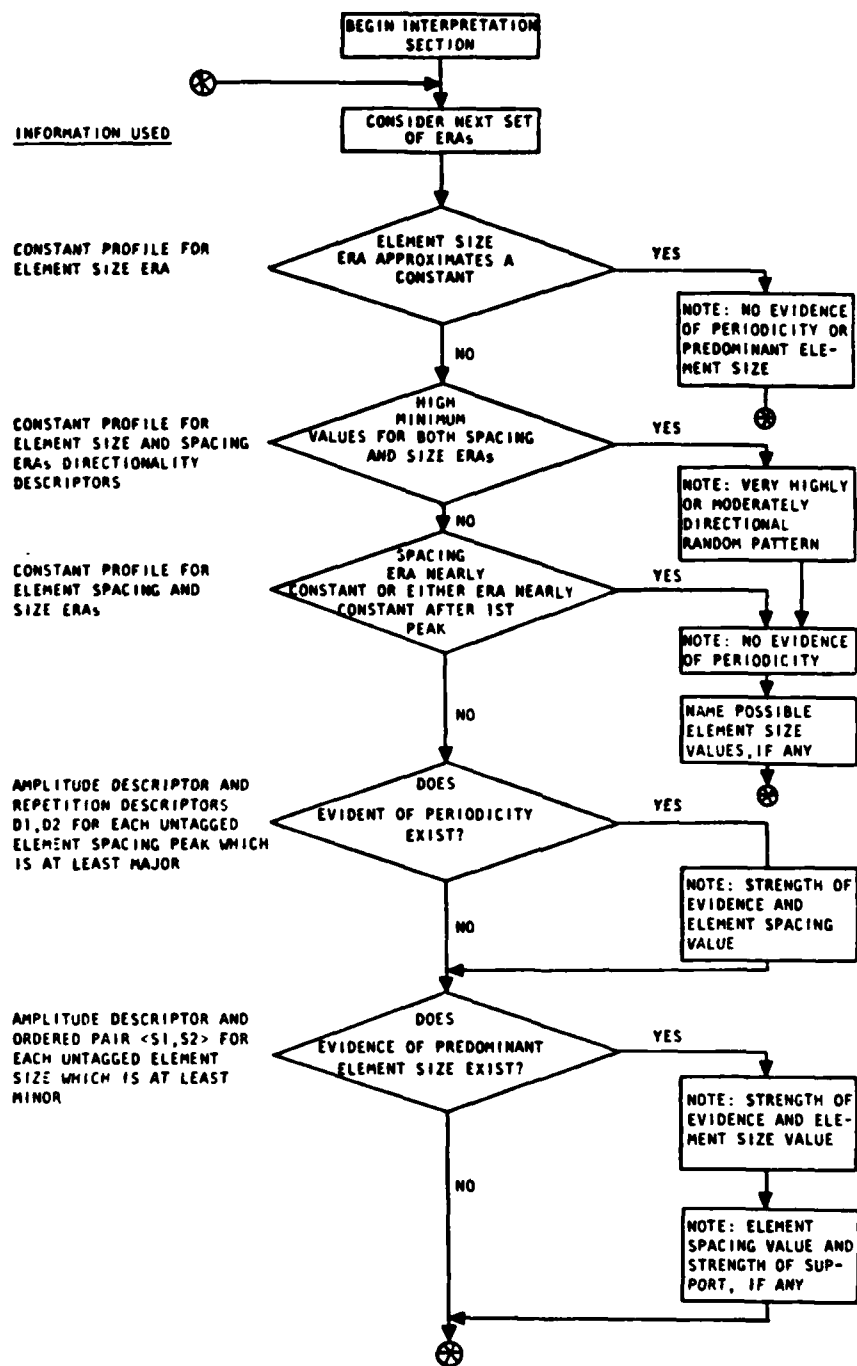
Figure 2-23. Texture Interpretation Algorithm

AND (Element size graph has constant profile 0)

AND (There is a major peak at element spacing value, N, having amplitude descriptor STRONG)

AND (Element spacing repetition descriptor, D1, for N is MPK)

AND (Element size repetition descriptor, D2, for N is MPK)

THEN PRINT ("There is VERY STRONG evidence of periodicity with element spacing N").

Rule 4: IF(Element spacing graph has constant profile 0)

AND (Element size graph has constant profile 0)

AND (There is a major peak at element size value N)

AND (Amplitude descriptor for N is at least STRONG)

AND (N is not permanently tagged)

AND (S2 associated with N is MPK)

THEN PRINT ("There is STRONG evidence of element size N with STRONG support for element spacing S1").

For descriptions of D1, D2, S1, and S2, see the repetition descriptor calculation section.

The CPU time needed to compute the peak-valley signature, amplitude and directionality descriptors, and

constant profile depends only on the range of pixel distances to be considered. However, the time needed to extract major peaks, collect peak information, and calculate repetition descriptors depends on the number and types of peaks in each graph. The time needed for description generation depends on the results of the above mentioned calculations. The average time recorded for 31 pixel distances is .6 seconds. In the following section some automatically generated ERA descriptions are examined and discussed.

2.4.4 Automatically Generated ERA Descriptions

Figures 2-24 through 2-36 are descriptions of the ERAs from Figs. 2-7 through 2-22. These descriptions were automatically generated by the program described in Section 2.4.3. They have been shortened by excluding all messages of the form: "No evidence of periodicity or predominant element size."

In Fig. 2-24, raffia is described as a texture which is strongly periodic in the vertical direction. Vertical element dimensions are given as 3 for dark objects and 5 for light objects. There is also strong evidence to support the existence of thin light elements found in the horizontal scan direction. However, no period could be established for these.

99

FILENAME = RAFFIA

DARK OBJECT DESCRIPTIONS

30 DEGREE SCAN DIRECTION

NO EVIDENCE OF PERIODICITY
WEAK EVIDENCE OF PREDOMINANT ELEMENT SIZE   25.40)

VERTICAL SCAN DIRECTION

THERE IS STRONG EVIDENCE OF PERIODICITY (SPACING 8.00)

THERE IS STRONG EVIDENCE OF PREDOMINANT ELEMENT SIZE (3.00)
WITH MODERATE SUPPORT FOR ELEMENT SPACING (8.00)
RATIO OF SIZE TO PERIOD IS .38

LIGHT OBJECT DESCRIPTIONS

HORIZONTAL SCAN DIRECTION

NO EVIDENCE OF PERIODICITY
STRONG EVIDENCE OF PREDOMINANT ELEMENT SIZE (3.00)

VERTICAL SCAN DIRECTION

THERE IS STRONG EVIDENCE OF PERIODICITY (SPACING 8.00)

THERE IS STRONG EVIDENCE OF PREDOMINANT ELEMENT SIZE (5.00)
WITH MODERATE SUPPORT FOR ELEMENT SPACING (8.00)
RATIO OF SIZE TO PERIOD IS .63

Figure 2-24.   Raffia Texture Description

In Figs. 2-25 and 2-26, there are descriptions for the two aerial city texture subwindows. They both report periodicity, but in different directions. The first is periodic in the horizontal and vertical scan directions while the second reports periodicity at 30 degrees. In the second description multiple element sizes are found at 30 degrees for both dark and light objects. This is as predicted, see Fig. 2-10(b).

In Fig. 2-27, the herringbone material texture is described. This texture is found to be periodic in the vertical and horizontal directions. The existence of multiple dark and light element sizes in both of these scan directions is reported, see Fig. 2-11(b).

In Fig. 2-28, the floor grating image texture description is given. The 30°, 90°, and 150° comments show no evidence of periodicity, while all other directions exhibit strong evidence of a period of approximately 14. This is due to the fact that in all other directions the period was too large to show any repetitions of the element spacing peak. Note that the dark circular dots were found as elements in every scan direction.

The water and wood texture descriptions given in Figs. 2-29 and 2-30 are extremely similar. In both cases, the texture are labelled as highly directional random

FILENAME = CITY1

DARK OBJECT DESCRIPTIONS

HORIZONTAL SCAN DIRECTION

THERE IS STRONG EVIDENCE OF PERIODICITY (SPACING 7.00)

THERE IS STRONG EVIDENCE OF PREDOMINANT ELEMENT SIZE (3.00)
WITH MODERATE SUPPORT FOR ELEMENT SPACING (7.00)
RATIO OF SIZE TO PERIOD IS .43

60 DEGREE SCAN DIRECTION

NO EVIDENCE OF PERIODICITY
WEAK EVIDENCE OF PREDOMINANT ELEMENT SIZE (32.33)

VERTICAL SCAN DIRECTION

THERE IS VERY STRONG EVIDENCE OF PERIODICITY (SPACING 16.00)

THERE IS STRONG EVIDENCE OF PREDOMINANT ELEMENT SIZE (13.00)
WITH STRONG SUPPORT FOR ELEMENT SPACING (16.00)
RATIO OF SIZE TO PERIOD IS .81

Figure 2-25. City1 Texture Description

102

FILENAME = CITY1

LIGHT OBJECT DESCRIPTIONS

HORIZONTAL SCAN DIRECTION

THERE IS VERY STRONG EVIDENCE OF PERIODICITY (SPACING 7.00)

THERE IS STRONG EVIDENCE OF PREDOMINANT ELEMENT SIZE (4.00)
WITH STRONG SUPPORT FOR ELEMENT SPACING (7.00)
RATIO OF SIZE TO PERIOD IS .57

VERTICAL SCAN DIRECTION

THERE IS STRONG EVIDENCE OF PERIODICITY (SPACING 16.00)

THERE IS STRONG EVIDENCE OF PREDOMINANT ELEMENT SIZE (3.00)
WITH MODERATE SUPPORT FOR ELEMENT SPACING (16.00)
RATIO OF SIZE TO PERIOD IS .19

Figure 2-25. Continued

103

FILENAME = CITY2

DARK OBJECT DESCRIPTIONS

HORIZONTAL SCAN DIRECTION

NO EVIDENCE OF PERIODICITY
MODERATE EVIDENCE OF PREDOMINANT ELEMENT SIZE (6.00)

30 DEGREE SCAN DIRECTION

THERE IS STRONG EVIDENCE OF PERIODICITY (SPACING 15.01)

THERE IS MODERATE EVIDENCE OF PREDOMINANT ELEMENT SIZE (4.62)
WITH MODERATE SUPPORT FOR ELEMENT SPACING (15.01)
RATIO OF SIZE TO PERIOD IS .31

THERE IS STRONG EVIDENCE OF PREDOMINANT ELEMENT SIZE (10.39)
WITH STRONG SUPPORT FOR ELEMENT SPACING (15.01)
RATIO OF SIZE TO PERIOD IS .69

Figure 2-26. City2 Texture Description

104

FILENAME = CITY2

DARK OBJECT DESCRIPTIONS

60 DEGREE SCAN DIRECTION

NO EVIDENCE OF PERIODICITY
WEAK EVIDENCE OF PREDOMINANT ELEMENT SIZE (4.52)

VERTICAL SCAN DIRECTION

NO EVIDENCE OF PERIODICITY
WEAK EVIDENCE OF PREDOMINANT ELEMENT SIZE (6.00)

120 DEGREE SCAN DIRECTION

THERE IS WEAK EVIDENCE OF PREDOMINANT ELEMENT SIZE (28.87)

150 DEGREE SCAN DIRECTION

THERE IS WEAK EVIDENCE OF PREDOMINANT ELEMENT SIZE (31.18)

Figure 2-26. Continued

105

FILENAME = CITY2

LIGHT OBJECT DESCRIPTIONS

HORIZONTAL SCAN DIRECTION

THERE IS MODERATE EVIDENCE OF PREDOMINANT ELEMENT SIZE (5.00)

30 DEGREE SCAN DIRECTION

THERE IS STRONG EVIDENCE OF PERIODICITY (SPACING 13.86)

THERE IS STRONG EVIDENCE OF PREDOMINANT ELEMENT SIZE (4.62)
WITH MODERATE SUPPORT FOR ELEMENT SPACING (13.86)
RATIO OF SIZE TO PERIOD IS .33

THERE IS MODERATE EVIDENCE OF PREDOMINANT ELEMENT SIZE (10.39)
WITH MODERATE SUPPORT FOR ELEMENT SPACING (13.86)
RATIO OF SIZE TO PERIOD IS .75

Figure 2-26. Continued

106

FILENAME = CITY?

LIGHT OBJECT DESCRIPTIONS

VERTICAL SCAN DIRECTION

NO EVIDENCE OF PERIODICITY
MODERATE EVIDENCE OF PREDOMINANT ELEMENT SIZE (5.00)

120 DEGREE SCAN DIRECTION

THERE IS WEAK EVIDENCE OF PREDOMINANT ELEMENT SIZE (3.46)

THERE IS MODERATE EVIDENCE OF PREDOMINANT ELEMENT SIZE (36.95)

150 DEGREE SCAN DIRECTION

NO EVIDENCE OF PERIODICITY
MODERATE EVIDENCE OF PREDOMINANT ELEMENT SIZE (4.62)

Figure 2-26. Continued

107

FILENAME = HERRINGBONE MATERIAL

DARK OBJECT DESCRIPTIONS

HORIZONTAL SCAN DIRECTION

  THERE IS VERY STRONG EVIDENCE OF PERIODICITY (SPACING 11.00)

  THERE IS MODERATE EVIDENCE OF PREDOMINANT ELEMENT SIZE (3.00)
  WITH STRONG SUPPORT FOR ELEMENT SPACING (11.00)
  RATIO OF SIZE TO PERIOD IS .27

  THERE IS WEAK EVIDENCE OF PREDOMINANT ELEMENT SIZE (8.00)
  WITH MODERATE SUPPORT FOR ELEMENT SPACING (11.00)
  RATIO OF SIZE TO PERIOD IS .73

30 DEGREE SCAN DIRECTION

  NO EVIDENCE OF PERIODICITY
  MODERATE EVIDENCE OF PREDOMINANT ELEMENT SIZE (3.46)

60 DEGREE SCAN DIRECTION

  NO EVIDENCE OF PERIODICITY
  WEAK EVIDENCE OF PREDOMINANT ELEMENT SIZE (12.70)

Figure 2-27.   Herringbone Material Texture Description

FILENAME = HERRINGBONE MATERIAL

DARK OBJECT DESCRIPTIONS

VERTICAL SCAN DIRECTION

THERE IS STRONG EVIDENCE OF PERIODICITY (SPACING 13.00)

THERE IS MODERATE EVIDENCE OF PREDOMINANT ELEMENT SIZE (4.00)
WITH MODERATE SUPPORT FOR ELEMENT SPACING (13.00)
RATIO OF SIZE TO PERIOD IS .31

THERE IS WEAK EVIDENCE OF PREDOMINANT ELEMENT SIZE (9.00)
WITH MODERATE SUPPORT FOR ELEMENT SPACING (13.00)
RATIO OF SIZE TO PERIOD IS .69

THERE IS WEAK EVIDENCE OF PREDOMINANT ELEMENT SIZE (10.00)
WITH MODERATE SUPPORT FOR ELEMENT SPACING (13.00)
RATIO OF SIZE TO PERIOD IS .77

120 DEGREE SCAN DIRECTION

THERE IS WEAK EVIDENCE OF PREDOMINANT ELEMENT SIZE (4.62)

THERE IS WEAK EVIDENCE OF PREDOMINANT ELEMENT SIZE (12.70)

150 DEGREE SCAN DIRECTION

NO EVIDENCE OF PERIODICITY
WEAK EVIDENCE OF PREDOMINANT ELEMENT SIZE (4.62)

Figure 2-27.   Continued

109

FILENAME = HERRINGBONE MATERIAL

LIGHT OBJECT DESCRIPTIONS

HORIZONTAL SCAN DIRECTION

THERE IS STRONG EVIDENCE OF PERIODICITY (SPACING 11.00)

THERE IS MODERATE EVIDENCE OF PREDOMINANT ELEMENT SIZE (3.00)
WITH MODERATE SUPPORT FOR ELEMENT SPACING (11.00)
RATIO OF SIZE TO PERIOD IS .27

THERE IS WEAK EVIDENCE OF PREDOMINANT ELEMENT SIZE (8.00)
WITH MODERATE SUPPORT FOR ELEMENT SPACING (11.00)
RATIO OF SIZE TO PERIOD IS .73

THERE IS WEAK EVIDENCE OF PREDOMINANT ELEMENT SIZE (9.00)
WITH MODERATE SUPPORT FOR ELEMENT SPACING (11.00)
RATIO OF SIZE TO PERIOD IS .82

30 DEGREE SCAN DIRECTION

NO EVIDENCE OF PERIODICITY
MODERATE EVIDENCE OF PREDOMINANT ELEMENT SIZE (3.46)

50 DEGREE SCAN DIRECTION

NO EVIDENCE OF PERIODICITY
MODERATE EVIDENCE OF PREDOMINANT ELEMENT SIZE (3.46)

Figure 2-27. Continued

110

FILENAME = HERRINGBONE MATERIAL

LIGHT OBJECT DESCRIPTIONS

VERTICAL SCAN DIRECTION

THERE IS VERY STRONG EVIDENCE OF PERIODICITY (SPACING 13.00)

THERE IS MODERATE EVIDENCE OF PREDOMINANT ELEMENT SIZE (3.00)
WITH MODERATE SUPPORT FOR ELEMENT SPACING (13.00)
RATIO OF SIZE TO PERIOD IS .23

THERE IS MODERATE EVIDENCE OF PREDOMINANT ELEMENT SIZE (9.00)
WITH STRONG SUPPORT FOR ELEMENT SPACING (13.00)
RATIO OF SIZE TO PERIOD IS .69

THERE IS MODERATE EVIDENCE OF PREDOMINANT ELEMENT SIZE (10.00)
WITH STRONG SUPPORT FOR ELEMENT SPACING (13.00)
RATIO OF SIZE TO PERIOD IS .77

120 DEGREE SCAN DIRECTION

NO EVIDENCE OF PERIODICITY
WEAK EVIDENCE OF PREDOMINANT ELEMENT SIZE (3.46)

Figure 2-27. Continued

111

FILENAME = FLOOR GRATING

DARK OBJECT DESCRIPTIONS

HORIZONTAL SCAN DIRECTION

THERE IS VERY STRONG EVIDENCE OF PERIODICITY (SPACING 14.00)

THERE IS STRONG EVIDENCE OF PREDOMINANT ELEMENT SIZE (8.00)
WITH MODERATE SUPPORT FOR ELEMENT SPACING (14.00)
RATIO OF SIZE TO PERIOD IS .57

THERE IS STRONG EVIDENCE OF PREDOMINANT ELEMENT SIZE (10.00)
WITH STRONG SUPPORT FOR ELEMENT SPACING (14.00)
RATIO OF SIZE TO PERIOD IS .71

30 DEGREE SCAN DIRECTION

THERE IS STRONG EVIDENCE OF PREDOMINANT ELEMENT SIZE (8.08)

THERE IS STRONG EVIDENCE OF PREDOMINANT ELEMENT SIZE (32.33)

60 DEGREE SCAN DIRECTION

THERE IS STRONG EVIDENCE OF PERIODICITY (SPACING 13.86)

THERE IS STRONG EVIDENCE OF PREDOMINANT ELEMENT SIZE (8.08)
WITH STRONG SUPPORT FOR ELEMENT SPACING (13.85)
RATIO OF SIZE TO PERIOD IS .58

Figure 2-28. Floor Grating Texture Description

112

FILENAME = FLOOR GRATING

DARK OBJECT DESCRIPTIONS

VERTICAL SCAN DIRECTION

THERE IS STRONG EVIDENCE OF PREDOMINANT ELEMENT SIZE (8.00)

THERE IS STRONG EVIDENCE OF PREDOMINANT ELEMENT SIZE (10.00)

THERE IS STRONG EVIDENCE OF PREDOMINANT ELEMENT SIZE (32.00)

120 DEGREE SCAN DIRECTION

THERE IS VERY STRONG EVIDENCE OF PERIODICITY (SPACING 13.85)

THERE IS STRONG EVIDENCE OF PREDOMINANT ELEMENT SIZE (8.08)
WITH STRONG SUPPORT FOR ELEMENT SPACING (13.86)
RATIO OF SIZE TO PERIOD IS .58

150 DEGREE SCAN DIRECTION

THERE IS STRONG EVIDENCE OF PREDOMINANT ELEMENT SIZE (8.08)

THERE IS STRONG EVIDENCE OF PREDOMINANT ELEMENT SIZE (32.33)

Figure 2-28. Continued

113

FILENAME = FLOOR GRATING

LIGHT OBJECT DESCRIPTIONS

HORIZONTAL SCAN DIRECTION

THERE IS VERY STRONG EVIDENCE OF PERIODICITY (SPACING 14.00)

THERE IS STRONG EVIDENCE OF PREDOMINANT ELEMENT SIZE (4.00)
WITH STRONG SUPPORT FOR ELEMENT SPACING (14.00)
RATIO OF SIZE TO PERIOD IS .29

THERE IS STRONG EVIDENCE OF PREDOMINANT ELEMENT SIZE (5.00)

30 DEGREE SCAN DIRECTION

THERE IS STRONG EVIDENCE OF PREDOMINANT ELEMENT SIZE (15.01)

THERE IS STRONG EVIDENCE OF PREDOMINANT ELEMENT SIZE (16.17)

60 DEGREE SCAN DIRECTION

THERE IS STRONG EVIDENCE OF PERIODICITY (SPACING 13.85)

THERE IS STRONG EVIDENCE OF PREDOMINANT ELEMENT SIZE (5.77)
WITH MODERATE SUPPORT FOR ELEMENT SPACING (13.86)
RATIO OF SIZE TO PERIOD IS .42

Figure 2-28. Continued

114

FILENAME = FLOOR GRATING

LIGHT OBJECT DESCRIPTIONS

VERTICAL SCAN DIRECTION

THERE IS STRONG EVIDENCE OF PREDOMINANT ELEMENT SIZE (14.00)

THERE IS STRONG EVIDENCE OF PREDOMINANT ELEMENT SIZE (16.00)

120 DEGREE SCAN DIRECTION

THERE IS VERY STRONG EVIDENCE OF PERIODICITY (SPACING 13.86)

THERE IS STRONG EVIDENCE OF PREDOMINANT ELEMENT SIZE (5.77)
WITH STRONG SUPPORT FOR ELEMENT SPACING (13.86)
RATIO OF SIZE TO PERIOD IS .42

150 DEGREE SCAN DIRECTION

THERE IS STRONG EVIDENCE OF PREDOMINANT ELEMENT SIZE (16.17)

Figure 2-28. Continued

115

FILENAME = WATER

DARK OBJECT DESCRIPTIONS

HORIZONTAL SCAN DIRECTION

   HIGHLY DIRECTIONAL RANDOM PATTERN

   NO EVIDENCE OF PERIODICITY
   VERY STRONG EVIDENCE OF PREDOMINANT ELEMENT SIZE (3.00)

LIGHT OBJECT DESCRIPTIONS

HORIZONTAL SCAN DIRECTION

   HIGHLY DIRECTIONAL RANDOM PATTERN

   NO EVIDENCE OF PERIODICITY
   VERY STRONG EVIDENCE OF PREDOMINANT ELEMENT SIZE (3.00)

120 DEGREE SCAN DIRECTION

   NO EVIDENCE OF PERIODICITY
   MODERATE EVIDENCE OF PREDOMINANT ELEMENT SIZE (30.02)

Figure 2-29. Water Texture Description

116

FILENAME = WOOD

DARK OBJECT DESCRIPTIONS

HORIZONTAL SCAN DIRECTION

   NO EVIDENCE OF PERIODICITY
   VERY STRONG EVIDENCE OF PREDOMINANT ELEMENT SIZE (3.00)

30 DEGREE SCAN DIRECTION

LIGHT OBJECT DESCRIPTIONS

HORIZONTAL SCAN DIRECTION

   HIGHLY DIRECTIONAL RANDOM PATTERN

   NO EVIDENCE OF PERIODICITY
   VERY STRONG EVIDENCE OF PREDOMINANT ELEMENT SIZE (3.00)

VERTICAL SCAN DIRECTION

   NO EVIDENCE OF PERIODICITY
   MODERATE EVIDENCE OF PREDOMINANT ELEMENT SIZE (3.00)

Figure 2-30. Wood Texture Description

117

patterns in the horizontal scan direction description.
The strongest evidence reported is for an element size of
3 in the horizontal scan direction for both light and dark
objects.

The 2 straw images are described in Figs. 2-31 And
2-32. The major difference between these 2 descriptions
is the fact that light element sizes are reported in 5 out
of 6 of the scan direction descriptions in Fig. 2-32. On
the other hand, predominant element sizes are indicated in
only 2 scan directions in Fig. 2-31. Looking at the
corresponding straw images (Fig. 2-13(a) bottom row)
clarifies this question. The pieces of straw are stacked
in one direction in the first straw image. In the second
picture of straw, the pieces are placed in a much more
random fashion. The descriptions are, therefore, quite
reasonable.

The remaining 4 texture images have roughly the same
descriptions, see Figs. 2-33 through 2-36. In all 4
cases, there are no texture periods given. No texture
period is apparent in the corresponding texture images.
The element sizes are all roughly the same size and they
occur in the same directions. One noticeable difference
in these descriptions is that the grass image is described
as a moderately directional random pattern while the

118

```
FILENAME = STRAW1

DARK OBJECT DESCRIPTIONS

60 DEGREE SCAN DIRECTION

    NO EVIDENCE OF PERIODICITY
    VERY STRONG EVIDENCE OF PREDOMINANT ELEMENT SIZE ( 2.31 )

VERTICAL SCAN DIRECTION

    THERE IS MODERATE EVIDENCE OF PREDOMINANT ELEMENT SIZE ( 3.00 )

LIGHT OBJECT DESCRIPTIONS

50 DEGREE SCAN DIRECTION

    HIGHLY DIRECTIONAL RANDOM PATTERN

    NO EVIDENCE OF PERIODICITY
    STRONG EVIDENCE OF PREDOMINANT ELEMENT SIZE ( 2.31 )

VERTICAL SCAN DIRECTION

    NO EVIDENCE OF PERIODICITY
    MODERATE EVIDENCE OF PREDOMINANT ELEMENT SIZE ( 3.00 )
```

Figure 2-31. Strawl Texture Description

119

```
FILENAME = STRAW2

DARK OBJECT DESCRIPTIONS

30 DEGREE SCAN DIRECTION

    NO EVIDENCE OF PERIODICITY
    WEAK EVIDENCE OF PREDOMINANT ELEMENT SIZE ( 2.31 )

60 DEGREE SCAN DIRECTION

    NO EVIDENCE OF PERIODICITY
    STRONG EVIDENCE OF PREDOMINANT ELEMENT SIZE ( 2.31 )

LIGHT OBJECT DESCRIPTIONS

HORIZONTAL SCAN DIRECTION

    NO EVIDENCE OF PERIODICITY
    STRONG EVIDENCE OF PREDOMINANT ELEMENT SIZE ( 3.00 )

30 DEGREE SCAN DIRECTION

    NO EVIDENCE OF PERIODICITY
    MODERATE EVIDENCE OF PREDOMINANT ELEMENT SIZE ( 2.31 )

60 DEGREE SCAN DIRECTION

    MODERATELY DIRECTIONAL RANDOM PATTERN

    NO EVIDENCE OF PERIODICITY
    STRONG EVIDENCE OF PREDOMINANT ELEMENT SIZE ( 2.31 )

VERTICAL SCAN DIRECTION

    NO EVIDENCE OF PERIODICITY
    MODERATE EVIDENCE OF PREDOMINANT ELEMENT SIZE ( 3.00 )

120 DEGREE SCAN DIRECTION

    NO EVIDENCE OF PERIODICITY
    WEAK EVIDENCE OF PREDOMINANT ELEMENT SIZE ( 2.31 )
```

Figure 2-32. Straw2 Texture Description

```
FILENAME = GRASS

DARK OBJECT DESCRIPTIONS

HORIZONTAL SCAN DIRECTION

    MODERATELY DIRECTIONAL RANDOM PATTERN

    NO EVIDENCE OF PERIODICITY
    MODERATE EVIDENCE OF PREDOMINANT ELEMENT SIZE ( 3.00 )

VERTICAL SCAN DIRECTION

    NO EVIDENCE OF PERIODICITY
    WEAK EVIDENCE OF PREDOMINANT ELEMENT SIZE ( 3.00 )

LIGHT OBJECT DESCRIPTIONS

HORIZONTAL SCAN DIRECTION

    NO EVIDENCE OF PERIODICITY
    STRONG EVIDENCE OF PREDOMINANT ELEMENT SIZE ( 3.00 )

30 DEGREE SCAN DIRECTION

    NO EVIDENCE OF PERIODICITY
    WEAK EVIDENCE OF PREDOMINANT ELEMENT SIZE ( 2.31 )

VERTICAL SCAN DIRECTION

    NO EVIDENCE OF PERIODICITY
    STRONG EVIDENCE OF PREDOMINANT ELEMENT SIZE ( 3.00 )

150 DEGREE SCAN DIRECTION

    NO EVIDENCE OF PERIODICITY
    WEAK EVIDENCE OF PREDOMINANT ELEMENT SIZE ( 2.31 )
```

Figure 2-33. Grass Texture Description

```
FILENAME = SAND

DARK OBJECT DESCRIPTIONS

HORIZONTAL SCAN DIRECTION

    NO EVIDENCE OF PERIODICITY
    MODERATE EVIDENCE OF PREDOMINANT ELEMENT SIZE ( 3.00 )

VERTICAL SCAN DIRECTION

    NO EVIDENCE OF PERIODICITY
    STRONG EVIDENCE OF PREDOMINANT ELEMENT SIZE ( 3.00 )

LIGHT OBJECT DESCRIPTIONS

HORIZONTAL SCAN DIRECTION

    NO EVIDENCE OF PERIODICITY
    MODERATE EVIDENCE OF PREDOMINANT ELEMENT SIZE ( 4.00 )

VERTICAL SCAN DIRECTION

    NO EVIDENCE OF PERIODICITY
    MODERATE EVIDENCE OF PREDOMINANT ELEMENT SIZE ( 3.00 )
```

Figure 2-34. Sand Texture Description

FILENAME = WOOL1

DARK OBJECT DESCRIPTIONS

HORIZONTAL SCAN DIRECTION

THERE IS MODERATE EVIDENCE OF PREDOMINANT ELEMENT SIZE (3.00)

VERTICAL SCAN DIRECTION

NO EVIDENCE OF PERIODICITY
MODERATE EVIDENCE OF PREDOMINANT ELEMENT SIZE (3.00)

LIGHT OBJECT DESCRIPTIONS

VERTICAL SCAN DIRECTION

THERE IS WEAK EVIDENCE OF PREDOMINANT ELEMENT SIZE (3.00)

Figure 2-35. Wool 1 Texture Description

123

FILENAME = WOOL2

DARK OBJECT DESCRIPTIONS

HORIZONTAL SCAN DIRECTION

NO EVIDENCE OF PERIODICITY
MODERATE EVIDENCE OF PREDOMINANT ELEMENT SIZE (3.00)

VERTICAL SCAN DIRECTION

NO EVIDENCE OF PERIODICITY
STRONG EVIDENCE OF PREDOMINANT ELEMENT SIZE (3.00)

LIGHT OBJECT DESCRIPTIONS

HORIZONTAL SCAN DIRECTION

THERE IS MODERATE EVIDENCE OF PREDOMINANT ELEMENT SIZE (3.00)

THERE IS MODERATE EVIDENCE OF PREDOMINANT ELEMENT SIZE (4.00)

Figure 2-36. Wool 2 Texture Description

others are not. It would seem that this characterization is quite reasonable.

2.5 Summary and Conclusions

In this chapter some earlier approaches to structural texture feature description were discussed. The edge repetition array method was presented and examined in detail. ERA results were displayed and discussed for a set of natural texture images containing both regular and random texture patterns. A systematic process for interpreting ERA results was presented, and both an outline and a detailed description of the algorithm were given. Finally, descriptions automatically generated for the original set of texture images were presented and discussed.

It has been shown that ERAs can be used to extract textural information which can, in turn, be automatically interpreted to produce structural texture descriptions. Such features as periodicity, directionality, and predominant element size of both light and dark intensity textural elements can be extracted from ERA results using the algorithm described above. A basic assumption for use of this technique is that textural elements are locally bounded by pairs of oppositely oriented parallel edges. If this were not the case then element sizes would not be

found. An image composed of perfectly triangular objects might produce a texture period peak in some directions but no element size peaks for the triangular elements would be found. A similar problem occurs when a textural element is bordered by a lighter element on one side and a darker element on the other. In this case, the element size for the darkest element will be found as well as an element size for the combined darkest and middle intensity element. However, the middle intensity element boundaries are mistakenly seen as period boundaries. Extensions to this basic method should include mechanisms to handle such special cases.

CHAPTER 3

EXTRACTION AND ANALYSIS OF TEXTURAL PRIMITIVES

3.1 Introduction

In the previous chapter a technique for automatically generating descriptions of natural texture images was presented. These descriptions provide regularity (periodicity), direction, element size, and element relative intensity information. The element size information is the dimension of the element in the particular scan direction for which the description was generated. Therefore, we have only one-dimensional descriptions for 2-dimensional texture primitives. In this chapter, a technique for extracting and analyzing texture primitives is presented. The starting point of this process is the texture description generated by the algorithm discussed in Chapter 2. The end product is a set of primitive masks (one for each texture primitive type) and descriptions of each primitive type found. A composite primitive image is also produced. All of the separate primitive masks are included in this image. However, the intensity of a particular primitive is set to

127

the average intensity found for that primitive. After the algorithm is described in detail the results generated for the texture images analyzed in Chapter 2 will be presented and discussed.

3.2 Texture Primitive Extraction Methods

Texture primitives have been defined as line segments, uniform intensity regions, parallelogram tiles or even pixels. The primitive extraction technique one uses depends on the type of primitive to be isolated. The following is a brief overview of some previously used primitive extraction methods.

Conners and Harlow [12] define texture primitives to be parallelogram tiles which are repeated in 2 non-collinear directions to cover the plane. The size, shape, and orientation of the basic textural primitive is found by examining the inertia measure values for spatial gray level dependence matrices calculated for a number of different directions. Valleys in these graphs correspond to the texture period in the given direction. By choosing the 2 directions giving the smallest texture period (in Euclidean magnitude) the orientation, size, and placement rules of the tile can be obtained. Size, shape, and orientation do not completely characterize the texture tile or unit cell. A painting function or tile pattern

128

must also be specified. One problem with this method is that many different tiles or unit cells can be found for a given texture. Also, this characterization is only meaningful when working with periodic textures.

The texture primitive representation used by Ehrich and Foith [17] does not share this latter restriction. The unit patterns which they extract are aggregates of 2-dimensional gray level peaks. The atomic regions are light intensity areas bounded by darker intensity areas on either side in a given scan direction. More complex regions are formed by recursive clustering using the method of relational trees. One problem with this method is the assumption that a textural element will be centered at an intensity peak. There may be a problem if an element is relatively light in one scan direction and relatively dark in another. In this case the element will not be at an intensity peak, it will be at a saddle point.

In [18] Wang, Velasco, Wu, and Rosenfeld describe and contrast 3 different thresholding based primitive extraction methods. Their primitives are connected regions whose pixel intensities are above or below a given threshold.

An alternative method for characterizing textural elements is to define them as uniform intensity regions

129

within the texture. Such a characterization is used by Tsuji and Tomita [29], and Matsuyama, Saburi, and Nagao [20]. Maleson, Brown, and Feldman [19] use a region growing technique to divide the image into uniform intensity regions which are then approximated by ellipses. These elliptical texture primitives are then classified with respect to similar intensity and shape characteristics.

The texture primitive characterization to be presented here requires that individual textural elements be regions of like relative intensity. However, primitive intensity need not be uniform over the entire primitive group. The intensity constraint used here has to do with relative and not absolute intensity. That is, texture primitives of the same type must exhibit the same relative intensity with respect to surrounding regions in a particular scan direction. Primitive groups are not only able to contain elements of various intensities; but they are not constrained to contain all uniform intensity areas exhibiting the same average gray level. This primitive extraction technique should therefore be less sensitive to intensity differences due to natural variation and illumination over the texture images. Other constraints, e.g., element size and orientation are also used. All of this information is available in the set of ERA

descriptions calculated for the texture.

3.3 The Primitive Extraction Process

3.3.1 Descriptive Overview

The primitive extraction process to be presented here uses the one-dimensional texture descriptions generated by the algorithm discussed in Chapter 2.   For example, the primitive   search   for   the   raffia   texture   image   of Fig. 2-2(a) would begin with the   internal   form   of   the texture   description   found   in   Fig. 2-24.   One might be tempted to try to use the individual components of the description to form a two-dimensional description of some of the textural elements. Since a light element size of 3 is found in the horizontal scan direction and one of 5 is found in the vertical scan direction, the existence of a light   element with horizontal dimension 3 pixels and vertical dimension 5 pixels would be assumed. This is, in fact,   not   the   case.   Fig. 3-1   is   an   abstract representation of the basic raffia primitive cluster. The light element found in the vertical scan direction is the medium intensity block A of Fig. 3-1, while the light element found by the horizontal scan is the high intensity block C in Fig. 3-1. If both dimensions of block A were found then the vertical dimension would be characterized as belonging to a light element while the horizontal

131
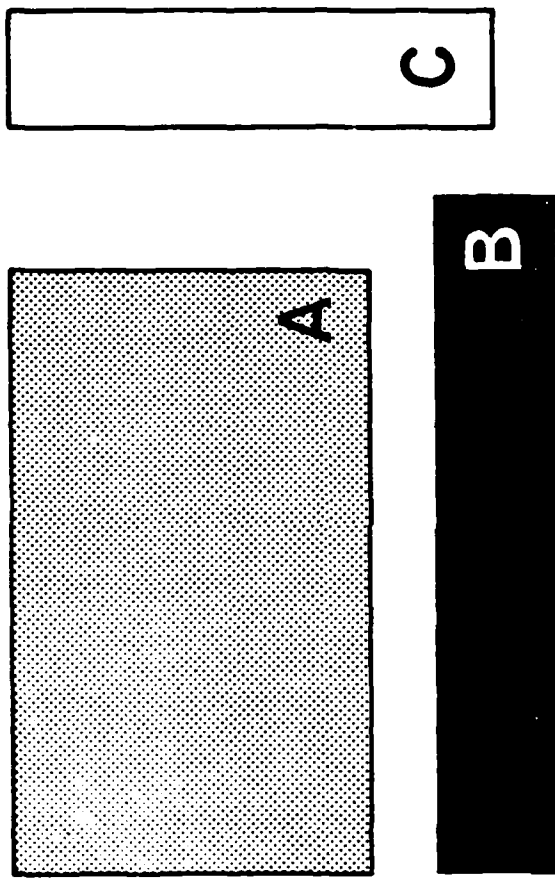
Figure 3-1. Abstract Representation of Raffia
Primitives

dimension would be described as belonging to a dark element. Clearly, a two dimensional description of the texture cannot be constructed by combining its one-dimensional parts. However, the one-dimensional descriptions are of use in the primitive extraction process.

Consider again the texture description given in Fig. 2-24. There are 3 strong indications of predominant element size. Light elements of size 5 and dark elements of size 3 are strongly indicated in the vertical scan direction, while light elements of size 3 are strongly indicated in the horizontal scan direction. Each of these predominant element sizes is the location of a strong peak in an element size edge repetition array for the raffia image in Fig. 2-2(a). Knowing the exact locations, within the original texture image, where the edge matches contributing to a particular strong peak occur would be useful. It would then be possible to isolate those regions being measured. The regions, or textural elements, would then be automatically grouped according to relative intensity and size with respect to the given scan direction. It is also known that one set of edges bounding each element of the group is oriented in the direction perpendicular to the direction of scan. By analyzing this set of textural elements, or primitives,

one could determine the average area and intensity of members of the group, and determine predominant element placement characteristics as well.

The primitive extraction process presented in this thesis is an implementation of the above idea. When considering an element size indicated for a particular scan direction and relative intensity, the directional scan is repeated for a restricted range of distances. When a match occurs the locations of the matching edges and their interior pixels are marked in an intermediate mask image. After the scan is completed the marked primitive interior slices are expanded to their "natural boundaries" in a direction perpendicular to the original scan direction. The criteria for expansion is based on the local pixel intensities within the original texture image as well as the locations of edges within the corresponding edge image. The final primitive mask image contains the expanded primitive interiors. The individual elements are then analyzed to determine an average primitive size and intensity for the group as well as predominant inter-element spacings for 2 perpendicular directions. If it can be established that the primitive type under consideration forms part of the background then this information is also noted. If it is determined that enough primitives of this type have been found to make

134

further analysis meaningful the primitive description is catalogued and the primitive mask is saved.

It is conceivable that a particular primitive can be detected in more than one scan direction. When this happens more than one mask image will refer to the same class of primitives. It is also possible to find 2 different primitive types having the same dimension and relative intensity in a particular scan direction. In this case, one primitive mask may contain primitives of more than one type. Primitive masks are merged or separated to rectify these situations.

At the end of this analysis there exists a set of reduced primitive masks and their respective descriptions. In the following section the primitive extraction algorithm will be explained in detail.

3.3.2 The Primitive Extraction Algorithm

The details of the primitive extraction algorithm are given in this section. This algorithm is composed of four major parts as follows:

1) Ordering of the information resulting from ERA interpretation with respect to relative significance.

2) Creating the individual and composite primitive masks.

135

3) Analyzing the primitive masks.

4) Merging or separating primitive masks when they are sufficiently overlapped.

Information Ordering

One part of the internal texture description which was calculated but not used before this algorithm is the significance number. A significance number is calculated for each (intensity, direction) pair. It is used to classify the 12 pairs of ERAs in terms of their relative "importance." The importance of each (element spacing, element size) ERA pair depends on the maximum peak amplitudes in each ERA and the number of potential matching edges found by each directional scan. The maximum peak amplitudes are easily found and the maximum normalization number for a given ERA reflects the number of properly oriented edges encountered. The significance number of ERA set, I, where $I \epsilon \{1,2,...,12\}$, is simply the average of the four ratios given below:

1) (Maximum Amplitude for Element Spacing ERA [I])/(Maximum Amplitude Over All Element Spacing ERAs)

2) (Maximum Amplitude for Element Size ERA [I])/(Maximum Amplitude Over All Element Size ERAs)

136

3) (Maximum Normalization Number for Element Spacing ERA [I])/(Maximum Normalization Number Over All Element Spacing ERAs)

(4) (Maximum Normalization Number for Element Size ERA [I])/(Maximum Normalization Number Over All Element Size ERAs).

The descriptive information calculated for each (intensity, direction) pair is considered for primitive extraction in order of decreasing significance number of the given pair. Both the relative ordering of information and the significance numbers themselves will be used in the classification scheme presented in Chapter 5.

Primitive Mask Creation

At this point the (intensity, direction) pairs have been sorted according to significance number. The descriptive information for each pair is considered in turn. When evidence of a predominant element size is found for a given (direction, intensity) pair a scan similar to the original ERA scan is initiated. Since the object of this scan is to pinpoint only certain matches it will differ from the original ERA scan in the following ways:

137

1) The scan is over a restricted range of distances. This range will contain the element size peak distances with a margin of one pixel in distance at either end.

2) Only the indicated scan direction is used; and matches are sought only for element sizes of the indicated relative intensity.

3) Instead of recording the edge matches in an edge repetition array the 2 matching edges are marked in a blank image in locations corresponding to their locations in the original edge image. The interior points, points lying between the 2 matching edges along the direction of scan, are also marked.

In Fig. 3-2, the marking scheme is illustrated. Both edges are marked by "E"'s. The edge exhibiting the lower row location (and if this test fails the lower column location) is marked in a special way as a starred edge. The points between the 2 edges along the line of scan are marked as interior points, "I."

The image produced by this process is the intermediate primitive image. This image consists of zeros except where edge matches and their interior points are marked as in Fig. 3-2.

```
0    0    0    0    0    0    0    0

0    0    0    E*   0    0    0    0

0    0    0    I    0    0    0    0

0    0    0    I    0    0    0    0

0    0    0    I    0    0    0    0

0    0    0    E    0    0    0    0

0    0    0    0    0    0    0    0
```

Figure 3-2.   Non-Expanded Primitive in Vertical
              Scan Direction

```
0    0    0    0    0    0    0    0

0    0    0    Ա    0    0    0    0

0    1    1    1    1    1    0    0

0    0    1    1    1    1    1    0

0    1    1    1    1    1    0    0

0    0    0    0    0    0    0    0

0    0    0    0    0    0    0    0
```

Figure 3-3.   Expanded Primitive for Fig. 3-2

139

The next step is the expansion of the interiors of the primitive slices to form a binary mask image for the primitive set. In the expansion process the original texture image and the edge image are used.

The intermediate primitive image is searched until a starred "E" is encountered. Proceeding in the direction of scan the first interior point, "I," is found. A "1" is placed in the binary mask image at this point and the texture image intensity of this point is noted. This is repeated until the edge mark at the end of the primitive slice is encountered. The range of intensity values for the interior pixels of the primitive slice is now known. At this point the primitive interior can be expanded to its "natural boundary." The natural boundary of a primitive is made up of:

1) the edges given in the edge image;

2) pixels whose intensities are outside of the interior intensity range by more than 10 gray levels; and,

3) the boundary of the texture image itself.

Expansion of the primitive slice proceeds outward from its interior points in a direction perpendicular to the direction of scan. Figure 3-3 shows the expanded primitive within the primitive mask image corresponding to

140

the primitive slice in Fig. 3-2. During the primitive expansion process the composite primitive masks image is being updated to include the current set of textural elements. The value of the entries is the average intensity of the particular textural element being expanded.

After all of the elements have been expanded both the primitive mask and the intermediate primitive mask are used to estimate predominant inter-element spacing in the scan direction and in the direction perpendicular to the direction of scan. Both of these quantities are used later in the program when the expected number of elements of this type is calculated.

Primitive Mask Analysis

After all the primitives of a given type have been expanded the primitive set can be analyzed. A region extractor is used so that each individual texture element can be examined to determine its area in pixels and its average intensity value. At the time of examination any pixel sized holes found in individual textural elements are filled in the primitive mask and are examined as part of the element. Due to the nature of the primitive expansion technique, the primitive dimension in the direction perpendicular to the direction of scan can be

141

approximated by dividing the primitive area by the scan direction dimension.

When all of the elements have been examined the average primitive intensity value, size in pixels and dimensions in 2 perpendicular directions are calculated. This information forms part of the description of the primitive type defined by the mask being analyzed.

Another part of the primitive description is the background flag. The importance of this flag is to indicate that the primitive dimensions may not be meaningful. Also, when distances between the centroids of different textural elements are being calculated and analyzed in the primitive placement rule detection section (see Chapter 4) primitives of this type are automatically marked for exclusion.

During primitive mask analysis two conditions, either of which would indicate that the primitive under consideration forms part of the image background, are watched for. The two background tests are given below. (Note that the second dimension of a primitive is its dimension oriented perpendicular to the direction of scan.)

1) If the ratio of (primitive size in pixels) to (maximum

possible element dimension in the scan direction) for any textural element is greater than twice the maximum possible dimensional distance, given the image boundaries, then this primitive forms part of the image background.

2) If at last 40% of the elements of a given type have their second dimension greater than or equal to 95% of the maximum possible dimensional distance, given the boundaries of the image, then this primitive forms part of the image background.

Consider the dark dot pattern in Fig. 2-8(a). Obviously, the high intensity area surrounding the dots forms the image background. Light intensity elements are found in the vertical scan direction for this texture pattern. They are the spaces between vertically neighboring dots. Expanding these primitive slices in the horizontal direction will cause them to be joined to neighboring strips. The resulting primitive mask will contain one huge primitive. Since the vertical element dimension is obtained from the ERA description and the element area is the actual pixel count the second dimension calculation will produce an impossibly large number. This condition would be detected by the first background test.

The second background test detects textural elements which extend from one end of the image to the other. An example of this type of primitive is the vertical mortar strips in the non-shifted brick pattern of Fig. 1-1).

The final task to be performed in this section is to determine if enough textural elements were found to consider this primitive type a meaningful component of the texture.

If the primitive type forms part of the background then a sample set size of 1 is sufficient. In all other cases a_ least 10, and possibly more, textural elements must be found. In any case, 30 elements are deemed sufficient to qualify the primitive type. A special floor value is calculated to handle borderline cases with sample set size of less than 30, but at least 10 elements. In these cases at least one third of the expected number of textural primitives must be found. The expected number of texture primitives, E, is calculated as follows:

$$E = \frac{\text{Image area}}{(DIM1 + ELSP1) * (DIM2 + ELSP2)} \quad ,$$

where DIM1 and DIM2 are the primitive dimensions in the scan direction and the direction perpendicular to the direction of scan, respectively. Similarly, ELSP1 and ELSP2 are the predominant inter-element spacings in these

144

2 directions. The image area, as well as all of the distances are in pixels.

As explained earlier background elements may merge to form only one primitive, therefore, a floor value of 1 is sufficient for them. Any primitive group with less than 10 elements is highly suspect. If the element dimensions or spacings are so big that not even ten elements can fit into the image, then a window size problem is indicated. If there is no size or spacing problem then the primitive type is even more questionable and should be dismissed. In either case, the averages calculated for so small a sample set are of little value. Between 10 and 30 primitives is still a fairly small sample set size for elements of a texture. However, if this set represents at least one third of the expected number of primitives then it is accepted. This range is marginal; but it does represent a substantial percentage of the expected number of samples. 30 is assumed to be a large enough set size so that the average measurements calculated will be meaningful. These conclusions are based on tests with a wide range of texture types for texture windows of 128 x 128 or 256 x 256 pixels. If one is dealing with much larger texture windows then other thresholds might be more meaningful. If the textures being considered were artificially generated perfect patterns then the

145

thresholds discussed above would be unnecessary. However, when dealing with natural textures there can be considerable elemental variation, hence, the need for a reasonably-sized set of elements.

If it is determined that too few samples have been found then the primitive expansion process is repeated for the next potential element size value for the current (intensity, direction) pair. If the sample set size is acceptable then the ERA description for the next (intensity, direction) pair is considered. Only one primitive type for each (intensity, direction) pair is currently handled. Extending the program to handle more than this would be a natural next step.

Merging and Separation of Primitive Types

The final part of the algorithm deals with merging primitive masks when it is determined that they are defining the same primitive type; and separating primitive masks when it is recognized that more than one primitive type is being defined.

After a primitive mask is analyzed and accepted as defining a bona fide primitive type it is ANDed with the primitive masks of each other existing primitive type to check for overlap. When overlap is more than one third of

146

the pixels covered by either mask separately, then the masks will be either merged or separated.

The primitive masks will be separated only when all of the following occur:

1) Neither primitive type forms part of the background.

2) The scan directions used to create the 2 primitive sets are perpendicular.

3) There is a discrepancy in the average primitive areas of the 2 primitive sets. (The average area of the smaller primitive is less than two thirds of the average area for the larger one.)

4) There is a discrepancy in the average intensities of the 2 separated mask areas. (The average intensity of the masked area defining the smaller primitives differs by at least 30 gray levels from the average intensity of the masked area defining the larger primitives minus the area of intersection).

If all 4 conditions hold then the mask containing the smaller primitives is subtracted from the mask containing the larger primitives. Next, the average intensity and element size found for the larger primitive type is adjusted using a region extractor on the updated primitive

147

mask. If the 4 conditions do not hold then the 2 masks
are merged (ORed) and their descriptions are linked. In
this case no new primitive type is defined.

The requirement that the 2 primitive masks be defined
having perpendicular directions of scan before separation
is considered stems from the particular type of problem
being corrected and the nature of the expansion technique.
Consider the primitives in Fig. 3-4(a). Both type A and
type B primitives have the same relative intensity and
element size with respect to the vertical scan direction.
When relatively light vertical elements with element size,
d, are extracted both element types will be represented by
the same primitive mask. Clearly, only elements with
vertical edges found by a horizontal scan will be useful
in separating these primitives. The intensity requirement
4) is used to prevent texture primitives like the one in
Fig. 3-4(b) from being subdivided.

In the following section primitive extraction results
for the texture samples analyzed in Chapter 2 will be
presented and discussed. The amount of CPU time needed
for the entire primitive extraction process depends on the
number of potential primitive types and their respective
numbers of textural elements. Sixteen 128 x 128 pixel
floor grating texture samples averaged approximately 1
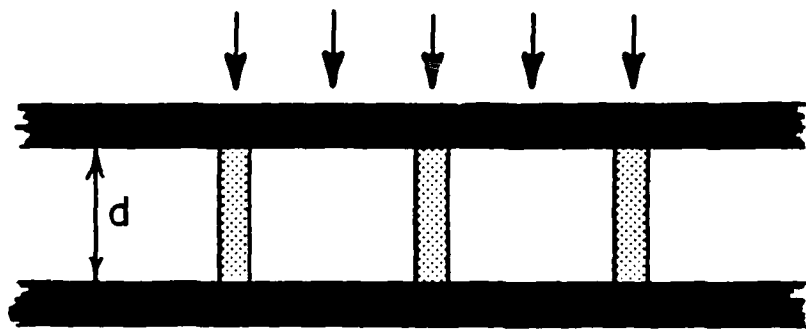
(a)   2 Different Primitives Found in a
       Single Scan Direction
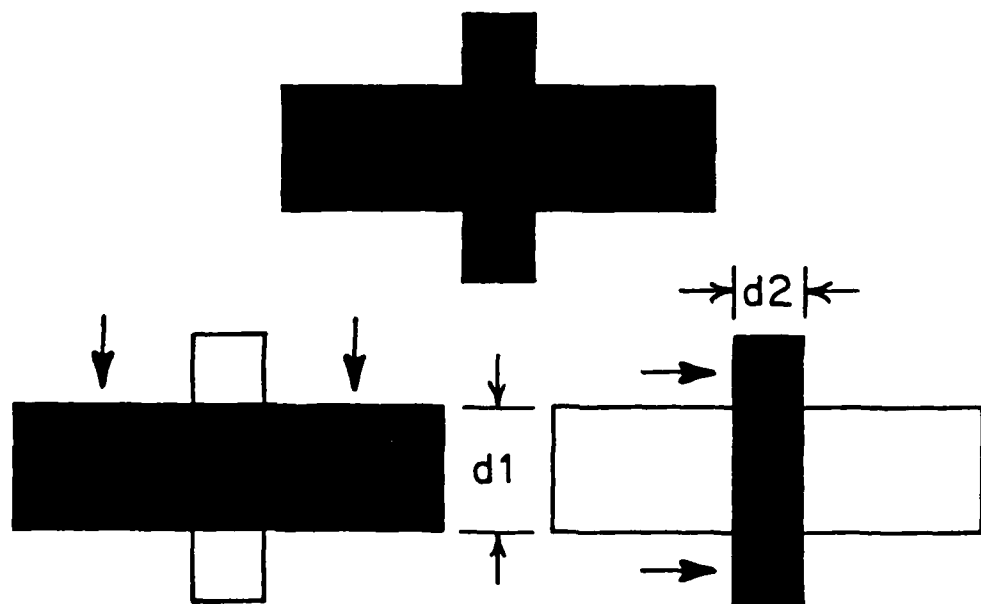
(b) Parts of a Single Primitive Found in 2
     Scan Directions

Figure 3-4.   Primitive Separation and Merging Examples

149

minute of CPU time each on a DEC KL-10 processor. A potential textural element was sought for each intensity, direction pair for every one of the 16 subwindows.

3.4 Primitive Extraction Results

In this section primitive extraction results are presented for the texture samples discussed in Chapter 2. Consider the raffia texture image in Fig. 2-2(a). Its corresponding ERA description is given in Fig. 2-24. There are 3 strong indications of element size in this description. Dark elements of size 3 are found in the vertical scan direction. This element type corresponds to the B type element of Fig. 3-1. Light elements of size 3 in the horizontal scan direction, and 5 in the vertical scan direction are also noted. These correspond to primitives of type C and A (of Fig. 3-1), respectively. In Fig. 3-5, the individual primitive masks for the 3 raffia primitives are given. They correspond to the primitives of type A, B, and C (of Fig. 3-1), respectively. Figure 3-6(a) and (b) are the original raffia texture image and its composite primitive mask. The diagonally oriented elements represent a primitive type which was rejected because too few textural elements were found. These elements were caused by irregularities in the texture. (See Fig. 3-6(a)). The composite
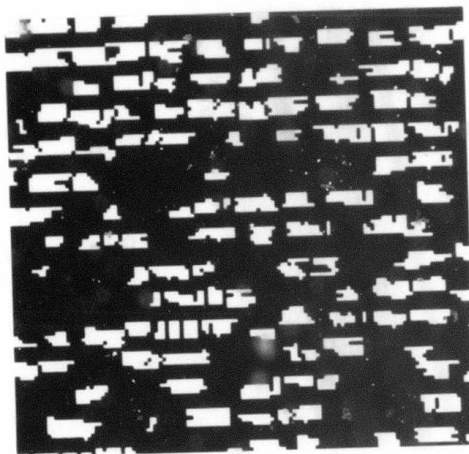
(a) Raffia Texture Primitive Type A
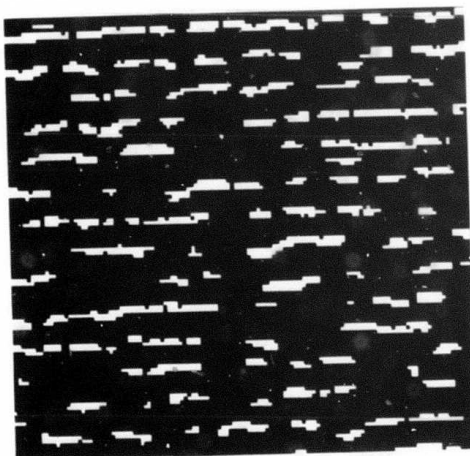
(b) Raffia Texture Primitive
Type B
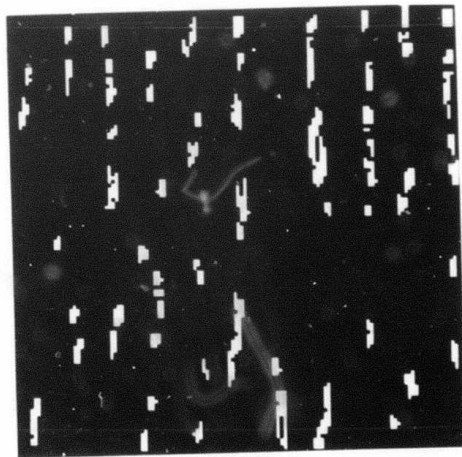
(c) Raffia Texture Primitive
Type C

Figure 3-5.   Raffia Primitives
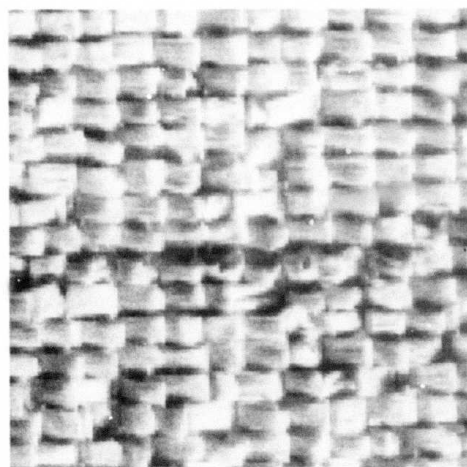
(a) Raffia Texture Image

(b) Composite Primitive Mask Image for (a)

(c) Composite Primitive Mask Image for (a) with Rejected Primitives Excluded

Figure 3-6. Raffia and Composite Primitive Masks

primitive mask would appear like the image in Fig. 3-6(c) if these rejected elements were not included.

There is considerable intensity variation over different primitives of the same type in both the texture image and the composite mask images. The intensities used in these masks are the average intensities for the individual textural elements. In Fig. 3-7, the primitive descriptions for the 3 raffia primitive types are given. None of these primitives are merged or separated.

Only tabular primitive descriptions and composite primitive masks will be presented for the rest of the image samples. The composite primitive masks show all of the texture elements considered.

In Fig. 3-8(a) and (b), the periodic texture mosaic analyzed in Chapter 2 is presented with its corresponding set of composite texture primitive masks. The primitive descriptions for these textures is given in Tables 3-1 through 3-4.

The primitive descriptions for the first aerial city texture image are summarized in Table 3-1. Four primitives are found. The fourth texture primitive is a dark primitive found in the vertical scan direction with dimensions 12 in the vertical direction and 4 in the

PRIMITIVE ANALYSIS FOR RAFFIA

RELATIVE INTENSITY IS DARK   DIRECTION IS VERTICAL

    PRIMITIVE NUMBER IS: 1

NUMBER OF SAMPLES: 104   SIGNIFICANCE NUMBER: 1.00

    AVERAGE PRIMITIVE DIMENSIONS ARE: (2.00 AND 10.71)

    AVERAGE PRIMITIVE SIZE IN PIXELS IS: (20.93)

    AVERAGE PRIMITIVE INTENSITY IS: (128.37)

    PRIMITIVES REPEAT AT ELEMENT SPACING: (8.00)
    IN ABOVE MENTIONED DIRECTION

RELATIVE INTENSITY IS LIGHT   DIRECTION IS VERTICAL

    PRIMITIVE NUMBER IS: 2

NUMBER OF SAMPLES: 102   SIGNIFICANCE NUMBER: .83

    AVERAGE PRIMITIVE DIMENSIONS ARE: (4.00 AND 9.49)

    AVERAGE PRIMITIVE SIZE IN PIXELS IS: (37.31)

    AVERAGE PRIMITIVE INTENSITY IS: (172.48)

    PRIMITIVES REPEAT AT ELEMENT SPACING: (8.00)
    IN ABOVE MENTIONED DIRECTION

RELATIVE INTENSITY IS LIGHT   DIRECTION IS HORIZONTAL

    PRIMITIVE NUMBER IS: 3

NUMBER OF SAMPLES: 68   SIGNIFICANCE NUMBER: .48

    AVERAGE PRIMITIVE DIMENSIONS ARE: (2.00 AND 7.79)

    AVERAGE PRIMITIVE SIZE IN PIXELS IS: (14.99)

    AVERAGE PRIMITIVE INTENSITY IS: (190.44)

        Figure 3-7. Primitive Descriptions for Raffia

TABLE 3-1. PRIMITIVE DESCRIPTIONS FOR CITY1

PRIM NUMBER	REL INT	SCAN DIR	NUMBER OF SAMPLES	SIG NUMBER	DIM1*	DIM2**	AVERAGE AREA IN PIXELS	AVERAGE INT	PERIOD*** IN PIXELS	SEPARATED FROM
1	D	0°	144	.98	2.00	12.57	24.60	97.51	7.00	-
2	L	0°	59	.89	3.00	27.15	81.36	143.14	7.00	-
3	L	90°	51	.41	2.00	11.71	22.98	142.06	16.00	-
4	D	90°	68	.33	12.00	3.71	44.31	105.82	16.00	1,2

* Dimension in scan direction in pixels
** Average dimension perpendicular to scan direction in pixels
*** Period in the direction of scan

Legend: PRIM – PRIMITIVE
REL – RELATIVE
INT – INTENSITY
D – DARK
L – LIGHT
DIR – DIRECTION
SIG – SIGNIFICANCE

155
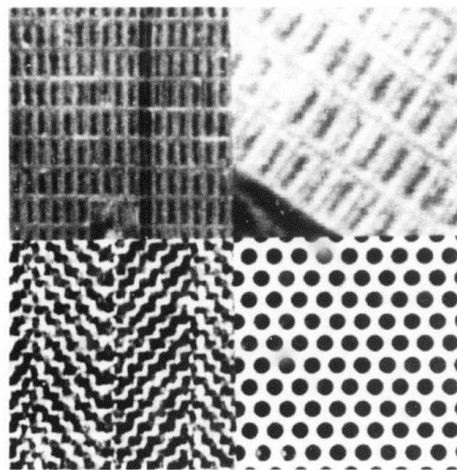
(a) Texture Mosaic Including City1, City2,
Herringbone and Grating Images
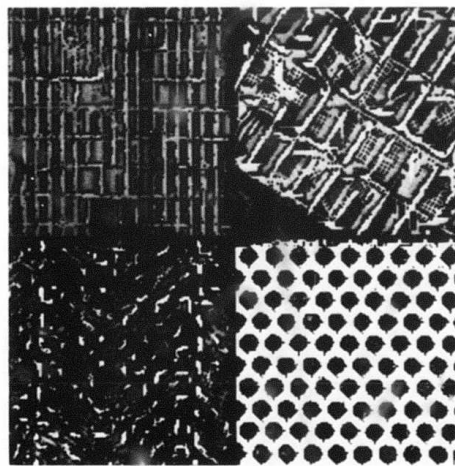
(b) Composite Primitive Images form (a)

Figure 3-8. Periodic Texture Mosaic and Composite
Primitive Masks

156

horizontal direction. This primitive is first separated from primitives of type 1, (dark, horizontal elements with dimensions 13 and 2) then from the primitive of type 2 (light, horizontal elements with dimensions 3 and 27). The primitive descriptions for the second aerial city image are given in Table 3-2. There are two sets of links to finally produce 3 texture element types. In Table 3-3 the herringbone material texture primitives are described. There are 6 separate primitive types. It seems that the dark vertical and horizontal texture elements expand to produce elongated primitives oriented at 45 and 135 degrees. These primitives correspond to the dark stripes in the herringbone pattern. The description generated for the grating primitives is quite lengthy. (See Table 3-4). Eleven primitive masks and descriptions are generated; but all of these primitives are merged into 2 primitive types, namely, the black dots and the white background. New primitive descriptions are not generated after merging. It is enough to know that all of the merged texture element descriptions actually refer to the same texture primitive type.

In Fig. 3-9(a) and (b) the first non-periodic texture mosaic (from Chapter 2) is presented with its corresponding set of composite texture primitive masks. The primitive descriptions for these textures is given in

157

(a) Texture Mosaic Including Water,
Wood, Straw1, and Straw2 Images
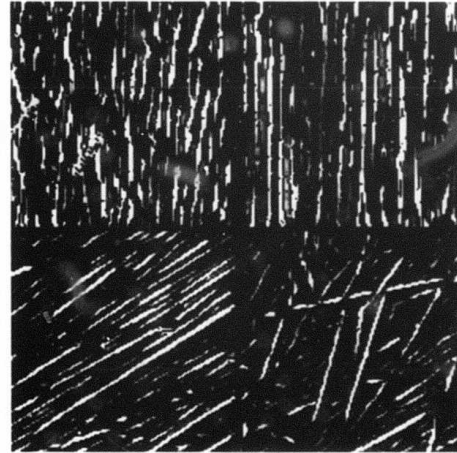
(b) Composite Primitive Images from (a)

Figure 3-9.   Non-Periodic Texture Mosaic and
Composite Primitive Masks

158

TABLE 3-2. PRIMITIVE DESCRIPTIONS FOR CITY2

PRIM NUMBER	REL INT	SCAN DIR	NUMBER OF SAMPLES	SIG NUMBER	DIM1*	DIM2**	AVERAGE AREA IN PIXELS	AVERAGE INT	PERIOD*** IN PIXELS	MERGED WITH
1	L	30°	27	.94	3.46	26.90	69.78	197.37	12.00	5
2	D	30°	30	.90	3.46	18.98	49.23	150.27	13.00	3
3	D	0°	29	.47	5.00	6.76	33.41	152.34	-	-
4	L	90°	29	.44	4.00	8.38	32.86	192.10	-	-
5	L	0°	26	.41	4.00	7.58	29.65	196.42	-	-
6	D	90°	19	.39	5.00	7.95	40.05	158.21	-	-
7	L	120°	15	.32	2.31	14.78	25.00	191.73	-	-
8	L	150°	11	.19	3.46	8.61	22.64	181.64	-	-

*Dimension in scan direction in pixels
**Average dimension perpendicular to scan direction in pixels
***Period in the direction of scan

Legend: PRIM - PRIMITIVE
REL - RELATIVE
INT - INTENSITY
D - DARK
L - LIGHT
DIR - DIRECTION
SIG - SIGNIFICANCE

159

Tables 3-5 through 3-8.

Note that the primitive descriptions for water and wood given in Table 3-5 and 3-6 are extremely similar. The one distinguishing characteristic seems to be the length of the two types of primitives. The wood primitives are considerably longer than the primitives found for water. The same comparison can be made for the original texture images and for the composite primitive masks as well.

In Tables 3-7 and 3-8, the straw primitive texture descriptions are given. One obvious difference is that the first straw texture sample has primitives oriented in only one direction while the second straw sample has 4 primitive types generated by 3 different scan directions. Both the texture and composite mask images bear out the directionality of the first sample and the lack of directionality in the second.

In Fig. 3-10(a) and (b) the mosaic composed of the most random texture group to be considered is presented along with its set of composite primitive masks. The primitive descriptions for these texture samples are given in Tables 3-9 through 3-12. The primitive descriptions for all 3 texture types (grass, sand, and wool) are quite similar as are the composite primitive masks in
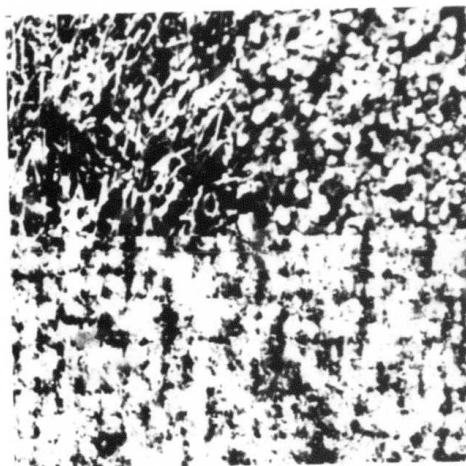
(a) Texture Mosaic Including Grass,
Sand, Wool 1, and Wool 2 Images
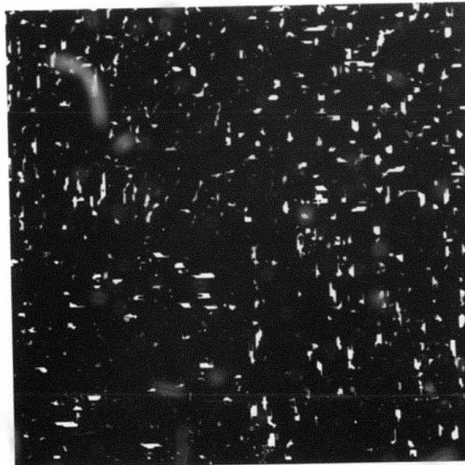
(b) Composite Primitive Images from (a)

Figure 3-10.   Random Texture Mosaic   and Composite
Primitive Masks

TABLE 3-3. PRIMITIVE DESCRIPTIONS FOR HERRINGBONE MATERIAL

PRIM NUMBER	REL INT	SCAN DIR	NUMBER OF SAMPLES	SIG NUMBER	DIM1*	DIM2**	AVERAGE AREA IN PIXELS	AVERAGE INT	PERIOD*** IN PIXELS
1	D	0°	70	.90	2.00	5.19	9.81	62.47	11.00
2	L	90°	50	.88	2.00	5.10	9.60	230.48	13.00
3	D	90°	92	.86	3.00	3.90	11.60	55.23	13.00
4	L	0°	80	.84	2.00	5.71	10.86	222.26	11.00
5	∼D	30°	20	.32	2.31	5.60	9.05	49.40	-
6	L	120°	17	.25	2.31	6.66	10.88	226.71	-

*Dimension in scan direction in pixels
**Average dimension perpendicular to scan
 direction in pixels
***Period in the direction of scan

Legend: PRIM - PRIMITIVE
 REL - RELATIVE
 INT - INTENSITY
 D - DARK
 L - LIGHT
 DIR - DIRECTION
 SIG - SIGNIFICANCE

162

TABLE 3-4. PRIMITIVE DESCRIPTIONS FOR FLOOR GRATING

| PRIM NUMBER	REL INT	SCAN DIR	NUMBER OF SAMPLES	SIG	DIM1*	DIM2**	AVERAGE AREA IN PIXELS	AVERAGE INT	PERIOD*** IN PIXELS	BACK-GROUND	MERGED WITH
1	D	90°	94	.89	7.00	5.89	41.10	34.94	–	–	4
2	L	90°	1	.87	–	–	7917.00	251.00	–	YES	3
3	L	0°	97	.81	3.00	10.52	31.59	252.97	14.00	–	7
4	D	0°	83	.80	7.00	6.43	44.70	31.95	14.00	–	5
5	D	60°	67	.54	6.93	5.20	26.48	20.84	12.00	–	6
6	D	120°	61	.47	6.93	5.07	25.59	20.56	12.00	–	8
7	L	120°	68	.46	4.62	11.56	39.74	253.80	12.00	–	10
8	D	30°	68	.46	6.93	5.30	27.12	22.46	–	–	9
9	D	150°	64	.45	6.93	5.21	26.63	22.28	–	–	–
10	L	60°	62	.43	4.62	11.71	39.92	253.60	12.00	–	11
11	L	30°	1	.33	–	–	4815.00	253.00	–	YES	–

*Dimension in scan direction in pixels
**Average dimension perpendicular to scan
   direction in pixels
***Period in the direction of scan

Legend: PRIM - PRIMITIVE
       REL - RELATIVE
       INT - INTENSITY
       D - DARK
       L - LIGHT
       DIR - DIRECTION
       SIG - SIGNIFICANCE

163

TABLE 3-5.   PRIMITIVE DESCRIPTIONS FOR WATER

PRIM NUMBER	REL INT	SCAN DIR	NUMBER OF PIXELS	SIG NUMBER	DIM1*	DIM2**	AVERAGE AREA IN PIXELS	AVERAGE INT
1	D	0°	111	.99	2.00	14.11	27.74	54.68
2	L	0°	99	.90	2.00	17.54	34.68	206.57

*Dimension in scan direction in pixels
**Average dimension perpendicular to scan
direction in pixels

Legend: PRIM - PRIMITIVE
         REL - RELATIVE
         INT - INTENSITY
         D - DARK
         L - LIGHT
         DIR - DIRECTION
         SIG - SIGNIFICANCE

TABLE 3-6. RPIMITIVE DESCRIPTIONS FOR WOOD GRAIN

PRIM NUMBER	REL INT	SCAN DIR	NUMBER OF SAMPLES	SIG NUMBER	DIM1*	DIM2**	AVERAGE AREA IN PIXELS	AVERAGE INT
1	D	0°	52	1.00	2.00	32.71	64.98	70.94
2	L	0°	69	.86	2.00	26.30	52.01	190.13

*Dimension in scan direction in pixels
**Average dimension perpendicular to scan direction in pixels

Legend: PRIM – PRIMITIVE
REL – RELATIVE
INT – INTENSITY
D – DARK
L – LIGHT
DIR – DIRECTION
SIG – SIGNIFICANCE

165

TABLE 3-7. PRIMITIVE DESCRIPTIONS FOR STRAW1

PRIM NUMBER	REL INT	SCAN DIR	NUMBER OF SAMPLES	SIG NUMBER	DIM1*	DIM2**	AVERAGE AREA IN PIXELS	AVERAGE INT
1	D	60°	79	.95	1.15	19.37	16.77	76.62
2	L	60°	62	.91	1.15	42.82	37.08	228.52

*Dimension in scan direction in pixels
**Average dimension perpendicular to scan direction in pixels

Legend: PRIM – PRIMITIVE
REL – RELATIVE
INT – INTENSITY
D – DARK
L – LIGHT
DIR – DIRECTION
SIG – SIGNIFICANCE

166

TABLE 3-8. PRIMITIVE DESCRIPTIONS FOR STRAW2

PRIM NUMBER	REL INT	SCAN DIR	NUMBER OF SAMPLES	SIG NUMBER	DIM1*	DIM2**	AVERAGE AREA IN PIXELS	AVERAGE INT
1	L	60°	31	.95	1.15	17.06	14.77	203.84
2	D	60°	36	.90	1.15	14.24	12.33	50.17
3	L	0°	31	.74	2.00	12.68	24.87	193.87

*Dimension in scan direction in pixels
**Average dimension perpendicular to scan direction in pixels

Legend: PRIM - PRIMITIVE
REL - RELATIVE
INT - INTENSITY
D - DARK
L - LIGHT
DIR - DIRECTION
SIG - SIGNIFICANCE

167

TABLE 3-9. PRIMITIVE DESCRIPTIONS FOR GRASS

PRIM NUMBER	REL INT	SCAN DIR	NUMBER OF SAMPLES	SIG NUMBER	DIM1*	DIM2**	AVERAGE AREA IN PIXELS	AVERAGE INT
1	L	0°	82	.95	2.00	6.89	13.12	180.96
2	D	0°	76	.94	2.00	6.57	12.58	47.34
3	L	90°	41	.67	2.00	5.05	9.56	187.49

*Dimension in scan direction in pixels
**Average dimension perpendicular to scan direction in pixels

Legend: PRIM - PRIMITIVE
        REL - RELATIVE
        INT - INTENSITY
        D - DARK
        L - LIGHT
        DIR - DIRECTION
        SIG - SIGNIFICANCE

TABLE 3-10. PRIMITIVE DESCRIPTIONS FOR SAND

PRIM NUMBER	REL INT	SCAN DIR	NUMBER OF SAMPLES	SIG NUMBER	DIM1*	DIM2**	AVERAGE AREA IN PIXELS	AVERAGE INT
1	D	90°	67	.99	2.00	5.61	10.69	71.73
2	L	90°	72	.89	2.00	5.88	11.11	192.93
3	D	0°	57	.88	2.00	5.70	10.82	54.49
4	L	0°	71	.82	3.00	4.69	14.01	204.58

*Dimension in scan direction in pixels
**Average dimension perpendicular to scan direction in pixels

Legend: PRIM – PRIMITIVE
        REL – RELATIVE
        INT – INTENSITY
        D – DARK
        L – LIGHT
        DIR – DIRECTION
        SIG – SIGNIFICANCE

TABLE 3-11. PRIMTIVE DESCRIPTIONS FOR WOOL1

PRIM NUMBER	REL INT	SCAN DIR	NUMBER OF SAMPLES	SIG NUMBERS	DIM1*	DIM2**	AVERAGE AREA IN PIXELS	AVERAGE INT
1	D	0°	70	.99	2.00	5.87	11.21	92.01
2	D	90°	44	.80	2.00	4.66	8.70	95.66
3	L	90°	44	.70	2.00	6.23	11.77	224.05

*Dimension in scan direction in pixels
**Average dimension perpendicular to scan direction in pixels

Legend: PRIM - PRIMITIVE
REL - RELATIVE
INT - INTENSITY
D - DARK
L - LIGHT
DIR - DIRECTION
SIG - SIGNIFICANCE

170

TABLE 3-12. PRIMITIVE DESCRIPTIONS FOR WOOL2

PRIM NUMBER	REL INT	SCAN DIR	NUMBER OF SAMPLES	SIG NUMBER	DIM1*	DIM2**	AVERAGE AREA IN PIXELS	AVERAGE INT
1	D	0°	57	.91	2.00	6.61	12.61	89.14
2	D	90°	61	.88	2.00	5.00	9.43	94.16
3	L	0°	69	.87	2.50	6.35	15.83	207.10

*Dimension in scan direction in pixels
**Average dimension perpendicular to scan direction in pixels

Legend: PRIM – PRIMITIVE
REL – RELATIVE
INT – INTENSITY
D – DARK
L – LIGHT
DIR – DIRECTION
SIG – SIGNIFICANCE

171

Fig. 3-10(b). In the following section a comparison is drawn between the primitive extraction method presented in this thesis and a simple thresholding scheme.

3.5 Thresholding Versus ERA Cues for
Primitive Extraction

The texture primitive extraction method presented in this thesis extracts texture primitive sets according to the following criterion. Elements belonging to the same primitive class should have similar relative intensity with respect to surrounding regions, similar size, similar shape and similar orientation. The size, orientation, and relative intensity information used is provided by the descriptors calculated in the ERA interpretation program discussed in Chapter 2.

For artificially generated textures where all like elements have the same intensity a simple thresholding scheme would work well for primitive extraction. It would also be quite adequate for textures like the floor grating pattern of Fig. 2-8(a) which have high contrast and good element separation. However, in a low contrast texture image like the raffia texture image of Fig. 2-2(a) an adequate thresholding range might be difficult to compute. In Fig. 3-11, a comparison can be made between thresholded raffia image masks (a), (c), and (e) and the corresponding

172

raffia primitive masks (b), (d), and (f) created using size, orientation and intensity cues. The thresholding ranges used for (a), (c), and (e) were set at the approximate average primitive intensity of the corresponding primitive mask plus and minus 10 (gray levels). (All of the texture images used in this thesis are 8 bit images. Therefore, 256 gray levels are possible for each image.) The primitive regions in (b), (d), and (f) are much more uniform than the regions found in the corresponding thresholded image masks. Thus, size, shape, and placement analysis should produce better results using primitive masks created using this primitive extraction scheme. Next, consider what happens when the lower left straw texture image of Fig. 2-13(a) is thresholded to extract the light straw elements. Figure 3-12(a) is a thresholded version of this image. It can be seen that a number of the pieces of straw appear as pairs of dotted lines. Others are blended with neighboring elements. The corresponding straw primitive mask image appears in Fig. 3-12(b). There is much more uniformity with respect to primitive shape and orientation. Each element appears to come from a separate piece of straw and not from a number of different pieces. Hence, thresholding schemes may encounter difficulties even in high contrast images.
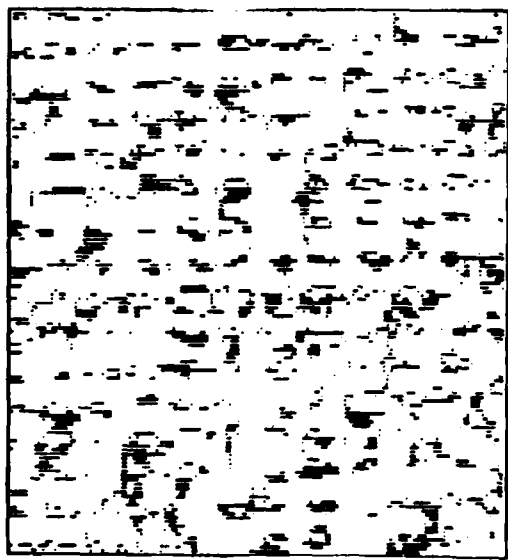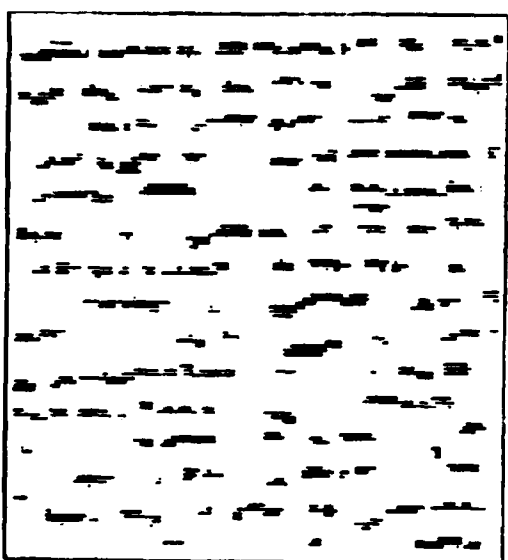
(a) Thresholded Image of Raffia (b) Raffia Primitive Mask
    (Range: 115-140)   Image (Average
                                        Intensity = 128.4)
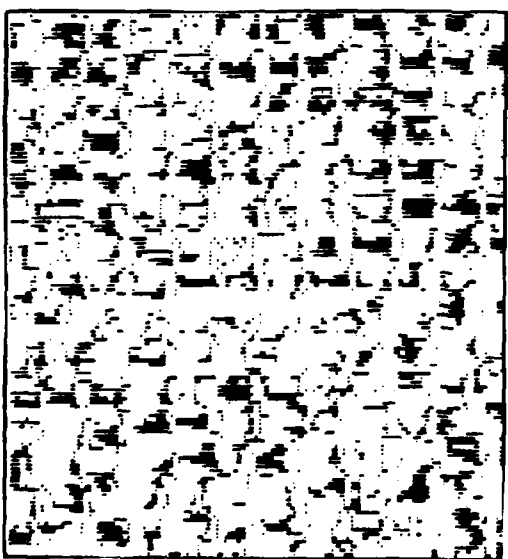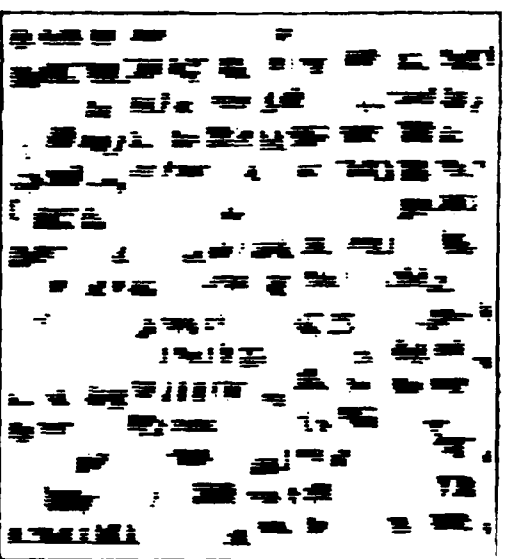
(c) Thresholded Image of Raffia (d) Raffia Primitive Mask
    (Range: 160-185)   Image (Average
                                        Intensity = 172.5)

Figure 3-11. Raffia Comparison

174
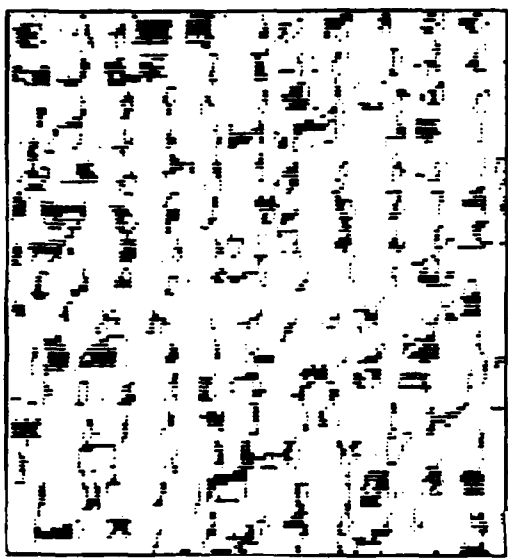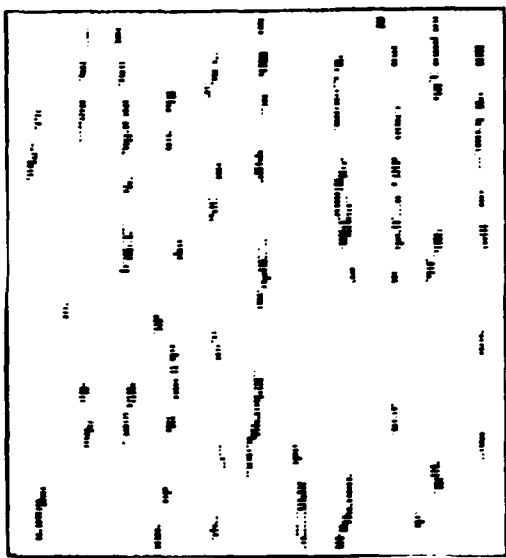
(e) Thresholded Image of Raffia (f) Raffia Primitive Mask
    (Range: 180-200)   Image (Average
                                    Intensity = 190.4)

Figure 3-11.   Continued
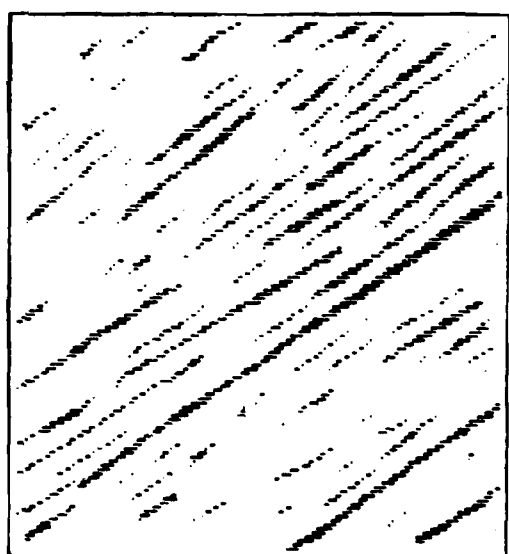
(a) Thresholded Image of   (b) Straw Primitive Mask
     Straw   Image

Figure 3-12.   Straw Comparison

3.6 Summary and Conclusions

In this chapter a primitive extraction algorithm was presented. The starting point of the algorithm is the internal form of the set of ERA descriptions generated for the given texture. Algorithm details were discussed in Section 3.3 and texture primitive masks and descriptions were presented for a large group of textures (Section 3.4). In Section 3.5 the primitive extraction technique presented in this thesis is compared to a simple thresholding scheme. Results seem to indicate that the type of information contained in the ERA description is valuable with respect to the primitive extraction process.

CHAPTER 4

AUTOMATIC DETERMINATION OF INTER-PRIMITIVE
SPATIAL RELATIONS

4.1 Introduction

A structural description for a given texture should consist of a description of the different types of primitives comprising the texture and the rules governing their placement. In the previous chapter a scheme was presented for extracting and analyzing textural primitives. The present chapter deals with the analysis of their spatial relations.

The two types of texture descriptions discussed up to this point contain only partial primitive placement information. In the ERA descriptions only the element spacing information pertains to placement. However, this information is only useful for relating a primitive to other primitives of the same type, and in only one scan direction. Similarly, the texture primitive descriptions contain only information relative to a single primitive type. Consider the upper and lower left brick subimages in Fig. 4-1(a). It is clear that the arrangements of

177
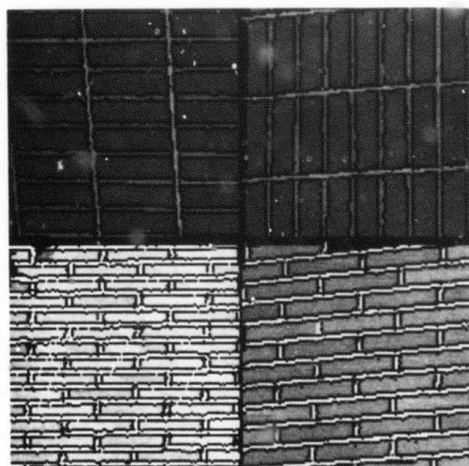
(a) Brick Mosaic

(b) Composite Primitive Image from (a)

Figure 4-1. Brick Mosaic and Composite Primitives

these 2 brick patterns are different. However, this
difference is not captured in the texture descriptions of
Figs. 4-2 and 4-3 or the brick primitive descriptions of
Tables 4-1 and 4-2. Both sets of bricks were found by
expanding elements discovered by the vertical scan. The
bricks and horizontal mortar strips separating them were
found to be periodic in this same direction. It is clear
that further analysis is necessary before the spatial
arrangements of these primitive sets can be completely
characterized.

This analysis begins with the set of primitive masks
created by the primitive extraction algorithm discussed in
the previous chapter. These masks contain the exact
locations of all the primitives of each type. (See the
composite primitive masks in Fig. 4-1(b).) The method used
to extract the primitive placement information from these
masks will be discussed in detail later in this chapter.
In the following section a brief overview of other work
done in this area is discussed.

4.2 Spatial Arrangement Analysis Methods

A number of different methods for determining
inter-primitive spatial relationships will be briefly
discussed below.

FILENAME = BRICK1

DARK OBJECT DESCRIPTIONS

VERTICAL SCAN DIRECTION

THERE IS STRONG EVIDENCE OF PERIODICITY (SPACING 15.00)

THERE IS STRONG EVIDENCE OF PREDOMINANT ELEMENT SIZE (12.00)
WITH STRONG SUPPORT FOR ELEMENT SPACING (15.00)
RATIO OF SIZE TO PERIOD IS .80

LIGHT OBJECT DESCRIPTIONS

HORIZONTAL SCAN DIRECTION

NO EVIDENCE OF PERIODICITY
VERY STRONG EVIDENCE OF PREDOMINANT ELEMENT SIZE (3.00)

VERTICAL SCAN DIRECTION

THERE IS VERY STRONG EVIDENCE OF PERIODICITY (SPACING 15.00)

THERE IS STRONG EVIDENCE OF PREDOMINANT ELEMENT SIZE (3.00)
WITH STRONG SUPPORT FOR ELEMENT SPACING (15.00)
RATIO OF SIZE TO PERIOD IS .20

150 DEGREE SCAN DIRECTION

NO EVIDENCE OF PERIODICITY
MODERATE EVIDENCE OF PREDOMINANT ELEMENT SIZE (5.77)

Figure 4-2. Brick1 Texture Description

180

FILENAME = BRICK3

DARK OBJECT DESCRIPTIONS

VERTICAL SCAN DIRECTION

THERE IS STRONG EVIDENCE OF PERIODICITY (SPACING 8.00)

THERE IS STRONG EVIDENCE OF PREDOMINANT ELEMENT SIZE (6.00)
WITH STRONG SUPPORT FOR ELEMENT SPACING (8.00)
RATIO OF SIZE TO PERIOD IS .75

120 DEGREE SCAN DIRECTION

NO EVIDENCE OF PERIODICITY
MODERATE EVIDENCE OF PREDOMINANT ELEMENT SIZE (34.64)

LIGHT OBJECT DESCRIPTIONS

HORIZONTAL SCAN DIRECTION

NO EVIDENCE OF PERIODICITY
VERY STRONG EVIDENCE OF PREDOMINANT ELEMENT SIZE (3.00)

VERTICAL SCAN DIRECTION

THERE IS STRONG EVIDENCE OF PERIODICITY (SPACING 8.00)

THERE IS STRONG EVIDENCE OF PREDOMINANT ELEMENT SIZE (3.00)
WITH STRONG SUPPORT FOR ELEMENT SPACING (8.00)
RATIO OF SIZE TO PERIOD IS .38

Figure 4-3. Brick3 Texture Description

181

TABLE 4-1. PRIMITIVE DESCRIPTIONS FOR BRICK1

PRIM NUMBER	REL INT	SCAN DIR	NUMBER OF SAMPLES	SIG	DIM1*	DIM2**	AVERAGE AREA IN PIXELS	AVERAGE INT	PERIOD*** IN PIXELS	BACK-GROUND
1	L	90°	21	1.0	2.00	56.81	113.10	121.90	15.00	–
2	D	90°	25	.95	11.00	36.68	403.04	100.52	15.00	–
3	L	0°	3	.36	–		250.00	131.00	–	YES

*Dimension in scan direction in pixels
**Average dimension perpendicular to scan direction in pixels
***Period in the direction of scan

Legend: PRIM – PRIMITIVE
REL – RELATIVE
INT – INTENSITY
D – DARK
L – LIGHT
DIR – DIRECTION
SIG – SIGNIFICANCE

182

TABLE 4-2. PRIMITIVE DESCRIPTIONS FOR BRICK3

PRIM NUMBER	REL INT	SCAN DIR	NUMBER OF SAMPLES	SIG	DIM1*	DIM2**	AVERAGE AREA IN PIXELS	AVERAGE INT	PERIOD*** IN PIXELS	SEPARATED FROM
1	L	90°	30	.97	2.00	59.70	10.04	219.63	8.00	-
2	D	90°	65	.94	5.00	22.24	111.44	179.94	8.00	-
3	L	0°	47	.30	2.00	5.21	118.87	218.14	-	2

*Dimension in scan direction in pixels
**Average dimension perpendicular to scan direction in pixels
***Period in the direction of scan

Legend: PRIM – PRIMITIVE
REL – RELATIVE
INT – INTENSITY
D – DARK
L – LIGHT
DIR – DIRECTION
SIG – SIGNIFICANCE

183

Syntactic approaches to texture analysis have been explored by Carlucci [13], Zucker [16], Lu and Fu [14], [15] and others. Carlucci [13] designed a graph-like language to be used in the generation of structural descriptions for simple textures. Zucker [16] defines textures in terms of ideal (perfect) highly structured patterns which undergo certain transformations to produce natural (observable) textures. In [14] and [15] Lu and Fu present a structural analyzer which uses tree grammars to describe the spatial arrangement of texture primitives within square subwindows of a texture. The subwindows are of a predetermined size. The texture elements are pixels. Like intensity pixels belong to the same primitive class. The primitive types correspond to the number of gray levels found in the image. On the next level the square subwindows must be placed according to another set of syntax rules. Recognition and synthesis results have been shown for a number of binary textures.

Conners and Harlow [12] use the inertia measure of the SGLDM to define the size, shape, and orientation of the unit tiles comprising a texture. The SGLDMs must be calculated for angles between 0° and 180° to determine the direction in which the smallest periods (in Euclidean magnitude) occur. The period in a given direction corresponds to the valleys of the inertia measure graph

184

for that direction. The two smallest periods and their corresponding directions define the underlying grid pattern of the given texture. In order to completely characterize the texture the tile pattern or painting function must then be defined.

In [21] Davis outlines a method for determining the spatial arrangement of a texture pattern when the underlying structure is a rectangular grid. After noting centroid locations for the set of texture primitives, size and direction histograms are calculated. First, size histograms are calculated for K 4 nearest neighbors to determine the 2 smallest texture periods. These correspond to the 2 leftmost peaks in the histogram. The direction histograms are then calculated for the 2 chosen distances. The final step is to determine the strongest pair of peaks (one from each direction histogram) such that their angular difference is approximately 90°.

Matsuyama, Saburi, and Nagao [20] use "regularity vectors" to characterize texture primitive arrangement. A regularity vector is similar to a placement rule. It defines a frequently occurring relative vector between elements in the texture. Along with each regularity vector is the set of the individual element pairs related by that vector. Initially, the vectors are defined only

for like element pairs. Next, the regularity vectors are defined on regularity vector sets to characterize more complex arrangements. Results were shown for a number of complex artificially generated textures and one homogeneous, regular natural texture sample.

The final spatial arrangement analysis technique to be discussed is the method presented by Maleson, Brown, and Feldman in [19]. Initially, regions of similar intensity within the texture field are approximated by ellipses. These elliptical texture primitives are then grouped into equal intensity, similar shape classes. Spatial relations are then defined among textural elements within these classes. Primitives are considered to be collinear if their major axes line up and parallel if their minor axes are in the same line. T-joints and V-joints are also considered to be important spatial relationships.

In the following section a technique for extracting inter-primitive placement rules is presented. In the event that the texture under consideration is homogeneous and regular a minimum set of rules can be extracted which characterize the underlying grid pattern. A comparison using the original texture image and a reconstructed texture image (using this minimum set of rules along with

a set of average textural primitives) can be made.

The algorithms for minimum placement rule extraction and texture reconstruction are presented in section 4.3. Texture reconstructions and placement rule sets for a number of natural, regular textures are then presented and discussed.

4.3 The Spatial Arrangement Analysis Method

4.3.1 Descriptive Overview

The spatial arrangement analysis method to be presented here uses the texture primitive masks generated by the algorithm discussed in Chapter 3. Clearly, the placement information for all the primitives extracted is preserved in their respective primitive mask images. Using these primitive masks one can determine the most frequently occurring spatial relations for all combinations of non-background texture primitive type pairs. This set of placement rules along with their respective rates of occurrence within the texture image provide a reasonable description of the predominant spatial relations inherent in the given texture pattern.

If the texture pattern under consideration is homogeneous and regular then this analysis can be taken a step further. A minimum set of rules necessary to

characterize the texture pattern can be extracted. The constraints necessary for extracting this minimum set are high frequency of occurrence and minimum Euclidean distance. Without the minimum distance constraint the underlying texture pattern may not be captured. Without the high frequency constraint the rules selected may represent an anomaly in the texture pattern rather than the actual pattern being analyzed.

The best test of the selection processes is to compare the original texture image with an image created using the placement rules selected and a set of average texture primitives. The comparison should be made only with respect to the spatial relations of the two images. Images created using average texture primitives rarely look exactly like the natural textures they represent.

In the following subsection the details of the spatial arrangement analysis process are given.

4.3.2 The Spatial Arrangement Analysis Algorithm

The details of the algorithm used to analyze the underlying structure of a given texture are presented in this section. This algorithm uses the set of texture primitive masks created by employing the method discussed in Chapter 3. There are 3 major parts to this algorithm:

1) Primitive Placement Rule Generation - A set of predominant primitive placement rules is generated for every possible pair of non-background primitive types.

2) Grid Relation Extraction - If the texture under consideration is homogeneous and regular then a minimum set of placement rules, which characterizes the texture pattern, can be extracted.

3) Texture Reconstruction - This algorithm section uses the minimum set of placement rules produced in part 2 and a set of average texture primitives in order to produce a reconstructed texture image. The reconstructed texture image serves as a means for visually comparing the inferred set of inter-primitive spatial relations with the ones inherent in the original texture image.

No placement rules are generated for primitives which form part of the background. (See Chapter 3, Section 3.3.2 for the details of the background test.) However, after the non-background primitives have been placed in their proper grid locations for the texture reconstruction the background intensity is filled in if a background primitive has been indicated for the texture. (This can also be done before the non-background

189

primitives are placed.)

The thresholds used in the remainder of this section were chosen after numerous tests with many kinds of texture samples. The need for thresholding is due to the fact that only natural texture images, which are sometimes quite noisy, are used.

Primitive Placement Rule Generation

1)   Primitive Centroid Calculation

Since the images being analyzed are natural texture images there can be considerable variation among the texture primitives of a given primitive type. Therefore, it is reasonable to define placement rules in terms of distances and angular separation between the centroids of textural elements.

The centroid is calculated for each individual texture primitive. The centroid locations are stored in a primitive centroid list along with the primitive type of the textural element. During the centroid calculation process a new mask image is simultaneously created for each primitive type. It uses the index into the primitive centroid list as the mask value for each of its primitives. See

Fig. 4-4. This primitive index mask image, along with the primitive centroid list are all that is needed for the placement rule determination process.

2)   Placement Rule Determination

A set of placement rules is generated for each possible pair of non-background primitives. In order to determine the frequency of placement rules relating primitives of type A to primitives of type B a 12-directional scan is initiated from each type A primitive centroid location within the type B primitive index mask image. When a primitive is encountered which is different from the primitive of origin, the index value is used to retrieve the corresponding centroid location. At this point the angle and distance between the 2 primitive centroids are calculated and the frequency of that particular placement rule is increased by one. Placement rules are noted to the nearest 10 degrees and the nearest 3 pixels. Therefore, when a placement rule is observed the frequency for the rule relating primitives of type A to primitives of type B at the observed distance divided by 3 and the observed angle divided by 10 is increased by one.

191

```
0  0  0  0  0  0  0  0  0  0  0
0  7  7  7  0  0  0  0  0  0  0
0  7  7  7  0  0  0  0  0  0  0
0  7  7  7  0  0  0  0  C  0  0
0  0  0  0  0  0  0  0  0  0  0
0  0  0  0  8  8  8  0  0  0  0
0  0  0  0  8  8  8  0  0  0  0
0  0  0  0  8  8  8  0  0  0  0
0  0  0  0  0  0  0  0  0  0  0
```

(a) Primitive Index Mask Image for Primitive
    Type N.

Index	Row	Col	Type
⋮	⋮	⋮	⋮
7	3	3	N
8	7	6	N
⋮	⋮	⋮	⋮

(b) Primitive Centroid List Showing Entries
    for (a).

Figure 4-4.   Primitive Indexing Scheme

There are 2 reasons for having the placement rules represent a range of 3 pixels in distance and 10 degrees in angular separation:

a) The first consideration has to do with the types of images encountered. For noisy images like raffia, placement rules may cluster around a certain range of directions and distances but a significant amount of variation will be encountered. Having larger angle, distance bins will help to concentrate the results so that predominant placement rules will be more obvious.

b) Another consideration is storage. The temporary matrix used to store placement rule frequencies needs to have N x M x 39 locations, where N is the number of primitive types, M = Max{#Rows, #Columns}/3 + 1, and the angular bins go from −19 to +19 to provide the overlap needed for further processing. When working with 128 x 128 pixel images the requirement is 1677 locations for every primitive type.

3) <u>Frequency Normalization</u>

The raw frequencies for the individual placement rules will depend upon the number of primitives of

the type from whose centroids the scan is being initiated, e.g., the number of primitives of type A in the previous example. These frequencies also depend upon the distance and angle of the spatial relationship itself. Therefore, the frequencies of the individual placement rules will be normalized as follows. Let F be the number of times the placement rule relating primitives of type A to primitives of type B at angle and distance D occurred. Then

Normalized(F) =

$$100 \times \cfrac{F}{\left(\begin{array}{c}\text{\# Primitives}\\\text{of Type A}\end{array}\right) \times \cfrac{(\text{\# Rows}-D\text{Sin}\theta)(\text{\#Cols}-D\text{Cos}\theta)}{(\text{\# Rows} \times \text{\# Cols})}}$$

Normalized (F) is the percentage of time the rule occurs given that a primitive of type A is encountered. Note that the number of primitives of type A is multiplied by the ratio of the useful area within the image (given the angle and distance constraint) over the entire image area. In short, it may not be possible for all of the primitives of type A to exhibit the particular inter-primitive spatial relationship under consideration. Multiplying by the above ratio should provide an approximate correction.

194

4) <u>Primitive</u> <u>Placement</u> <u>Rule</u> <u>Selection</u>

The final step is the selection process. At this point a decision must be made concerning the relative importance of the different placement rules. If the image under consideration is a perfect homogeneous, regular texture image then all of the placement rules with non-zero frequency would have percentages close to 100%. Hence, all of them would be selected as members of the final set. However, when working with natural texture images it is not unusual for a certain amount of dispersion to take place. Under these conditions a method for selecting the most significant, or most frequently occurring set of rules must be developed. The selection method used here is outlined as follows:

a) First, the maximum percentage of occurrence, $M1$, for any placement rule for a given primitive type, say A, is noted. Any type A placement rule with percentage at least as great as half of the value of $M1$, but not less than 15% is kept.

b) Any placement rule surviving the first set of thresholds has its percentage of occurrence replaced by the sum of the nine matrix entries. These nine entries are those whose degree and

195

distance indices are different from the original entry's indices by at most one. This should insure that any large volume peak which is spread out will not be passed over in the next thresholding process.

c) Next, the maximum percentage of occurrence, M2, over the new set of entries is noted. Any placement rule with a percentage at least as great as half the value of M2, but not less than 20% is kept if it is a local maximum. That is, its value must be at least as great as its eight closest matrix neighbors.

d) If there is no remaining rules relating a specific primitive type pair then the highest placement rule relating these 2 types is kept even if its percentage is less than 20%.

The remaining placement rules belong to the final set of inter-primitive spatial relations for the given primitive type. These rules are of the form:

PRIM1 = A   PRIM2 = B   Angle = θ DIST = D   PER = P

This relationship states that the centroid of a primitive of type A is separated from the centroid of

a primitive of type B by a distance of D pixels at
angle θ, P percent of the time that a primitive of
type A is encountered. This final set of placement
rules is stored in order of decreasing frequency of
occurrence.

Automatic Grid Relation Extraction for Homogeneous Regular Textures

If we are working with a homogeneous regular texture,
i.e., a periodic texture in which each primitive of a
given kind exhibits the same kind of inter-primitive
spatial relationships, then we should be able to extract a
minimum, not necessarily unique, set of rules which
completely characterize the underlying texture pattern.

In the event that the texture under consideration is
a striped pattern the program would report that each
primitive type repeats in the same direction and forms
part of the background. Upon detecting this condition the
program would only have to select one placement rule for
each type of primitive.   The rules would relate each
primitive type to a given primitive type, say A, in the
direction of scan which is precisely the direction of
repetition for each primitive type detected.

The algorithm presented here was designed for

197

homogeneous regular textures in which there is more than one direction of repetition.

Suppose we are given such a texture. If all of the primitives of one type, say type A, are extracted a single primitive "subtexture" of the original texture can be formed. Choosing the 2 nearest neighbors of a type A primitive so that the 3 primitives are not collinear, we have a configuration similar to the one in Fig. 4-5(a). This is equivalent to choosing 2 noncollinear placement rules relating primitive type A to primitive type A which minimize distance. Since each element of a given type has the same environment the structure in Fig. 4-5(a) can be propagated to form a triangular or parallelogram grid pattern as in Fig. 4-5(b), all of whose nodes correspond to type A elements contained in the subtexture pattern.

Suppose there exists a primitive of type A in the subtexture which is not represented in the grid pattern. Placing this primitive in the grid, but not in the position of a grid node presents a problem. There is no position that this primitive can take where it would be at least as far from every grid node as the maximum distance of the 2 relationships chosen above, and these relationships were chosen so that inter-primitive distances would be minimized. This is a contradiction.
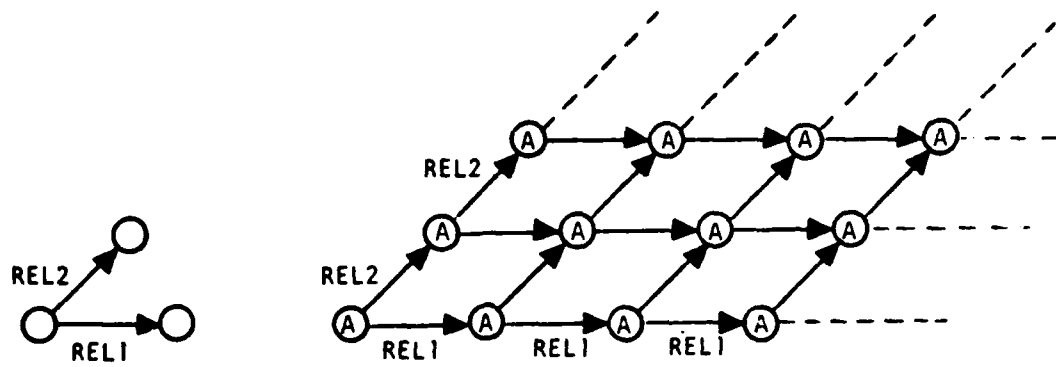
(a) 2 Non-collinear Single
Primitive Placement
Rules.

(b) Since each type A primitive
has the same environment a
parallelogram grid is
propagated.
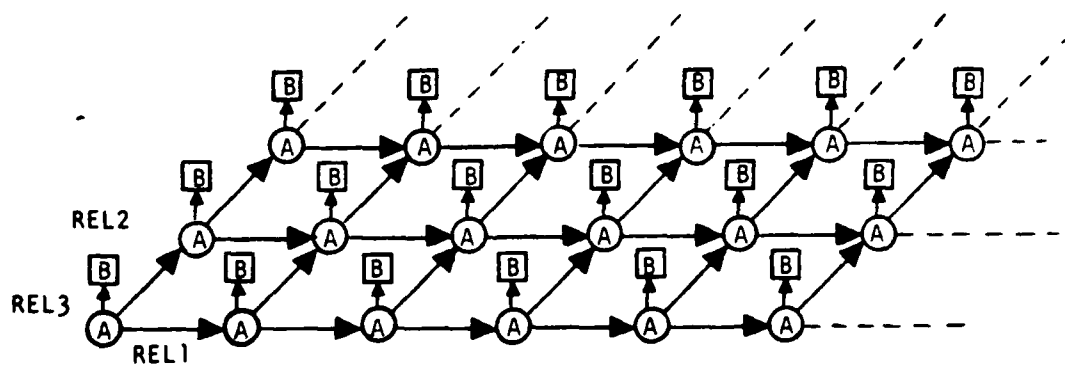
(c) Using an additional relationship,
REL3, to add type B primitives
to the grid.

Figure 4-5. Texture Reconstruction Scheme

Hence, there is no primitive of type A in the texture which is not included in the grid.

In order to reconstruct the original texture pattern only one placement rule need be used to relate each additional primitive type to the grid. In each case the relationship would be between a primitive type already included in the grid and a type not yet included.

For example, suppose there exists a placement rule relating type A primitives to primitives of type B. This rule could be used to place one type B primitive in the grid for each type A primitive already included, see Fig. 4-5(c). All type B primitives placed in this way correspond to a type B primitives in the original texture. Likewise, it can be argued that there exists no type B primitive in the original texture which is not now included in the grid. If there were such a primitive it would not exhibit the inter-primitive spatial relationship used to place all of the type B primitives already included in the grid.

Hence, we need only establish the underlying grid pattern using 2 single primitive placement rules, both referring to the same primitive type. Then only one placement rule for each additional non-background primitive type need be used to include the remaining

200

primitive types in this grid structure.

The major steps in this grid relation selection process are as follows:

1) <u>Combine</u> <u>Redundant</u> <u>Single</u> <u>Primitive</u> <u>Placement</u> <u>Rules</u>

Rules relating a primitive to itself at a distance, D, and an angle, θ , are combined with rules relating this same primitive to itself at distance, D, and angle $\theta + 180$ or $\theta - 180$.

2) <u>Determine</u> <u>the</u> <u>Underlying</u> <u>Grid</u> <u>Pattern</u>

From the reduced set of single primitive placement rules created in 1 choose two rules to span the image space as follows:

a) Find the maximum percentage of occurrence among all single primitive placement rules. Any single primitive rule with percentage at least two thirds of this value will be considered a candidate for the first grid axis.

b) Only those rules exhibiting the minimum inter-primitive distance among the candidate placement rules will be given further consideration.

c) The rule with maximum percentage of occurrence which exhibits the minimum inter-primitive distance will be chosen as the first grid axis.

d) The second grid axis is chosen the same way as the first grid axis with the exception that the initial set of candidates is somewhat reduced. This initial set of placement rules contains only those single primitive rules which pertain to the same primitive used in the first grid axis. Also, the angle at which the primitives are related cannot be within 10° of the angle used in the first grid axis (or its opposite).

3) Relate the Remaining Primitives to the Grid

All non-background primitives which are not specified in the 2 grid axis placement rules must be related to the underlying grid pattern. This is done as follows:

a) Note all placement rules which are STRONG. Let P1 be a placement rule relating a primitive of type A to a primitive of type B at angle θ and distance D. P1 is STRONG if there exists a placement rule, P2, relating a primitive of type B to a primitive of type A at distance D and

202

angle $\theta + 180$ degrees or $\theta - 180$ degrees.

b) Consider the set of placement rules relating a primitive included in the grid structure to one which is not yet included. Note the maximum percentage of occurrence among all of these rules. Any of the rules whose percentage is below two thirds of the maximum value is dismissed from the group.

c) If any placement rules within the new group are STRONG then the maximum percentage, STRONG placement rule is chosen as the next grid relation. If none are STRONG then the only constraint used will be maximum percentage of occurrence. The relationship chosen adds another primitive type to the grid structure.

(This process is repeated until all non-background primitives are included in the grid.)

Texture Pattern Reconstruction

After the grid relations have been selected it would be desirable to be able to estimate how closely they approximate the relations inherent in the original texture image. This can be done by reconstructing the texture using the selected grid relations and a set of average

203

texture primitives. The texture pattern reconstruction process is outlined below.

1) <u>Create</u> <u>Primitive</u> <u>Templates</u>

An "average" primitive mask is created for each non-background primitive type as follows:

a) Using a blank image, each primitive of a given type is superimposed so that their centers of mass lie on the same pixel. Each pixel value equals the number of primitives covering that pixel.

b) All pixels with values less than the total number of primitives of that type multiplied by a user specified threshold value are set to zero.

c) After thresholding, the reduced "average" primitive mask is stored and the starting row and column, the location of the center of mass, and the maximum length and width are recorded.

2) <u>Construct</u> <u>Grid</u> <u>Skeleton</u>

Using the grid relation set, mark primitive *centroid locations* with the primitive type number as follows:

a) Starting at the center of the image the primitive centroid locations for one axis are marked using the angle and distance information in the first grid axis placement rule as shown in Fig. 4-6(a).

b) An axis of centroids is constructed through each of the first axis centroid locations using the angle and distance information in the second grid axis placement rule. (See Fig. 4-6(b).)

c) The rest of the centroids are marked in a similar manner. Using each of the remaining placement rules from the grid relation set, the centroid locations of each "new" primitive type are marked. That is, the placement rule information is used to relate a primitive of one type to a primitive of another type whose centroids have already been marked in the image.

3) Fill in Primitives and Background

Using the average primitive templates created in 1 and the average primitive intensities calculated earlier in the program the texture pattern can be reconstructed. The reconstructed texture image will have an "average" primitive region centered at each of the primitive centroid markers. The intensity of

205

```
0    0    0    0    0    0    0    0    0

0    0    0    0    0    0    0    0    0

0    0    0    0    0    0    0    0    0

0    0    0    0    0    0    0    0    0

1    0    0    0    1    0    0    0    1

0    0    0    0    0    0    0    0    0

0    0    0    0    0    0    0    0    0

0    0    0    0    0    0    0    0    0

0    0    0    0    0    0    0    0    0
```

(a) First Grid Axis Centroids for Placement.
     Rule: PRIM1 = 1   PRIM2 = 1   ANGLE = 0°
           DISTANCE = 4.

```
0    0    0    0    1    0    0    0    1

0    0    0    0    0    0    0    0    0

0    0    1    0    0    0    1    0    0

0    0    0    0    0    0    0    0    0

1    0    0    0    1    0    0    0    1

0    0    0    0    0    0    0    0    0

0    0    1    0    0    0    1    0    0

0    0    0    0    0    0    0    0    0

1    0    0    0    1    0    0    0    0
```

(b) Second Grid Axis Centroids for Placement.
     Rule: PRIM1 = 1   PRIM2 = 1   ANGLE = 45°
             DISTANCE = 2√2.

Figure 4-6. Grid Axis Placement Scheme

206

this region will be equal to the average primitive intensity of the respective primitive type. All pixels not covered by a primitive will take on the background intensity if a background has been detected.

In the following section the spatial arrangement analysis for a number of periodic textures will be presented and discussed. It should be noted that all placement rule angles are assigned according to the scheme shown in Fig. 4-7. Also, all single and double starred rules represent the first and second grid axes, respectively. Triple starred rules relate remaining primitives to the underlying grid pattern.

The amount of CPU time needed for the spatial arrangement analysis process depends mainly on the number of primitive types and the number of individual primitives per type. In Table 4-3 five textures are compared with respect to CPU time needed for spatial analysis arrangement processing. All samples are 128 x 128 pixel images. All processing was done on a DEC KL-10 processor.

4.4 Spatial Arrangement Analysis Results

Consider the brick mosaic of Fig. 4-1(a). In the first brick subwindow the bricks are arranged in unshifted
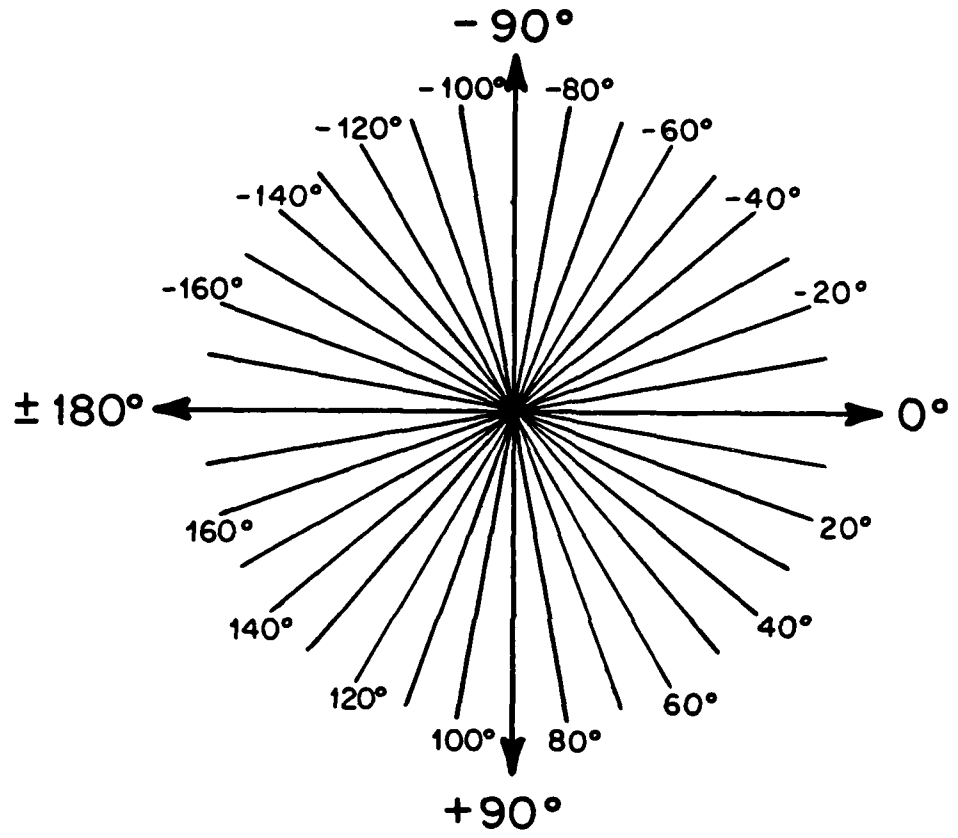
Figure 4-7.   Placement Rule Angles

TABLE 4-3. SPATIAL ARRANGEMENT ANALYSIS TIMING

Texture	#Non-Background PRIM Types	PRIM Type	# PRIMS Per Type	CPU Time (Secs)
Floor Grating	1	1	94	5.8
Brick (Unshifted)	2	1 2	21 25	8.0
Brick (Shifted)	3	1 2 3	30 66 47	13.5
Raffia	3	1 2 3	104 102 68	18.9
Herringbone Material	6	1 2 3 4 5 6	70 50 92 80 20 17	66.2

rows. Three types of primitives are found for this texture. (See Table 4-1.) The first primitive type described is the horizontal mortar strip. The second primitive type is the brick primitive. The third primitive type is the vertical mortar strip between the neighboring brick columns. The vertical mortar strips extend from one end of the image to the other. Hence, they are labelled as background primitives. The placement rules will then only refer to the first 2 primitive types. In Fig. 4-8 the placement rules for this brick subwindow are given. The grid axes are formed by the 2 highest percentage single primitive placement rule sets. These are the single and double starred rules shown in Fig. 4-8. (In some cases two equivalent rules were found for each grid axis.) These 2 sets of rules refer to brick primitives. Another rule is needed to related the horizontal mortar strip primitives to the grid of brick. The triple starred rule is the one chosen. For the remaining samples only the underlying grid relations and links will be shown. The grid relations will refer to the placement rules chosen as grid axes, while the grid links will refer to the placement rules selected to relate the remaining primitives to the grid.

The upper right brick subimage in Fig. 4-1(a) is a rotated version of the upper left brick subimage. The

210

FILENAME = BRICK1

PRIM1 = 1	PRIM2 = 1	DEG = -90	DIST = 15	PER = 49.84	
PRIM1 = 1	PRIM2 = 1	DEG = 90	DIST = 15	PER = 49.83	
PRIM1 = 1	PRIM2 = 1	DEG = 180	DIST = 56	PER = 48.05	
PRIM1 = 1	PRIM2 = 1	DEG = 180	DIST = 45	PER = 33.30	
PRIM1 = 1	PRIM2 = 1	DEG = 0	DIST = 45	PER = 32.32	
PRIM1 = 1	PRIM2 = 1	DEG = 160	DIST = 45	PER = 27.73	
PRIM1 = 1	PRIM2 = 1	DEG = -20	DIST = 45	PER = 27.08	
PRIM1 = 1	PRIM2 = 1	DEG = -150	DIST = 27	PER = 20.87	
PRIM1 = 1	PRIM2 = 1	DEG = 30	DIST = 27	PER = 20.61	
PRIM1 = 1	PRIM2 = 2	DEG = 80	DIST = 9	PER = 58.47	***
PRIM1 = 1	PRIM2 = 2	DEG = 20	DIST = 24	PER = 25.54	
PRIM1 = 1	PRIM2 = 2	DEG = 160	DIST = 21	PER = 20.41	
PRIM1 = 2	PRIM2 = 1	DEG = -100	DIST = 9	PER = 49.15	
PRIM1 = 2	PRIM2 = 2	DEG = -90	DIST = 15	PER = 87.92	*
PRIM1 = 2	PRIM2 = 2	DEG = 90	DIST = 15	PER = 87.90	*
PRIM1 = 2	PRIM2 = 2	DEG = 180	DIST = 42	PER = 74.18	**
PRIM1 = 2	PRIM2 = 2	DEG = 0	DIST = 42	PER = 72.05	**
PRIM1 = 2	PRIM2 = 2	DEG = 160	DIST = 45	PER = 32.46	

Figure 4-8. Placement Rule Set for Brick1

211

rotation is clockwise through 90 degrees. A comparison can be made between the texture descriptions of Figs. 4-2 and 4-9 and the primitive descriptions of Tables 4-1 and 4-4. The descriptions are nearly identical except for the directional difference of 90 degrees. Likewise, the starred placement rules chosen for the rotated brick (Fig. 4-10) are very similar to those chosen for the original (Fig. 4-8) with the exception of a 90 degree difference for each rule. The reconstructions of both of these texture subwindows is given in the reconstruction mosaic of Fig. 4-11(b). (Figure 4-11(a) is the original brick mosaic.) Since a background primitive was indicated for both images their reconstructed images are completely filled in.

The brick subimage in the lower left section of the brick texture mosaic, Fig. 4-11(a), is a shifted brick pattern. Successive rows are shifted by half of a brick in distance. The texture descriptions and primitive descriptions for this image are given in Fig. 4-3 and Table 4-2, respectively. The placement rules selected for this subimage are the starred rules of Fig. 4-12.

The highest percentage single primitive placement rule and its counterpart are selected for the first grid axis. However, the placement rule set with the next

212

FILENAME = BRICK2

DARK OBJECT DESCRIPTIONS

HORIZONTAL SCAN DIRECTION

THERE IS VERY STRONG EVIDENCE OF PERIODICITY (SPACING 15.00)

THERE IS STRONG EVIDENCE OF PREDOMINANT ELEMENT SIZE (12.00)
WITH STRONG SUPPORT FOR ELEMENT SPACING (15.00)
RATIO OF SIZE TO PERIOD IS .80

LIGHT OBJECT DESCRIPTIONS

HORIZONTAL SCAN DIRECTION

THERE IS STRONG EVIDENCE OF PERIODICITY (SPACING 15.00)

THERE IS STRONG EVIDENCE OF PREDOMINANT ELEMENT SIZE (3.00)
WITH STRONG SUPPORT FOR ELEMENT SPACING (15.00)
RATIO OF SIZE TO PERIOD IS .20

VERTICAL SCAN DIRECTION

NO EVIDENCE OF PERIODICITY
VERY STRONG EVIDENCE OF PREDOMINANT ELEMENT SIZE (3.00)

Figure 4-9. Brick2 Texture Description

213

FILENAME = BRICK2

GRID RELATIONS ARE AS FOLLOWS:

PRIM1 = 1   PRIM2 = 1   ANGLE = 180.00   DIST = 15.00   PER = 88.30   *
       PRIM1 = 1   PRIM2 = 1   ANGLE = .00   DIST = 15.00   PER = 87.42   *

PRIM1 = 1   PRIM2 = 1   ANGLE = -90.00   DIST = 42.00   PER = 73.14   **
       PRIM1 = 1   PRIM2 = 1   ANGLE = 90.00   DIST = 42.00   PER = 73.14   **

GRID LINKS ARE AS FOLLOWS:

PRIM1 = 2   PRIM2 = 1   ANGLE = 170.00   DIST = 9.00   PER = 70.37   ***

Figure 4-10.   Grid Relations and Links for Brick2

214
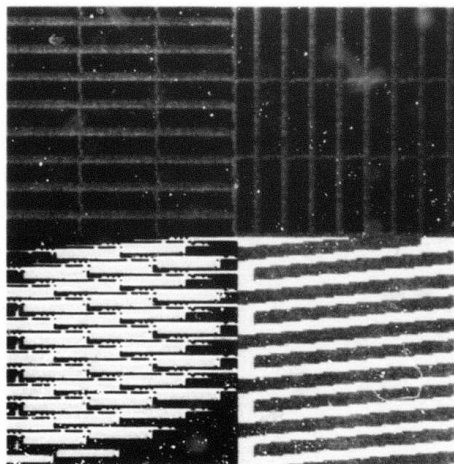
(a) Brick Mosaic

(b) Reconstruction for (a)

Figure 4-11. Brick Mosaic and ⌐ruction

215

FILENAME = BRICK3

GRID RELATIONS ARE AS FOLLOWS:

PRIM1 = 3   PRIM2 = 3   ANGLE = -90.00   DIST = 18.00   PER = 78.43   *
    PRIM1 = 3   PRIM2 = 3   ANGLE = 90.00   DIST = 18.00   PER = 56.04   *

PRIM1 = 3   PRIM2 = 3   ANGLE = -30.00   DIST = 21.00   PER = 54.18   **
    PRIM1 = 3   PRIM2 = 3   ANGLE = 150.00   DIST = 21.00   PER = 38.77   **

GRID LINKS ARE AS FOLLOWS:

PRIM1 = 3   PRIM2 = 2   ANGLE = 180.00   DIST = 18.00   PER = 81.55   ***

PRIM1 = 1   PRIM2 = 3   ANGLE = 60.00   DIST = 15.00   PER = 31.31   ***

Figure 4-12.   Grid Relations and Links for Brick3

216

TABLE 4-4. PRIMITIVE DESCRIPTIONS FOR BRICK2

PRIM NUMBER	REL INT	SCAN DIR	NUMBER OF SAMPLES	SIG	DIM1*	DIM2**	AVERAGE AREA IN PIXELS	AVERAGE INT	PERIOD*** IN PIXELS	BACK-GROUND
1	D	0°	25	1.00	11.00	36.20	397.92	100.52	15.00	-
2	L	0°	19	.94	2.00	58.11	115.74	121.00	15.00	-
3	L	90°	4	.38	-	-	182.50	127.00	-	YES

*Dimension in scan direction in pixels
**Average dimension perpendicular to scan
   direction in pixels
***Period in the direction of scan

Legend: PRIM - PRIMITIVE
       REL - RELATIVE
       INT - INTENSITY
       D - DARK
       L - LIGHT
       DIR - DIRECTION
       SIG - SIGNIFICANCE

highest percentage is not chosen. Instead, rules with lower percentage and distance are selected. Figure 4-13 shows the underlying grid pattern produced using the highest percentage placement rules with no attempt to minimize distance. This pattern looks similar to the brick pattern shown in the top row of Fig. 4-11(a). The shifted rows are completely lost.

In the lower left corner of Fig. 4-11(b) the reconstruction using the starred set of placement rules is shown. It appears that the original subimage in Fig. 4-11(a) is less slanted than the corresponding reconstruction. This is due to the angular error introduced by rounding to the nearest 10 degrees. Instead of -30 degrees, the second grid axis rule should be approximately -26.6 degrees. In an application, where more precision is necessary, a higher resolution placement rule search could be implemented. The black gaps in the reconstruction exist because the primitive templates used are averages of the original texture elements. There is no guarantee that they will fit together as precisely as the originals. The lack of primitives around the edges, and especially in the lower right hand corner of the subimage is due to the reconstruction process. It if were necessary to cover the entire 128 x 128 pixel image are with the reconstructed pattern this could be done.
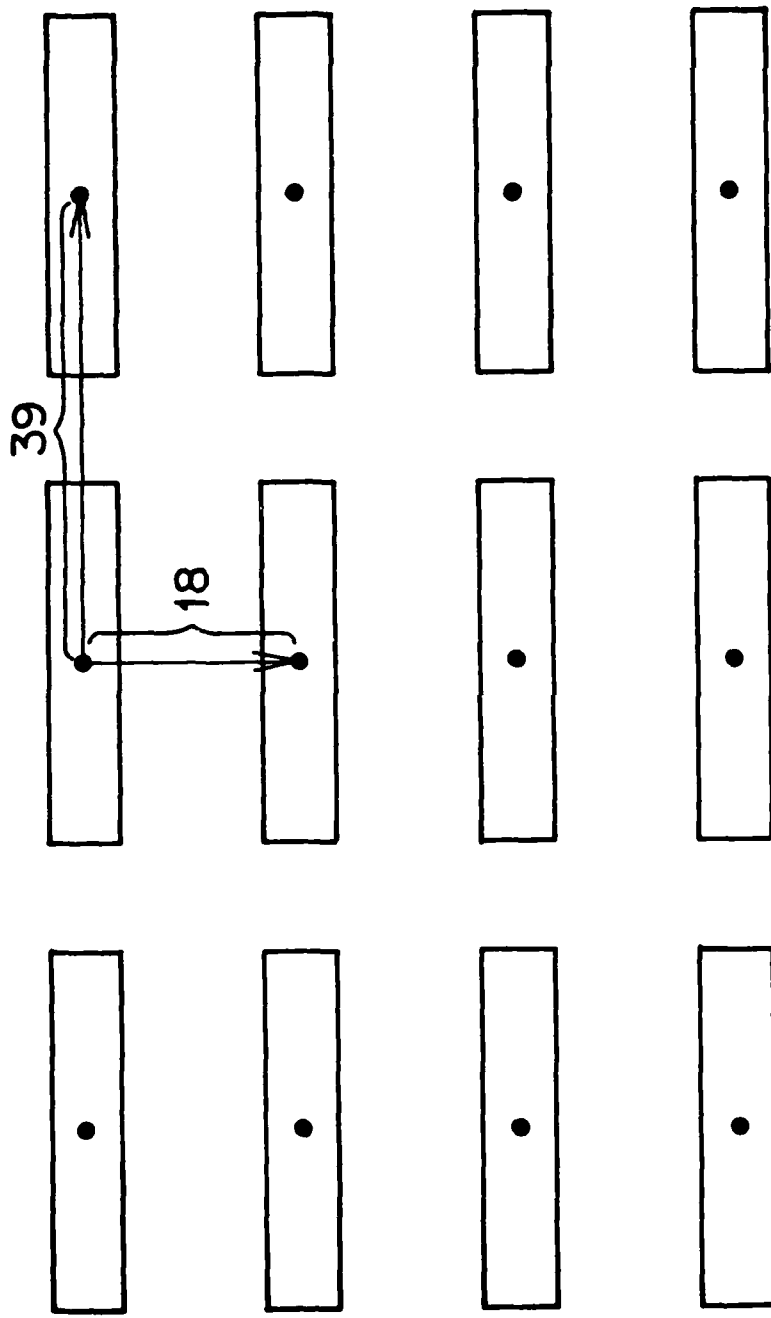
Figure 4-13. Incorrect Brick Reconstruction

However, the intent here is to provide enough textured area for a visual comparison of the basic textural structure.

The last brick subimage in the mosaic is taken from a different brick wall image. It has the same basic pattern as the last brick image analyzed. The texture descriptions and primitive descriptions for this subimage are given in Fig. 4-14 and Table 4-5, respectively. The selected grid relations and grid links are shown in Fig. 4-15. One obvious difference between the 2 shifted brick patterns is the difference in the sizes of the bricks. There are only 10 complete rows of brick on the right, as opposed to 14 on the left. Each of the rows on the left contain 3 nearly complete bricks. On the right only 5 rows show 3 complete bricks. The remaining 5 rows have half bricks on either end. Since there are fewer full size primitives in the lower right image the edge effects will have a much more pronounced effect. The texture reconstruction for this image (Fig. 4-11(b)) shows that these effects produced enough confusion to inhibit the discovery of the underlying textural structure.

If the problem is, in fact, subwindow size, then a larger window from the same image should be analyzed correctly. Consider Fig. 4-16(a). The lower right

FILENAME = BRICK4

DARK OBJECT DESCRIPTIONS

VERTICAL SCAN DIRECTION

THERE IS VERY STRONG EVIDENCE OF PERIODICITY (SPACING 11.00)

THERE IS STRONG EVIDENCE OF PREDOMINANT ELEMENT SIZE (8.00)
WITH STRONG SUPPORT FOR ELEMENT SPACING (11.00)
RATIO OF SIZE TO PERIOD IS .73

LIGHT OBJECT DESCRIPTIONS

HORIZONTAL SCAN DIRECTION

NO EVIDENCE OF PERIODICITY
VERY STRONG EVIDENCE OF PREDOMINANT ELEMENT SIZE (3.00)

VERTICAL SCAN DIRECTION

THERE IS STRONG EVIDENCE OF PERIODICITY (SPACING 11.00)

THERE IS STRONG EVIDENCE OF PREDOMINANT ELEMENT SIZE (3.00)
WITH MODERATE SUPPORT FOR ELEMENT SPACING (11.00)
RATIO OF SIZE TO PERIOD IS .27

Figure 4-14.   Brick4 Texture Description

221

FILENAME = BRICK4

GRID RELATIONS ARE AS FOLLOWS:

PRIM1 = 2   PRIM2 = 2   ANGLE = -150.00   DIST = 21.00   PER = 57.93   *
       PRIM1 = 2   PRIM2 = 2   ANGLE = 30.00   DIST = 21.00   PER = 57.31   *

PRIM1 = 2   PRIM2 = 2   ANGLE = 90.00   DIST = 24.00   PER = 14.08   **
       PRIM1 = 2   PRIM2 = 2   ANGLE = -90.00   DIST = 24.00   PER = 30.28   **

GRID LINKS ARE AS FOLLOWS:

PRIM1 = 3   PRIM2 = 2   ANGLE = -90.00   DIST = 12.00   PER = 85.26   ***

Figure 4-15.   Grid Relations and Links for
               Brick4

222

(a) Brick Texture Image
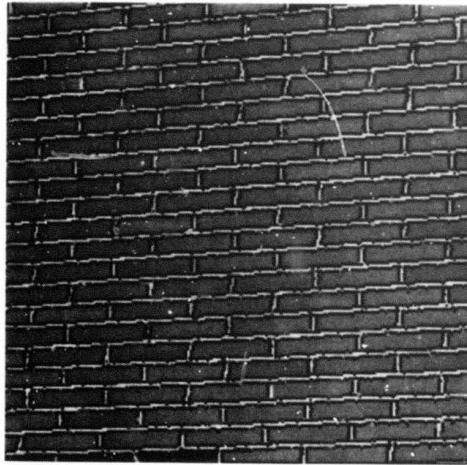
(b) Composite Primitive Image for (a)
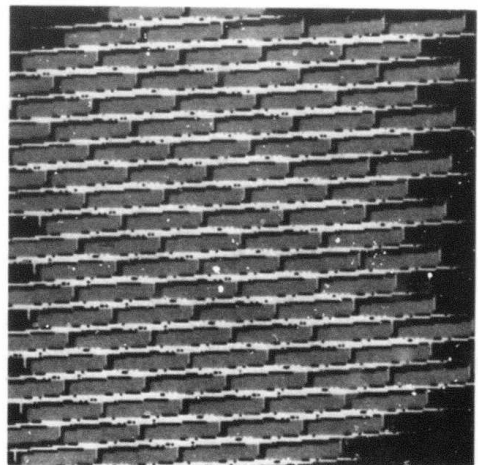
(c) Reconstruction for (a)

Figure 4-16.   Brick Texture, Composite Primitives and Reconstruction

223

TABLE 4-5. PRIMITIVE DESCRIPTIONS FOR BRICK4

PRIM NUMBER	REL INT	SCAN DIR	NUMBER OF PIXELS	SIG NUMBER	DIM1*	DIM2**	AVERAGE AREA IN PIXELS	AVERAGE INT	PERIOD*** IN PIXELS	BACK- GROUND	SEPARATED FROM
1	L	90°	16	.98	-	-	172.00	176.31	11.00	YES	-
2	D	90°	39	.90	7.00	34.97	244.33	134.77	11.00	-	-
3	L	0°	30	.30	2.00	7.33	14.20	171.67	-	-	2

*Dimension in scan direction in pixels
**Average dimension perpendicular to scan
    direction in pixels
***Period in the direction of scan

Legend: PRIM - PRIMITIVE
         REL - RELATIVE
         INT - INTENSITY
         D   - DARK
         L   - LIGHT
         DIR - DIRECTION
         SIG - SIGNIFICANCE

subwindow of Fig. 4-11(a) is the upper left hand quarter of this 256 x 256 pixel brick texture image. A comparison can be made of the composite texture primitive images from Fig. 4-1(b) and 4-16(b), and the texture and primitive descriptions from Fig. 4-3, Table 4-2, Fig. 4-17, and Table 4-6. Both texture descriptions are very similar. However, the brick (dark) element size in the vertical scan direction is larger by one pixel for the 256 x 256 image. This is probably due to a slight texture gradient in the image. It appears that the upper left hand corner of the wall was further from the camera lens than the central or lower parts.

The 2 texture primitive descriptions for the brick textural element show a large discrepancy (approximately 80 pixels) in average element size. This is due to the fact that the half bricks represent a much higher percentage of the total number of bricks in the smaller subimage than in the image shown in Fig. 4-16(a). The 2 sets of grid relations and links are shown in Figs. 4-15 and 4-18. The corresponding texture reconstruction, Figs. 4-11(b) and 4-16(c), are quite different. The larger brick wall reconstruction is quite close to the original with respect to brick size and relative placement. It would seem that the reason for the poor reconstruction in Fig. 4-11(b) (lower right) is the window

225

FILENAME = BRICK5

DARK OBJECT DESCRIPTIONS

VERTICAL SCAN DIRECTION

THERE IS STRONG EVIDENCE OF PERIODICITY (SPACING 12.00)

THERE IS STRONG EVIDENCE OF PREDOMINANT ELEMENT SIZE (9.00)
WITH MODERATE SUPPORT FOR ELEMENT SPACING (12.00)
RATIO OF SIZE TO PERIOD IS .75

LIGHT OBJECT DESCRIPTIONS

HORIZONTAL SCAN DIRECTION

NO EVIDENCE OF PERIODICITY
VERY STRONG EVIDENCE OF PREDOMINANT ELEMENT SIZE (3.00)

VERTICAL SCAN DIRECTION

THERE IS STRONG EVIDENCE OF PERIODICITY (SPACING 12.00)

THERE IS STRONG EVIDENCE OF PREDOMINANT ELEMENT SIZE (3.00)
WITH MODERATE SUPPORT FOR ELEMENT SPACING (12.00)
RATIO OF SIZE TO PERIOD IS .25

Figure 4-17. Brick5 Texture Description

FILENAME = BRICK5

GRID RELATIONS ARE AS FOLLOWS:

PRIM1 = 3   PRIM2 = 3   ANGLE = 30.00   DIST = 24.00   PER = 79.41   *
         PRIM1 = 3   PRIM2 = 3   ANGLE = -150.00   DIST = 24.00   PER = 77.28   *

PRIM1 = 3   PRIM2 = 3   ANGLE = -30.00   DIST = 27.00   PER = 85.68   **
         PRIM1 = 3   PRIM2 = 3   ANGLE = 150.00   DIST = 27.00   PER = 86.35   **

GRID LINKS ARE AS FOLLOWS:

PRIM1 = 3   PRIM2 = 2   ANGLE = 170.00   DIST = 21.00   PER = 90.96   ***

PRIM1 = 1   PRIM2 = 2   ANGLE = -30.00   DIST = 12.00   PER = 33.92   ***

Figure 4-18. Grid Relations and Links for Brick5

227

TABLE 4-6. PRIMITIVE DESCRIPTIONS FOR BRICK5

PRIM NUMBER	REL INT	SCAN DIR	NUMBER OF SAMPLES	SIG	DIM1*	DIM2**	AVERAGE AREA IN PIXELS	AVERAGE INT	PERIOD*** IN PIXELS	SEPARATED FROM
1	L	90°	39	.99	2.00	143.13	285.74	175.69	12.00	-
2	D	90°	122	.99	8.00	40.40	322.65	134.22	12.00	-
3	L	0°	121	.32	2.00	8.50	16.54	171.81	-	2

*Dimension in scan direction in pixels
**Average dimension perpendicular to scan
  direction in pixels
***Period in the direction of scan

Legend: PRIM - PRIMITIVE
        REL - RELATIVE
        INT - INTENSITY
        D - DARK
        L - LIGHT
        DIR - DIRECTION
        SIG - SIGNIFICANCE

228

size problem.

In Fig. 4-19, the grid relations and grid links extracted for the raffia image (Fig. 4-20(a)) are shown. The primitives referred to in this list correspond to the 3 primitive types described in Fig. 3-11. The texture reconstruction is given in Fig. 4-20(b). The unusual primitive shapes are a direct result of the wide variation in texture element shape in the original texture image. The set of placement rules selected seem to capture the basic relations inherent in the abstract primitive cluster of Fig. 3-3. The elongated light primitive in the reconstruction seems to have a varying spatial relationship with respect to the broad light primitive. This is due to the fact that except for certain directions angular displacements must be approximated in a digital image. The interactions of the approximations needed for 2 of the 4 placement rules used help to cause this oscillating effect.

In Figs. 4-21 through 4-24 the sets of grid relations and links for the 4 texture samples of Fig. 4-25(a) are given. The primitives refer to the primitives described in Tables 3-1 through 3-4 except where merging has taken place. For example, the placement rules for the floor grating pattern refer to only 1 (non-background) primitive

FILENAME = RAFFIA

GRID RELATIONS ARE AS FOLLOWS:

PRIM1 = 2   PRIM2 = 2   ANGLE = 180.00   DIST = 12.00   PER = 43.88   *
            PRIM1 = 2   PRIM2 = 2   ANGLE = .00   DIST = 12.00   PER = 40.48   *

PRIM1 = 2   PRIM2 = 2   ANGLE = -100.00 DIST = 9.00   PER = 27.25   **
            PRIM1 = 2   PRIM2 = 2   ANGLE = 80.00   DIST = 9.00   PER = 26.23   **

GRID LINKS ARE AS FOLLOWS:

PRIM1 = 2   PRIM2 = 1   ANGLE = -90.00   DIST = 3.00   PER = 44.73   ***

PRIM1 = 3   PRIM2 = 1   ANGLE = 150.00   DIST = 9.00   PER = 51.46   ***

Figure 4-19. Grid Relations and Links for Raffia

230

(a) Raffia Texture Image
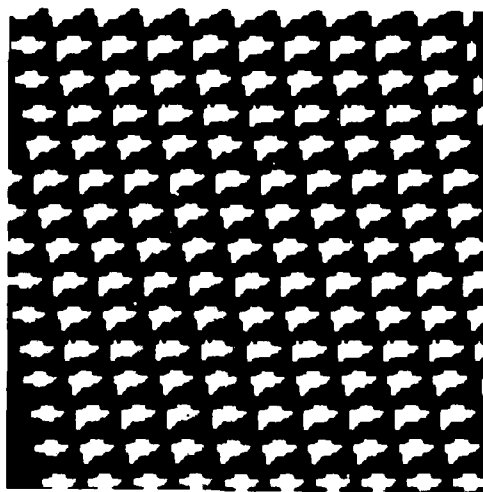
(b) Reconstruction for (a)

Figure 4-20. Raffia and Reconstruction

FILENAME = CITY1

GRID RELATIONS ARE AS FOLLOWS:

PRIM1 = 1   PRIM2 = 1   ANGLE = 180.00   DIST = 6.00   PER = 56.03   *
        PRIM1 = 1   PRIM2 = 1   ANGLE = .00   DIST = 6.00   PER = 55.80   *

PRIM1 = 1   PRIM2 = 1   ANGLE = -90.00   DIST = 15.00   PER = 63.94   **
        PRIM1 = 1   PRIM2 = 1   ANGLE = 90.00   DIST = 15.00   PER = 63.93   **

GRID LINKS ARE AS FOLLOWS:

PRIM1 = 3   PRIM2 = 1   ANGLE = 140.00   DIST = 12.00   PER = 54.79   ***

PRIM1 = 4   PRIM2 = 1   ANGLE = .00   DIST = 3.00   PER = 50.63   ***

PRIM1 = 2   PRIM2 = 1   ANGLE = -10.00   DIST = 3.00   PER = 33.57   ***

Figure 4-21.   Grid Relations and Links for City1

FILENAME = CITY2

GRID RELATIONS ARE AS FOLLOWS:

PRIM1 = 2   PRIM2 = 2   ANGLE = -150.00   DIST = 15.00   PER = 44.20   *
            PRIM2 = 2   ANGLE = 30.00   DIST = 15.00   PER = 43.91   *

PRIM1 = 2   PRIM2 = 2   ANGLE = 130.00   DIST = 30.00   PER = 25.14   **

GRID LINKS ARE AS FOLLOWS:

PRIM1 = 6   PRIM2 = 2   ANGLE = 80.00   DIST = 24.00   PER = 68.60   ***

PRIM1 = 6   PRIM2 = 1   ANGLE = 150.00   DIST = 18.00   PER = 38.64   ***

PRIM1 = 3   PRIM2 = 2   ANGLE = -70.00   DIST = 15.00   PER = 57.51   ***

PRIM1 = 5   PRIM2 = 2   ANGLE = 90.00   DIST = 24.00   PER = 57.33   ***

PRIM1 = 4   PRIM2 = 2   ANGLE = 160.00   DIST = 21.00   PER = 39.25   ***

Figure 4-22.   Grid Relations and Links for City2

233

FILENAME = HERRINGBONE MATERIAL

GRID RELATIONS ARE AS FOLLOWS:

PRIM1 = 3   PRIM2 = 3   ANGLE = -90.00   DIST = 12.00   PER = 48.60   *
             PRIM1 = 3   PRIM2 = 3   ANGLE = 90.00   DIST = 12.00   PER = 45.20   *

PRIM1 = 3   PRIM2 = 3   ANGLE = -50.00   DIST = 9.00   PER = 27.88   **
             PRIM1 = 3   PRIM2 = 3   ANGLE = 130.00   DIST = 9.00   PER = 25.84   **

GRID LINKS ARE AS FOLLOWS:

PRIM1 = 4   PRIM2 = 3   ANGLE = -90.00   DIST = 6.00   PER = 39.53   ***

PRIM1 = 6   PRIM2 = 3   ANGLE = 70.00   DIST = 18.00   PER = 49.51   ***

PRIM1 = 1   PRIM2 = 4   ANGLE = -30.00   DIST = 3.00   PER = 28.83   ***

PRIM1 = 6   PRIM2 = 2   ANGLE = 150.00   DIST = 27.00   PER = 25.71   ***

PRIM1 = 5   PRIM2 = 3   ANGLE = 30.00   DIST = 15.00   PER = 36.49   ***

Figure 4-23.   Grid Relations and Links for Herringbone Material

234

FILENAME = FLOOR GRATING

GRID RELATIONS ARE AS FOLLOWS:

PRIM1 = 1   PRIM2 = 1   ANGLE = 180.00   DIST = 12.00   PER = 83.82   *
       PRIM1 = 1   PRIM2 = 1   ANGLE = .00   DIST = 12.00   PER = 83.03   *

PRIM1 = 1   PRIM2 = 1   ANGLE = 120.00   DIST = 12.00   PER = 80.13   **
       PRIM1 = 1   PRIM2 = 1   ANGLE = -60.00   DIST = 12.00   PER = 79.88   **

Figure 4-24.   Grid Relations for Floor Grating

235
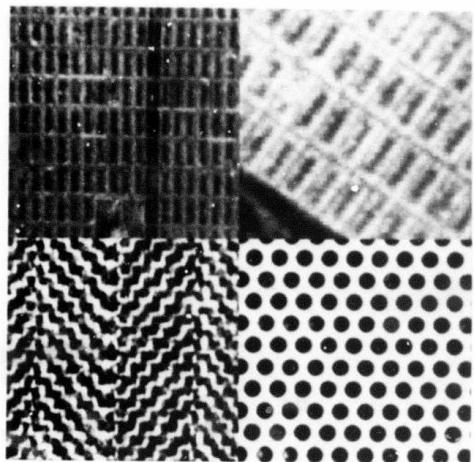
(a) Regular Texture Mosaic
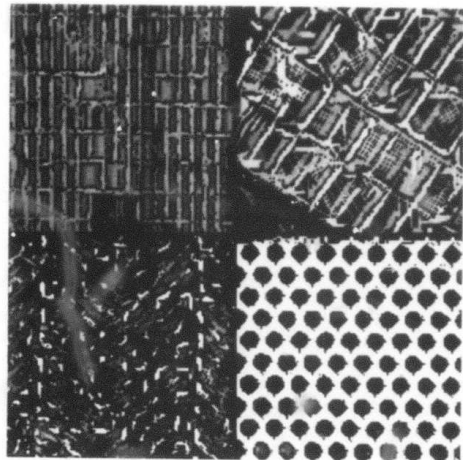
(b) Composite Primitive
Image for (a)
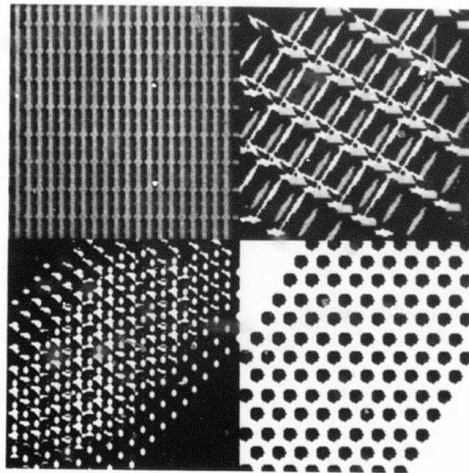
(c) Reconstruction for (a)

Figure 4-25.   Periodic Texture Mosaic, Composite
Primitives and Reconstruction

236

type. This is because all of the dark primitives were recognized as belonging to the same primitive type and so were merged. Figure 4-25(c) is the reconstruction mosaic corresponding to the texture samples in Fig. 4-25(a). The grid like appearance of the first aerial city texture sample is captured in its corresponding reconstruction. The reconstruction for the second city texture sample seems much more abstract. The elongated light rows and dark primitives seem to be well placed; but the reconstruction seems less complete than for its neighbor to the left. It should be noted that the reconstruction process has only the extracted texture primitive types to work with. These primitives are included in the composite primitive images of the mosaic in Fig. 4-25(b). The texture primitive composite mask image for the rightmost aerial city image seems to be less complete than the one on the left. In this case, one can only determine if the spatial arrangement of the reconstruction is consistent with the original texture image. It is not meaningful to ask how closely it duplicates the original.

The herringbone material pattern is not a homogeneous regular texture pattern (as previously defined). It is, instead, a texture made up of alternating texture strips. All of the texture primitives of a given type do not have the same environment. Their environment depends on where

237

they are located in the original texture image. The minimum set of placement rules extracted do not completely characterize the spatial arrangement of the primitives within the herringbone texture image. Although the texture reconstruction might look similar to the herringbone texture, it does not capture the underlying textural structure completely.

The last texture sample in this mosaic (Fig. 4-25(a)) is the floor grating texture. Only 2 placement rules are needed to characterize the underlying grid pattern (Fig. 4-24) since there is only one non-background primitive type after merging. The spatial arrangement of the grating pattern is successfully captured in the texture reconstruction. (See Fig. 4-25(c).)

4.5 Summary and Conclusions

In this chapter an algorithm for analyzing the spatial arrangement of the primitives comprising a given texture was presented. The starting point of the algorithm is the set of texture primitive masks extracted by using the algorithm discussed in Chapter 3. The results produced are a set of primitive placement rules, a minimum, not necessarily unique, set of rules needed to completely characterize the underlying textural grid, and a texture reconstruction image. The latter 2, i.e., the

minimum set of rules and the texture reconstruction are only meaningful when the texture under consideration is homogeneous and regular.

Results for a number of regular texture images were presented and discussed. The textures samples analyzed include 2 aerial city images, a raffia sample, a herringbone material subimage, a floor grating texture sample and a number of brick texture subwindows. In most cases, the underlying grid structure was captured by the minimum set of placement rules extracted.

CHAPTER 5

STRUCTURAL TEXTURE ANALYSIS APPLICATIONS

5.1 Introduction

In Chapters 2, 3, and 4, a number of texture analysis techniques were presented. These techniques are useful for generating structural texture descriptions. However, they can also be applied to other texture analysis tasks. Two such tasks are texture recognition, and surface orientation determination.

In Section 5.2 a texture classification scheme is presented. This scheme uses the information contained in the general texture description produced by the ERA interpretation algorithm. It also uses the information contained in the individual primitive descriptions created by the primitive extraction algorithm. These types of descriptions were discussed in Chapters 2 and 3, respectively. In Section 5.2.2, texture classification results for eleven types of textures are presented and discussed.

In Section 5.3 the problem of determining the

240

orientation of textured surfaces is discussed. The discussion centers around the use of the gradient of the texture as the primary surface orientation cue. Work done by Bajcsy [5] and Stevens [23], [30] in this area is briefly discussed. An orientation analysis scheme is suggested which is based on these methods and incorporates some of the texture analysis techniques presented earlier in this thesis. Preliminary results for a number of texture images exhibiting texture gradients are discussed.

5.2 Texture Recognition

The texture recognition scheme presented here is basically a decision tree classifier. It uses the one-dimensional ERA interpretations and the 2-dimensional texture element descriptions presented and discussed earlier. The first describes a texture in terms of characteristics which can be detected from analyzing the ERA results for a given texture image. The second describes classes of individual texture primitive types. A texture recognition scheme (for 11 types of textures) is discussed below. It uses the information from both of these types of texture descriptions.

5.2.1 Texture Recognition Algorithm

The structure of the algorithm used for texture

classification is shown in Fig. 5-1. The 11 texture classified are: floor grating (dark dot pattern), brick wall, aerial view of city, raffia (woven palm), herringbone material, wood grain, aerial view of water, straw, grass, sand, and wool.

Most of the textures used are from the Brodatz album [22]. The exceptions are the floor grating, brick wall, and aerial city patterns. Aerial city pictures taken at different orientations and different scales were used. (See the top row of Fig. 3-8(a)). Only 11 samples are found. All other texture groups consist of 16 samples each. The 2 basic brick wall patterns of Fig. 1-1 are used.

The decision tree form was chosen for this texture classification scheme. The structure of the tree allows the classification information to be weighted by means of relative ordering. For example, the test for periodicity is encountered at an earlier stage than any of the aspect ratio tests. Clearly texture period information is being given more significance than aspect ratio information according to this classification scheme. An equivalent production system or graph matching scheme could have been used. However, it was decided that the tree structure would be the most efficient method to use (in terms of
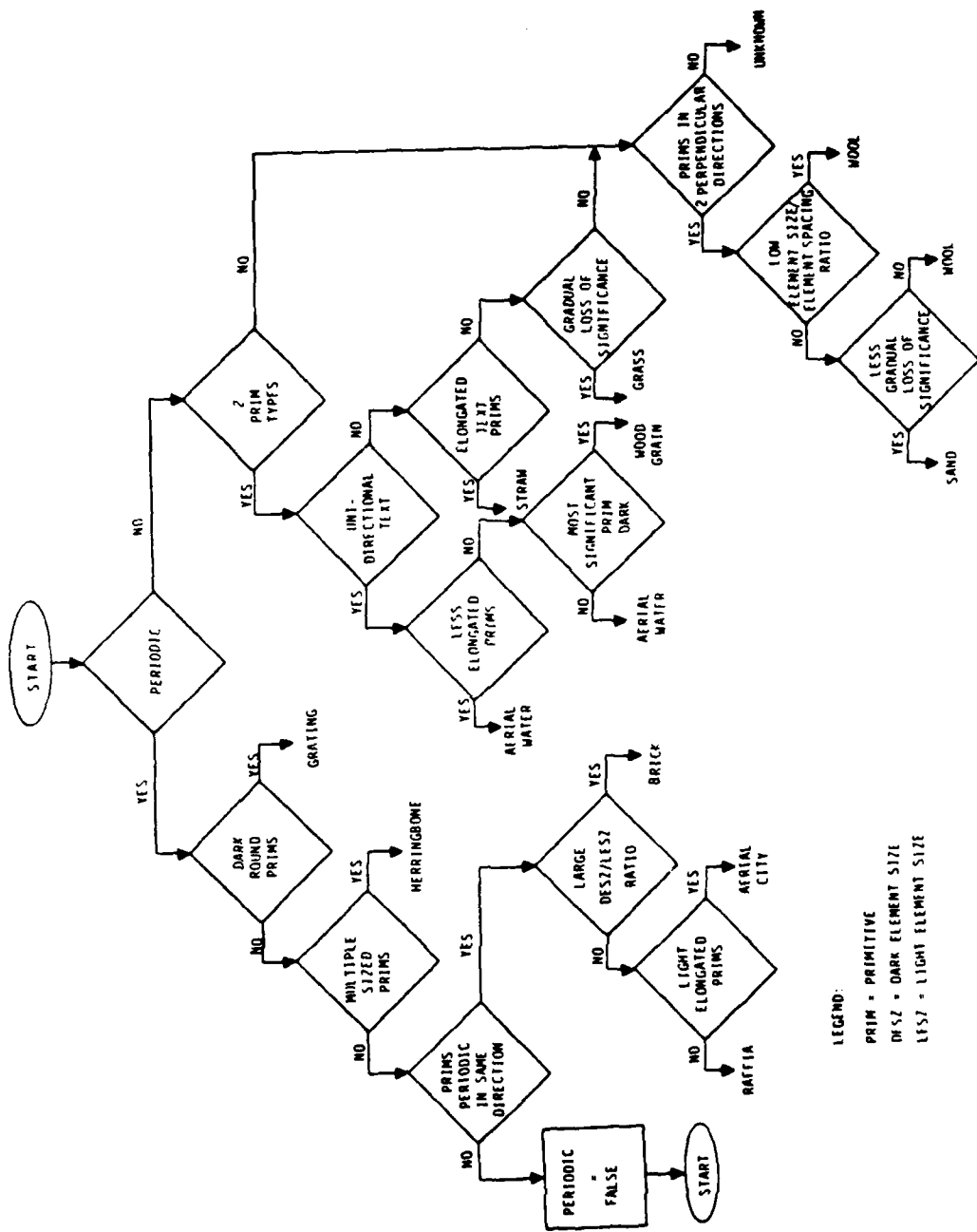
Figure 5-1. Decision Tree Classifier

LEGEND:

PRIM = PRIMITIVE

DESZ = DARK ELEMENT SIZE

LESZ = LIGHT ELEMENT SIZE

243

programming ease and computational complexity) which would
be adequate for classifying this set of textures.

The first texture characteristic considered is
periodicity. If a texture is non-periodic it will be
classified by the subtree to the right of the root node.
However, if the texture exhibits signs of periodicity but
fails the tests for each of the 5 regular texture patterns
it is sent back to the root node re-labeled as a
non-periodic texture. Due to this loop in the structure,
the classification algorithm does not have the exact form
of a binary decision tree. However, for convenience tree
terminology will be used in the discussion. The loop is
introduced to accommodate textures which are basically
non-periodic, but may show evidence of periodicity some of
the time. The wood grain, water and straw textures
exhibit this characteristic. The opposite is not as
likely to occur, i.e., none of the periodic textures are
ever mistakenly sent down the non-periodic branch.

No absolute texture element dimensions or intensity
values are used; and all directional information is
relative as well. In this way, the analysis should be
insensitive to scaling, rotation and degree of contrast
within the image. Measures which are used are primitive
eccentricity, dimension to period ratio, the number and

significance of texture element types, and relative
intensities and orientations of texture primitive types.
The details of each decision box for the two main decision
branches is given below:

Periodic Branch

1) Dark Round Primitives - More than four dark
    primitives are merged into one primitive type.

2) Multiple Sized Primitives - Multiple sized primitives
    are found in two perpendicular directions. The
    texture period is equal to the sum of the element
    sizes. The sum of the (size/period) ratios for the
    four most significant primitives is less than .2.

3) Most Significant Primitives are Periodic in the Same
    Direction - The two most significant primitives
    exhibit an element spacing value for the same scan
    direction.

4) Large (Dark Element Size/Light Element Size) Ratio -
    The dark primitive is at least twice as wide as the
    light primitive in the most significant scan
    direction.

5) Light Elongated Primitives - The ratio of the
    dimension in the most significant scan direction to

the dimension in the direction perpendicular to the direction of scan is less than .4.

Non-Periodic Branch

1) Uni-Directional Texture - The two most significant primitives are found in the same scan direction. The significance numbers associated with these two primitive types are greater than all other significance numbers by at least .66 (out of a possible 1.0).

2) Less Elongated Primitives - The sum of the aspect ratios for the two most significant primitives is at least as great as .175.

3) Most Significant Primitive is Relatively Dark.

4) Elongated Texture Primitives - The minimum aspect ratio of the four most significant texture primitives is no larger than .18.

5) Two Primitives Types - Primitives are found for the two most significant (intensity,direction) pairs.

6) Gradual Loss of Significance - There is no abrupt loss of significance after the fourth (intensity,direction) pair. The difference is smaller than .3.

7) Primitives Found in Two Perpendicular Directions.

8) Low Size/Spacing Ratio - There is a low (element size/element spacing) ratio for relatively dark primitives in two perpendicular directions. The sum of both ratios is less than .53.

9) Less Gradual Loss of Significance - The loss of significance after the fourth (intensity,direction) pair is at least .3.

No attempt has been made to optimize this decision scheme. The classification results are discussed in the following section.

5.2.2 Classification Results

Classification results are given in the confusion matrix shown in Table 5-1. The types of samples to be classified are listed to the left of the matrix. Each row shows how a specific set of samples was classified. For example, 15 aerial water texture samples were correctly classified, while one sample was incorrectly classified as wood grain. One hundred seventy-one samples were classified in all. In most cases the samples came from 512 x 512 pixel texture images. These were divided into sixteen 128 x 128 pixel non-overlapping texture

TABLE 5-1. CONFUSION MATRIX

Type	Floor Grating	Herring-Bone	Raffia	Brick	Aerial City	Aerial Water	Wood Grain	Straw	Grass	Sand	Wool
Floor Grating	16	0	0	0	0	0	0	0	0	0	0
Herring-Bone	0	16	0	0	0	0	0	0	0	0	0
Raffia	0	0	16	0	0	0	0	0	0	0	0
Brick	0	0	0	16	0	0	0	0	0	0	0
Aerial City	0	0	0	0	11	0	0	0	0	0	0
Aerial Water	0	0	0	0	0	15	1	0	0	0	0
Wood Grain	0	0	0	0	0	2	14	0	0	0	0
Straw	0	0	0	0	0	0	0	16	0	0	0
Grass	0	0	0	0	0	0	0	0	11	5	0
Sand	0	0	0	0	0	0	0	0	0	14	2
Wool	0	0	0	0	0	0	0	0	2	3	11

248

subwindows. However, in the case of the aerial city samples only 11 samples were available. These were cropped from two different satellite images of the San Francisco area. The 16 brick wall samples were taken from three separate brick wall images. One hundred fifty-six samples were correctly classified to give an overall success rate of 91.23%. It should be noted that additional contextual information, e.g., color, scale, and type of scene would probably have improved the results obtained. However, no information of this type was used in the classification scheme in order that the strength of the texture descriptions used could be tested in isolation.

There are no mismatches for the highly structured, regular texture group. However, there are a number of non-periodic texture samples which are classified incorrectly. One source of confusion is between the water and wood grain textures. Both are one-dimensional textures made up of elongated texture primitives. The wood grain primitives tend to be more elongated than the water wave primitives. There is little else which is noticeably different from a structural point of view. Hence, confusion of these two texture types is predictable. Additional contextual information, e.g., the scale information for both textures, would improve the

classification results.

Another area for confusion is the set of textures in Fig. 3-10(a). These textures (grass, sand, and wool) exhibit the least amount of structure of the entire set. The edge images (Fig. 2-18(b), ERAs (Figs. 2-19 to 2-22), ERA descriptions (Figs. 2-33 to 2-36), composite texture primitive masks (Fig. 3-10(b)), and texture primitive descriptions (Tables 3-9 to 3-12) are very similar for all three types. This is because the program is not designed to measure the types of features which most readily differentiate these textures. In light of these description similarities, confusion among members of this group is to be expected. It should be noted that none of these texture samples *were confused with textures from* outside of the group and none of the other texture samples were mistakenly classified as one of these. The same can be said of the subgroup formed by the water and wood grain textures.

In summary 156 samples out of 171 were correctly classified to give an overall success rate of 91.23% for this classification scheme. These results are extremely encouraging. It would seem that the information extracted by the algorithms presented earlier in this thesis describe meaningful texture characteristics.

250

5.3 Surface Orientation Analysis

In Figs. 5-2 and 5-3 two texture gradient images are shown. Figure 5-2 is an image of a brick wall and Fig. 5-3 is an image of a redwood shake ɔof. In each case the textured surface is at a non - zero angle with respect to the image plane. The brick wall recedes to the left of the image, while the shake roof slants away from the viewer toward the top of the image.

One cue which we use to infer information about the orientation of textured surfaces is the texture gradient, i.e., the relative change in size or period of the elements making up the textured region within the image. Assuming that the textured surface being viewed is homogeneous, the element sizes of like texture primitives should decrease with increased distance from the viewer. The direction of maximum rate of change of depth with respect of the observer should be discernible as well as the degree of surface slant in this direction. A convenient way to represent these two surface characteristics is via the gradient space (as introduced by Mackworth [31]).

Let $z = f(x,y)$ be a function defining a planar surface in 3-Space, where the image plane is parallel to
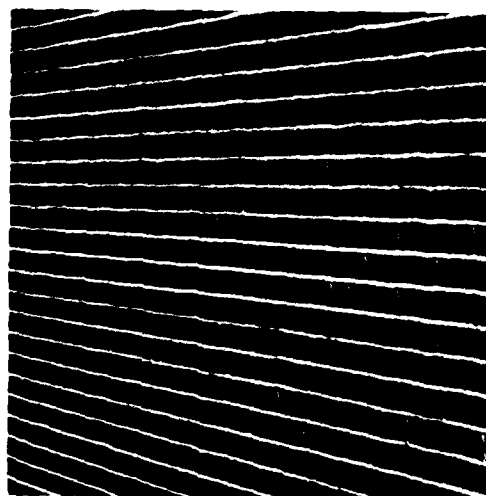
Figure 5-2. Brick Wall

Figure 5-3. Redwood Shake Roof

252

the x-y plane, (see Fig. 5-4). The surface normal, N, can be defined as follows: $N = (f_x, f_y, -1)$. Letting $p = f_x$, and $q = f_y$, we have the gradient vector, $G = (p,q)$. The direction of G is $TAN^{-1}(q/p)$, while the magnitude of G is $SQRT(p^2 + q^2)$. The direction of G denotes the direction of the greatest rate of change within the image, while the magnitude of G determines its quantity. Also, the tangent of the angle that the surface makes with the x-y (or image) plane is equal to the magnitude of G. Therefore, the orientation of a surface in 3-Space can be represented as a point in the gradient space.

In [23] Stevens suggests an alternate set of coordinates to represent surface orientation. He suggests the pair (σ, τ), where

$$\sigma = \tan^{-1}((p^2 + q^2)^{1/2}) \ ,$$

and

$$\tau = \tan^{-1}(q/p) \ ,$$

Stevens' slant and tilt angle terminology will be used. The tilt angle, τ , is an angle made with the horizontal axis of the image plane. It is the projection of the surface normal onto the image plane. Stevens has shown that this direction coincides with the direction which exhibits the greatest rate of change of distance from the

253
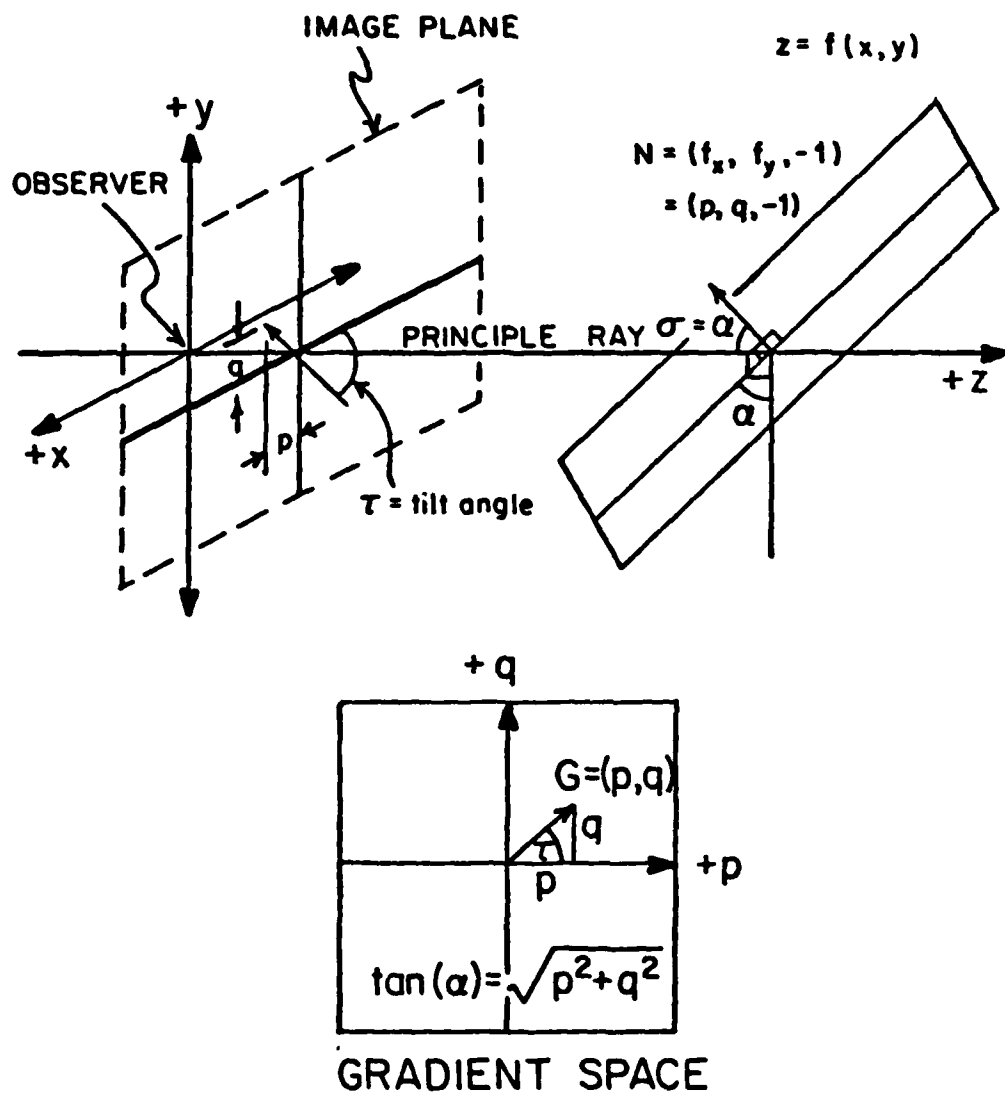
Figure 5-4.   Gradient Space Scheme

observer to the surface. This is precisely the direction of the texture gradient. Therefore, by calculating the texture gradient one can determine the tilt angle. The slant angle, σ, is the angle which defines how much the image plane orientation differs from the surface plane orientation. For a discussion of various forms of surface orientation representation see the works of Stevens [23] and Kender [32].

5.3.1 Methods for Determining Surface Orientation

In [23] Stevens proposed a method for determining the gradient direction, or tilt angle, and the angle made by the surface normal and the line of sight to the surface at that point. He calls the latter the slant angle. They are τ and σ as described above. (When the line of sight is the principle ray, then the slant angle is equal to the angle made by the surface and the image plane.)

Calculating the tilt angle is fairly straightforward. It entails determining the direction of the gradient of any texture measure which is scaled (due to distance), foreshortened (due to surface orientation), or both scaled and foreshortened.

Determining the slant angle, σ, is more involved. One method suggested is to determine which texture measure

corresponds to the characteristic dimension. That is, which texture measure is scaled but not foreshortened. The normalized gradient of this dimension, taken in the direction of the texture gradient, is equal to the tangent of the slant angle.

$$\frac{\nabla d}{d} = \tan \sigma , \qquad (5\text{-}1)$$

where d is the characteristic dimension. Characteristic dimensions are parallel to the image plane and are perpendicular to the local surface tilt. Therefore, after the surface tilt has been determined the orientation of the characteristic dimension is known. This scheme for calculating σ cannot be used if the image is an orthographic projection, or if the elements exhibit successive occlusion. Alternative schemes are explored in [23] for handling these problems. Here it will be assumed that neither problem exists.

In [5] Bajcsy presents a method for calculating the angle formed by the image and surface planes. However, the dimension used in this case is the dimension oriented in the gradient direction. Therefore, it is both foreshortened and scaled.

Using the principles of projective geometry, the

256

trigonometric rules pertaining to similar triangles and some small angle approximations, Bajcsy derives an expression for α, the angle formed by the surface and image planes.

$$\frac{-\tan\alpha}{\text{Focal distance}} = \frac{\text{Fractional change in element size}}{\text{Baseline in image}} \qquad (5-2)$$

where the fractional change in element size and the baseline within the image are both measured in the direction of the texture gradient. Details of the derivation can be found in [5].

Both methods assume proximity to the line of sight defining the local image plane. All of the examples used in Section 5.3.2 have maximum off center angle less than 10 degrees. Further work is necessary to define the transformation needed to correct for large off center angular separations. This transformation should take into account the image plane and lens system characteristics as well as the geometry needed for coordinate transformations.

5.3.2 A General Orientation Analysis Technique

Application of the structural texture analysis techniques presented earlier in this thesis to the surface orientation analysis problem is in a preliminary stage.

The process has not been fully defined or automated. An outline of a proposed algorithm is discussed below, and some preliminary results are presented in the following section. Although only part of the program is operational, see 2 below, most of the remaining program sections are defined and seem feasible from a programming point of view.

One effect which must be anticipated by this technique is the possible changing orientation of the texture primitives. If the texture gradient was strong enough the height of the brick primitives in Fig. 5-2 would be found in the 120 degree scan direction in the lower left hand part of the image and in the vertical scan direction in the right and central areas. One possible solution is discussed in (3) below.

A possible scenario for detecting surface orientation is as follows:

1. Divide the textured region into locally uniform subwindows, i.e., subwindows which exhibit very little, if any, element size variation. This algorithm is not yet defined. However, as a first approximation the image can be divided into subwindows which accommodate the largest texture elements. Then element sizes can be averaged over each texture

subwindow to produce an element size for that location in the image. This was done manually for the two examples discussed below. (In order to automatically determine the largest element size, one might calculate modified ERAs (see 2 below) for a large range of distances, say up to one third of the largest image dimension, over the entire texture image. Then an ERA interpretation routine, similar to the one presented in Chapter 2, can be used to determine the largest texture element dimensions.)

2. Calculate modified ERAs for each subwindow within the region. Only the first atch encountered will be recorded for a particular directional scan. Hence, no element size or spacing repetitions should be counted. It is hoped that this will prevent repetitions from being interpreted as element size variations within a given subwindow. The modified ERA calculation scheme is operational and has been used to produce the results shown in Fig. 5-5.

3. Look for a dimension exhibiting strong results for each subwindow. A dimension, d, which is locally uniform but which reflects the gradient of the texture is sought. It should be verified that all of the ERA results chosen refer to the same texture primitive
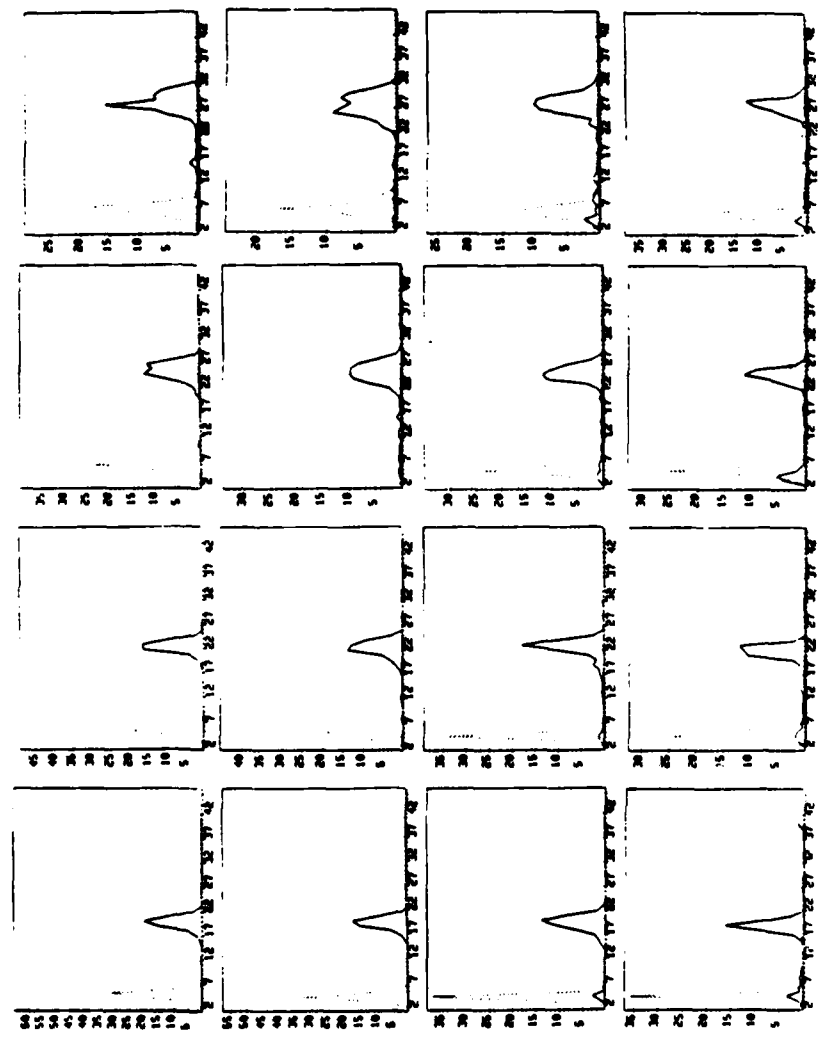
Figure 5-5. Vertical Brick Element Size Graphs for Example 1

260

type. One way to achieve this end is to extract texture primitives for overlapping subwindows and verify that enough of the primitives extracted belong to both subwindow neighbors. In this way textural elements which shift orientation due to the effect of angular perspective can be found in each subwindow.

4. Create a matrix, M, of the centroid values of the element size peaks for d. Use a gradient operator on M to calculate the value of the tilt, or gradient, angle of the surface within the image. (A discussion of gradient operators can be found in [33].)

5. Knowing the tilt angle means that the orientation of the characteristic dimension is also known. It can then be ascertained if either the characteristic dimension or the gradient dimension is already available as part of the set of ERA results. If this is the case then the rest of this step can be skipped. If this is not true then the characteristic or gradient dimension of some non-background texture primitive type must be measured from texture primitive masks. (These measurements should proceed outward from the elemental centers of mass.) Either of these two dimensions can be used for the slant angle calculation. Histograms of these dimensions should be

261

kept so that the final calculations can be made using the highest amplitude/lowest standard deviation results. When measuring the characteristic dimension the original set of subwindows can be used. However, when calculating the gradient dimension the subwindows might have to be recropped to provide the correct center to center angle.

6. At this point either (5-1) or (5-2) can be used to calculate the surface slant angle to complete the procedure. If the characteristic dimension is known then (5-1) would be used. If the dimension oriented in the texture gradient direction is known then (5-2) would be used. (See Section 5.3.1 for a brief description of both slant angle calculation methods.)

5.3.3 Texture Gradient Examples

In this section two texture gradient examples are presented and discussed. They make use of the general method outlined in Section 5.3.

Example 1

Consider the brick wall image in Fig. 5-2. This image is 512 x 512 pixels. It was divided into 16 128 x 128 pixel subimages, and ERAs were calculated for each of these. The vertical element size ERAs for each

subwindow are shown in Fig. 5-5. As expected the element sizes decrease toward the left side of the image. Figure 5-6(a) shows the brick vertical element size dimension matrix. In Fig. 5-6(b), the results of the gradient calculation are shown; and Fig. 5-6(c) shows the results of the tilt and slant angle calculations. In this case the vertical brick dimension is the characteristic dimension, hence, the method developed by Stevens will be used to calculate the surface slant. The slant and tilt calculations are carried out for the 4 interior subwindows of the image (Fig. 5-2). The tilt angle measured from the image is approximately 3°. The tilt angle results range from $.967^{\circ}$ to 4.52°. Unfortunately, the actual slant angle is not known for this image. However, the results found for this angle seem to be reasonable. The angle made by the image and surface planes, or similarly, the angle between the principle ray and the surface normal seem to be in the neighborhood of 45°. In the next example the approximate angle formed by the surface and the image plane is known.

Example 2

Consider the shake roof image in Fig. 5-3. This image is 512 x 512 pixels. It was divided into 9 170 x 170 pixel subimages. (The last two rows and columns

19.759	22.547	25.644	28.551
19.515	22.406	25.176	27.450
19.368	22.496	25.306	28.182
18.938	21.868	24.965	28.029

(a) Brick Vertical Dimension Matrix. Each value, d, is a dark, vertical element size.

$$S_x = -23.146$$
$$S_y = -.83 \tag{1}$$

$$S_x = 21.778$$
$$S_y = -1.094 \tag{2}$$

$$S_x = -23.566$$
$$S_y = -1.864 \tag{3}$$

$$S_x = -22.577$$
$$S_y = -.381 \tag{4}$$

(b) Gradient Results for (a).

$$\tau = \tan^{-1}\left(\frac{S_y}{S_x}\right) \qquad \sigma = \tan^{-1}\left(\frac{\sqrt{S_x^2 + S_y^2}}{d}\right)$$

| 2.05° | 2.88° |
| 4.52° | .967° |

| 45.95° | 40.90° |
| 46.42° | 41.74° |

(c) Tilt and Slant Angle Matrices.

Figure 5-6. Analysis for Example 1

264

were not used.) ERAs were calculated for each of the nine subimages. The vertical element size ERAs for each subwindow are shown in Fig. 5-7. As expected the element sizes decrease toward the top of the image. Figure 5-8(a) is the matrix of the centers of mass for the vertical element size ERAs of Fig. 5-7. In Fig. 5-8(b) the results of the gradient and tilt angle calculations are shown, and Fig. 5-8(c) shows the results of the slant angle calculation for three image locations. The gradient direction dimension, i.e., the vertical dimension, of the wood shake elements was already known via ERA calculation. Therefore, the the surface slant angle was calculated using the method developed by Bajcsy. (It would be very difficult to use the characteristic dimension in this example since the widths of the wood shake are variable.) The slant angle computations are carried out for 3 sets of data. The tilt angle is calculated once since there are only enough windows for one gradient computation. The tilt angle for the image (Fig. 5-3) is approximately 90°. The tilt angle was computed to be 88.49°. The slant angle was calculated to be approximately 71.97°. (See Fig. 5-9.) The slant angle calculation results range from 72.405° to 74.167°.

Determination of window size is a problem which must be addressed. One possible solution is to calculate a set
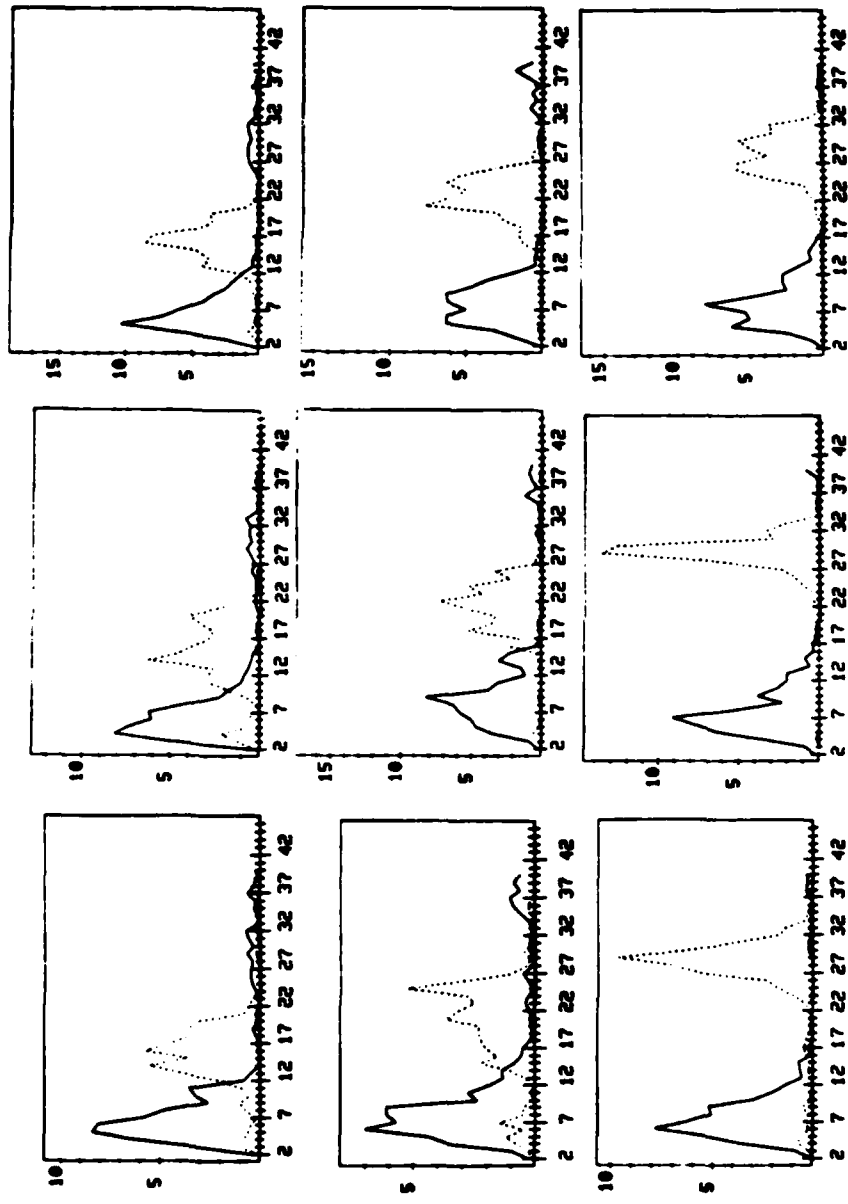
Figure 5-7. Vertical Wood Shake Element Size Graphs for Example 2

266

	1	2	3
d_1	16.029	15.855	16.286
d_2	21.223	21.317	22.104
d_3	28.808	29.347	28.146

Image Baseline
(340 pixels)

(a) Redwood Shake Vertical Dimension Matrix. Each value, d, is a light vertical element size.

$$S_x = 1.357 \qquad \tau = \tan^{-1}(\frac{S_y}{S_x})$$

$$S_y = 51.623 \qquad \tau = 88.49^{\circ}$$

(b) Gradient and Tilt Angle Calculation.

$$\alpha = \tan^{-1}\left(\frac{(d_3-d_1)* \text{ Focal Distance}}{\frac{1}{2}(d_3+d_1)* \text{ Image Baseline}}\right)$$

Focal Distance = 50 mm = 2008.33 pixels

α_1	α_2	α_3
73.46°	74.17°	72.41°

(c) Slant Angle Result Matrix.

Figure 5-8. Analysis for Example 2

267
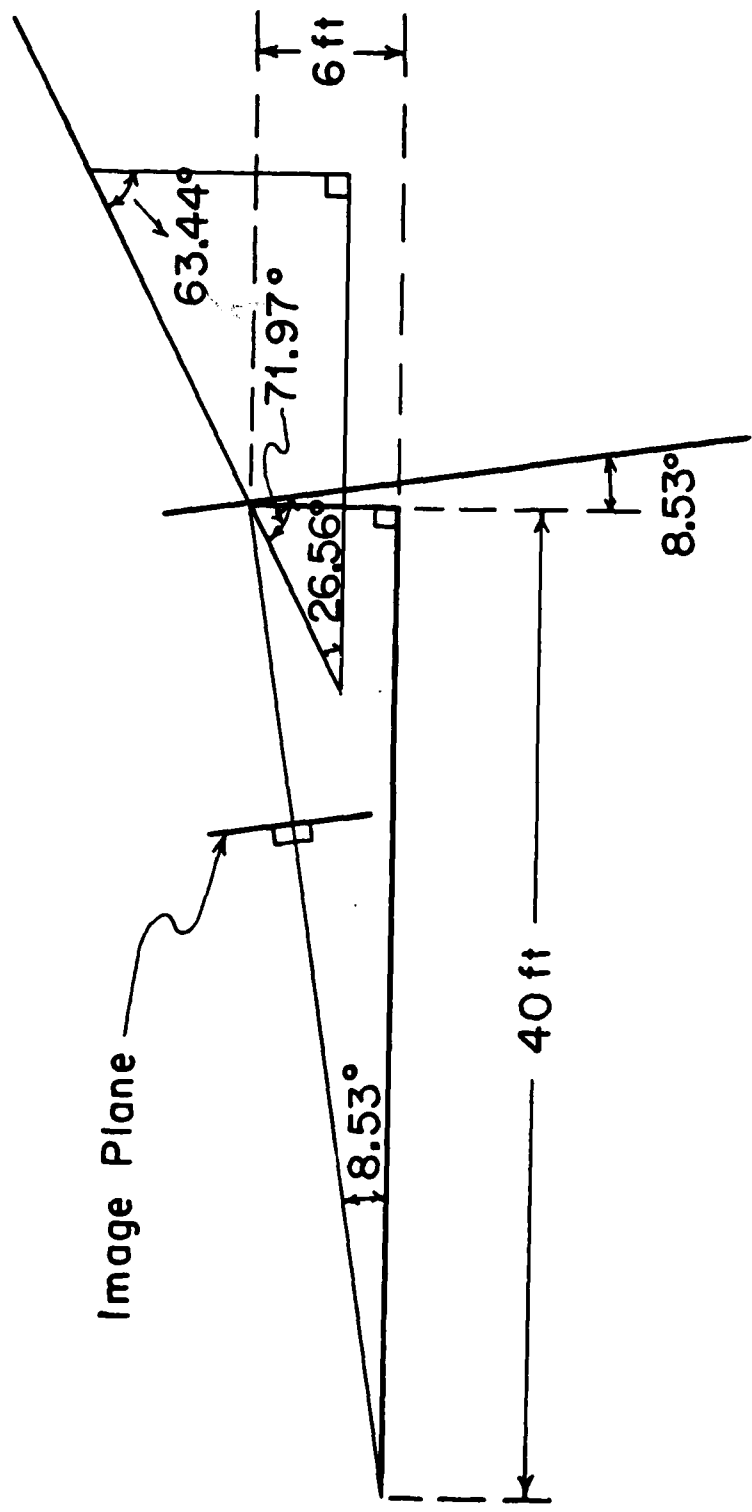
Figure 5-9. Geometry for Surface in Fig. 5-3

268

of ERAs for the entire image, initially, for a wide range of distances. The maximum element sizes found would then dictate the appropriate window size.

5.4 Summary and Conclusions

In this chapter the structural texture analysis techniques developed earlier were applied to 2 texture analysis problems, namely, texture recognition and surface orientation determination. The results obtained in both cases appear to be very promising.

In Section 5.2 a classification scheme using both one-dimensional texture descriptions and texture primitive descriptions was presented and classification results were discussed. The algorithm was designed to classify 11 different types of textures, including 6 random and 5 periodic textures. The random textures were taken from the Brodatz album [22]. These are grass, sand, wool, water, wood, and straw. The 5 periodic textures came from a variety of sources ranging from aerial imagery to pictures taken by the author. They are raffia, herringbone material, floor grating, aerial city, and brick wall. The algorithm achieved an overall success rate of 91.23%. The classification scheme worked well for the non-periodic texture group, and extremely well for the highly structured regular textures, achieving 100% correct

269

classification for this group. In those cases where there was confusion additional contextual information would have been helpful. For example, knowing scale information would have aided in distinguishing wood grain from the aerial water texture. As might be expected the amount of algorithm success varied directly with the amount of structure present in the texture. Since the range of textures handled by this algorithm is varied and any confusion encountered is restricted to small groups, (2-3) of similar textures it is fair to say that the description information extracted thus far corresponds to meaning textural features.

The surface orientation determination scheme presented in Section 5.3 is in preliminary form. The method described is only partly automated. It uses schemes developed by Bajcsy [5] and Stevens [23]. It also utilizes the techniques developed in the earlier chapters of this thesis. Some preliminary results are presented and discussed. Tilt and slant angles are calculated for two images exhibiting non-zero texture gradients. The results for all known quantities are accurate to within 5 degrees. These results appear to be promising. However, more work needs to be done to completely automate the process.

CHAPTER 6

SUMMARY AND CONCLUSIONS

In this dissertation a general method for structural texture analysis was presented. In chapter 2, edge repetition arrays were defined. It was explained how they could be used to extract certain structural information, such as periodicity, directionality, and predominant element size from the edge and direction images corresponding to a natural texture image. An algorithm was presented which automatically interprets these arrays and outputs a structural texture description. ERA results were shown for a number of different natural texture images. The texture descriptions generated for these arrays were also presented. In most cases, the texture periods, predominant element sizes, primitive orientations, and relative elemental intensities were correctly reported in the texture description.

The ERAs, and hence, the texture descriptions derived from them are produced by analyzing lines of pixels (in 6 different directions) within the edge and direction images. Therefore, these descriptions are one-dimensional

271

in nature. The element sizes reported describe a single dimension of the elements comprising the texture. Although these texture descriptions do not provide enough information in themselves to completely describe the two-dimensional texture elements they can serve as the starting point for a two-dimensional texture primitive search.

In Chapter 3, a primitive extraction algorithm was presented. It uses the internal form of the one-dimensional texture description to pinpoint the actual locations of the individual primitives within the texture image. As a result, individual and composite primitive masks are produced along with a set of texture primitive descriptions, one *for each texture primitive type*. Texture primitive masks and descriptions were presented and discussed for a number of different types of natural textures. The algorithm performed very well for most textures whose primitives exhibited at least one uniform dimension.

A structural texture description should include information pertaining to the arrangement of the elements of which the texture is composed. In Chapter 4, an algorithm was presented which extracts the most frequently occurring inter-primitive placement rules. In the event

that the natural texture being considered is homogeneous and regular, a minimum, not necessarily unique, set of rules is extracted which completely describes the underlying texture pattern. As part of the algorithm, a texture pattern is constructed using the minimum set of placement rules along with a set of average primitive templates. This texture reconstruction can be used to visually determine how closely the minimum placement rule set characterizes the underlying texture pattern. Texture reconstructions are presented and discussed for all of the homogeneous, regular textures examined up to this point. In most cases, the underlying grid pattern was captured in the texture reconstruction. A logical extension of this algorithm would be to include increasingly complex texture types in the class of natural textures for which a minimum set of placement rules can be extracted.

In Chapter 5, the texture analysis techniques presented in the first 4 chapters are applied to two texture analysis applications, namely, texture recognition and determination of surface orientation using texture gradient cues. A texture classification scheme for the 11 natural texture types used in this thesis was devised. An overall success rate of 91.23% was achieved. Since the range of textures classified by this algorithm is varied and any confusion which was encountered was restricted to

small groups of similar textures, it would seem to indicate that the descriptive information extracted by the texture analysis scheme corresponds to meaningful textural features.

A surface orientation detection scheme was outlined and partially automated. Preliminary results for two images exhibiting textured surfaces with non-zero gradients were presented and discussed. All known quantities were calculated to within 5° of their actual value. These results are very promising. However, more work needs to be done in order to fully automate the surface orientation analysis process.

APPENDIX A

STATISTICAL ANALYSIS OF ERA DEGRADATION

A.1 Introduction

In Chapter 2, an ERA interpretation algorithm was presented. The peak values of every ERA are examined and classified as major, minor, and subminor. The classification decision depends on the peak amplitude and the peak to valley separation. (See Chapter 2, Section 2.4.3 for details.) Given perfect edge and direction images for a periodic texture image, we would expect to get ERA values of 100 at element size or spacing distances, and zeros everywhere else. However, the edge and direction images analyzed are seldom free from some form of degradation. In low contrast images some edges may be missed, in noisy images edges may be found where there are no corresponding object edges, and at times edges are out of place by a small number of pixels. It is the object of this study to determine the robustness of the ERA peak classification scheme when one of these types of degradation occurs. In short, we want to determine the expected ERA values for certain pixel distances, assuming

a particular non-degraded edge image line and probability of an edge being deleted, inserted, or shifted.

Disregarding the factor of 100, each ERA entry is the number of a particular type of matches occurring at a given pixel distance and for a particular scan direction divided by a similarly defined normalization count. (See Chapter 2 for details.) The number of matches and normalization count is calculated separately for each line of pixels within the image. Therefore, this number can be thought of as the ratio of two sums. For a given line, the number of matches and normalization count are correlated. Only certain normalization counts can occur given a certain number of matches. However, the numbers of matches (or normalization counts) found for separate lines are independent. We want to find the expected value of this ratio.

The problem will be modelled as the ratio, X/Y, of 2 correlated random variables, which are themselves sums of independent random variables. ($X = X_1 + X_2 +...+ X_N$) and ($Y = Y_1 + Y_2 +...+ Y_N$), where N is the number of lines in the image, and $X_i(Y_i)$ is the random variable corresponding to the number of matches(normalization count) for line i. The X_i are identically distributed because the initial conditions are assumed to be the same

276

for each image line. This is also true of the Y_i. Therefore, we can find the expected values and (because of independence) the variance for X(or Y) in terms of N and the expected value and variance for X (or Y). These values will be used to calculate the expected value of the ratio (X/Y). See Section A.3.

The expected values, $E\{X_i\}$, of the number of matches for a line is calculated as follows:

(For the purpose of illustration the degradation will be assumed to be edge deletions.)

1) Assume an initial non-degraded line configuration, that is, a line with a periodic spacing of edges, and a non-zero probability, p, that an edge is deleted.

2) Given the number of edges, E, and the probability that an edge is deleted, calculate the probability of zero through E deletions occurring by using the binomial density.

3) For each possible number of deletions (zero through E) enumerate all of the line configurations with that number of deletions.

4) Calculate $P(M|D)$, that is, calculate the probability that M matches occur given D edge deletions. This can

be calculated for $D = 0,1,\ldots,E$ and $M = 0,1,\ldots,E-1$.

5) Calculate $P(M)$, the probability of M matches occurring by forming the sum

$$P(M|D=0)P(D=0)+P(M|D=1)P(D=1)+\ldots+P(M|D=E)P(D=E).$$

This can be done for $M = 0,1,\ldots,E-1$.

6) Calculate the expected value, $E\{X_i\}$, by forming the sum of the products $M(P(M))$ for $M = 0,1,\ldots,E-1$.

The same procedure can be followed to determine $E\{Y_i\}$ and $E\{X_iY_i\}$.

By evoking the law of large numbers we can use the approximations for $E\{g(X,Y)\}$ and $\sigma^2_{g(X,Y)}$ found in [34]. The details of this analysis are given in Section A.3.

The results (for element spacing ERAs) can be summarized as follows:

1) If the only kind of degradation is edge deletions, then the true texture period can be expected to be classified as a major peak for probability of deletion as great as .8.

2) If insertions are the only kind of degradation then peak to valley separation will decrease with increased probability of an edge being inserted and increased

278

texture period. In particular, for a texture period of 3, 5, or 7 pixels and probability of insertion equal to .1, .3, or .5 the true texture period would be expected to be classified as a major peak.

3) If edge shifting is the only source of degradation then with increasing shift probabilities the texture period peak and peak valley separations will decrease. For shift probabilities up to 1/3, (for left or right one pixel shifts) the texture period peak would still be correctly classified as major for element spacings of 4, 6, or 8 pixels.

4) In all cases the standard deviation was smaller (by roughly a factor of ten) than the corresponding expected peak value.

In spite of the fact that the standard deviations were calculated along with the expected peak values no attempt was made to calculate the precise probability of correct peak classification in any case. This is due to the fact that the dynamic thresholds and peak to valley separations used in the classification scheme are also affected by the imposed degradation. Thus, a more complex study is necessary to examine the combination of effects. However, the results can be used to indicate the general effects of such degradations.

A.2 Assumptions and Goals

This analysis is for element spacing ERAs calculated for periodic texture images. Hence, all matches are assumed to be between edges with exactly the same orientation. A similar analysis can be carried out for element size ERAs. The scan direction is assumed to be horizontal. These results can be applied to the vertical scan direction by interchanging "length of line" with "number of lines". However, analysis for other scan directions would have to take into account the varying line lengths for square or rectangular images. It is assumed that once a non-degraded line configuration is defined the analysis proceeds with no alterations. For example, if the non-degraded configuration of Fig. A-1(a) is assumed, then there can be no insertions two pixels to the left of the first edge, even if the rightmost pixel is deleted to keep the line length the same. Although only certain line configurations are examined the method can be used to analyze arbitrary non-degraded line configurations.

The purpose of this analysis is to determine the expected values of element spacing ERA peaks and valleys given the element spacing, line length, and the probability of edges being deleted, inserted, or shifted.

280

Combinations of these effects are not considered. In Fig. A-1, an example of each of these types of degradations is shown. The method used in each case is basically the same. (This is the subject of the following section.) The primary reference is by Papoulis [34].

A.3 General Scheme

The ERA entry for distance, d, is defined as follows:

$$100 \times \frac{\text{Number of matches at distance d}}{\text{Normalization count for d}} \quad . \qquad \text{(A-1)}$$

Since each line is considered independently, we can rewrite (A-1) for distance d as follows:

$$100 \times \frac{\displaystyle\sum_{i=1}^{N} \text{Number of matches for line i}}{\displaystyle\sum_{i=1}^{N} \text{Normalization count for line i}} \quad , \qquad \text{(A-2)}$$

where N is the number of lines in the image. (The factor of 100 will be ignored for the rest of this analysis.) The aim here is to derive an expression for the expected value of second factor in (A-2).

Let S be the space of all possible degraded line configurations for a given initial non-degraded line and non-zero probability of one kind of degradation. For

281

NORMALIZATION NUMBER = 6

NUMBER OF MATCHES = 6

(a) NO DEGRADATION

NORMALIZATION NUMBER = 6

NUMBER OF MATCHES = 4

(b) ONE EDGE DELETED

NORMALIZATION NUMBER = 8

NUMBER OF MATCHES = 6

(c) ONE EDGE INSERTED

NORMALIZATION NUMBER = 10

NUMBER OF MATCHES = 2
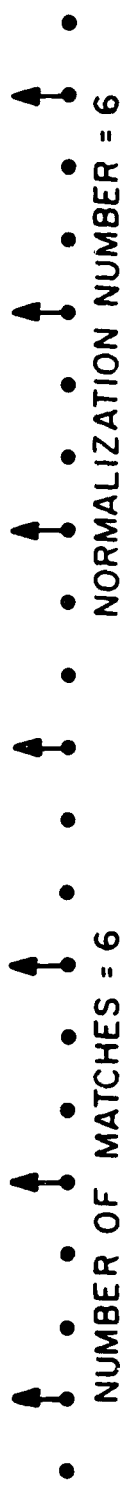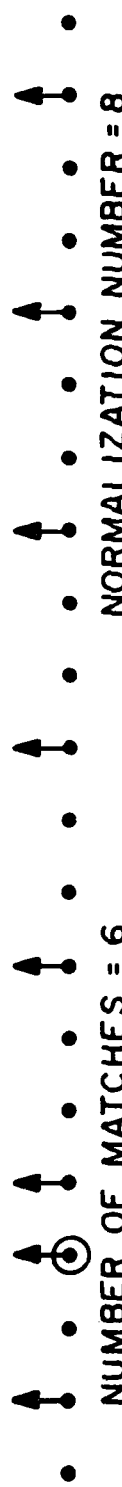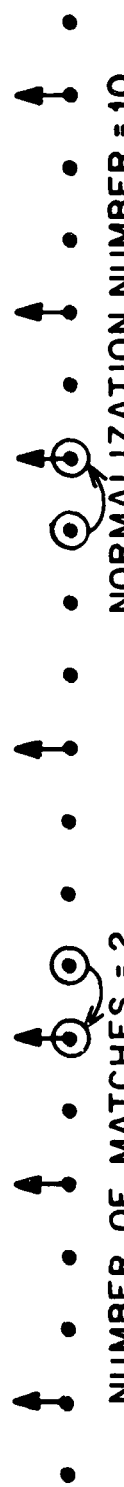
(d) TWO EDGES SHIFTED

Figure A-1. Line Configuration and Degradations

282

example, if the degradation is deletions, then S is the set containing the initial line configuration with all possible numbers of deletions, from no deleted edges to all deleted edges. In this case $S = \{l_1, l_2, \ldots, l_{2^E}\}$, where E is the number of equally spaced edges in the non-degraded line. Let X_i be the random variable (r.v.) associated with line i in the image which assigns each line configuration, l_j, its number of matches for some predetermined element spacing distance. For example, if l_j is the degraded configuration of Fig. A-1(b) then $X_i(l_j) = 4$ for element spacing 3 for all i.

Let $P(X_i = k)$ be the probability that a particular line configuration with non-zero probability of degradation will have k matches at a given element spacing. Then

$$E\{X_i\} = \eta_{X_i} = \sum_j k_j P\{X_i = k_j\} \tag{A-3}$$

is the mean or expected value of X and

$$\sigma^2_{X_i} = \sum_j (k_j - \eta_{X_i})^2 P\{X_i = k_j\} \tag{A-4}$$

is the variance or dispersion of X_i. The number of matches for each line in the image is calculated independently. Therefore, the random variables

283

$X_1, X_2, \ldots, X_N$ are independent. Since all of the initial conditions, that is, the non-degraded line configuration, probability of degradation, and element spacing, are the same for each line the expected values and variances are also identical for all i.

Let $\eta_{X_0} = \eta_{X_i}$ for i and $\sigma^2_{X_0} = \sigma^2_{X_i}$ for all i. We can now define the r.v. $X = X_1 + X_2 + \ldots + X_N$ where N is the number of lines in the image. Then

$$\eta_X = N\eta_{X_0} \quad , \tag{A-5}$$

and since the X_i are uncorrelated we have

$$\sigma^2_X = N\sigma^2_{X_0} \quad . \tag{A-6}$$

A similar argument can be made for the normalization counts to produce the r.v. $Y = Y_1 + Y_2 + \ldots + Y_{N'}$ with

$$\eta_Y = N\eta_{Y_0} \quad , \tag{A-7}$$

and

$$\sigma^2_Y = N\sigma^2_{Y_0} \quad . \tag{A-8}$$

Now let

$$g(X,Y) = \left(\frac{X}{Y}\right) = \left(\frac{\sum_{i=1}^{N} X_i}{\sum_{i=1}^{N} Y_i}\right) \tag{A-9}$$

284

be a function of the random variables X and Y. The statistics of g are the object of this analysis. That is, we are interested in the expected value and standard deviation of g(X,Y). (The standard deviation is simply the square root of the variance).

Since we are working with large sums of identically distributed random variables, it is reasonable to assume by the law of large numbers that the joint density is concentrated near its mean, (η_X, η_Y). Then since (X/Y) is smooth in the regions of interest, the following approximation from [34,p.212] can be used:

$$E\{g(X,Y)\} \simeq g(\eta_X, \eta_Y) + \frac{1}{2}\left(\mu_{20}\frac{\partial^2 g}{\partial X^2} + 2\mu_{11}\frac{\partial^2 g}{\partial X \partial Y} + \mu_{02}\frac{\partial^2 g}{\partial Y^2}\right) \quad , \quad (A-10)$$

and

$$\sigma^2_{g(X,Y)} \simeq (\frac{\partial g}{\partial X})^2 \mu_{20} + (\frac{\partial g}{\partial Y})^2 \mu_{02} + 2 \frac{\partial g}{\partial X} \frac{\partial g}{\partial Y} \mu_{11} \quad , \quad\quad (A-11)$$

where

$$\mu_{11} = E\{XY\} - E\{X\}E\{Y\} \quad , \quad\quad (A-12)$$

$$\mu_{20} = \sigma_X^2 = N\sigma_{X_0}^2 \ , \qquad\qquad (A-13)$$

and

$$\mu_{02} = \sigma_Y^2 = N\sigma_{Y_0}^2 \ \ . \qquad\qquad (A-14)$$

We would like a simpler expression for μ_{11}, the covariance of X and Y. By substituting in (A-12) we get

$$\mu_{11} = E\left\{\sum_{i=1}^{N} X_i \sum_{j=1}^{N} Y_j\right\} - N\eta_{X_0} N\eta_{Y_0} \ . \qquad\qquad (A-15)$$

(A-15) can be rewritten as follows

$$\mu_{11} = E\left\{\sum_{i=1}^{N} \sum_{j=1}^{N} X_i Y_j\right\} - N^2 \eta_{X_0} \eta_{Y_0} \ . \qquad\qquad (A-16)$$

The double sum can be broken into 2 sums to give

$$\mu_{11} = E\left\{\sum_{i=1}^{N} X_i Y_i\right\} + E\left\{\sum_{\substack{i,j\in I_N \\ i\neq j}} X_i Y_j\right\} - N^2 \eta_{X_0} \eta_{Y_0} \ , \qquad\qquad (A-17)$$

where I_N is the set $\{1,2,\ldots,N\}$. The sum on the right is the sum of products of independent random variables since the number of matches and normalization numbers are constrained to be from 2 different lines in the image. This means that (A-17) can be rewritten as follows

$$\mu_{11} = \sum_{i=1}^{N} E\{X_i Y_i\} + (N^2 - N)\eta_{X_0}\eta_{Y_0} - N^2 \eta_{X_0}\eta_{Y_0} \ . \quad (A-18)$$

286

Simplifying, we obtain

$$\mu_{11} = N(E\{X_i Y_i\} - \eta_{X_0} \eta_{Y_0}) \quad . \tag{A-19}$$

Now (A-10) can be rewritten as follows

$$E\{g(X,Y)\} \simeq \frac{N\eta_{X_0}}{N\eta_{Y_0}} - \frac{N(E\{X_i Y_i\}\eta_{X_0}\eta_{Y_0})}{(N\eta_{Y_0})^2} + \frac{N^2 \sigma_{Y_0}^2 \eta_{X_0}}{(N\eta_{Y_0})^3} \quad , \tag{A-20}$$

and further simplified as follows

$$E\{g(X,Y)\} \simeq \frac{\eta_{X_0}}{\eta_{Y_0}} - \frac{(E\{X_i Y_i\} - \eta_{X_0}\eta_{Y_0})}{N\eta_{Y_0}^2} + \frac{\sigma_{Y_0}^2 \eta_{X_0}}{N\eta_{Y_0}^3} \quad . \tag{A-21}$$

Finally, we have

$$E\{\frac{X}{Y}\} \simeq \frac{\eta_{X_0}}{\eta_{Y_0}} - \left(E\{X_i Y_i\} - \eta_{X_0}\eta_{Y_0} - \frac{\sigma_{Y_0}^2 \eta_{X_0}}{\eta_{Y_0}} \right) \frac{1}{N\eta_{Y_0}^2} \quad , \tag{A-22}$$

where N is the number of lines in the image, η_{X_0} is the expected value of the number of matches on a line, η_{Y_0} is the expected value for the normalization count on a line, and $\sigma_{Y_0}^2$ is the variance for the normalization count. $E\{X_i Y_i\}$ is the expected value of the product of the

287

matching and normalization numbers for a line. All of these will be calculated by enumeration for a given non-degraded line configuration, element spacing distance and probability of degradation. A similar simplification of (A-11) will produce

$$\sigma_{g(X,Y)}^2 \simeq \frac{N\sigma_{X_0}^2}{(Nn_{Y_0})^2} + \frac{(Nn_{X_0})^2}{(Nn_{Y_0})^4} N\sigma_{Y_0}^2 - 2\mu_{11} \frac{(Nn_{X_0})}{(Nn_{Y_0})} \, , \quad (A-23)$$

which becomes

$$\sigma_{g(X,Y)}^2 \simeq \frac{1}{Nn_{Y_0}^2} \left[\sigma_{X_0}^2 + \left(\frac{n_{X_0}}{n_{Y_0}}\right)^2 \sigma_{Y_0}^2 - 2\left(\frac{n_{X_0}}{n_{Y_0}}\right)(E\{X_i Y_i\} - n_{X_0} n_{Y_0}) \right] \, .$$

$$(A-24)$$

In the remaining sections some results for the three types of degradations mentioned above will be presented and discussed. It will be assumed in these studies that the number of image rows is large (over 100). This is not unreasonable in light of the fact that all images used in this thesis are at least 128x128 pixel images.

A.4 Deletions

Since deletions are considered independent of shifts and insertions, we need only consider the expected value of (X/Y) at the element spacing distance. All values for

(X/Y) at distances other than the element spacing or its multiples will be zero. It is also true that the results will be the same for different element spacing distances provided the probability that an edge is deleted is the same and the number of edges per line (given no deletions) is the same.

If E is the number of edges per line given no deletions then the expected value of the number of matches at the element spacing distance is defined as

$$n_{X_0} = \sum_{M=0}^{E-1} M \cdot P(M) \ , \qquad (A-25)$$

where

$$P(M) = \sum_{D=0}^{E} P(M|D) P(D) \ , \qquad (A-26)$$

M is the number of matches, and D is the number of deletions. Since each edge is equally likely to be deleted we have

$$P(D) = \binom{E}{D} p^D (1-p)^{E-D} \qquad (A-27)$$

for each D where p is the probability of an edge being deleted. $P(M|D)$ is the probability that the number of matches is M given D deletions occur. This number, as well as $P(C|D)$ which is used in (A-30), is calculated as

explained in the outline given in Section A.1. The variance is defined as

$$\sigma_{X_0}^2 = \sum_{M=0}^{E-1} (M - n_{X_0})^2 P(M) \quad . \tag{A-28}$$

Similarly,

$$n_{Y_0} = \sum_{C=0}^{E-1} C \cdot P(C), \tag{A-29}$$

$$P(C) = \sum_{D=0}^{E} P(C|D) P(D), \tag{A-30}$$

and

$$\sigma_{Y_0}^2 = \sum_{C=0}^{E-1} (C - n_{Y_0})^2 P(C) \tag{A-31}$$

for normalization count, C.

It remains to define $E\{X_i Y_i\}$ to provide all that is necessary for the computations shown in (A-22) and (A-24). $E\{X_i Y_i\}$ is the expected value of the product of the number of matches and normalization count for a given line. That is, each (X_i, Y_i) pair must be a valid pair of counts for at least one degraded line configuration (or for the original non-degraded line). (The method used to calculate $E\{X_i Y_i\}$ is outlined in Section A.1.) Let T be

290

the set of valid (number of matches, normalization count) ordered pairs. Then

$$E\{X_i Y_i\} = \sum_{(X_j, Y_j) \epsilon T} (X_j Y_j) P(X_j, Y_j) \quad , \qquad \text{(A-32)}$$

where

$$P(X_j, Y_j) = \sum_{D=0}^{E} P((X_j, Y_j) | D) P(D) \quad . \qquad \text{(A-33)}$$

The graph in Fig. A-2 shows the expected value of (X/Y) for the given texture period as a function of the probability of deletion. Only the 1st term of (A-22) is used since the second term is insignificant for N equal to 100 (which was used in this example). The expected value of (X/Y) at the element spacing value depends only on the probability that an edge is deleted. The number of edges per line and the element spacing distance have no effect on the result. However, the standard deviation decreases as the number of edges per line increases. For 100 image lines the standard deviation; is less than one tenth of the expected value for probability of deletion less than or equal to .5, for lines with at least 5 edges. The results shown in Fig. A-2 seem to indicate that if no other type of degradation is present the peak at the element spacing distance will be classified as major for
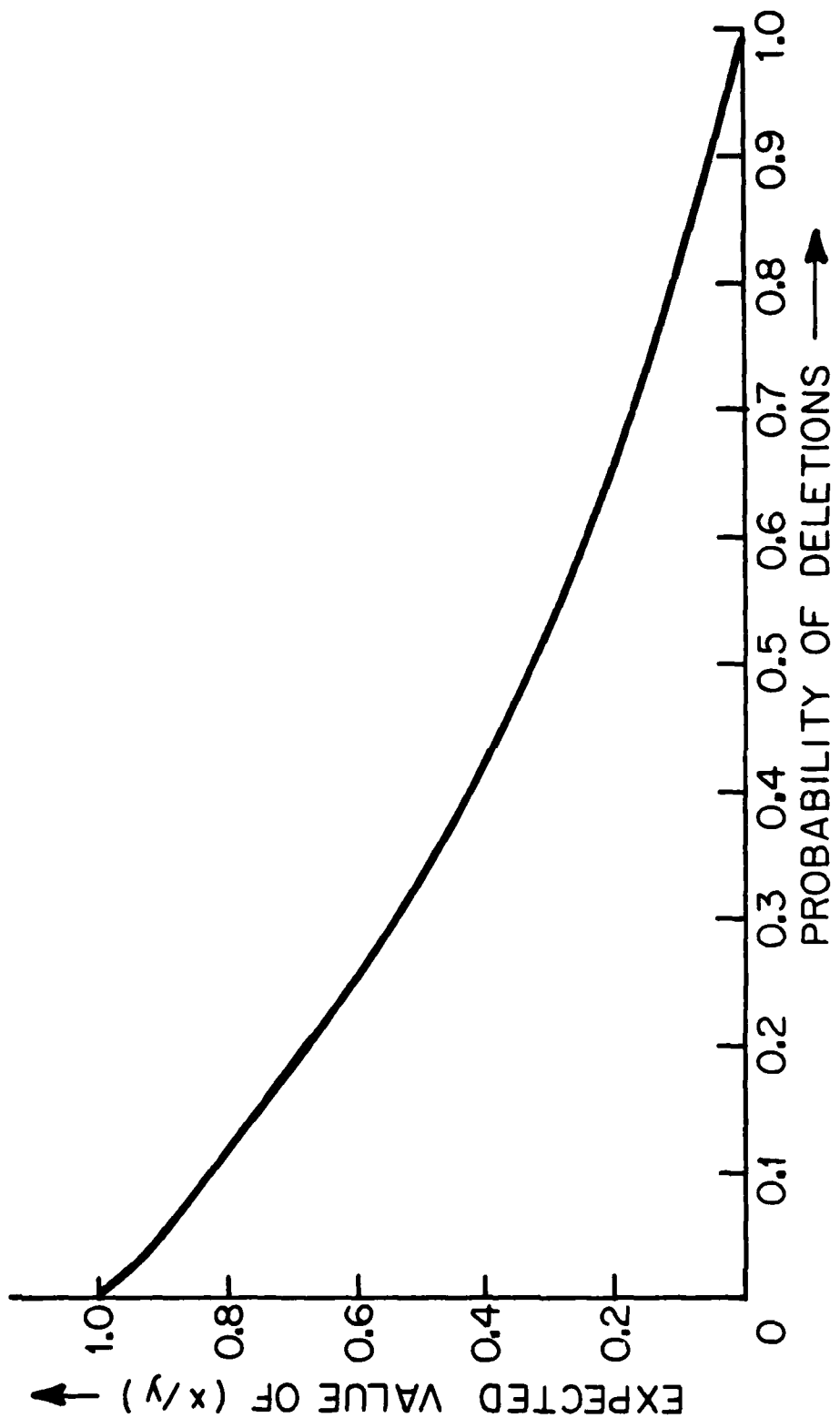
Figure A-2. Expected Value of Texture Period Peak

probability of deletion as high as .8.

The specific probability of correct classification is not given because the threshold used in the classification scheme is dynamically computed. It is subject to the same degradation effects as the peak amplitudes. Hence, we can only use these results to get an indication of general trends.

A.5 Insertions

In the case of insertions, we need to consider the expected value of the element spacing peak, as well as the expected values at the surrounding pixel distances. In this way the expected peak to valley separation can be examined. In the case of deletions only the element spacing ERA value (and its multiples) could be expected to be non-zero. The initial, non-degraded line configuration has more of an impact in the case of insertions, i.e., the length of the line, the number of edges per line and the placement of these edges within the line can influence the final result.

If L is the number of non-edge pixels on a line given no insertions and E is the number of edges on the line then the expected value of the number of matches at distance, D, is defined as

$$\eta_{X_0} = \sum_{M=0}^{L+E-D} M \cdot P(M) \quad , \qquad (A-34)$$

where

$$P(M) = \sum_{I=0}^{L} P(M|I) P(I) \quad , \qquad (A-35)$$

M is the number of matches, and I is the number of insertions. Since each non-edge pixel is equally likely to become an insertion we have

$$P(I) = \binom{L}{I} p^I (1-p)^{(L-I)} \quad , \qquad (A-36)$$

for each I where p is the probability of an edge being inserted in a non-edge location. $P(M|I)$ is the probability that the number of matches is M given that I insertions occur. The variance is defined as

$$\sigma_{X_0}^2 = \sum_{M=0}^{L+E-D} (M-\eta_{X_0})^2 P(M) \quad . \qquad (A-37)$$

Similarly,

$$\eta_{Y_0} = \sum_{C=0}^{L+E-D} C \cdot P(C) \quad , \qquad (A-38)$$

294

$$P(C) = \sum_{I=0}^{L} P(C|I)P(I) \quad , \tag{A-39}$$

and

$$\sigma_{Y_0}^2 = \sum_{C=0}^{L+E-D} (C-\eta_{Y_0})^2 P(C) \tag{A-40}$$

for normalization count C.

In order to perform the computations shown in (A-22) and (A-24), $E\{X_iY_i\}$ is needed. $E\{X_iY_i\}$ is the expected value of the product of the number of matches and normalization count for a given line. That is, each (X_i,Y_i) pair must be a valid pair of counts for at least one degraded line configuration (or for the original non-degraded line). Let T be the set of valid (number of matches, normalization count) ordered pairs. Then

$$E\{X_iY_i\} = \sum_{(X_j,Y_j)\epsilon T} (X_jY_j)P(X_j,Y_j) \quad , \tag{A-41}$$

where

$$P(X_j,Y_j) = \sum_{I=0}^{L} P((X_j,Y_j)|I)P(I) \quad . \tag{A-42}$$

The graphs shown in Fig. A-3(a), (b), and (c) show the expected value of (X/Y) as a function the element

295
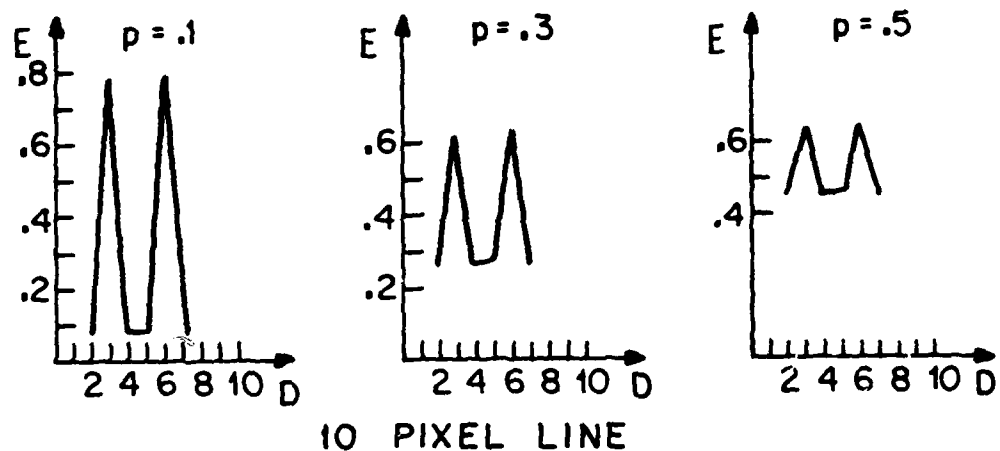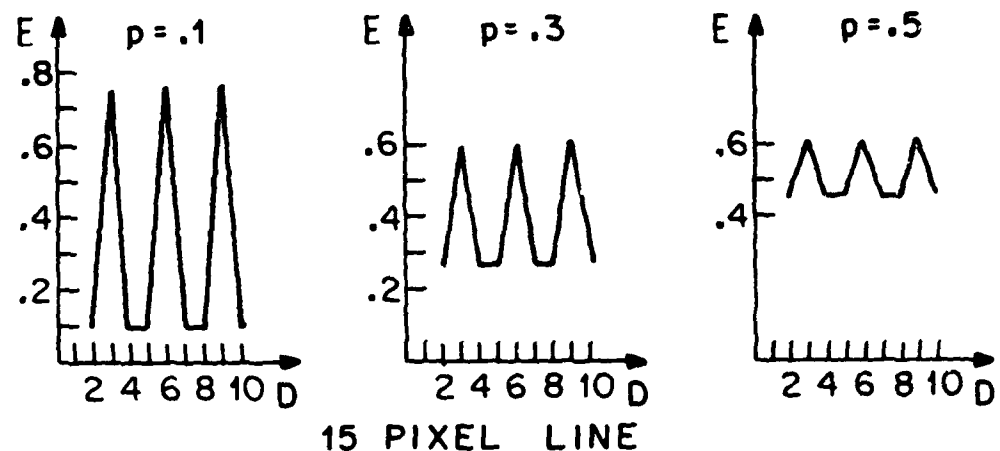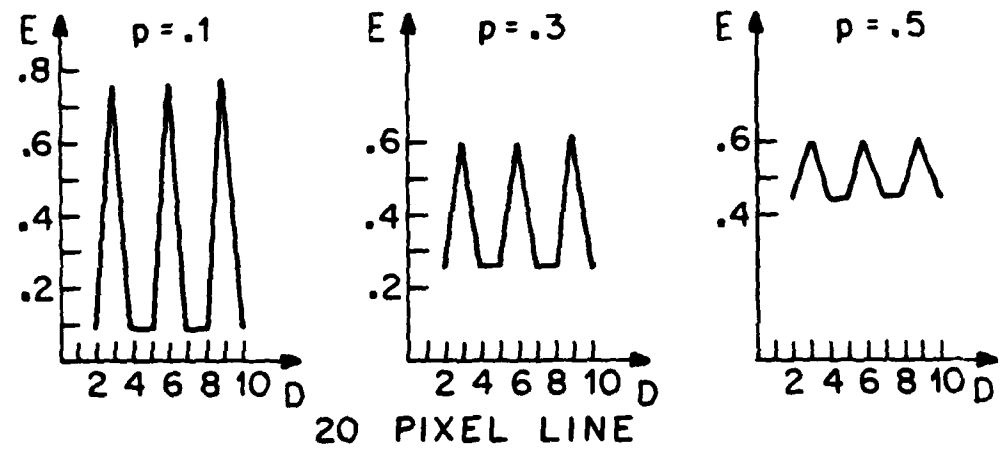
Figure A-3(a).   Expected Value (E) of (X/Y) at Distance
(D) for Texture Period 3
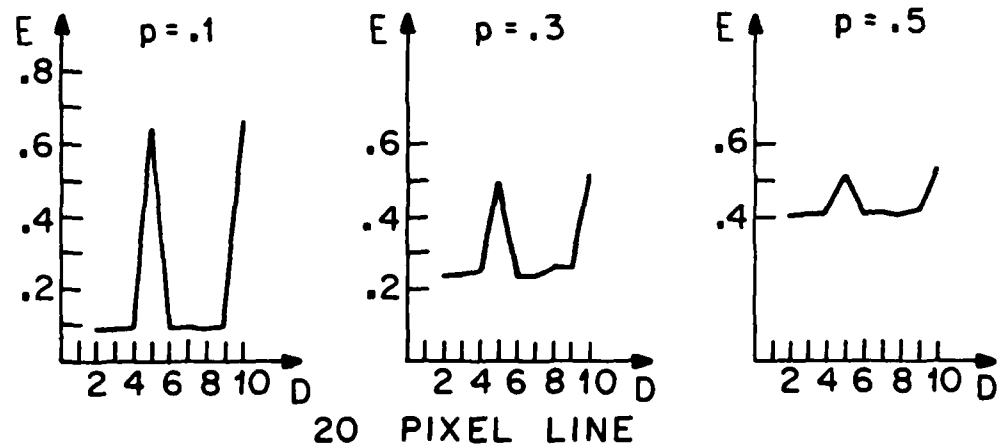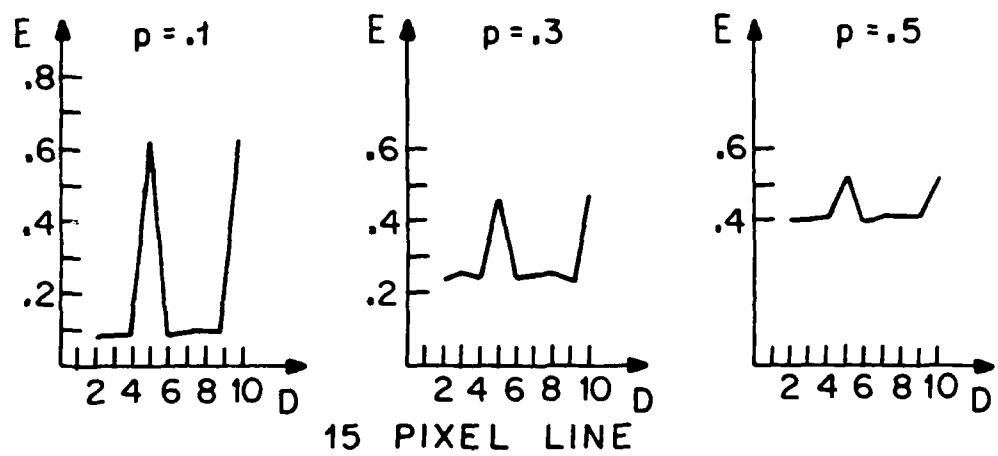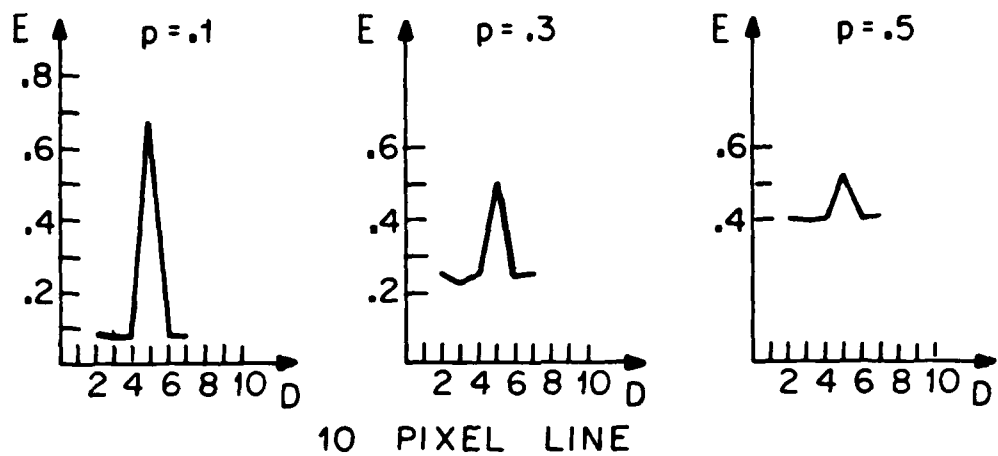
Figure A-3(b). Expected Value (E) of (X/Y) at Distance (D) for Texture Period 5
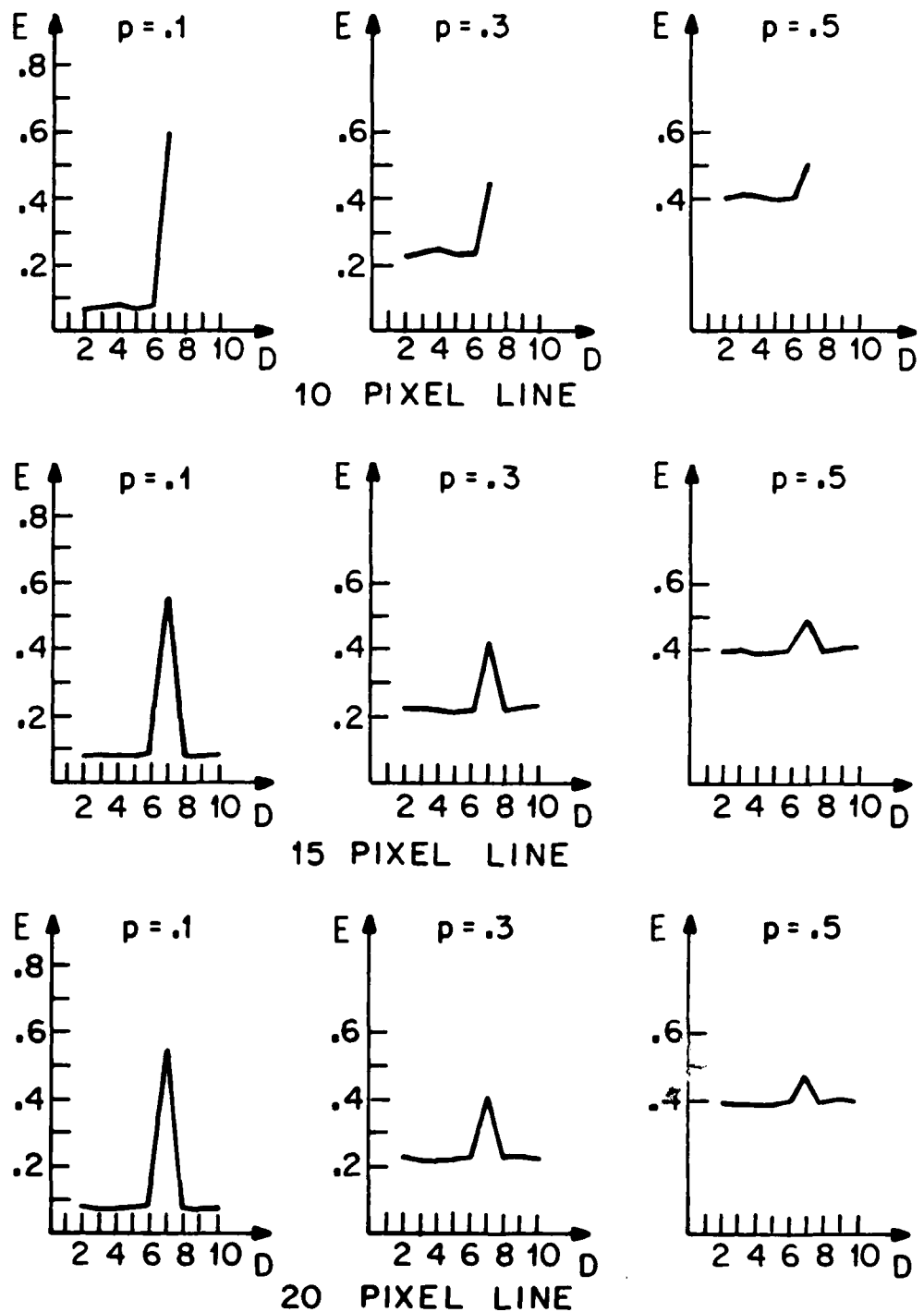
Figure A-3(c). Expected Value (E) of (X/Y) at Distance (D) for Texture Period 7

298

spacing distance and the probability of insertion for specific initial non-degraded line configurations. Only the first term of (A-22) is used since the second term is insignificant for large N. (N = 100 is assumed.) It would seem from the above mentioned graphs that length of line has less effect on expected value results than the spacing between valid edges in the line. The expected value decreases for a given probability of insertions as the period increases. As the probability of insertions increases, the peak valley separation for the element spacing edge repetition array decreases. None of the graphs shown in Fig. A-3 would pose a problem in terms of major peak selection since the values shown will be multiplied by 100. However, further decreases in peak valley separation would begin to have an affect.

Assuming a one hundred line image, the standard deviation for the texture period peaks and their multiples is more than a factor of ten less than the expected values at those element spacing distances for all cases shown. As the length of the line increases the expected value, standard deviation ratio increases. However, for a given length of line, as the element period increases the ratio decreases. Also the standard deviation decreases as the square of the number of image rows.

Again, no precise probabilities can be given for correct classification. In this case not only do the peak classification thresholds depend on the probability of degradation, but the peak to valley separation for each graph does as well.

A.6 Shifts

For this study is is assumed that each edge in the image line has a non-edge pixel to its right and left so that each edge can be shifted in either direction. This was done for ease of notation. In the computed cases, the probability that an edge is shifted one pixel to the right is the same as the probability of a similar left shift. This need not be the case as long as the sum of the two probabilities does not exceed 1.0. An in place edge is never assumed to have been shifted right one pixel and then shifted left this amount. Hence, each edge can only be right shifted, left shifted or unshifted. In the case of shifts, as for insertions, the expected values for the element spacing peak, as well as the expected values at surrounding pixel distances are shown. This is done so that the expected peak to valley separations can be examined. In the case of shifts, the expected value at the texture period distance is the same for different length lines and different texture periods, given a

particular left shift, right shift probability pair. (See Fig. A-4(a), (b), and (c).) Only the first term of (A-22) is used since the second term is less than the first by at least a factor of N. (N at least 100 has been assumed.)

Let L be the number of non-edge pixels within the line and E be the number of edges in the line, then the expected value of the number of matches at distance, D, is

$$\eta_{X_0} = \sum_{M=0}^{L+E-D} M \cdot P(M) \quad , \tag{A-43}$$

where

$$P(M) = \sum_{\substack{L, R \varepsilon S \\ L+R < E}} (M \mid L, R) P(L, R) \quad , \tag{A-44}$$

M is the number of matches, and L(R) is the number of left (right) shifted edges, and $S = \{0, 1, \ldots, E\}$. Since each edge is equally likely to be left shifted, right shifted or remain unshifted we have

$$P(L, R) = \binom{E}{L} \binom{E-L}{R} p^L q^R (1-p-q)^{(E-L-R)} \tag{A-45}$$

for each L,R pair such that $L \varepsilon S$, $R \varepsilon S$, and $L+R \leq E$, where p is the probability of an edge being shifted left, and q is the probability of an edge being shifted right. $P(M \mid L, R)$ is the probability that the number of matches is

301

M given L left shifts and R right shifts occur on a previously determined line. The variance is defined as

$$\sigma_{X_0}^2 = \sum_{M=0}^{L+E-D} (M-\eta_{X_0})^2 P(M) \quad .$$
(A-46)

Similarly,

$$\eta_{Y_0} = \sum_{C=0}^{L+E-D} C \cdot P(C) \quad ,$$
(A-47)

$$P(C) = \sum_{\substack{L,R \in S \\ L+R \leq E}} (C|L,R) P(L,R),$$
(A-48)

and,

$$\sigma_{Y_0}^2 = \sum_{C=0}^{L+E-D} (C-\eta_{Y_0})^2 P(C)$$
(A-49)

for normalization count C.

$E\{X_i Y_i\}$ will now be defined. $E\{X_i Y_i\}$ is the expected value of the product of the number of matches and normalization count for a given line. That is, each (X_i, Y_i) pair must be a valid pair of counts for at least one degraded line configuration (or for the original non-degraded line). Let T be the set of valid (number of matches, normalization count) ordered pairs. Then

302

$$E\{X_i Y_i\} = \sum_{(X_j,Y_j)\varepsilon T} (X_j Y_j) P(X_j,Y_j) \quad , \qquad \text{(A-50)}$$

where

$$P(X_j,Y_j) = \sum_{\substack{L,R\varepsilon S \\ L+R\leq E}} P((X_j,Y_j)|L,R) P(L,R) \quad . \qquad \text{(A-51)}$$

The graphs shown in Fig. A-4(a), (b), and (c) show the expected value of (X/Y) as a function of p, q, the texture period for specific non-degraded line configurations. Again only the first term of (A-22) is used. From the graphic results it seems that only p and q exert significant influence over the expected value results. When p=q=(1/3) the peak-valley separation is close to the point at which the texture period peak will not be classified as major. For higher probabilities of shift these peaks are likely to fail the major peak test.

As the length of the line increases the standard deviation for a given texture period decreases. However, as the texture period increases for a given length line, the standard deviation increases. For the texture period results shown, the standard deviations for N = 100 are given in Table A-1. (That is, the standard deviations are shown only for the texture period peaks.)

303
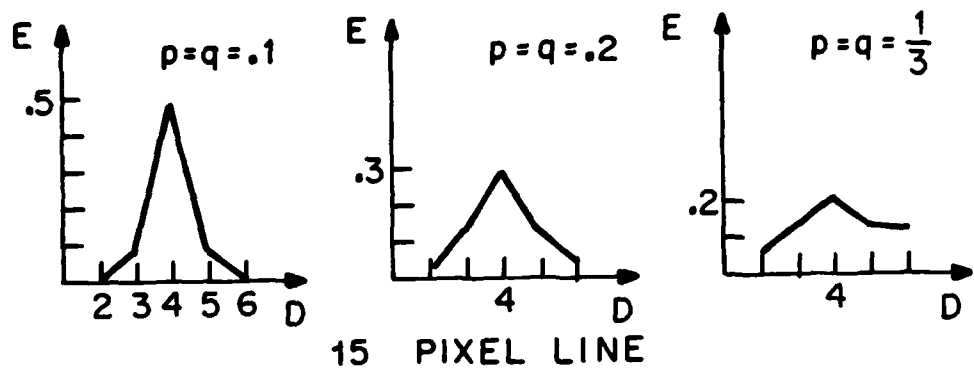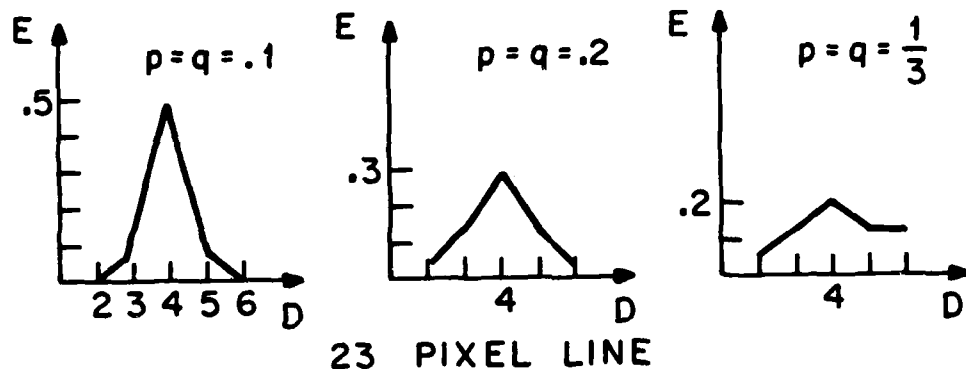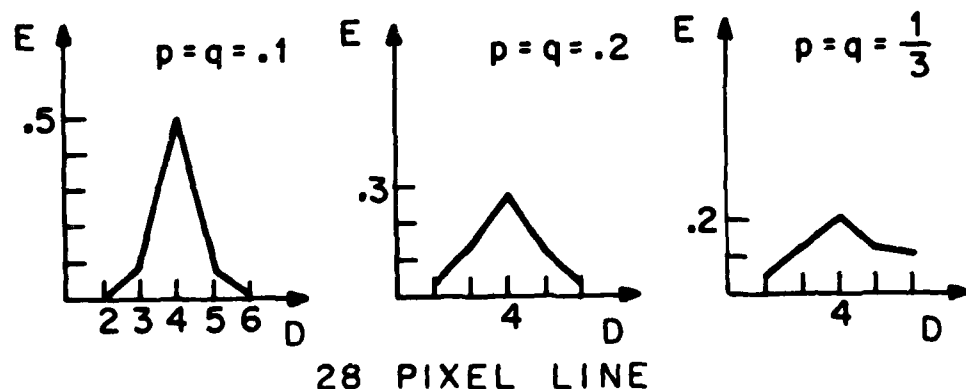
Figure A-4(a). Expected Value (E) at Distance (D) for
Texture Period 4
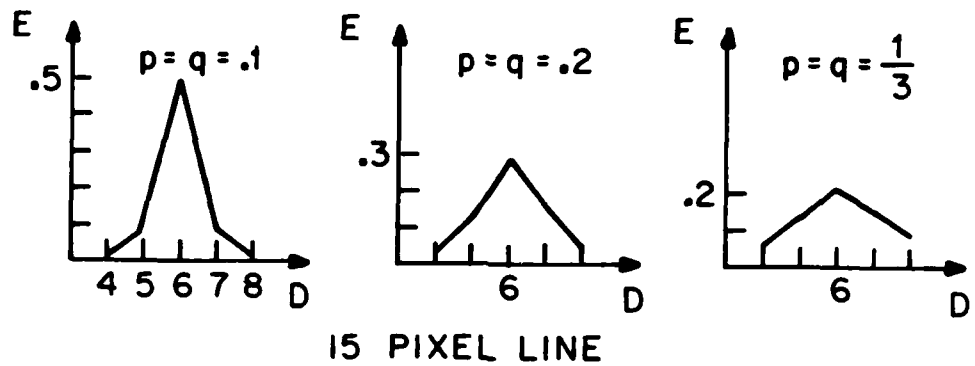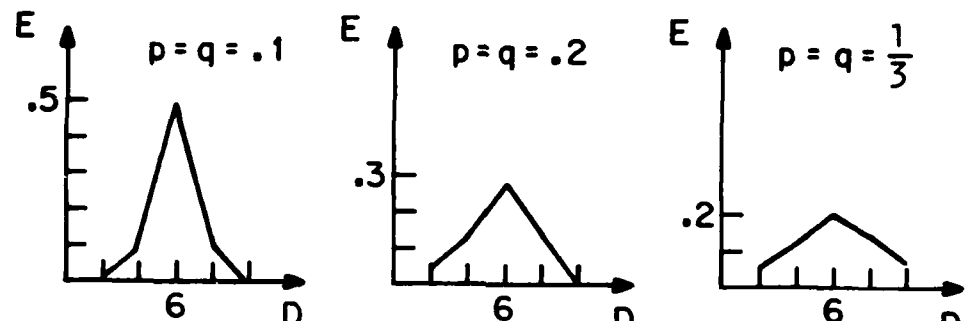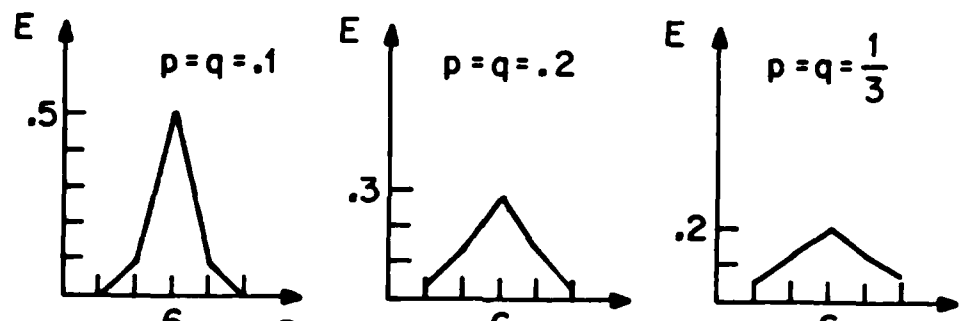
Figure A-4(b). Expected Value (E) at Distance (D) for
Texture Period 6

305
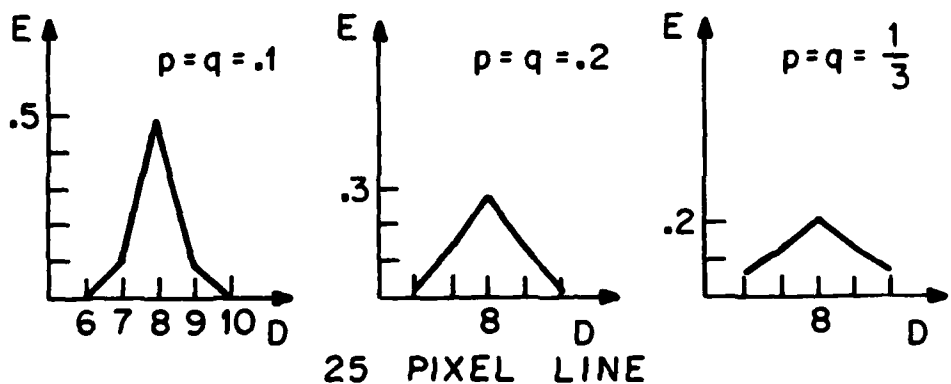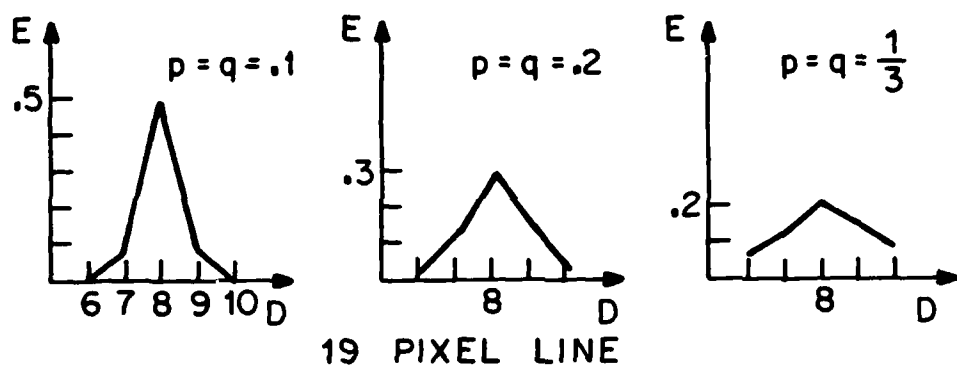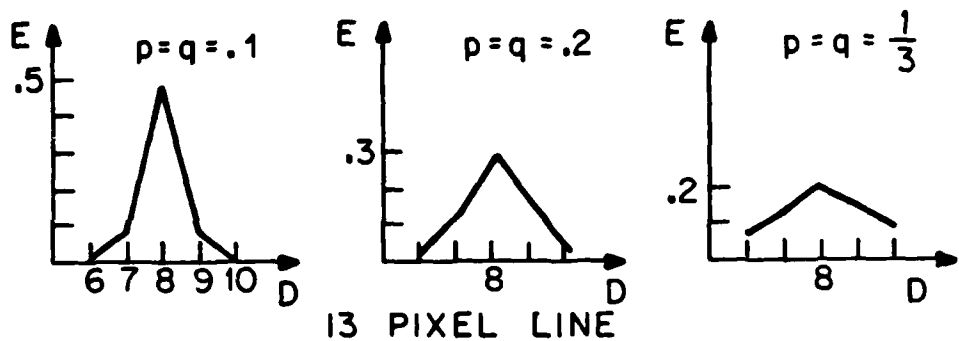
Figure A-4(c).   Expected Value (E) at Distance (D) for
Texture Period 8

TABLE A-1. EXPECTED VALUE AND STANDARD DEVIATION OF (X/Y) AT THE TEXTURE PERIOD FOR 100 IMAGE LINES

Line Length (In pixels)	Texture Period (In pixels)	p=q= .1		p=q= .2		p=q= 1/3	
		E(X/Y)	σX/Y	E(X/Y)	σX/Y	E(X/Y)	σX/Y
15	4	.49	.038	.28	.025	.2	.019
15	6	.49	.043	.28	.310	.2	.024
13	8	.49	.052	.28	.040	.2	.033
23	4	.49	.029	.28	.020	.2	.015
21	6	.49	.036	.28	.025	.2	.019
19	8	.49	.043	.28	.031	.2	.024
28	4	.49	.027	.28	.018	.2	.013
33	6	.49	.032	.28	.022	.2	.016
25	8	.49	.043	.28	.031	.2	.024

Further analysis would be required in order to determine the precise probability of correctly classifying texture period peaks. This is due to the dynamic thresholding scheme used and the use of peak to valley separations.

REFERENCES

[1] B. Julesz, "Experiments in the Visual Perception of Texture," Scientific American, vol. 232, pp. 34-43, April 1975.

[2] W.K. Pratt, O.D. Faugeras, and A. Gagalowicz, "Visual Discrimination of Stochastic Texture Fields," IEEE Trans. on Systems, Man, and Cybernetics, vol. SMC-8, pp. 460-473, June 1978.

[3] R. Nevatia, Machine Perception. To be published, Prentice-Hall.

[4] R.M. Haralick, "Statistical and Structural Approaches to Texture," Proceedings of IEEE, vol. 67, pp. 786-804, May 1979.

[5] R. Bajcsy, "Computer Identification of Textured Visual Scenes," Ph.D. Dissertation, Stanford University, 1972.

[6] R. Bajcsy, and L. Lieberman, "Texture Gradient as a Depth Cue," Computer Graphics and Image Processing, vol. 5, pp. 52-57, 1976.

[7]   R.M. Haralick,   K. Shanmugan,   and   I. Dinstein,
      "Textural Features for Image Classification," IEEE
      Trans.   on Systems, Man, and   Cybernetics,
      vol. SMC-3, pp. 610-621, Nov. 1973.

[8]   K.E. Price and R. Nevatia, "Experiments in Natural
      Texture Description," USCIPI Report 840, pp. 77-89,
      Sept. 1978.

[9]   L.S. Davis, A.J. Johns, and J.K. Aggarwal, "Texture
      Analysis Using Generalized Co-Occurrence Matrices,"
      IEEE Trans.   Pattern Analysis and   Machine
      Intelligence, vol. PAMI-1, pp. 251-259, July 1979.

[10] S.W. Zucker, and D. Terzopoulos, "Finding Structure
      in Co-Occurrence Matrices for Texture Analysis,"
      Computer Graphics and Image Processing, vol. 12,
      pp. 286-308, 1980.

[11] R.W. Conners, "Towards a Set of Statistical Features
      Which Measure Visually Perceivable Qualities of
      Textures," Procedings: Pattern Recognition and Image
      Processing, pp. 382-390, 1979.

[12] R.W. Conners and   Charles A. Harlow,   "Toward   a
      Structural Textural Analyzer Based on Statistical
      Methods," Computer Graphics and Image Processing,
      vol. 12, pp. 224-256, 1980.

310

[13] L. Carlucci, "A Formal System for Texture Languages," _Pattern Recognition_, vol. 4, pp. 53-72, 1972.

[14] S.Y. Lu and K.S. Fu, "A Syntactic Approach to Texture Analysis," _Computer Graphics and Image Processing_, vol. 7, pp. 303-330, 1978.

[15] S.Y. Lu and K.S. Fu, "Stochastic Tree Grammar Inference for Texture Synthesis and Discrimination," _Computer Graphics and Image Processing_, vol. 9, pp. 234-245, 1979.

[16] S.W. Zucker, "Toward a Model of Texture," _Computer Graphics and Image Processing_, vol. 5, pp. 190-202, 1976.

[17] R.W. Ehrich and J.P. Foith, "A View of Texture Topology and Texture Description," _Computer Graphics and Image Processing_, vol. 8, pp. 174-202, 1978.

[18] S. Wang, F.R.D. Velasco, A.Y. Wu, and A. Rosenfeld, "Relative Effectiveness of Selected Texture Primitive Statistics for Texture Discrimination," _IEEE Trans. on Systems, Man, and Cybernetics_, vol. SMC-11, pp. 360-370, May 1981.

[19] J. Maleson, C. Brown, and J. Feldman, "Understanding

Natural Textures," Proceedings: Image Understanding Workshop, pp. 19-27, Oct. 1977.

[20] T. Matsuyama, K. Saburi, and M. Nagao, "A Structural Description of Regularly Arranged Textures," Proceedings: International Conference of Pattern Recognition, pp. 1115-1118, Dec. 1980.

[21] L.S. Davis, "Computing the Spatial Structures of Cellular Textures," Computer Graphics and Image Processing, vol. 11, pp. 111-122, 1979.

[22] P. Brodatz, Texture: A Photographic Album for Artists and Designers. New York: Dover, 1966.

[23] K.A. Stevens, "Analysis and Representation of Visual Surface Orientation," Ph.D. Dissertation, MIT, 1978.

[24] R. Nevatia, K.E. Price, and F. Vilnrotter, "Describing Natural Textures," USCIPI Report 860, pp. 29-52, March 1979.

[25] H. Tamura, S. Mori, and T. Yamawaki, "Textural Features Corresponding to Visual Perception," IEEE Trans. on Systems, Man, and Cybernetics, vol. SMC-8, pp. 460-473, June 1978.

[26] J.S. Weszka, C.R. Dyer, and R. Rosenfeld, "A

Comparative Study of Texture Measures for Terrain Classification," IEEE Trans. on Systems, Man, and Cybernetics, vol. SMC-6, pp. 269-285, April 1976.

[27] R.W. Conners, and C.A. Harlow, "A Theoretical Comparison of Texture Algorithms," IEEE Trans. on Pattern Analysis and Machine Intelligence, vol. PAMI-2, pp. 204-222, May 1980.

[28] R. Nevatia and K.R. Babu, "Linear Feature Extraction and Description," Computer Graphics and Image Processing, vol. 13, pp. 257-269, 1980.

[29] S. Tsuji and F. Tomita, "A Structural Analyzer for a Class of Textures," Computer Graphics and Image Processing, vol. 2, pp. 216-231, Dec. 1973.

[30] K.A. Stevens, "Representing and Analyzing Surface Orientation," Artificial Intelligence: An MIT Perspective, pp. 104-125, Cambridge: MIT Press, 1979.

[31] A.K. Mackworth, "Interpreting Pictures of Polyhedral Scenes," Artificial Intelligence, vol. 4, pp.121-137, 1973.

[32] J.R. Kender, "Shape From Texture," Ph.D. Dissertation, Carnegie-Mellon University, 1980.

[33] R.O. Duda and P.E. Hart, <u>Pattern</u> <u>Classification</u> <u>and</u> <u>Scene</u> <u>Analysis</u>. New York: Wiley-Interscience, 1973.

[34] A. Papoulis, <u>Probability,</u> <u>Random</u> <u>Variables,</u> <u>and</u> <u>Stochastic</u> <u>Processes</u>. New York: McGraw-Hill Book Company, 1965.